論文 / 著書情報
Article / Book Information

題目(和文)	GaInAsP/InP長波長帯量子細線レーザに関する研究
Title(English)	A study of GaInAsP/InP long-wavelength quantum-wire lasers
著者(和文)	小島隆
Author(English)	
出典(和文)	学位:博士(工学), 学位授与機関:東京工業大学, 報告番号:甲第4121号, 授与年月日:1999年3月26日, 学位の種別:課程博士, 審査員:
Citation(English)	Degree:Doctor (Engineering), Conferring organization: Tokyo Institute of Technology, Report number:甲第4121号, Conferred date:1999/3/26, Degree Type:Course doctor, Examiner:
学位種別(和文)	博士論文
Type(English)	Doctoral Thesis

A Study of GaInAsP/InP Long-Wavelength Quantum-Wire Lasers

by
Takashi KOJIMA

Department of Applied Electronics
Interdisciplinary Graduate School of Science and Engineering
Tokyo Institute of Technology

A DOCTORAL DISSERTATION

Directed by : Professor **Shigehisa ARAI**

2-12-1 O-okayama, Meguro-ku, Tokyo, 152-8552, Japan
Research Center for Quantum Effect Electronics
Tokyo Institute of Technology

March 1999

Contents

Chapter 1 Introduction........ **1**

1.1 Introduction........ 1
1.2 Semiconductor Laser for Optical Communication........ 2
1.3 Low-Dimensional Quantum-Well Lasers........ 3
1.3.1 Low-Dimensional Quantum-Well........ 3
1.3.2 Strained Quantum-Wire Lasers........ 5
1.3.3 Fabrication Technique........ 6
1.3.4 Long-Wavelength Quantum-Wire Lasers........ 16
1.4 Objective and Outline of This Thesis........ 19
References........ 23

Chapter 2 Theoretical Characteristics—Requirements to Density and Size Fluctuation of Quantum Wire Structure........ **37**

2.1 Introduction........ 37
2.2 Requirement for Optical Gain........ 38
2.3 Requirement to Optical Confinement Factor and Size Fluctuation........ 47
2.3.1 Threshold Current of Single Quantum-Well Laser........ 47
2.3.2 Threshold Current of Quantum-Wire Laser........ 53
2.4 Conclusion........ 68
References........ 69

Chapter 3 Fabrication of Quantum-Wire Lasers........ **71**

3.1 Introduction........ 71
3.2 Crystal Growth Technique........ 72
3.2.1 Organometallic Vapor Phase Epitaxy........ 72
3.2.2 GaInAsP Compressively-Strained Quantum-Well........ 75
3.3 Measurement of Size Fluctuation of Quantum-Wire Structure........ 81
3.3.1 Measurement of Size Fluctuation of EB Pattern........ 81
3.3.2 Reduction of Size Fluctuation........ 83
3.4 Fabrication Process of Quantum-Wire laser........ 87
3.5 Conclusion........ 96
References........ 97

Chapter 4 Photoluminescence Properties of Quantum-Wire Structures........ **100**

4.1 Introduction........ 100
4.2 Polarization Dependence........ 101
4.3 Temperature Dependence........ 111
4.4 Conclusion........ 113
References........ 114

Chapter 5 Lasing Properties of Quantum-Wire Lasers.................................. **116**

5.1 Introduction.. 116
5.2 I-L Characteristics.. 117
5.3 Cavity Length Dependence... 120
5.4 Temperature Dependence... 123
5.4.1 Threshold Current and Lasing Wavelength................................. 123
5.4.2 Differential Quantum Efficiency.. 126
5.4.3 Internal Quantum Efficiency... 131
5.4 Quantum-Wire DFB Lasers... 142
5.5 Conclusion... 146
References... 148

Chapter 6 Optical Gain Properties of Quantum-Wire Lasers.............................. **151**

6.1 Introduction.. 151
6.2 Measurement of Optical Gain... 152
6.3 Comparison to Theoretical Analysis.. 159
6.3.1 Gain Spectrum... 159
6.3.2 Intraband Relaxation Time.. 161
6.3.3 Differential Gain.. 165
6.4 Conclusion... 170
References... 171

Chapter 7 Approach for Improvement of Temperature Characteristics of Quantum-Wire Lasers.. **173**

7.1 Introduction.. 173
7.2 Approach for Improvement of Temperature Characteristics of Quantum-Wire lasers... 174
7.2.1 Multiple-Stacked Quantum-Wire Laser Using Dry Etching............ 174
7.2.2 Introduction of Al-Containing Materials..................................... 176
7.2.3 High Optical Confinement Structure Laser.................................. 178
7.3 Conclusion... 179
References... 180

Chapter 8 Conclusions.. **181**

Acknowledgments.. **185**

Publication List.. **189**

Chapter 1

Introduction

1.1 Introduction............ 1
1.2 Semiconductor Laser for Optical Communication............ 2
1.3 Low-Dimensional Quantum-Well Lasers............ 3
1.3.1 Low-Dimensional Quantum-Well............ 3
1.3.2 Strained Quantum-Wire Lasers............ 5
1.3.3 Fabrication Technique............ 6
1.3.4 Long Wavelength Quantum-Wire Lasers............ 16
1.4 Objective and Outline of This Thesis............ 19
References............ 23

1.1 Introduction

NOW, in the last few years of the 20th century, technology has made rapid progress, and international cooperation and international standards are necessary for global improvement, not selfish innovation. Under this situation, what should one do in the university? One should have a basis to go out into the world, and a disposition to contribute to sound development. First, one should do one thing thoroughly. Fortunately, a student has a good opportunity to deal with anything positively and optimistically, fearless of failure. Then he will become a professional. If one can understand a narrow but deep field, that is, one can have a root, his views will spread globally. We should become specialists before generalists.

Now the world is changing from a material culture to an information society. Businesses work in networks, as the networks become global. The amount of information in Japan this year is about 200,000 Tbytes, and data communication occupies 30% of telecommunication. A few years later, the amount of information will be twice what it is now and that of data communication will be more than 5 times the present amount. For such a huge amount of information to come and go around the world, an optical communication network system will be indispensable.

In this chapter, the importance of optical fiber communication system for intelligent communication society is discussed in §1.2 and the progresses in the development of quantum-wire and quantum-box lasers are reviewed in §1.3. Finally the purpose and outline of this thesis are given.

1.2 Semiconductor Laser for Optical Communication

The semiconductor laser is a key device for the optical fiber communication system. The semiconductor laser is used as a transmitter in the present optical fiber communication system. First lasing operation of GaAs semiconductor lasers was obtained in 1962[1-1]-[1-4], and continuous wave (CW) operation at room temperature (RT) was achieved in 1970 using GaAs/AlGaAs double heterostructure[1-5]. At the same time, a very low loss, 20dB/km, optical fiber was also fabricated. Since then, the optical fiber communication system made rapid progress. At first, 0.8μm wavelength optical fiber communication system, which is lasing wavelength of GaAs semiconductor laser, was made for practical use, as decreasing the loss of optical fiber, GaInAsP semiconductor laser emitting at 1.3 and 1.55μm was studied because fiber dispersion is minimum at a wavelength of 1.3μm and fiber loss is minimum at 1.55μm. In 1979, an extremely low loss optical fiber was achieved i.e., 0.2dB/km at 1.55μm, which is almost theoretical limit (0.16dB/km)[1-6], and the GaInAsP semiconductor laser emitting 1.3μm[1-7]-[1-9], and 1.55μm[1-10]-[1-13] was also fabricated.

Until now, optical technology have been introduced to trunk-line communication in need of large transmission capacity and/or long transmission distance. Recently this technology will be more familiar due to the use of the access network system. In such a huge and high-grade information society, all kinds of information are digitalized and independent of the original sources (such as voice/sound, image, data, character, etc.). For an intelligent communications network in 2015, a communication capacity of 5Tb/s for the trunk network systems will be necessary to satisfy the demand of 100Mb/s for homes[1-14]. Optical fiber will be utilized for most of the network and a high-performance semiconductor laser will be required as a transmitter. Almost all Japanese companies make many low-cost and practical systems toward the project FTTH (Fiber To The Home). The priority seems to have moved from research and development (R & D) to the pursuit of the ultimately highest performance to R & D for how to use this technology easily. However the present technology is not sufficient and the fundamental study is essential to obtain even higher performance. As universities are academic, it is important to pursue extremely high performance in any study, considering the contribution to the future. Concerning optoelectronic technology, we, companies and universities, should pursue both technological diffusion and technological innovation at the end of the 20th century.

1.3 Low-Dimensional Quantum-Well Lasers

1.3.1 Low-Dimensional Quantum-Well

The semiconductor laser is one of most successful photonic devices benefited by the quantum-size effect, since their operation characteristics have been drastically improved by introducing lattice-matched (LM)[1-15] and strained[1-16]-[1-20] quantum-well (QW) structure, due to developments in epitaxial growth technology to realize high quality QW structures of precisely controlled thickness and compositions. Introducing low-dimensional QW structures, such as quantum-wire (Q-Wire) and quantum-box (Q-Box or Q-Dot) structures, carriers are confined into them stronger than into QW in order to further modified band structure and density of states (DOS) distribution[1-21]. Figure 1.1 shows a schematic diagram of DOS of (a) Q-Wire and (b) Q-Box structures. The DOS distributions of them are sharper than that of QW, step-like function. However it should be noted that these sharp features can be

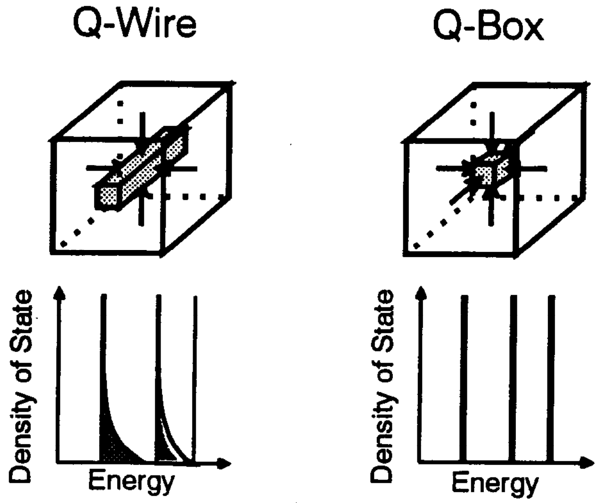

(a) (b)

Fig. 1.1 Density of states of low dimensional quantum-well
(a) Q-Wire and (b) Q-Box structure

inferior because of size fluctuation of Q-Wire or Q-Box structures, leading to inhomogeneous broadening of the energy spectrum[1-22],[1-23]. The broadening effects significantly reduce the impact of the modified DOS on the optical gain and lasing properties, which is discussed in the next chapter.

Due to strong confinement of carriers into low-dimensional QW structures because of a narrower DOS profile, higher optical gain and narrow gain spectrum features are obtained at the same injection current density, although the same intraband relaxation time (0.1ps) is assumed for Q-Wire and Q-Box structures. In other words, a higher differential gain property can be obtained. Figure 1.2 shows, for example, the calculated gain spectra for different quantized dimension in case of LM GaInAs/InP material under the same injection carrier density[1-24]. The size of quantum structures is 10nm for quantum-film (Q-Film), $10 \times 10\text{nm}^2$ for Q-Wire, and

10×10×10nm^3 for Q-Box, respectively. As a result, the threshold current of the Q-Wire laser is lower than that of the Q-Film laser, since the Q-Wire laser can obtain necessary gain for lasing i.e., threshold gain, by a lesser injection carrier density. Furthermore higher efficiency properties of the Q-Wire laser are also obtained due to the smaller size of the active region.

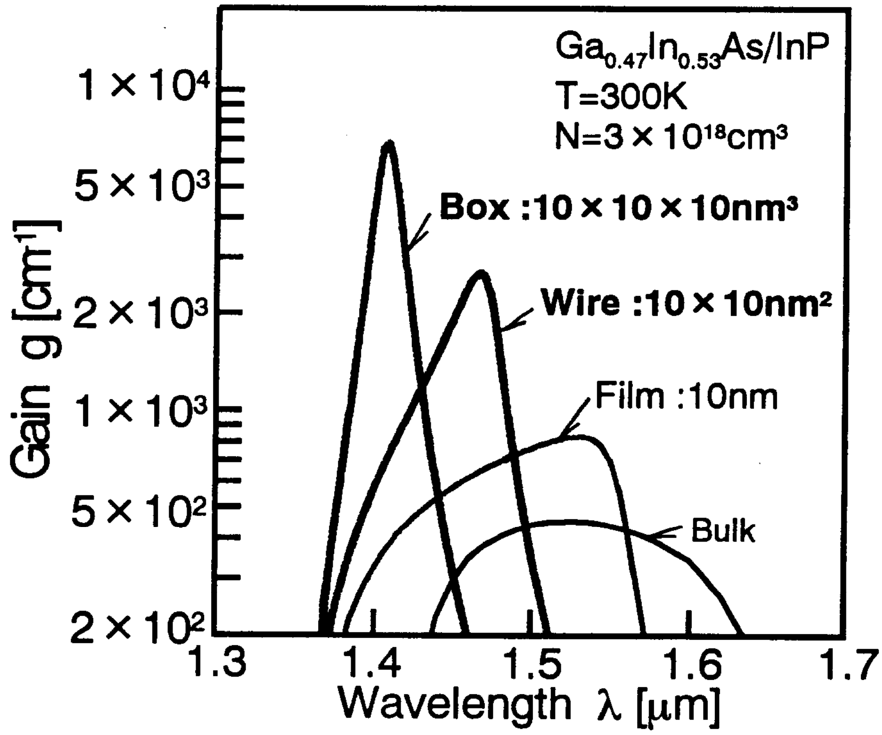

Fig. 1.2 Calculated optical gain spectra of quantum structures.
(After M. Asada et al. [1-24].)

1.3.2 Strained Quantum-Wire Lasers

Semiconductor lasers can be operated at a high level of performance due to the narrow gain spectrum feature by introducing the Q-Wire/Q-Box structures as an active region, such as high characteristic temperature T_0 of threshold current[1-21], higher modulation bandwidth[1-25], and lower threshold current[1-24]-[1-26]. Narrower linewidth operation as well as small wavelength chirping under a direct modulation due to a lower linewidth enhancement factor is also expected[1-27],[1-28]. Further improvements by a combination of strain effect and low-dimensional quantum-well structures are also expected[1-29]-[1-32]. In addition, the wire width of a strained Q-Wire laser is estimated to be 2.5 times wider than that of an unstrained one to obtain a sufficient separation of 30meV between quantized energy levels, and the broadening of energy levels due to wire width fluctuation can be reduced by half that of an unstrained one[1-30].

Because drive current of a laser for a certain required power level is given by the threshold current I_{th} and the differential quantum efficiency η_d, it is very important to design a proper laser cavity. An introduction of a high gain medium leads to a reduction of the threshold and an increase in the efficiency. Figure 1.3 shows calculated relation between them for an almost optimum condition of the volume of the active medium, where n is the number of stacked layers of Q-Wires or Q-Boxes and ρ is the in-plane space filling factor of them[1-33]. As can be seen in Fig.1.3, an introduction of both compressive- and tensile-strained (CS- and TS-) QW structures will lead to much lower threshold current operation as well as high efficiency. Relatively larger size of the Q-Wire and Q-Box can be adopted compared with unstrained one because the effective mass of holes can be reduced[1-30]. However these properties are attributed to the sharp gain spectrum of Q-Wire and Q-Box structures, their size fluctuation affects much[1-22],[1-23], it should be less than 10% to 20%.

1.3.3 Fabrication Technique

Semiconductor Q-Wire and Q-Box structures are very attractive for application to optoelectronic devices because of their inherent advantages of high differential quantum gain under carrier injection and large refractive index variation induced by

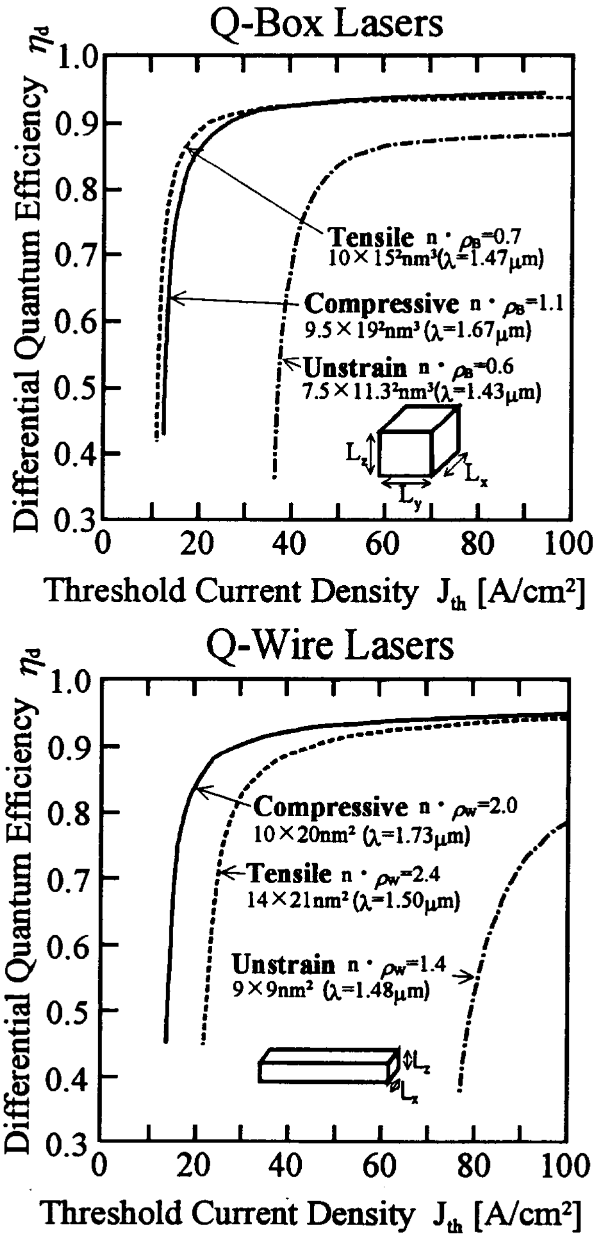

Fig. 1.3 Relation between differential quantum efficiency and threshold current density for the optimal Q-Box and Q-Wire lasers.
(After H. Hirayama, [1-33].)

electric field. As for semiconductor lasers, expected high-performance properties are discussed in the previous section. Concerning other optical devices, reduction of the noise figure in semiconductor laser amplifiers is also expected[1-34]-[1-36]. Large electric-field-induced refractive index variation was theoretically predicted[1-37],[1-38], and was experimentally observed to be approximately 4%[1-39] and 7%[1-40] for GaInAs/InP Q-Wire and Q-Box structures, respectively. The possibility of high-performance operations of intersection waveguide type was theoretically given, while a much larger optical confinement factor of Q-Wire or Q-Boxes is required for these devices[1-41]. Fundamental physics of Q-Wire and Q-Box structures were also analyzed, such as excitons and biexcitons in Q-Wires[1-42], nonlinear effects in Q-Wire structure[1-43], optical absorption of Q-Wires by multiband effective mass theory[1-44], spectral hole burning in Q-Wire lasers[1-45], many-body effect[1-46], cross-sectional shape dependence of band structure[1-47] and electronic states[1-48] in Q-Wire, and so on.

In order to realize high performance operation of low dimensional quantum structures as optical and/or electrical devices, very low-damage fabrication technology of ultra-fine structures with high accuracy is required, and various fabrication methods using various materials have been investigated. The first attempt was done in 1982, using an orthodox method to fabricate GaAs Q-Wire structures– i.e., a growth of QW structure followed by conventional lithography and a burying growth on it[1-49] Similar technology was employed, that is, using electron beam (EB) direct drawing and wet chemical etching for the Q-Wire[1-50] and Q-Box[1-51], or dry etching[1-52],[1-53] followed by embedding growth[1-54]-[1-56] for the GaInAsP/InP system, AlGaAs/GaAs[1-57], InGaAs/GaAs[1-58]-[1-60], and $Si/Si_{1-x}Ge_x$ system[1-61]. On another similar technique, electrochemical anodization[1-62] and impact lithography[1-63] was also attempted.

For GaAs/Al(In)GaAs systems, fractional layer growth on tilted substrate[1-64] or on multi atomic steps on vicinal substrate[1-65]-[1-69] for Q-Wire, and growth of QW structure on patterned substrate[1-70]-[1-74] or on very fine V-grooves for Q-Wire[1-

75]-[1-78] and for Q-Box structures[1-79],[1-80] are used because oxidation of AlGaAs/GaAs is much severer and the surface recombination velocity of this system is much faster than GaInAsP/InP systems[1-81]. Recently, for GaInAsP/InP system, selective growth on a patterned substrate for Q-Wire[1-82],[1-83] and Q-Box structures[1-84],[1-85] or on V-grooves for Q-Wire structures[1-86]-[1-90] or fractional layer growth on vicinal InP substrate for Q-Wire and Q-Box structures[1-91] was also carried out for application to single electron devices or optical devices. Concerning other selective growth methods, the Q-Wires fabricated on grooved side walls[1-92], on cleaved edge[1-93], at giant step edges on vicinal (110) surfaces[1-94], and on (111)B facet by glancing-angle molecular beam epitaxy[1-95] were attempted.

These fabrication techniques of Q-Wire and Q-Box structures mentioned above are much more difficult compared with the case of QW, which is due to developments in epitaxial growth technology to realize high quality QW structures of precisely controlled thickness and compositions. However recently, simple technology to fabricate Q-Wire or Q-Box structures in direct has been investigated only using the growth technique, i.e., these structures can be self-organized by adjusting the growth condition. So a great number of researchers have studied actively. Strain-induced lateral-layer ordering (SI-LO) method of binary superlattices was used for Q-Wire[1-96]-[1-98], and for Q-Box structures[1-99]. Stranski-Krastanow (SK) epitaxial growth mode was done for Q-Wire[1-100] and for Q-Box[1-101]-[1-104], or by strain-induced self-organized (SI-SO) growth on (311) oriented substrate was done for Q-Wire[1-105] and Q-Box structures[1-106]-[1-109]. SI-LO method is similar to SI-SO growth method except for the substrate orientation used. SI-SO growth on patterned substrate for the position control of Q-Box structures[1-110] and SK-mode Q-Box on InP substrate for approaching long-wavelength emission[1-111] were attempt lately. Besides III-V materials, self-organization methods of Q-Wire and Q-Box structures were investigated, such as Si Q-Wire[1-112], GeSi Q-Wire[1-113], Si Q-Box[1-114], ZeSe Q-Box[1-115], and so on. Recently electroluminescence from Si Q-Box structures was observed[1-116].

A fabrication technology to produce high density and uniformly sized low dimensional structures became very important in order to reveal the lateral confinement effect for high performance semiconductor lasers. Here, recent progress in the development of Q-Wire and Q-box lasers is reviewed with an emphasis on the fabrication technology, though the stimulated emission properties of Q-Wire or Q-Box structures were ever reported[1-117]-[1-121]. Several fabrication methods of Q-Wire and Q-Box lasers have been reported up to now as illustrated in Fig. 1.4; (1) a fractional (sub-monoatomic) layer growth on the step edge of a vicinal substrate[1-49], [1-122]-[1-125], (2) a combination of lithography and embedding growth[1-117],[1-126]-[1-128], (3) selective growth on a patterned substrate[1-129], (4) strain-induced lateral-layer ordering (SI-LO) of binary superlattices[1-97], (5) strain-induced self-organized (SI-SO) growth[1-101], and (6) cleaved edge overgrowth[1-130].

GaInAsP/InP long wavelength Q-Wire lasers were fabricated by a combination of lithography, chemical etching, and embedding growth[1-131]-[1-137],[1-138]. A relatively low threshold current density J_{th}=816A/cm^2 under room temperature CW conditions was achieved[1-133],[1-134], but was still twice higher than that of the original quantum-film laser made on the same wafer. Recently, a lower threshold current as well as a higher differential quantum efficiency was observed at low temperatures (J_{th}=34A/cm^2 at T=90K)[1-138]. Five layered $Ga_xIn_{1-x}As$ quantum-wires (15nm wide, 10nm thick) laser, fabricated by SI-LO method, showed a relatively better threshold current (J_{th}=1kA/cm^2 at T=300K, and J_{th}=200A/cm^2 at T=77K)[1-139]. Very clear polarization dependence particularly for quantum-wire structure, i. e. higher gain hence lower threshold current for the electric field of the propagating light parallel to the quantum-wire, was reported[1-139]. In this year, InAs Q-Box lasers fabricated by SI-SO method on InP substrate emitting at 1.9μm[1-140] and 1.4μm[1-141] were achieved at T=77K, which very low threshold current density of 11.4cm^{-1} was obtained with four-cleaved facets[1-140].

As for GaAs/AlGaAs Q-Wire lasers, low threshold current operation due to a narrow striped active region[1-129],[1-142] and a CW operation of Q-Wire lasers

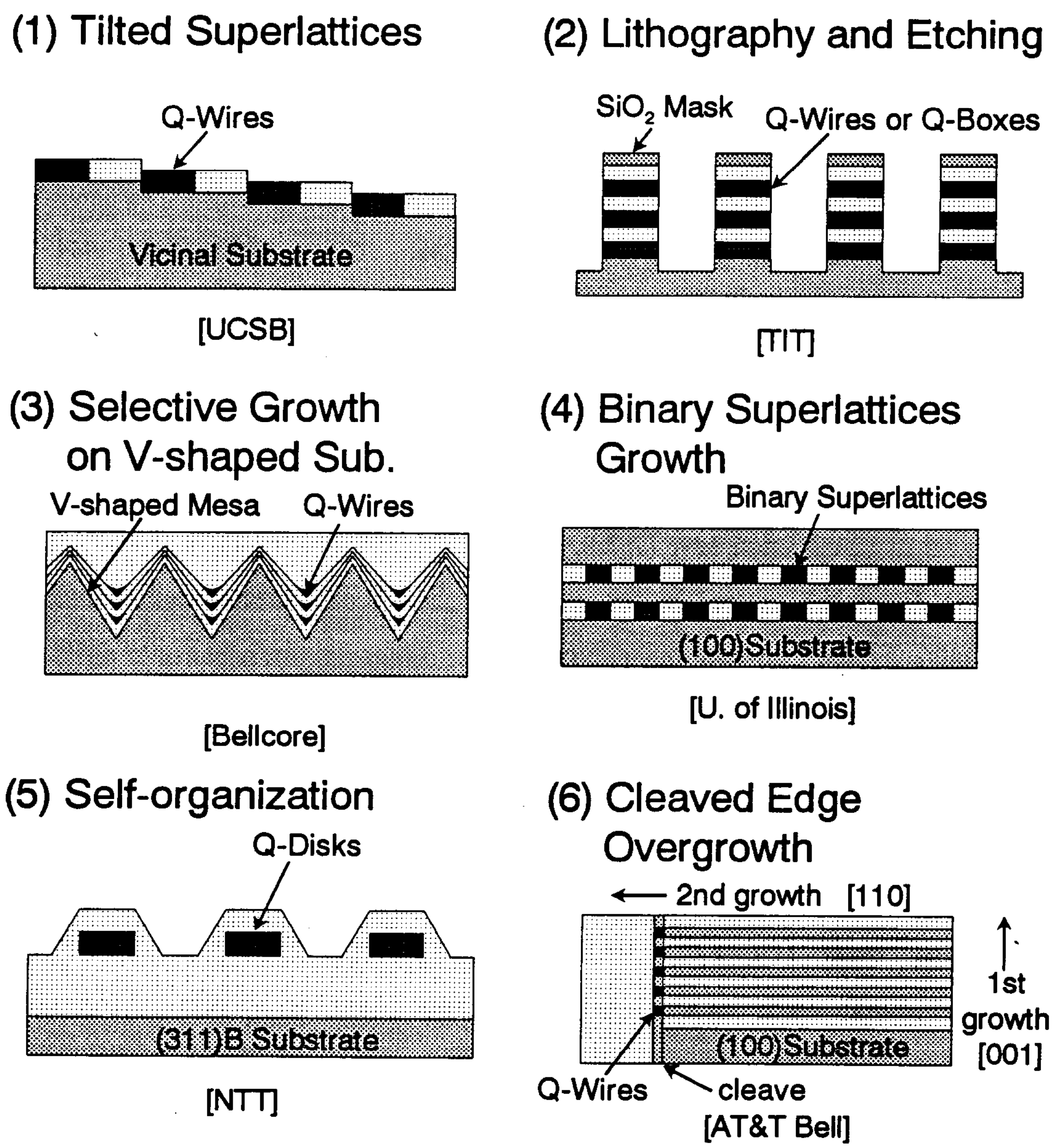

Fig. 1.4 Fabrication methods of Q-Wire and Q-Box Lasers

grown on Si substrate was achieved[1-143]. A combination of GaInAs/GaAs CS-QW material and selective growth on a patterned substrate demonstrated an extremely low threshold current operation(I_{th}=188μA)[1-144] as well as improved direct modulation speed[1-145]. Polarization dependence of threshold current was also observed for TS-GaAsP/AlGaAs Q-Wire laser fabricated on V-grooved substrate.[1-146].

Q-Wire lasers by SI-LO method[1-139],[1-147]-[1-150], and Q-Box lasers by SI-SO method[1-151]-[1-160] have been reported. A room temperature CW operation with low threshold current density (J_{th}=294A/cm^2) was achieved, which was comparable to the best GaInP/GaAs CS-QW lasers[1-149]. GaInAs/AlGaAs Q-Disk lasers grown on (311)B GaAs substrate showed a slightly lower threshold current than that of a double QW laser grown on (100) substrate[1-151]. Even though the diameter of the disk 60nm was not small enough to cause the lateral confinement effect, a sharp PL spectrum (FWHM=18meV at T=300K) was considered to be attributed to some gain enhancement effect since the space filling factor of the disk area was only 6%. High characteristic temperature T_0=330K (from 70K to 135K) was reported for a quantum-box laser with the size of 12nm and size fluctuation of 10%[1-152]. By an increase in the number of stacked Q-Box layers[1-154],[1-155] or by reducing the cavity loss[1-156], threshold current density was fairly reduced. Record low threshold current density at room temperature was achieved to be 62A/cm^2 for GaInAs/AlGaAs 3-layer-vertical-coupled Q-Dot (3VCQD) laser with 4-cleaved facets[1-157]. Low threshold current operation was also demonstrated by an adoption of a vertical cavity surface emitting laser (VCSEL) structure[1-158]. Recently, a room temperature CW operation with low threshold current (I_{th}=5.4mA) and high power (110mW)[1-159], and with low threshold current density (270A/cm^2) emitting at 1.31μm[1-160] were reported. Structure and threshold current of quantum-wire and quantum-box lasers reported up to now are summarized in Table 1.1(1) to (3).

Table 1.1 Summary of the structure and threshold current of Q-Wire and Q-Box lasers

(1) GaInAsP/InP System

Year	Method Growth	QWR/QB Size|Period	Barrier Sub.	Organi- zation	Threshold| Temperature	Wavelength Cavity	Ref.
1987	(2)Wet Etch OMVPE	GaInAsP SQB 100nm |204nm	GaInAsP InP	T.I.T.	EL|77K	1.37μm	[1-117]
1989	(2)EBX+W.E. OMVPE	LM-GaInAs SQWR 30nm |70nm	GaInAsP InP	T.I.T.	39.7kA/cm ^{2}|77K	1.226μm	[1-128]
1992	(2)EBX+W.E. OMVPE	LM-GaInAs 3QWR 10-30nm|70nm	GaInAsP InP	T.I.T.	5.86kA/cm ^{2} |RT-CW	1.522μm L=700μm	[1-161]
	(2)EBX+W.E. OMVPE	CS-GaInAs 5QWR 30-60nm|100nm	GaInAsP InP	T.I.T.	2.9kA/cm ^{2} |RT-CW	1.531μm L=910μm	[1-132]
1993	(2)EBX+W.E. OMVPE	TS-GaInAs SQWR 30-40nm|70nm	GaInAsP InP	T.I.T.	816A/cm ^{2}(16mA) |RT-CW	1.4635μm L=920μm	[1-133] [1-134]
1994	(2)EBX+W.E. OMVPE	TS-GaInAs SQB 30nm |70nm	GaInAsP InP	T.I.T.	7.6kA/cm ^{2}|77K	1.26μm L=2080μm	[1-135]
1995	(2)EB+Dry.E. MOVPE	GaInAs 4QWR 100-140nm	GaInAsP InP	U- Stuttgart	5.12kA/cm ^{2}|RT	1.55μm L=950μm	[1-136]
	(4)SI-LO MBE	GaInAs 5QWR 15nm |30nm	GaInAs InP	U- Illinors	1kA/cm ^{2} |300K 200A/cm ^{2}|77K	1.69μm|77K L=500μm	[1-139]
1996	(2)EBX+W.E. OMVPE	CS-GaInAsP SQWR +SQF 23nm|70nm	GaInAs InP	T.I.T.	10kA/cm ^{2}|RT 43A/cm ^{2} |98K	1.58μm|RT L=860μm	[1-137]
	(2)EBX+D.E. MOVPE	GaInAs 4QB 85nm |235nm	GaInAsP InP	U- Stuttgart	1.1-2.6kA/cm ^{2}|RT	1.533μm	[1-162]
	(2)EBX+W.E. OMVPE	CS-GaInAsP SQB +SQF 22nm|70nm	GaInAs InP	T.I.T.	603A/cm ^{2} |77K-CW	1.4552μm L=1500μm	
1997	(2)EBX+W.E. OMVPE	CS-GaInAsP SQWR +SQF 25nm|70nm	GaInAs InP	T.I.T.	2.4kA/cm ^{2} |RT 34A/cm ^{2} |90K	1.601μm|RT L=1050μm	[1-138]
	(2)EBX+W.E. OMVPE	CS-GaInAsP SQWR +SQF 20nm|50nm	GaInAs InP		2.65kA/cm ^{2}|RT 32A/cm ^{2} |80K	1.60μm|RT L=1000μm	[1-163]
1998	(5)SI-SO MBE	InAs 3QB 50nm	GaInAs InP	A.F.Ioffe	11.4A/cm ^{2} |77K	1.894μm 4-Cleaved	[1-140]
	(5)SI-SO MBE	InAs 7QB 43nm	InP (311)B	NEC	540A/cm ^{2} |77K	1.4μm L=2800μm	[1-141]

(2) GaAs(P)/AlGaAs System

Year	Method Growth	QWR/QB Size|Period	Barrier Sub.	Organi-zation	Threshold| Temperature	Wavelength Cavity	Ref.
1989	(1)Tilted SL MBE	GaAs SQWR 4nm |8nm	AlGaAs GaAs	UCSB	460A/cm²|RT	0.827μm L=1120μm	[1-123]
	(3)V-groove OMCVD	GaAs SQWR 90nm	AlGaAs GaAs	Bellcore	3.5mA|RT	0.84μm L=350μm	[1-129]
1991	(3)V-groove OMCVD	GaAs 3QWR 90nm	AlGaAs GaAs	Bellcore	0.6mA(HR)|RT	0.86μm L=135μm	[1-142]
1994	(3)V-groove MOCVD	GaAs 3QWR 100nm	AlGaAs Si	Nagoya I.T.	9.8mA|RT-Pulse 16mA |RT-CW	0.859μm L=135μm	[1-143]
	(6)T-shaped MBE	GaAs SQWR 7nm	AlGaAs GaAs	AT & T Bell	0.4mA|4.2K-CW	0.786μm L=400μm	[1-164]
1995	(3)V-groove MOCVD	GaAs 4QWR 60nm	AlGaAs GaAs	Chinese A.Sience	0.7A|RT	0.755μm L=200μm	[1-165]
1997	(3)V-groove MOCVD	GaAs 3QWR 40nm |700nm	AlGaAs GaAs	KIST	0.14kA/cm² 143mA|RT	0.825μm L=200μm	[1-166]
1998	(3)V-groove MOVPE	TS-GaAsP 2QWR 80nm	AlGaAs GaAs	U-Toyko	500A/cm² 125mA|RT	0.78μm L=500μm	[1-146]
	(1)Atom.Step MBE	GaAs 5QWR |12nm	AlGaAs (775)B	U-Osaka	1.5kA/cm²|RT	0.761μm L=500μm	[1-124] [1-167]
	(3)V-groove MOCVD	GaAs 3QWR 80nm	AlGaAs GaAs	KIST	40mA|RT-CW	0.8185μm L=200μm	[1-168]

(3) GaInAs/GaAs & GaInP/GaAs System

(Strain-Induced Lateral-Layer Ordering: SI-LO,
Strian-Induced Self-Organization: SI-SO)

Year	Method Growth	QWR/QB Size|Period	Barrier Sub.	Organi- zation	Threshold| Temperature	Wavelength Cavity	Ref.
1993	(3)V-groove MBE	GaInAs 3QWR 100nm	GaAs GaAs	IBM	188μA|RT-CW	0.98μm L=980μm	[1-144] [1-145]
	(4)SI-LO MBE	GaInP 5QWR 5nm |10nm	AlGaInP GaAs	U- Illinois	2.5kA/cm^2|RT	0.702μm L=500μm	[1-147]
	(3)V-groove OMCVD	GaInAs SQWR 70-80nm|250nm	GaAs GaAs	Bellcore	66A/cm^2 |80K 1.9kA/cm^2|RT	0.99μm|RT L=360μm	[1-169]
1994	(4)SI-LO MBE	GaInP 5QWR 5nm |10nm	AlGaInP GaAs	U- Illinois	250A/cm^2|77K 1kA/cm^2 |RT	0.729μm L=600μm	[1-145] [1-148]
	(4)SI-LO MBE	GaInP 6QWR 9nm |18nm	AlGaInP GaAs	U- Sophia	294A/cm^2|RT-CW	0.746μm L=570μm	[1-149]
	(5)SI-SO MBE	GaInAs SQB 12-17nm	GaAs GaAs	T.U- Berlin	120A/cm^2|77K 950A/cm^2|RT	0.94μm L=1000μm	[1-152] [1-170]
	(5)SI-SO MOCVD	GaInAs 2QB 60nm	AlGaAs (311)B	NTT	23mA |RT-CW	0.94μm L=900μm	[1-151] [1-171]
1995	(5)SI-SO ALE	GaInAs SQB 20nm	InGaAs GaAs	Fujitsu	815A/cm^2|80K	0.911μm L=900μm	[1-153]
1996	(5)SI-SO MBE	InAs SQB 7.4nm	GaAs GaAs	T.U- Berlin	80A/cm^2|77K 3kA/cm^2|RT	0.961μm L=2000μm	[1-172] [1-173]
	(5)SI-SO MBE	GaInAs 3QB 20nm	GaAs GaAs	Fujitsu	550mA |RT	1.02μm L=900μm	[1-174]
	(5)SI-SO MBE	GaInAs SQB 42nm	GaAs GaAs	UCSB	525A/cm^2|293K	1.02μm L=800μm	[1-175]
	(5)SI-SO MBE	GaInAs 10QB	GaAs GaAs	A.F. Ioffe	97A/cm^2|300K	1.045μm 4-Cleaved	[1-157] [1-176]
	(5)SI-SO MBE	GaInAs 3VCQD	AlGaAs GaAs	T.U- Berlin	62A/cm^2|300K	0.99μm 4-Cleaved	[1-157] [1-176]
	(5)SI-SO MBE	GaInAs 10QB 28nm	AlGaAs GaAs	NEC	32mA |RT-CW	0.96μm VCSEL	[1-155]
	(5)SI-SO MBE	GaInAs 3QB 20nm	GaAs GaAs	Fujitsu	3.1A/cm^2(HR) |RT-CW	1.105μm L=900μm	[1-154] [1-177]
1997	(5)SI-SO MBE	GaInAs SQB 20nm	GaAs GaAs	U- Michigan	1.67kA/cm^2|RT	1.0μm L=600μm	[1-178]
	(5)SI-SO MOCVD	InAs 5QB 15-18nm	GaAs GaAs	T.U- Berlin	100A/cm^2 |77K 1.3kA/cm^2|RT	1.088μm	[1-179] [1-180]
	(5)SI-SO MBE	GaInAs SQB	GaAs GaAs	AirForce I.Tech.	200μA|RT-CW	1.0μm VCSEL	[1-181]
	(5)SI-SO MBE	GaAlInAs SQB 22nm	GaAs GaAs	U-Texas	235μA|RT-CW	0.95μm VCSEL	[1-182]
	(5)SI-SO MOCVD	InAs SQB 9-12nm	GaInAs GaAs	T.U- Berlin	12.7A/cm^2 |77K 181A/cm^2 |RT	1.088μm L=2000μm	[1-156] [1-183]
1998	(5)SI-SO MBE	GaInAs VCQD	GaAs GaAs	A.F. Ioffe	170μA|RT-CW	1.0μm VCSEL	[1-158]
	(5)SI-SO MBE	InAs SQB	GaAs GaAs	U-Texas	502μA|RT-CW	1.15μm VCSEL	[1-184]
	(4)Atom.Step MOVPE	GaInAs SQWR |70nm	GaAs GaAs	U- Hokkaido	58A/cm^2|77K	0.864μm L=600μm	[1-125]
	(5)SI-SO MBE	InAs 2QB 15nm	GaAs GaAs	Fujitsu	5.4mA(HR) |RT-CW	1.15μm L=300μm	[1-159] [1-185]
	(5)SI-SO MBE	GaInAs 10VCQD 22nm	AlGaAs GaAs	A.F. Ioffe	290A/cm^2 |RT-CW	0.94μm L=1100μm	[1-186]
	(5)SI-SO MBE	InAs SQB 50nm	GaAs GaAs	U-Texas	270A/cm^2(HR) |RT-CW	1.31μm L=2100μm	[1-160]

1.3.4 Long Wavelength Quantum Wire Lasers

For optical fiber communication system, semiconductor lasers emitting at 1.3 and 1.55μm, so-called "long-wavelength," are necessary, because fiber dispersion is minimum at a wavelength of 1.3μm and fiber loss is minimum at 1.55mm. As mentioned in the previous section, various fabrication technologies for low-dimensional quantum structures, i.e. Q-Wire and Q-Box structures have been attempted to realize high-performance semiconductor lasers. In this section, long-wavelength Q-Wire and Q-Box lasers from the last ten years are reviewed with an emphasis on the fabrication technology, and their future prospect is also discussed. Figure 1.5 shows the development of the lasing wavelength of Q-Wire and Q-Box lasers, which are summarized in Table 1.1. Three kinds of methods, i.e. a combination of lithography and embedding growth, strain-induced lateral-layer ordering (SI-LO) of binary superlattices, and strain-induced self-organized (SI-SO) growth were obtained to emit at a wavelength above 1.3μm. In 1987, electroluminescence (EL) (and possibly amplified spontaneous emission) from GaInAsP Q-Box structures fabricated by etching and regrowth was observed at 77K under pulsed conditions[1-117], but lasing was not achieved. This technology is the most direct approach for fabrication of Q-Wire and Q-Box structures, and is easy to control the size, density, and position of them. Especially this method can control the lasing wavelength to design the initial QW and the size of Q-Wire or Q-Box structures. Relatively low threshold current density J_{th}=816A/cm^2 under room temperature CW condition of TS GaInAs Q-Wire laser was achieved[1-133],[1-134], but was still twice higher than that of the original QW laser made on the same wafer. $(GaAs)_m(InAs)_m$ Q-Wire laser, fabricated by SI-LO method, showed relatively better threshold current (J_{th}=1kA/cm^2 at T=300K, and J_{th}=200A/cm^2 at T=77K) with emitting at 1.69μm at T=77K[1-139]. Recently $(GaP)_x/(InAs)_y$ short period superlattices by SI-LO were fabricated on InP and clear polarization dependence of photoluminescence (PL) particular for quantum-wire structure, i.e. higher PL intensity for the electric field of the propagating light parallel to the quantum-wire, was reported, which the PL peak temperatures. Better lasing properties, i.e. a low threshold current and a high differential quantum efficiency of GaInAsP compressively-strained Q-Wire lasers at T<200K, were obtained[1-137],[1-138]. Very low threshold current density, 11.4 cm^{-1} of InAs/InP Q-Dot laser was obtained with four-cleaved facets at T=77K[1-140]. At room temperature, the threshold current density of GaAs-based Q-Box lasers was 405A/cm^2 (cavity length L=5.1mm, stripe width W_S=40μm) with cleaved facets and 270A/cm^2 (L=2.1mm, W_S=100μm) with HR coatings[1-160]. The lines in Fig.1.6 are fitted by least squares; a solid line shows the fitting line at low temperature and a dashed line does the one at room temperature. From this tendency in the development, the threshold current density less than 100A/cm^2 will be expected in 2001, and that of about 10A/cm^2 in 2006 with operation at room temperature.

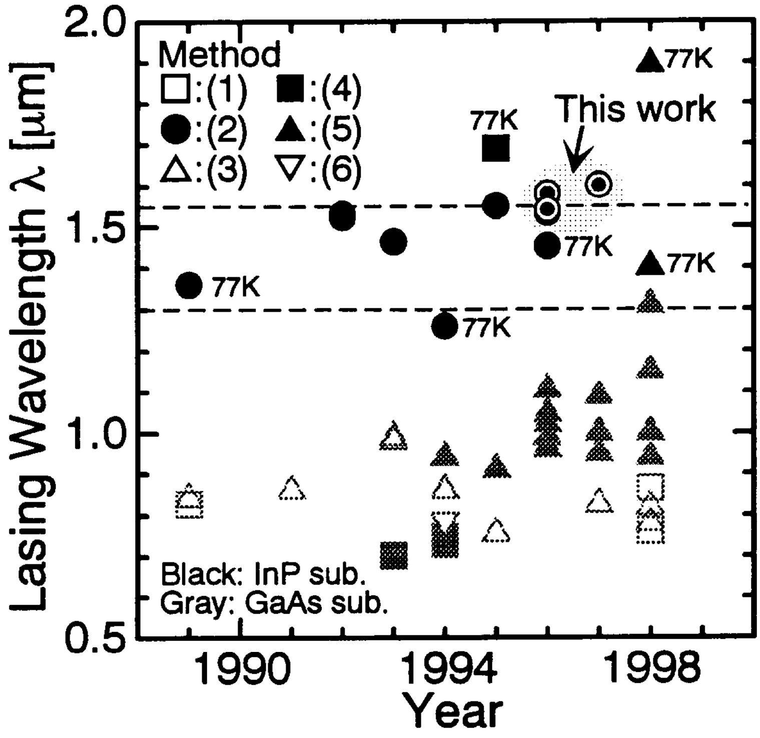

Fig. 1.5 Development in the lasing wavelength of Q-Wire and Q-Box lasers.

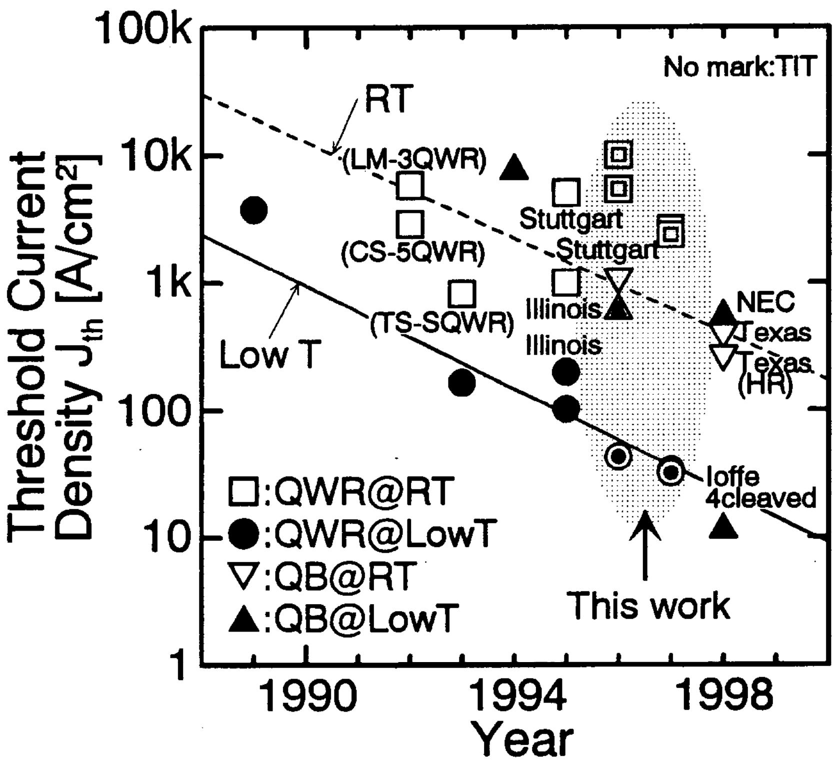

Fig. 1.6 Development in the threshold current density of long-wavelength Q-Wire and Q-Box lasers

1.4 Objective and Outline of This Thesis

Low-dimensional quantum structures, i.e. quantum-wire and quantum-box structures, attempted to realize high-performance semiconductor lasers are reviewed in the previous section. The fabrication technology using electron beam (EB) lithography and etching followed by an embedded growth with organometallic vapor phase epitaxy (OMVPE) is one of most effective methods for 1.55μm-wavelength Q-Wire or Q-Box lasers, which is a better technique for the position and size controllability of Q-Wire and Q-Box structures[1-132]-[1-134]. Furthermore, this fabrication technique is suitable for use in production of distributed feedback (DFB) lasers consisting of a Q-Wire or Q-Box active region[1-162],[1-192],[1-193]. However, due to a low optical confinement factor, ξ, of the active region and poor size uniformity of these Q-Wire structures, an improved performance over quantum-film (Q-Film) lasers fabricated from the initial quantum-well structures was not obtained within the investigated temperature range, T, between 150 K and 300 K[1-132]-[1-134]. Figure 1.7 shows the wire- or box-size dependence of the threshold current density of long-wavelength Q-Wire and Q-Box lasers as mentioned before. The size of Q-Wire was also considered to be insufficient to obtain clear lateral quantum confinement effect in case of GaInAs/GaInAsP/InP Q-Wire lasers[1-132]-[1-134].

The objective of this thesis is to realize high performance operation, i.e. lower threshold and higher efficiency of 1.55μm-wavelength Q-Wire laser compared with Q-Film laser using GaInAsP/InP system. The outline of this thesis is shown in Fig. 1.8.

In Chapter 2, the most effective size of Q-Wire is estimated from the point of material gain and threshold current density, considering the size fluctuation of Q-Wire structure and an optical confinement factor. In Chapter 3, the fabrication process of Q-Wire structure and the regrowth process are explained. A size fluctuation of 50nm periodic wire pattern of GaInAsP/InP structure was investigated. The size fluctuation was reduced taking the proximity effect of electron beam into account. In Chapter 4, the polarization dependence and temperature dependence of photoluminescence properties of the Q-Wire structure was measured and compared with the Q-Film structure fabricated on the same wafer. In Chapter 5, lasing properties, especially temperature dependence of threshold current, differential quantum efficiency, spontaneous emission efficiency, and internal quantum efficiency of Q-Wire lasers are compared with those of Q-Film lasers prepared on the same wafer. Fundamental lasing properties of Q-Wire DFB lasers are also shown in this chapter. In Chapter 6, the gain spectral characteristics of the Q-Wire lasers were measured and were compared with those of Q-Film laser fabricated on the same wafer. It was found that the material gain spectrum of Q-Wire lasers was narrower than that of the Q-Film laser. In Chapter 7, the improvement of temperature characteristics of the Q-Wire lasers are described in order to realize high performance operation of long-wavelength quantum-wire lasers at room temperature. Finally, this thesis is summarized in Chapter 8.

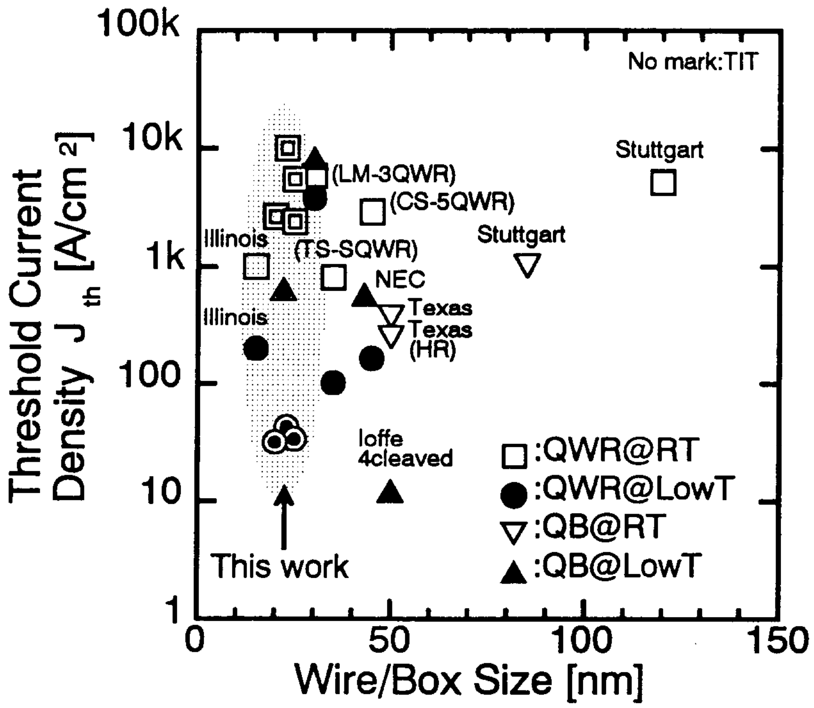

Fig. 1.7 Wire- and Box-size dependence of threshold current density of Q-wire and Q-Box lasers mentioned in §1.3.4.

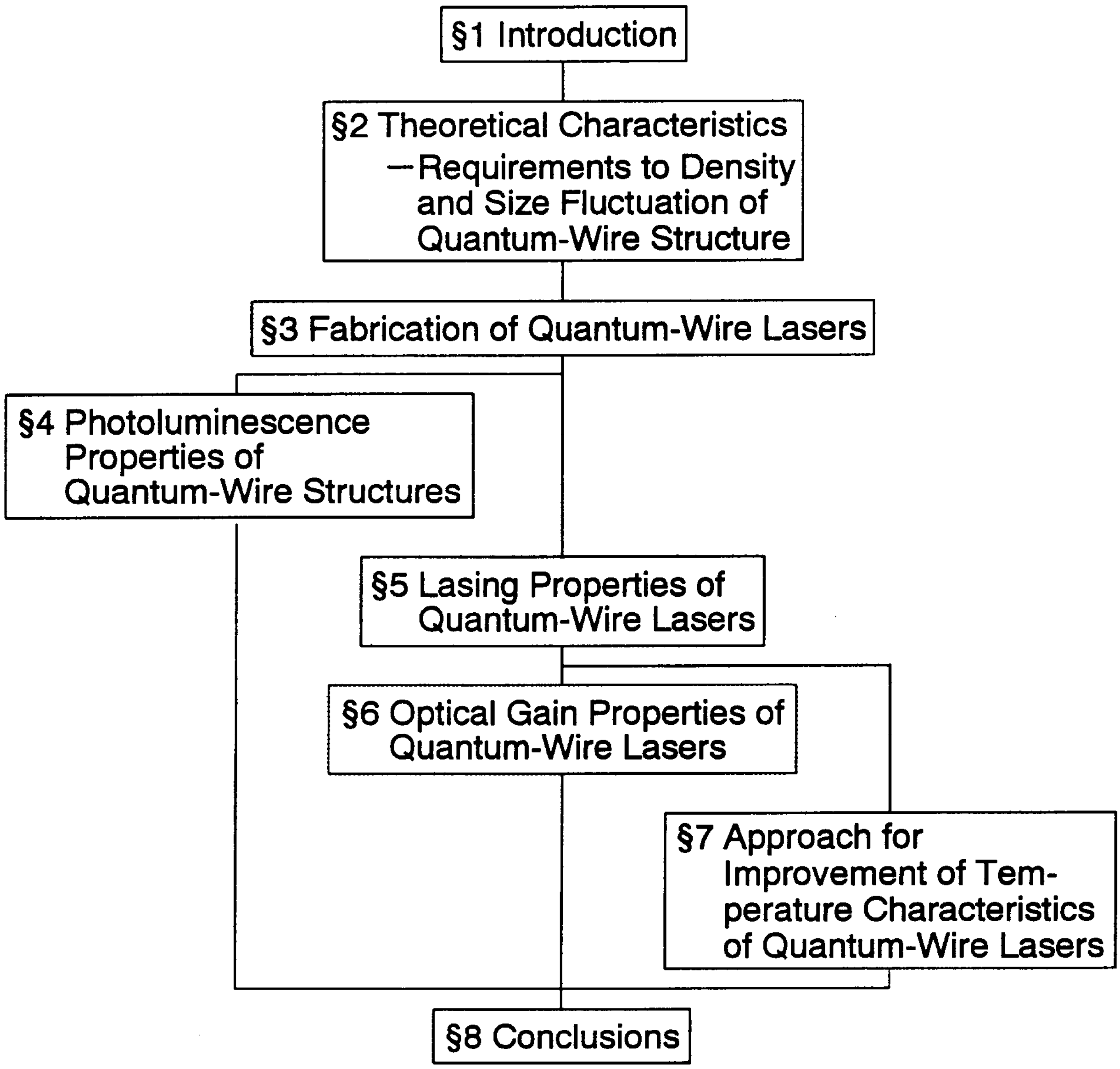

Fig. 1.8 Outline of this thesis.

References

[1-1] M. I. Nathan, W. P. Dumke, G. Burns, F. H. Dill, Jr. and G. Laher, "Stimulated emission of radiation from GaAs p-n junctions," *Appl. Phys. Lett.*, vol.1, no.3, p.62, 1962.

[1-2] N. Holonyak, Jr. and S. F. Bevacqua, "Coherent (visible) light emission from $Ga(As_{1-x}P_x)$ junctions," *Appl. Phys. Lett.*, vol.1, no.4, p.82, 1962.

[1-3] T. M. Quist, R. H. Rediker, R. J. Keyes, W. E. Krag, B. Lax, A. L. McWhorter and H. J. Zeiger, "Semiconductor maser of GaAs," *Appl. Phys. Lett.*, vol.1, no.4, p.91, 1962.

[1-4] R. N. Hall, G. H. Fenner, J. D. Kingsley, T. J. Solltys and R. D. Carlson, "Coherent light emission from GaAs junction," *Phys. Rev. Lett.*, vol.9, no.9, p.366, 1962.

[1-5] I. Hayashi, P. B. Panish, P. W. Foy and S. Sumski, "Junction lasers which operate continuously at room temperature," *Appl. Phys. Lett.*, vol.17, no.3, pp.109-111, 1970.

[1-6] T. Miya, Y. Terunuma, T. Hosaka and T. Miyashita, "An ultimately low-loss single-mode fiber at 1.55μm," *Electron. Lett.*, vol.15, no.7, pp.106-108, Feb. 1979.

[1-7] K. Oe and K. Sugiyama, "GaInAsP/InP double-hetero structure lasers prepared by a new LPE apparatus," *Jpn. J. Appl. Phys.*, vol.15, no.12, pp.740-741, Dec. 1976.

[1-8] T. Yamamoto, K. Sakai, S. Akiba and Y. Suematsu, "Fast pulse behavior of InGaAsP/InP double-hetero structure emitting at 1.27μm," *Electron. Lett.*, vol.13, no.3, pp.142-143, Mar. 1977.

[1-9] Y. Itaya, Y. Suematsu and K. Iga, "Carrier lifetime measurement of GaInAsP/InP double-hetero-structure lasers," *Jpn. J. Appl. Phys.*, vol.16, no.6, pp.1057-1058, Jun. 1977.

[1-10] S. Arai, Y. Suematsu and Y. Itaya, "1.6μm $Ga_{0.47}In_{0.53}As$/InP DH lasers double cladded with InP by LPE technique," *Jpn. J. Appl. Phys.*, vol.18, no.3, pp.709-710, Mar. 1979.

[1-11] S. Akiba, K. Sakai, Y. Matsushima and T. Yamamoto, "Room-temperature c.w. operation of InGaAsP/InP heterostructure lasers emitting at 1.55μm," *Electron. Lett.*, vol.15, no.9, pp.606-607, Sep. 1979.

[1-12] H. Kawaguchi, T. Takahei, Y. Toyoshima, H. Nagai and G. Iwane, "Room-temperature c.w. operation of InP/InGaAsP/InP double heterostructure diode lasers emitting at 1.55μm," *Electron. Lett.*, vol.15, no.10, pp.699-700, Oct. 1979.

[1-13] K. Utaka, K. Kobayashi, K. Kishino and Y. Suematsu, "1.5-1.6μm GaInAsP/InP integrated twin-guide lasers with first-order distributed Bragg reflectors," *Electron. Lett.*, vol.16, no.12, pp.455-456, Jun. 1980.

[1-14] Y. Arakawa, "Technology roadmap for opto-information technology in the 21st century," *IEEE 10th Int. Conf. on Indium Phosphide and Related Materials (IPRM'98)*, TuPL1-1, Tsukuba, p.3-5, May 1998.

[1-15] N. Holonyak, Jr., R. M. Kolbas, R. D. Dupuis and P. D. Dapkus, "Quantum-well heterostructure lasers," *IEEE J. Quantum Electron.*, vol.QE-16, no.2, pp.170-186, Feb. 1980.

[1-16] A. R. Adams, "Band-structure engineering for low-threshold high-efficiency semiconductor lasers," *Electron. Lett.*, vol.22, no.5, pp.249-250, Feb. 1986.

[1-17] E. Yablonobitch and E.O. Kane, "Reduction of lasing threshold current density by the lowering of valence band effective mass," *IEEE J. Lightwave Technol.*, vol.LT-4, no.5, pp.504-506, May 1986.

[1-18] P. J. A. Thijs, L. F. Tiemeijer, P. I. Kindersma, J. J. M. Binsma, and T. Van Dongen, "High-performance 1.5μm wavelength InGaAs-InGaAsP strained quantum well lasers and amplifiers," *IEEE J. Quantum Electron.*, vol.27, no.6, pp.1426-1439, Jun. 1991.

[1-19] P. J. A. Thijs, J. J. M. Binsma, L. F. Tiemeijer and T. van Dongen, "Submilliamp threshold current (0.62mA at 0℃) and high output power (220mW) 1.5μm tensile strained InGaAs single quantum well lasers," *Electron. Lett.*, vol.28, no.9, pp.829-830, Apr. 1992.

[1-20] M. P. C. M. Krijn, G. W. 't Hooft, M. J. B. Boermans, P. J. A. Thijs, T. van Dongen, J. J. M. Binsma, L. F. Tiemeijer and C. J. van der Poel, "Improved performance of compressively as well as tensile strained quantum-well lasers," *Appl. Phys. Lett.*, vol.61, no.15, pp.1772-1774, Oct. 1992.

[1-21] Y. Arakawa and H. Sakaki, "Multidimensional quantum well laser and temperature dependence of its threshold current," *Appl. Phys. Lett.*, vol.40, no.11, pp.939-941, June 1982.

[1-22] K. J. Vahala, "Quantum box fabrication tolerance and size limits in semiconductors and their effect on optical gain," *IEEE J. Quantum Electron.*, vol.24, no.3, pp.523-530, Mar. 1988.

[1-23] H. Zarem, K. Vahala, and A. Yariv, "Gain spectra of quantum wires with inhomogeneous broadening," *IEEE. J. Quantum Electron.*, vol.QE-25, no.4, pp.705-712, Apr. 1989.

[1-24] M. Asada, Y. Miyamoto, and Y. Suematsu, "Gain and the threshold current of three-dimensional quantum-box lasers," *IEEE J. Quantum Electron.*, vol.QE-22, no.9, pp.1915-1921, Sept. 1986.

[1-25] Y. Arakawa, K. Vahara and A. Yariv, "Dynamic and spectral properties of semiconductor lasers with quantum-well and quantum-wire effects," *Surf. Science*, vol.174, pp.155-162, 1986.

[1-26] A. Yariv, "Scaling laws and minimum threshold currents for quantum-confined semiconductor lasers," *Appl. Phys. Lett.*, vol.53, no.12, pp.1033-1035, Sep. 1988.

[1-27] Y. Miyake and M. Asada, "Spectral characteristics of linewidth enhancement factor α of multidimensional quantum wells," *Jpn. J. Appl. Phys.*, vol.28, no.7, pp.1280-1281, July 1989.

[1-28] Y. Arakawa and A. Yariv, "Quantum well lasers-gain, spectra, dynamics," *IEEE J. Quantum Electron.*, vol.QE-22, no.9, pp.1887-1899, Sep. 1986.

[1-29] Y. Arakawa: *IEICE Trans. Fundamental*, Vol.E75-A, No.1, pp.20-27, Jan. 1992.

[1-30] S. Ueno, Y. Miyake, and M. Asada, "Advantage of strained quantum wire lasers," *Jpn. J. Appl. Phys.*, vol.31, pt.1, no.2A, pp.286-287, Feb. 1992.

[1-31] T. Yamauchi, T. Takahashi, J. N. Schulman, and Y. Arakawa, "Theoretical analysis of band structures and lasing characteristics in strained quantum wire lasers," *IEEE J. Quantum Electron.*, vol.29., no.6, pp.2109-2116, Jun. 1993.

[1-32] H. Hirayama and M. Asada, "Reduction of size fluctuation effect in GaInAs/GaInAsP quantum-box lasers using tensile strained active region," *IEEE 14th Int. Semiconductor Laser Conf.*, P4, Hawaii, pp.89-90, Sep. 1994.

[1-33] H. Hirayama, "Fundamental study of quantum-box semiconductor lasers," ***Doctoral Dissertation,*** Graduate School of Science and Engineering, Tokyo Institute of Technology, Tokyo, 1994.

[1-34] Y. Arakawa, K. Vahala and A. Yariv, "Quantum noise and dynamics in quantum well and quantum wire lasers," *Appl. Phys. Lett.*, vol.45, no.9, pp.950-952, Nov. 1984.

[1-35] K. Komori, S. Arai and Y. Suematsu, "Noise in semiconductor laser amplifiers with quantum box structure," *IEEE. Photon. Technol. Lett.*, vol.3, no.1, pp.39-41, Jan. 1991.

[1-36] K. Komori, S. Arai and Y. Suematsu, "Noise study of low-dimensional quantum-well semiconductor laser amplifiers," ***IEEE. J. Quantum Electron.***, vol.28, no.9, pp.1894-1900, Sep. 1992.

[1-37] I. Suemune and L. A. Coldren, "Band-mixing effects and excitenic optical properties in GaAs quantum wire structures – comparison with the quantum wells," ***IEEE J. Quantum Electron.***, vol.24, no. , pp.1778-1790, Aug. 1988.

[1-38] K. G. Ravikumar, T. Aizawa, K. Matsubara, M. Asada and Y. Suematsu, "Analysis of electric field effect in quantum box structure and its application to low-loss intersectional type optical switch," *J. Lightwave Technol.* Vol.9, no.10, Oct. 1991.

[1-39] K. G. Ravikumar, T. Kikugawa, T. Aizawa, S. Arai and Y, Suematsu, "Field-induced refractive index variation spectrum in a GaInAs/InP quantum wire structure," *Appl. Phys. Lett.*, vol.58, no.10, pp.1015-1017, Mar. 1991.

[1-40] T. Aizawa, K. Shimomura, S. Arai and Y. Suematsu, "Observation of field-induced refractive index variation in quantum box structure," *IEEE. Photon. Technol. Lett.*, vol.3, no.10, pp.907-909, Oct. 1991.

[1-41] K. Shimomura, S. Arai and Y. Suematsu, "Operational wavelength range of GaInAs(P)-InP intersectional optical switches using field-induced electrooptic effect in low-dimensional quantum-well structures," ***IEEE. J. Quantum Electron.***, vol.28, no.2, pp.471-478, Feb. 1992.

[1-42] L. Bányai, I. Galbraith, C. Ell and H. Haug, "Excitons and biexcitons in semiconductor quantum wires," *Phys. Rev. B*, vol.36, no.11, pp.6099-6104, Oct. 1987.

[1-43] H. Ando, H. Oohashi and H. Kanbe, "Carrier-induced optical nonlinear effects in semiconductor quantum well wire structure," *J. Appl. Phys.*, vol.70, no.11, pp.7024-7032, Dec. 1991.

[1-44] H. Ando, S. Nojima and H. Kanbe, "Band-edge optical absorption spectra of GaAs quantum wires calculated by multiband effective mass theory," *J. Appl. Phys.*, vol.74, no.10, pp.6383-6390.

[1-45] I. Vurgaftman and J. Singh, "A self-consistent approach to spectral hole burning in quantum wire lasers," *J. Appl. Phys.*, vol.74, no.10, pp.6451-6453, Nov. 1993.

[1-46] M. Bayer, C. Schlier, C. Gréus, A. Forchel, S. Benner and H. Haug, "Many-body effects in the magneto plasma of $In_{0.13}Ga_{0.87}As$/GaAs quantum wires," *Jpn. J. Appl. Phys.*, vol.34, pt.1, no.8B, pp.4408-4410, Aug. 1995.

[1-47] T. Tanaka, T. Yamauchi, J. N. Schulman and Y. Arakawa, "Cross sectional shape dependence of quantum wire band structures and optical matrix elements," *Jpn. J. Appl. Phys.*, vol.32, pt.2, no.11A, pp.L1592-L1595, Nov. 1993.

[1-48] K. Komori and M. Arakawa, "Electronic states in crescent-shaped GaAs coupled quantum wires," *Jpn. J. Appl. Phys.*, vol.36, pt.1, no.3B, pp.1927-1932, Mar. 1997.

[1-49] P. M. Petroff, A. C. Gossard, R. A. Logan, and W. Wiegmann, "Toward quantum well wires: Fabrication and optical properties," *Appl. Phys. Lett.*, vol.41, no.7, pp.635-638, Oct. 1982.

[1-50] E. Inamura, Y. Miyamoto, S. Tamura, T. Takasugi and K. Furuya, "Wet chemical etching for ultrafine periodic structure: rectangular InP corrugations of 70nm pitch and 100nm depth," *Jpn. J. Appl. Phys.*, vol.28, no.10, pp.2193-3196, Oct. 1989.

[1-51] H. Hirayama, K. Matsunaga, M. Asada, T. Kakinuma and M. Kumazawa, "Observation of large quantum size effect "in GaInAs/GaInAsP strained quantum-box structures," *Int. Conf. on Solid State Devices and Materials (SSDM'93)*, LC-14, pp.982-983, Makuhari, Sep. 1993.

[1-52] K. G. Ravikumar, K. Kudo, S. Arai and Y. Suematsu, "Low-damage GaInAs(P)/InP nanometer structure by low-pressure ECR-RIBE," *Jpn. J. Appl. Phys.*, vol.29, no.10, pp.L1744-L1746, Oct. 1990.

[1-53] K. Kudo, Y. Nagashima, M. Tamura, S. Tamura, A. Ubukata and S. Arai, "Fabrication of GaInAs/GaInAsP/InP multi-quantum-wires and –boxes by substrate-potential-controlled electron cyclotron resonance reactive ion beam etching," *Jpn. J. Appl. Phys.*, vol.33, pt2, no.10A, pp.L1382-L1385, Oct. 1994.

[1-54] T. Yamamoto, E. Inamura, Y. Miyamoto and K. Furuya, "OMVPE buried ultrafine periodic structures in GaInAs and InP," *Microelectronic Engineering*, vol.11, pp.93-96, 1990.

[1-55] M. Notomi, M. Naganuma, T. Nishida, T. Tamamura, H. Iwamura, S. Nojima and M. Okamoto, "Clear energy level shift in ultranarrow InGaAs/InP quantum well wires fabricated by reverse mesa chemical etching," *Appl. Phys. Lett.*, vol.58, no.7, pp.720-722, Feb. 1991.

[1-56] T. Nishida, M. Notomi, R. Iga and T. Tamamura, "Quantum wire fabrication by e-beam lithography using high-resolution and high-sensitivity e-beam resist ZEP-520," *Jpn. J. Appl. Phys.*, vol.31, no.7, pp.4508-4514, Dec. 1992.

[1-57] S. Wakabayashi, Y. Toyoda, H. Tougou, T. Narusawa, Y. Nagamune and Y. Arakawa, "Fabrication of AlGaAs/GaAs multi-QWRs with 15nm wire width using two-step etching and MBE regrowth," *Springer Series in Materials Sciences*, vol.31, *Nanostructures and Quantum Effects*, ed. H Sakaki and H. Noge, *(Springer-Verlag Berlin Heidelberg, 1994)* pp.194-196.

[1-58] R. Steffen, F. Faller and A. Forchel, "Low-voltage electron beam lithography on GaAs substrates for quantum wire fabrication," *J. Vac. Sci. Technol. B*, vol.12, no.6, Nov/Dec 1994.

[1-59] K. Moriyasu, S. Osako, N. Mori and C. Hamaguchi, "Effect of quantum confinement and lattice relaxation on electronic states in GaAs/$In_{0.2}Ga_{0.8}As$/GaAs quantum dots," *Jpn. J. Appl. Phys.*, vol.36, pt.1, no.6B, pp.3932-3935, Jun. 1997.

[1-60] K. H. Wang, A. Pecher, E. Höfling and A. Forchel, "Low voltage electron-beam lithography based InGaAs/GaAs quantum dot arrays with 1meV luminescence linewidths," *J. Vac. Sci. Technol. B*, vol.15, no.6, pp.2829-2831, Nov/Dec 1997.

[1-61] Y. S. Tang, C. D. W. Wilkinson, D. W. Smith, T. E. Whall and E. H. C. Parker, "Optical properties of dry-etched Si/$Si_{1-x}Ge_x$ heterostructure wires," *Jpn. J. Appl. Phys.*, vol.33, pt.1, no.4B, pp.2348-2352, Apr. 1994.

[1-62] T. Takizawa, S. Arai and M. Nakahara, "Fabrication of vertical and uniform-size porous InP structure by electrochemical anodization," ***Jpn. J. Appl. Phys.***, vol.33, pt2, no.5A, pp.L643-L645, May 1994.

[1-63] S. Y. Chou, P. R. Krauss, W. Zhang, L. Guo and L. Zhuang, "Sub-10nm impact lithography and applications," ***J. Vac. Sci. Technol. B***, vol.15, no.6, pp.2897-2904, Nov/Dec 1997.

[1-64] M. Tsuchiya, J. M. Gaines, R. H. Yan, R. J. Simes, P. O. Holtz, L. A. Coldren, and P. M. Petroff, "Optical anisotropy in a quantum-well-wire array with two-dimensional quantum confinement," ***Phys. Rev. Lett.***, vol.62, no.4, pp.466-469, Jan. 1989.

[1-65] M. Kitamura, M. Nishioka, J. Oshinowo and Y. Arakawa, "Formation of InGaAs quantum dots on GaAs multi-atomic steps by metalorganic chemical vapor deposition growth," ***Jpn. J. Appl. Phys.***, vol.34, pt.1, no.8B, pp.4376-4379, Aug. 1995.

[1-66] S. Hara, J. Motohisa, T. Fukui and H. Hasegawa, "Quantum well wire fabrication method using self-organized multiatomic steps on vicinal (001) GaAs surfaces by Metalorganic vapor phase epitaxy," ***Jpn. J. Appl. Phys.***, vol.34, pt.1, no.8B, pp.4401-4404, Aug. 1995.

[1-67] M. Higashiwaki, M. Yamamoto, T. Higuchi, S. Shimomura, A. Adachi, Y. Okamoto, N. Sano and S. Hiyamizu, "High-density GaAs/AlAs quantum wires grown on (775)B-oriented GaAs substrates by molecular beam epitaxy," ***Jpn. J. Appl. Phys.***, vol.35, pt.2, no.5B, pp.L606-L608, May 1996.

[1-68] S. Hara, J. Motohisa and T. Fukui, "Formation and characterization of InGaAs strained quantum wires on GaAs multiatomic steps grown by metalorganic vapor phase epitaxy," ***J. Cryst. Growth***, vol.170, pp.579-584, 1997.

[1-69] T. Kato, T. Takeuchi, Y. Inoue, S. Hasegawa, K. Inoue and H. Nakashima, "Stacked GaAs multi-quantum wires grown on vicinal GaAs(110) surfaces by molecular beam epitaxy," ***Appl. Phys. Lett.***, vol.72, no.4, pp.465-467, Jan. 1998.

[1-70] S. Tsukamoto, Y. Nagamune, M. Nishioka and Y. Arakawa, "Fabrication of GaAs arrowhead-shaped quantum wires by metalorganic chemical vapor deposition selective growth," ***Appl. Phys. Lett.***, vol.62, no.1, pp.49-51, Jan. 1993.

[1-71] S. Tsukamoto, Y. Nagamune, M. Nishioka and Y. Arakawa, "Fabrication of GàAs quantum wires (~10nm) by metalorganic chemical vapor selective deposition growth," ***Appl. Phys. Lett.***, vol.62, no.3, pp.355-357, Jul. 1993.

[1-72] I. Matsuyama, M. López, N. Tanaka and T. Ishikawa, "Cathodoluminescence of wirelike GaAs/AlAs quantum well structures grown on substrate patterned with [001] mesa stripes," ***Jpn. J. Appl. Phys.***, vol.33, pt.2, no.5A, pp.L627-L630, May 1994.

[1-73] T. Yamada and Y. Horikoshi, "Comparison of GaAs facet formation on patterned substrate during molecular beam epitaxy and migration enhanced epitaxy," ***Jpn. J. Appl. Phys.***, vol.33, pt2, no.7B, pp.L1027-L1030, Jul. 1994.

[1-74] M. Kawabe, "Selective growth and other applications of hydrogen-assisted molecular beam epitaxy," ***J. Cryst. Growth***, vol.150, pp.370-376, 1995.

[1-75] T. Sogawa, S. Ando and H. Kanbe, "Lateral-size control of trench-buried quantum wires using GaAs/AlAs superlattice layers," ***Jpn. J. Appl. Phys.***, vol.34, pt.1, no.8B, pp.4405-4407, Aug. 1995.

[1-76] N. Hatori, T. Mukaihara, Y. Hayashi, N. Ohnoki, F. Koyama and K. Iga, "Design and fabrication of InGaAs/GaAs quantum wires for vertical-cavity surface emitting lasers," ***Jpn. J. Appl. Phys.***, vol.35, pt.1, no.3, pp.1777-1778, Mar. 1996.

[1-77] B. Dwir, F. Reinhardt, H. Wehman, A. Gustanfsson and E. Kapon, "Quantum wire self-ordered growth seeded by electron-beam lithography," ***Microelectronic Engineering***, vol.35, pp.269-272, 1997.

[1-78] E. Martinet, F. Reinhadt, A. Gustafsson, G. Biasiol and E. Kapon, "Self-ordering and confinement in strained InGaAs/AlGaAs V-groove quantum wires grown by low-pressure organometallic chemical vapor deposition," ***Appl. Phys. Lett.***, vol.72, no.6, pp.701-703, Feb. 1998.

[1-79] S. Ishida, Y. Arakawa and K. Wada, "Seeded self-assembled GaAs quantum dots grown in two-dimensional V grooves by selective metal-organic chemical-vapor deposition," ***Appl. Phys. Lett.***, vol.72, no.7, pp.800-802, Feb. 1998.

[1-80] Y. Sugiyama, Y. Sakuma, S. Muto and N. Yokoyama, "Novel InGaAs/GaAs quantum dots structures formed in tetrahedral-shaped recesses on (111)B GaAs substrate using metalorganic vapor phase epitaxy," ***Jpn. J. Appl. Phys.***, vol.34, pt.1, no.8B, pp.4384-4386, Aug. 1995.

[1-81] E. Yablonovitch, R. Bhat, C. E. Zah, T. J. Gmitter and M. A. Koza, "Nearly ideal InP/$In_{0.53}Ga_{0.47}As$ heterojunction regrowth on chemically prepared $In_{0.53}Ga_{0.47}As$ surfaces," ***Appl. Phys. Lett.***, vol.60, no.3, pp.371-373, Jan. 1992.

[1-82] H. Fujikura, M. Kubo and H. Hasegawa, "Excitation power dependent photoluminescence behavior in etched quantum wires having Silicon interlayer-based edge passivation and its interpretation," ***Jpn. J. Appl. Phys.***, vol.36, pt.1, no.3B, pp.1937-1943, Mar. 1997.

[1-83] M. Araki, Y. Hanada, H. Fujikura and H. Hasegawa, "Fabrication of InGaAs quantum wires and dots by selective molecular beam epitaxy growth on various mesa-patterned (001)InP substrates," ***Jpn. J. Appl. Phys.***, vol.36, pt.1, no.3B, pp.1763-1769, Mar. 1997.

[1-84] K. Kumakura, K. Nakakoshi, J. Motohisa, T. Fukui and H. Hasegawa, "Novel formation method of quantum dot structures by self-limited selective area metalorganic vapor epitaxy," ***Jpn. J. Appl. Phys.***, vol.34, pt.1, no.8B, pp.4387-4389, Aug. 1995.

[1-85] H. Fujikura, M. Araki, Y. Hanada, M. Kihara and H. Hasegawa, "Formation of two-dimensional arrays of InP-based InGaAs quantum dots on patterned substrates by selective molecular beam epitaxy," ***Jpn. J. Appl. Phys.***, vol.36, pt.1, no.6B, pp.4092-4096, Jun. 1997.

[1-86] J. Wang, D. A. Thompson, B. J. Robinson and J. G. Simmons, "Composition variation of InGaAsP grown on (111)B faceted V-groove InP substrates by gas source molecular beam epitaxy," ***IEEE 8th Int. Conf. on Indium Phosphide and Related Materials (IPRM'96)***, WP-C11, Schwäbisch Gmünd, pp.51-514, Apr. 1996.

[1-87] M. Kappelt, M. Grundmann, A. Krost, V. Türck and D. Bimberg, "InGaAs quantum wires grown on by low pressure metalorganic chemical vapor deposition on InP V-grooves," ***Appl. Phys. Lett.***, vol.68, no.25, pp.3596-3598, Jun. 1996.

[1-88] P. Bönsch, D. Wüllner, T. Schrimpf, H. –H. Wehmann and A. Schlachetzki, "Growth of InGaAs/InP quantum wires on patterned substrates," ***Int. Conf. on EW MOVPE VII***, C1, Berlin, Jun. 1997.

[1-89] M. Kappelt, V. Türck, O. Stier, D. Bimberg, H. Cerva, D. Stenkamp, P. Veit, T. Hempel and J. Christen, "Properties of ternary In(Al,Ga)As layers grown in InP V-grooves by MOCVD for the fabrication of quantum wire structures", ***Int. Conf. on EW MOVPE VII***, E5, Berlin, Jun. 1997.

[1-90] M. Geiger, F. Adler, U. A. Griesinger, H. Schweizer and F. Scholz, "GaInAsP/InP quantum wires grown by metalorganic vapor phase epitaxy on V-grooved InP substrates," ***Microelectronics Journal***, vol.28, pp.903-908, 1997.

[1-91] C. A. C. Mendonca E. Laureto, M. J. S. P. Brasil, M. A. Cotta, M. M. G. Carvalho and E. A. Meneses, "On the optical properties of InAs/InP systems: The role of two-dimensional structures and three-dimensional islands," ***Appl. Phys. Lett.***, vol.72, no.9, pp.1015-1017, Feb. 1998.

[1-92] K. Komori, A. Hamano, S. Arai, Y. Miyamoto and Y. Suematsu, "Fabrication of GaInAs/InP quantum wires by organometallic-vapor-phase-epitaxial (OMVPE) selective growth on grooved side walls of ultrafine multilayers," ***Jpn. J. Appl. Phys.***, vol.31, pt.2, no.5A, pp.L535-538, May 1992.

[1-93] W. Wegscheider, L. N. Pfeiffer, A. Pinczuk, K. W. West, M. M. Dignam, R. Hull and R. E. Leibenguth, "GaAs/AlGaAs quantum wire lasers fabricated by cleaved edge overgrowth," ***J. Cryst. Growth***, vol.150, pp.285-292, 1995.

[1-94] M. Takeuchi, K. Shiba, K. Sato, H. K. Huang, K. Inoue and H. Nakashima, "Formation and characterization of GaAs quantum wires at giant step edges on vicinal (110) GaAs surfaces," ***Jpn. J. Appl. Phys.***, vol.34, pt.1, no.8B, pp.4411-4413, Aug. 1995.

[1-95] N. Tomita, M. Tanaka, T. Saeki, S. Shimomura, S. Hiyamizu, K. Fujita, T. Watanabe, T. Higuchi, N. Sano and A. Adachi, "Improved chathodluminescence properties of GaAs/$Al_{0.3}Ga_{0.7}As$ tilted T-shaped quantum wires fabricated on (111)B facet by glancing-angle molecular beam epitaxy," ***J. Vac. Sci. Technol. B***, vol.14, no.6, pp.3550-3554, Nov/Dec 1996.

[1-96] K. C. Hsieh, J. N. Baillargeon and K. Y. Cheng, "Compositional modulation and long-range ordering in GaP/InP short-period superlattices grown by gas source molecular beam epitaxy," ***Appl. Phys. Lett.***, vol.57, no.19, pp.2244-2246, Nov. 1990.

[1-97] K. Y. Cheng, K. C. Hsieh and J. N. Baillargeon, "Formation of lateral quantum wells in vertical short-period superlattices by strain-induced lateral-layer ordering process," ***Appl. Phys. Lett.***, vol.60, no.23, pp.2892-2894, Jun. 1992.

[1-98] Y. Tang, D. H. Rich, A. M. Moy and K. Y. Cheng "An optical method for studying carrier diffusion in strained $(InP)_2/(GaP)_2$ quantum wires," ***Appl. Phys. Lett.***, vol.72, no.1, pp.55-57, Jan. 1998.

[1-99] S. J. Kim, H. Asahi, K. Asami, M. Takemoto, M. Fudeta and S. Gonda, "Vertical quantum confinement effect on optical properties of strain-induced quantum dots self-formed in GaP/InP short-period superlattices," ***Jpn. J. Appl. Phys.***, vol.37, pt.1, no.3B, pp.1540-1547, Mar. 1998.

[1-100] N. N. Ledentsov, "Self-organized quantum wires and dots: New challenge for device applications," ***Int. Conf. on EW MOVPE VII***, E0, Berlin, Jun. 1997.

[1-101] D. Leonard, M. Krisnamurthy, C. M. Reaves, S. P. Denbaas and P. M. Petroff, "Direct formation of quantum-sized dots from uniform coherent islands of InGaAs on GaAs surfaces," ***Appl. Phys. Lett.***, vol.63, no.23, pp.3203-3205, Dec. 1993.

[1-102] M. Kaneko, M. Shimoda, Y. Okada and M. Kawabe, "A molecular beam epitaxy approach to quantum dot arrays," ***Jpn. J. Appl. Phys.***, vol.34, pt.1, no.8B, pp.4390-4391, Aug. 1995.

[1-103] N. N. Ledentsov, J. Böhrer, D. Bimberg, I. V. Kochnev, M. V. Maximov, P. S. Kop'ev, Zh. I. Alferov, A. O. Kosogov, S. S. Ruvimov, P. Werner and U. Gösele, "Formation of coherent super dots using metal-organic chemical vapor deposition," ***Appl. Phys. Lett.***, vol.69, no.8, pp.1095-1097, Aug. 1996.

[1-104] F. Heinrichsdoff, A. Krost, N. Kirstaedter, M.-H. Mao, M. Grundmann, D. Bimberg, A.O. Kosogov and P. Werner, "InAs/GaAs quantum dots grown by metalorganic chemical vapor deposition," ***Jpn. J. Appl. Phys.***, nol.36, pt.1, no.6B, pp.4129-4133, Jun. 1997.

[1-105] R. Nötzel, M. Notomi, H. Kamada T. Furuta, T. Yanagawa and K. H. Ploog, "Room temperature performance of (311) GaAs quantum-wire structures," ***Jpn. J. Appl. Phys.***, vol.33, pt.1, no.1S, pp.900-904, Jan. 1994.

[1-106] R. Nötzel J. Temmyo and T. Tamamura, "Self-organization of boxlike microstructures on GaAs (311)B surfaces by metalorganic vapor-phase epitaxy," ***Jpn. J. Appl. Phys.***, vol.33, pt2, no.3A, pp.L275-L278, Mar. 1994.

[1-107] R. Nötzel, J. Temmyo, H. Kamada, T. Furuta and T. Tamamura, "Strong photoluminescence emission at room temperature of strained InGaAs quantum disks (200-30 nm diameter) self-organized on GaAs (311)B substrates," ***Appl. Phys. Lett.***, vol.65, no.4, pp.457-459, Jul. 1994.

[1-108] L. S. Freire, L. A. Cury, F. M. Matinaga, E. C. Valadares, M. V. B. Moreira, A. G. De Oliveira and A. R. Alves, "Quasi periodic microfacets on the surface of AlGaAs/GaAs quantum well structures grown by molecular beam epitaxy on (311)A high-index substrates," ***J. Vac. Sci. Technol. B***, vol.14, no.6, pp.3555-3558, Nov/Dec 1996.

[1-109] J. Temmyo, R. Nötzel and T. Tamamura, "Semiconductor nanostructures formed by the turning instability," ***Appl. Phys. Lett.***, vol.71, no.8, pp.1086-1087, Aug. 1997.

[1-110] E. Kuramochi, J. Temmyo, H. Kamada and T. Tamamura, "Perfect spatial ordering of self-organized InGaAs/AlGaAs quantum disks on GaAs (311)B substrate with Silicon-Nitride dot array," ***Jpn. J. Appl. Phys.***, vol.37, pt.1, no.3B, pp.1559-1564, Mar. 1998.

[1-111] V. M. Ustinov, A. E. Zhukov, A. F. Tsatsul'nikov, A. Yu. Egorov, A. R. Kovsh, M. V. Maximov, A. A. Suvorova, N. A. Bert and P. S. Kop'ez, "Arrays of strained InAs quantum dots in an (In Ga)As matrix, grown on InP substrates by molecular-beam epitaxy," ***Semiconductors***, vol.31, no.10, pp.1080-1083, Oct. 1997.

[1-112] C. Y. Yeh, S. B. Zhang and A. Zunger, "Pressure dependence of the band gaps in Si quantum wires," ***Appl. Phys. Lett.***, vol.64, no.26, pp.3545-3547, Jun. 1994.

1-113] C. Deng, T. W. Sigmon, J. C. Wu, M. N. Wybourne and J. Rack, "Formation and characterization of ultrasmall dimension GeSi wire structure by using pulsed laser-induced epitaxy," ***Appl. Phys. Lett.***, vol.68, no.26, pp.3734-3736, Jun. 1996.

[1-114] M. Watanabe, F. Iizuka and M. Asada, "Visible light emission from nanocrystalline Silicon embedded in CaF_2 layers on Si(111)," ***IEICE Trans. Electron.***, vol.E79-C, no.11, pp.1562-1567, Nov. 1996.

[1-115] S. B. Yin, L. Chen and W. F. Hsieh, "Fabrication and Raman analysis of ZnSe quantum dots in glass matrix thin films by pulsed laser evaporation," ***Jpn. J. Appl. Phys.***, vol.37, pt.1, no.7A, pp.4154-4157, Jul. 1998.

[1-116] M. Watanabe, T. Matsunuma, T. Maruyama and M. Asada, "Electroluminescence from Silicon nanoparticles embedded in CaF2 in Si(111)," ***Phantoms Strategic Domain Meetings (PHASDOM'97)***, D2.23c, Aachen, p.102, Mar. 1997.

[1-117] Y. Miyamoto, M. Cao, Y. Shingai, K. Furuya, Y. Suematsu, K. G. Ravikumar, and S. Arai, "Light emission from quantum-box structure by current injection," ***Jpn. J. Appl. Phys.***, vol.26, no.4, pp.L225-L227, Apr. 1987.

[1-118] J. P. Leburton, "Intersubband stimulated emission and opticl gain by "phonon pumping" in quantum wires," ***J. Appl. Phys.***, vol.74, no.2, pp.1417-1420, Jul. 1993.

[1-119] P. D. Wang, Y. P. Song, C. M. Sotomayor Torres, M. C. Holland, D. J. Lockwood, P. Hawrylak and J. J. Palacios, P. C. M. Christianen, J. C. Maan and J. A. A. J. Perenboom, "Optical emission and Raman scattering in modulation-doped GaAs-AlGaAs quantum wires and dots," ***Superlattices and Microstructures***, vol.15, no.1, pp.23-27, 1994.

[1-120] A. Orth, J. P. Reithmaier, A. Forchel, R. Nötzel and K. Ploog, "Room-temperature stimulated emission of optically pumped GaAs/AlAs quantum wires grown on (311)A-oriented substrates," ***Appl. Phys. Lett.***, vol.64, no.25, pp.3443-3445, Jun. 1994.

[1-121] L. Samuelson, N. Carlsson, P. Castrillo, A. Gustafsson, D. Hessman, J. Lindahl, L. Montelius, A. Petersson, M. E. Pistol and W. Seifert, "Nano-optical studies of individual nanostructures," ***Jpn. J. Appl. Phys.***, vol.34, pt.1, no.8B, pp.4392-4397, Aug. 1995.

[1-122] P. M. Petroff, A. C. Gossard, and W. Wiegmann, "Structure of AlAs-GaAs interfaces grown on (100) vicinal surfaces by molecular beam epitaxy," ***Appl. Phys. Lett.***, vol.45, no.6, pp.620-622, Sep. 1984.

[1-123] M. Tsuchiya, P. M. Petroff and L. A. Coldren, "Use of tilted-superlattices for quantum-well-wire lasers," ***IEEE Trans. Electron Devices***, vol.36, no.11, pp.2612-2613, Nov. 1989.

[1-124] M. Higashiwaki, Y. Ohno, Y. Okamoto, S. Shimomura and S. Hiyamizu, "High-density GaAs/$(GaAs)_4(AlAs)_2$ QWR lasers on (775)B GaAs substrates grown by MBE," ***Nat. Conv. Res. of Japan Soc. Appl. Phys.***, 30a-PC-16, Hachioji, p.1393, Mar. 1998.

[1-125] S. Hara, J. Motohisa and T. Fukui, "Self-organized InGaAs quantum wire lasers on GaAs multi-atomic steps," ***Electron. Lett.***, vol.34, no.9, pp.894-895, Apr. 1998.

[1-126] P. Dasté, Y. Miyake, M. Cao, Y. Miyamoto, S. Arai, Y. Suematsu and K. Furuya, "Fabrication technique for GaInAsP/InP quantum wire structure by LP-MOVPE," ***J. Cryst. Growth***, vol.93, pp.365-369, 1988.

[1-127] D. Gershoni, H. Temkin, G. J. Dolan, J. Dunsmuir, S. N. G. Chu, and M. B. Panish, "Effects of two-dimensional confinement on the optical properties of InGaAs/InP quantum wire structures," ***Appl. Phys. Lett.***, vol.53, no.11, pp.995-997, Sep. 1988.

[1-128] M. Cao, Y. Miyake, S. Tamura, H. Hirayama, S. Arai, Y. Suematsu and Y. Miyamoto, "Lasing action in GaInAs/GaInAsP quantum-wire structure," ***Trans. IEICE***, vol.E73, no.1, pp.63-70, Jan. 1990.

[1-129] E. Kapon, S. Simhony, R. Bhat, and D. M. Hwang, "Single quantum wire semiconductor lasers," ***Appl. Phys. Lett.***, vol.55, no.25, pp.2715-2717, Dec. 1989.

[1-130] W. Wegscheider, L. N. Pfeiffer, A. Pinczuk, K. W. West, M. M. Dignam, R. Hull and R. E. Leibenguth, "GaAs/AlGaAs quantum wire lasers fabricated by cleaved edge overgrowth," ***J. Cryst. Growth***, vol.150, pp.285-292, 1995.

[1-131] Y. Miyake, H. Hirayama, S. Arai, Y. Miyamoto and Y. Suematsu, "Room temperature operation of GaInAs-GaInAsP-InP SCH multiquantum-film laser with narrow wire-like active region," ***IEEE. Photon. Technol. Lett.***, vol.3, no.3, pp.191-192, Mar. 1991.

[1-132] K. Kudo, Y. Miyake, H. Hirayama, S. Tamura, S. Arai and Y. Suematsu, "Room temperature CW operation of $Ga_{0.3}In_{0.7}As$/GaInAsP/InP strained MQW lasers with wire active region," ***IEEE. Photon. Technol. Lett.***, vol.4, no.10, pp.1089-1092, Oct. 1992.

[1-133] K. Kudo, Y. Nagashima, S. Tamura, S. Arai, Y. Huang and Y. Suematsu, "$Ga_{0.66}In_{0.34}As$/GaInAsP/InP tensile-strained single-quantum-well lasers with 70-nm period wire active region," ***IEEE. Photon. Technol. Lett.***, vol.5, no.8, pp.864-867, Aug. 1993.

[1-134] K. C. Shin, S. Arai, Y. Nagashima, K. Kudo, and S. Tamura, "Temperature dependences of $Ga_{0.66}In_{0.34}As$ /InP tensile-strained quasi-quantum-wire laser fabricated by wet chemical etching and 2-step OMVPE growth," ***IEEE. Photon. Technol. Lett.***, vol.7, no.4, pp.345-347, Apr. 1995.

[1-135] H. Hirayama, K. Matsunaga, M. Asada, and Y. Suematsu, "Lasing action of $Ga_{0.67}In_{0.33}As$/GaInAsP/InP tensile-strained quantum-box laser," ***Electron. Lett.***, vol.30, no.2, pp.142-143, Jan. 1994.

[1-136] U. A. Griesinger, H. Schweizer, V. Härle, F. Barth, B. Höhing, B. Klepser, and F. Scholz "Dry-Etched Wire Distributed Feedback Laser," ***IEEE Photon. Technol. Lett.***, vol.7, no.9, pp.953-955, Sep. 1995.

[1-137] T. Kojima, M. Tamura, K. C. Shin, S. Tamura and S. Arai, "Temperature dependences of GaInAsP/InP compressively-strained quantum-wire lasers fabricated by EB-lithography and 2-step OMVPE growth," ***IEEE 8th Int. Conf. on Indium Phosphide and Related Materials (IPRM'96)***, ThA1-5, Schwäbisch Gmünd, pp.731-734, Apr. 1996.

[1-138] T. Kojima, M. Tamura, H. Nakaya, S. Tanaka, S. Tamura and S. Arai, "GaInAsP/InP compressively strained quantum-wire lasers fabricated by electron beam lithography and 2-step organometallic vapor phase epitaxy," ***Jpn. J. Appl. Phys.***, vol.37, pt.1, no.9A, pp.4792-4800, Sep. 1998.

[1-139] S. T. Chou, K. Y. Cheng, L. J. Chou and K. C. Hsieh, "$Ga_xIn_{1-x}As$ multiple-quantum-wire lasers grown by the strain-induced lateral-layer ordering process," ***Appl. Phys. Lett.***, vol.66, no.17, pp.2220-2222, Apr. 1995.

[1-140] V. M. Ustinov, A. E. Zhukov, A. Yu. Egorov, A. R. Kovsh, S. V. Zaitsev, N. Yu. Gordeev, V. I. Kopchatov, N. N. Lendentsov, A. F. Tsatsul'nikov, B. V. Volovik, P. S. Kop'ez, Z. I. Alferov, S. S. Ruvimov, Z. Liliental-Weber and D. Bimberg, "Low threshold quantum dot injection laser emitting at 1.9μm," ***Electron. Lett.***, vol.34, no.7, pp.670-672, April, 1998.

[1-141] K. Nishi, M. Yamada, T. Anan, A. Gomyo and S. Sugou, "Long-wavelength lasing from InAs self-assembled quantum dots on (311)B InP," ***Appl. Phys. Lett.***, vol.73, no.4, pp.526-528, Jul. 1998.

[1-142] S. Shimhony, E. Kapon, E. Colas, D. M. Hwang, N. G. Stoffel, and P. Worland, "Vertically stacked multiple-quantum-wire semiconductor diode lasers," ***Appl. Phys. Lett.***, vol.59, no.28, pp.2225-2227, Oct. 1991.

[1-143] Y. Hasegawa, T. Egawa, T. Jimbo and M. Umeno, "Vertically-stacked GaAs quantum wires grown on Si substrates by metalorganic chemical vapor deposition," ***J. Cryst. Growth***, vol.145, pp.728-733, 1994.

[1-144] S. Tiwari, G. D. Pettit, K. R. Milkove, F. Legoues, R. J. Davis and J. M. Woodall, "High efficiency and low threshold current strained V-groove quantum-wire lasers," ***Appl. Phys. Lett.***, vol.64, no.26, pp.3536-3538, Jun. 1994.

[1-145] S. Tiwari and J. M. Woodall, "Experimental comparison of strained quantum-wire and quantum-well laser characteristics," ***Appl. Phys. Lett.***, vol.64, no.17, pp.2211-2213, Apr. 1994.

[1-146] M. Ishikawa, W. Pan, Y. Kaneko, H. Yaguchi, K. Onabe, R. Ito and Y. Shiraki, "Polarization characteristics of crescent-shaped tensile-strained GaAsP/AlGaAs quantum-wire-like lasers," ***Jpn. J. Appl. Phys.***, vol.37, pt.1, no.3B, pp.1556-1558, Mar. 1998.

[1-147] E. M. Stellini, K. Y. Cheng, P. J. Pearah, A. C. Chen, A. M. Moy and K. C. Hsieh, "AlGaInP multiple-quantum-wire lasers grown by gas source molecular beam epitaxy," ***Appl. Phys. Lett.***, vol.62, no.5, pp.458-460, Feb. 1993.

[1-148] P. J. Pearah, E. M. Stellini, A. C. Chen, A. M. Moy, K. C. Hsieh and K. Y. Cheng, "Strained $Ga_xIn_{1-x}P$ multiple quantum wire light emitting diodes: A luminescence polarization study," ***Appl. Phys. Lett.***, vol.62, no.7, pp.729-731, Feb. 1993.

[1-149] J. Yoshida, K. Kishino, A. Kikuchi and I. Nomura, "Continuous-wave (CW) operation of GaInP-AlGaInP visible compressively strained multiple quantum-wire (CS-MQWR) lasers," ***IEEE J. Selected Topics in Quantum Electron.***, vol.1, no.2, pp.173-182, Jun. 1995.

[1-150] P. J. Pearah, A. C. Chen, A. M. Moy, K. C. Hsieh and K. Y. Cheng, "AlGaInP multiple quantum wire heterostructure lasers prepared by the strain-induced lateral-layer ordering process," ***IEEE J. Quantum Electron.***, vol.30, no.2, pp.608-618, Feb. 1994.

[1-151] J. Temmyo, E. Kuramochi, M. Sugo, T. Nishiya, H. Kamada, R. Nötzel and T. Tamamura, "Strained InGaAs quantum disk laser with self-organized box like nanostructure as active region," ***IEEE 14th Int. Semiconductor Laser Conf.***, PD-3, Hawaii, pp.8-9, Sep. 1994.

[1-152] N. Kirstaedter, N. N. Ledentsov, M. Grundman, M. Schell, D. Bimberg, V. M. Ustinov, M. V. Mazimov, P. S. Kop'ev, Zh. I. Alferov, S. V. Ruvimov, U. Richter, P. Wermer, and J. Heydenreich, "First observation of injection laser emission from InAs/GaAs quantum dots," ***14th IEEE Int. Semiconductor Laser Conf.***, PD-2, pp.6-7, Hawaii, Sep. 1994.

[1-153] H. Shoji, K. Mukai, N. Ohtsuka, Y. Uchida, and H. Ishikawa, "Lasing at three-dimensionally quantum-confined sublevel of self-organized $In_{0.5}Ga_{0.5}As$ quantum dots by current injection," ***IEEE. Photon. Technol. Lett.***, vol.7, no.12, pp.1385-1387, Dec. 1995.

[1-154] H. Shoji, Y. Nakata, K. Mukai, Y. Sugiyama, M. Sugawara, N. Yokoyama and H. Ishikawa, "Lasing characteristics of self-formed quantum dot lasers with multistacked dot layer," ***IEEE J. Selected Topics in Quantum Electron.***, vol.3, no.2, pp.188-195, Apr. 1997.

[1-155] H. Saito, K. Nishi, I. Ogura, S. Sugou and Y. Sugimoto, "Room-temperature lasing operation of a quantum-dot vertical-cavity surface-emitting laser," ***Appl. Phys. Lett.***, vol.69, no.21, pp.3140-3142, Nov. 1996.

[1-156] F. Heinrichsdoff, M.-H. Mao, N. Kirstaedter, A. Krost and D. Bimberg, A.O. Kosogov and P. Werner, "Room-temperature continuous-wave lasing from stacked InAs/GaAs quantum dots grown by metalorganic chemical vapor deposition," ***Appl. Phys. Lett.***, vol.71, no.1, pp.22-24, Jul. 1997.

[1-157] N. N. Ledentsov, V. A. Shchukin, M. Grundmann, N. Kirstaedter, J. Böhrer, O. G. Schmidt, D. Bimberg, V. M. Ustinov, A. Yu. Egorov, A. E. Zhukov, P. S. Kop'ev, S. V. Zaitsev, N. Yu. Gordeev, Zh. I. Alferov, A. I. Borovkov, A. O. Kosogov, S. S. Ruvimov, P. Werner, U. Gösele and J. Heydenreich, "Direct formation of vertically coupled quantum dots in Stranski-Krastanow growth," ***Phys. Rev. B***, vol.54, no.12, pp.8743-8750, Sep. 1996.

[1-158] N. N. Ledentsov, V. M. Ustinov, J. A. Lott, A. Yu. Egorov, A. E. Zhukov, M. V. Maximov, P. S. Kop'ev, Zh. I. Alferov and D. Bimberg, "Vertical cavity surface emitting lasers based on vertically coupled quantum dot," ***IEEE 10th Int. Conf. of Lasers and Electro-Optics Society (LEOS'97)***, ThY6, pp.502-503, Nov. 1997.

[1-159] K. Mukai, Y. Nakata, H. Shoji, M. Sugawara, K. Ohtsubo, Y. Sugiyama, N. Yokoyama and H. Ishikawa, "Low threshold and high output power lasing of columnar-shaped self-assembled InAs/GaAs quantum dots," ***IEEE 16th Int. Semicond. Laser Conf. (ISLC 1998)***, WA4, Nara, pp.213-214, Oct. 1998.

[1-160] D. L. Huffaker, G. Park, Z. Zou, O. B. Shchekin and D. G. Deppe, "1.3μm room-temperature GaAs-based quantum-dot laser," ***Appl. Phys. Lett.***, vol.73, no.18, pp.2564-2566, Nov. 1998.

[1-161] Y. Miyake, H. Hirayama, K. Kudo, S. Tamura, S. Arai, M. Asada, Y. Miyamoto and Y. Suematsu, "Room-Temperature Operation of GaInAs/GaInAsP/InP SCH lasers with quantum-wire size active region," ***IEEE. J. Quantum Electron.***, vol.QE-29, no.6, pp.2123-2133, Jun. 1993.

[1-162] U. A. Griesinger, H. Schweizer, S. Kronmüller, D. Ottenwälder, F. Scholz, and M. H. Pilkun, "Realization of dot DFB lasers," ***IEEE. Photon. Technol. Lett.***, vol.8, no.5, pp.587-589, May 1996.

[1-163] T. Kojima, H. Nakaya, S. Tanaka, S. Tamura and S. Arai, "Evaluation of internal efficiency and waveguide loss of 50nm-period GaInAsP/InP quantum-wire lasers," ***IEEE 10th Int. Conf. on Indium Phosphide and Related Materials (IPRM'98)***, WA2-4, Tsukuba, p.365-368, May 1998.

[1-164] W. Wegscheider, L. Pfeiffer, K. West and R. E. Leibenguth, "Current injection GaAs/AlGaAs quantum wire lasers fabricated by cleaved edge overgrowth," ***Appl. Phys. Lett.***, vol.65, no.20, pp.2510-2512, Nov. 1994.

[1-165] Y. Qian, Z. T. Xu, J. M. Zhang, L. H. Chen, Q. M. Wang, L. X. Zhen, and X. W. Hu, "High-power two-dimensional quantum wire laser arrays," ***Electron. Lett.***, vol.31, no.2, pp.102-104, Jan. 1995.

[1-166] T. G. Kim, E. K. Kim S. K. Min and J. H. Park, "Improvement of carrier capture efficiency of short-period GaAs/AlGaAs quantum wire array by a new lithography method," ***Appl. Phys. Lett.***, vol.69, no.7, pp.955-956, Aug. 1996.

[1-167] M. Higashiwaki, S. Ikawa, S. Shimomura and S. Hiyamizu, "High-density GaAs/ $(GaAs)_4(AlAs)_2$ QWR lasers on (775)B GaAs substrates grown by MBE," ***Nat. Conv. Res. of Japan Soc. Appl. Phys.***, 15a-A-20, Hirohsima, p.997, Sep. 1998.

[1-168] T. G. Kim, K. H. Park, S. M. Hwang, Y. Kim, E. K. Kim, S. K. Min, S. J. Leem, J. I. Jeon, J. H. Park and W. S. C. Chang, "Performance of GaAs-AlGaAs V-grooved inner stripe quantum-well wire lasers with different current blocking configurations," ***IEEE J. Quantum Electron.***, vol.34, no.8, pp.1461-1468, Aug. 1998.

[1-169] M. Walther, E. Kapon, C. Caneau, D. M. Hwang, and L. M. Schiavone, "InGaAs/GaAs strained quantum wire lasers grown by organometallic chemical vapor deposition on nonplanar substrates," ***Appl. Phys. Lett.***, vol.62, no.18, pp.2170-2172, May 1993.

[1-170] N. Kirstaedter, N. N. Ledentsov, M. Grundman, D. Bimberg, V. M. Ustinov, S. S. Ruvimov, M. V. Mazimov, P. S. Kop'ev, Zh. I. Alferov, U. Richter, P. Wermer, U. Gösele and J. Heydenreich, "Low threshold, large T_0 injection laser emission from (InGa)As quantum dots," ***Electron. Lett.***, vol.30, no.17, pp.1416-1417, Aug. 1994.

[1-171] J. Temmyo, E. Kuramochi, M. Sugo, T. Nishiya, R. Nötzel, and T. Tamamura, "Strained InGaAs quantum disk laser with nanoscale active region fabricated with self-organization on GaAs (311)B substrate," ***Electron. Lett.***, vol.31, no.3, pp.209-211, Feb. 1995.

[1-172] O. G. Schmidt, N. Kirstaedter, N. N. Ledentsov, D. Bimberg, V. M. Ustinov, A. Yu. Egorov, A. E. Zhukov, M. V. Maximov, P. S. Kop'ev and Zh. I. Alferov, "InAs/GaAs quantum dot lasers," ***IEEE 8th Int. Conf. on Indium Phosphide and Related Materials (IPRM'96)***, ThA1-4, Schwäbisch Gmünd, pp.727-730, Apr. 1996.

[1-173] N. Kirstaedter, O. G. Schmidt, N. N. Ledentsov, D. Bimberg, V. M. Ustinov, A. Yu. Egorov, A. E. Zhukov, M. V. Maximov, P. S. Kop'ev and Zh. I. Alferov, "Gain and differential gain of single layer InAs/GaAs quantum dot injection lasers," ***Appl. Phys. Lett.***, vol.69, no.9, pp.1226-1228, Aug. 1996.

[1-174] H. Shoji, Y. Nakata, K. Mukai, Y. Sugiyama, M. Sugawara, N. Yokoyama and H. Ishikawa, "Self-formed InGaAs quantum dot lasers with multi-stacked dot layer," ***Jpn. J. Appl. Phys.***, vol.35, pt.2, no.7B, pp.L903-L905, Jul. 1996.

[1-175] R. Mirin, A. Gossard and J. Bowers, "Room temperature lasing from InGaAs quantum dots," ***Electron. Lett.***, vol.32, no.18, pp.1732-1733, Aug. 1996.

[1-176] S. V. Zaitsev, N. Yu. Gordeev, Yu. M. Shernniakov, V. M. Ustinov, A. E. Zhukov, A. Yu. Egorov, M. V. Maximov, P. S. Kop'ez, Zh. I. Alferov, N. N. Lendentsov, N. Kirstaedter, and D. Bimberg "Radiation characteristics of injection lasers based on vertically coupled quantum dots," ***Superlattices and Microstructures***, vol.21, no.4, pp.559-564, 1997.

[1-177] H. Shoji, Y. Nakata, K. Mukai, Y. Sugiyama, M. Sugawara, N. Yokoyama and H. Ishikawa, "Room temperature CW operation at the ground state of self-formed quantum dot lasers with multi-stacked dot layer," ***Electron. Lett.***, vol.32, no.21, pp.2023-2024, Oct. 1996.

[1-178] K. Kamath, J. Phillips, H. Jiang, J. Singh and P. Bhattacharya, "Small-signal modulation and differential gain of single-mode self-organizad $In_{0.4}Ga_{0.6}As$/GaAs quantum dot lasers," ***Appl. Phys. Lett.***, vol.70, no.22, pp.2952-2953, Jun. 1997.

[1-179] D. Bimberg, N. Kirstaedter, N. N. Lendentsov, Zh. I. Alferov, P. S. Kop'ez and V. M. Ustinov, "InGaAs-GaAs quantum-dot lasers," ***IEEE J. Selected Topics in Quantum Electron.***, vol.3, no.2, pp.196-205, Apr. 1997.

[1-180] F. Heinrichsdoff, A. Krost, N. Kirstaedter, M.-H. Mao, M. Grundmann, D. Bimberg, A.O. Kosogov and P. Werner, "InAs/GaAs quantum dots grown by metalorganic chemical vapor deposition," ***Jpn. J. Appl. Phys.***, nol.36, pt.1, no.6B, pp.4129-4133, Jun. 1997.

[1-181] J. A. Lott, N. N. Ledentsov, V. M. Ustinov, A. Y. Egorov, A. E. Zhukov, P. S. Kop'ev, Zh. I.. Alferov and D. Bimberg, "Vertical cavity lasers based on vertically coupled quantum dots," ***Electron. Lett.***, vol.33, no.13, pp.1150-1151, Jun. 1997.

[1-182] D. L. Huffaker, L. A. Graham and D. G. Deppe, "Low-threshold continuous-wave operation of an oxide-confined vertical cavity surface emitting laser based on a quantum dot active region and half-wave cavity," ***Electron. Lett.***, vol.33, no.14, pp.1225-1226, Jul. 1997.

[1-183] M.-H. Mao, F. Heinrichsdorff, A. Krost and D. Bimberg, "Study of high frequency response of self-organized stacked quantum dot lasers at room temperature," ***Electron. Lett.***, vol.33, no.19, pp.1641-1642, Sep. 1997.

[1-184] D. L. Huffaker, H. Deng and D. G. Deppe, "1.15μm wavelength oxide-confined quantum-dot vertical cavity surface-emitting laser," ***IEEE Photon. Technol. Lett.***, vol.10, no.2, pp.185-187, Feb. 1998.

[1-185] K. Mukai, Y. Nakata, H. Shoji, M. Sugawara, K. Ohtsubo, T. Futatsugi, Y. Sugiyama, N. Yokoyama and H. Ishikawa, "Low threshold CW lasing of closely-stacked self-organized InAs/GaAs quantum dots," ***IEEE 10th Int. Conf. on Indium Phosphide and Related Materials (IPRM'98)***, WB1-4, Tsukuba, p.345-348, May 1998.

[1-186] M. V. Maximov, Yu. M. Shermyakov, A. F. Tsatsul'nikov, A. V. Lunev, A. V. Sakharov, V. M. Ustinov, A. Yu. Egorov, A. E. Zhukov, A. R. Kovsh, P. S. Kop'ez, L. V. Asryan, Zh. I. Alferov, N. N. Lendentsov, D. Bimberg, A. O. Kosogov and P. Werner, "High-power continuous-wave operation of a InGaAs/AlGaAs quantum dot laser," ***J. Appl. Phys.***, vol.83, no.10, pp.5561-5563, May 1998.

[1-189] A. M. Moy, L. J. Chou, K. C. Hsieh and K. Y. Cheng, "Molecular beam epitaxial growth of quantum wire heterostructures using $(GaP)_x/(InAs)_y$ short period superlattices on InP," ***IEEE 9th Int. Conf. on Indium Phosphide and Related Materials (IPRM'97)***, MP13, Hyannis, pp.90-91, May 1997.

[1-190] A. M. Moy, A. C. Chen, K. Y. Cheng, L. J. Chou and K. C. Hsieh, "Growth of GaInAsP quantum wire heterostructures using the strain-induced lateral-layer ordering process," ***J. Cryst. Growth***, vol.175/176, pp.819-824, 1997.

[1-191] H. Saito, K. Nishi and S. Sugou, "Influence of GaAs capping on the optical properties of InGaAs/GaAs surface quantum dots with 1.5μm emission," ***Appl. Phys. Lett.***, vol.73, no.19, pp.2742-2744, Nov. 1998.

[1-192] A. Orth, H. Zull, J. P. Reithmaier and A. Forchel, "GaInAs/GaAs quantum wire laser structures with strong gain coupling defined by reactive ion etching," ***Electron. Lett.***, vol.31, no.6, pp.457-458, Mar. 1995.

[1-193] J. P. Reithmaier, A. Orth, J. Müller and A. Forchel, "First order gratings for gain coupled GaInAsP DFB-lasers made by maskless focused ion beam patterning," ***IEEE 7th Int. Conf. on Indium Phosphide and Related Materials (IPRM'95)***, ThP53, Sapporo, pp.569-572, May 1995.

Chapter 2

Theoretical Characteristics —Requirements to Density and Size Fluctuation of Quantum-Wire Structure

2.1 Introduction... 37
2.2 Requirement for Optical Gain.. 38
2.3 Requirement to Optical Confinement Factor and Size Fluctuation.. 47
2.3.1 Threshold Current of Single Quantum-Well Laser........... 47
2.3.2 Threshold Current of Quantum-Wire Laser.................. 53
2.4 Conclusion.. 68
References.. 69

2.1 Introduction

LOW threshold current as well as high quantum efficiency operation is one of the most attractive improvements expected in quantum-wire (Q-Wire) lasers, but it strongly depends on the cavity structure, namely the optical confinement factor of the Q-Wire active region, due to the extremely small volume of the Q-Wire potential well[2-1],[2-2]. In addition, size fluctuation, particularly of the quantum-wire cross section, can significantly broaden the gain spectra and reduce the attainable peak gain[2-3]. The technology used to fabricate quantum wells relies on growth techniques capable of atomic layer tolerances, leading to actual quantum-well (QW) devices, which exhibit nearly ideal properties. Confinement in directions other than the growth direction requires lithographic patterning and the best lithographic techniques have resolutions on the order of 10nm. To obtain lateral quantum confinement effect is sufficiently, it is important to consider the effects of fabricational inhomogeneities on quantum wire structures. Variations in the size of quantum wires will smear some of the sharpness out of the density of the states of these structures, reducing some of the benefits of lower dimensionality.

Therefore in this chapter, the most effective size of Q-Wire is estimated from the point of material gain and threshold current density, considering the size fluctuation of Q-Wire structure and the optical confinement factor.

2.2 Requirement for optical gain

The very small volume of inverted materials, higher optical gain and reduced cavity losses in QW lasers result in very low threshold currents[2-4]-[2-6]. In addition, QW lasers exhibit reduced temperature sensitivity and potential for higher modulation bandwidths and narrower spectral linewidths. Further improvement in semiconductor laser performance is expected with the introduction of quantum confinement in more than one dimension. The resulting Q-Wire laser structures employ quasi-1-dimensional carriers which are quantum confined to wire-like potential wells of sufficiently small lateral dimensions (less than a few tens of nm).

The linear gain coefficient is given by[2-7]

$$g(\omega)=\frac{\omega}{n_r}\sqrt{\frac{\mu_0}{\varepsilon_0}}\int_{Eg}^{\infty}\left\langle R_{ch}^2\right\rangle\cdot g_{ch}(E_{ch})\cdot\{f_c-f_v\}\cdot\frac{\hbar/\tau_{in}}{(E_{ch}-\hbar\omega)^2+(\hbar/\tau_{in})^2}dE_{ch},\quad(2.1)$$

where the subscripts c and h denote the conduction and valence band, respectively, E_{ch} is the transition energy between conduction and valence band, $\hbar$ is the Plank's constant, ω is the angular frequency of input light, ε_0 and μ_0 are permittivity and permeability in the vacuum, τ_{in} is the intraband relaxation time[2-8], n_r is the refractive index without dispersion, and $\langle R_{ch}^2 \rangle$ is the matrix element of transition dipole moment[2-9],[2-10]. The Fermi functions in the conduction and the valence band are f_c and f_v, respectively, which are

$$f_c = \frac{1}{1+exp\{(E_c - E_{fc})/k_B T\}}, \tag{2-2}$$

$$f_v = \frac{1}{1+exp\{-(E_h - E_{fv})/k_B T\}}, \tag{2-3}$$

where E_{fc} and E_{fv} are quasi-Fermi energies in conduction band and valence band. g_{ch}, which is a density of state for electron, can be given by,

$$g_{ch}(E_{ch}) = \left(\frac{m_c^* \cdot m_h^*}{m_c^* + m_h^*}\right)\frac{1}{\pi\hbar^2 W_y} u(E_{ch} - E_{cy,1} - E_{hy,1} - E_g) \qquad \text{for Q-Film,} \tag{2-4}$$

$$g_{ch}(E_{ch}) = \left(\frac{2m_c^* \cdot m_h^*}{m_c^* + m_h^*}\right)^{1/2} \frac{1}{\pi\hbar W_x W_y} \Big/ (E_{ch} - E_{cxy,1,m} - E_{hxy,1,m} - E_g)^{1/2}$$

for Q-Wire, (2-5)

where m_c^* and m_h^* are the effective mass of electron and hole, respectively, E_g is the bandgap energy, $E_{cy,l}$, $E_{hy,l}$, $E_{cxy,l,m}$, and $E_{hxy,l,m}$ is the quantized energy level of quantum-film (Q-Film) and Q-Wire in the conduction band and the valence band, respectively. W_y and W_x is the thickness of Q-Wire or Q-Film, and the width of Q-Wire, respectively. E_{fc} and E_{fv} can be obtained from the density of electron N, and hole $P(\approx N)$ in the Q-Wire or Q-Film as[2-11]

$$N = \int_{E_c}^{\infty} g_c(E) \cdot \frac{dE}{1+exp\left(\frac{E - E_{fc}}{k_B T}\right)}, \tag{2-6}$$

$$P \approx N$$
$$= \int_{-\infty}^{E_h} g_h(E) \cdot \frac{dE}{1+exp\left(-\frac{E - E_{fv}}{k_B T}\right)}. \tag{2-7}$$

The size fluctuation of Q-Wires used in this analysis is shown in Fig. 2.1. In the case of Q-Wire structures fabricated by carving the Q-Film layer, the size fluctuation

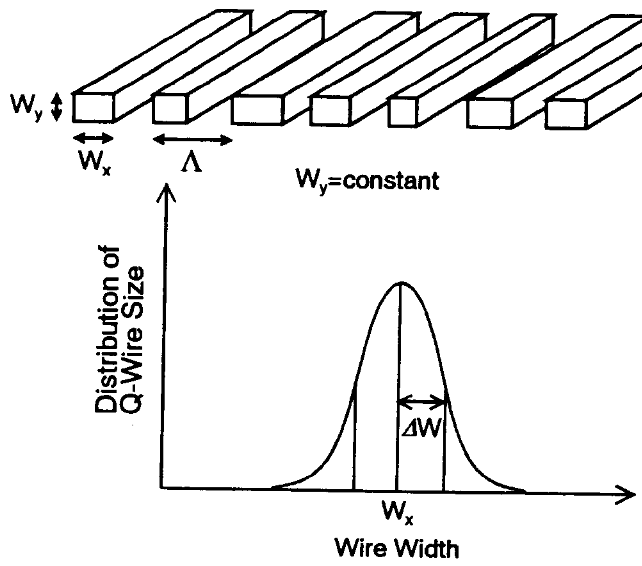

Fig. 2.1 Model of size-fluctuation distribution of Q-Wire structures used in this analysis

in the later thickness can be neglected because a flat heterointerface with less than one atomic layer can be grown by molecular beam epitaxy (MBE) or organometallic vapor phase epitaxy (OMVPE). In this analysis, strained Q-Wire structures are introduced because the merit of Q-Wire effect is more improved, that is, to obtain high gain and differential gain[2-12], by means of spreading the quantized energy levels in the valence band due to the small effective mass of the hole[2-13],[2-14]. Figure 2.2 shows the injection carrier density N dependence of maximum gain g_{max} for Q-Film at T=300K. The material of active region is compressively strained (1%-CS) GaInAsP, whose composition is $Ga_{0.18}In_{0.82}As_{0.73}P_{0.27}$ in this case. The thickness W_y is 8, 10, 12, and 15nm, respectively. The intraband relaxation time of all cases is assumed to be 0.1ps. In case of W_y=8nm, the size fluctuation of thickness is considered, which is assumed to be ±0.6nm (2 mono layer (ML)). As can be seen, the influence of size fluctuation is negligibly small. So the fluctuation of the thickness is not considered in this analysis after this. The peak gain shifts to higher subbands with increase in injected carrier density for W_y>10nm. The thicker the Q-Film becomes, the smaller the carrier density shifting to high subbands due to the small quantum confinement effect, i.e., the small separation of the density of states for thick Q-Film; therefore, the saturation of the maximum gain of ground level becomes small. In case of the injected carrier density of 1-3 × 10^{18}cm^{-3}, the largest maximum gain and differential gain is obtained at W_y=8nm. In this analysis, a thinner Q-Film less than 8nm is not calculated because the thin Q-Film is severe for lasing of single-layer QW lasers due to a low optical confinement factor in the active region.

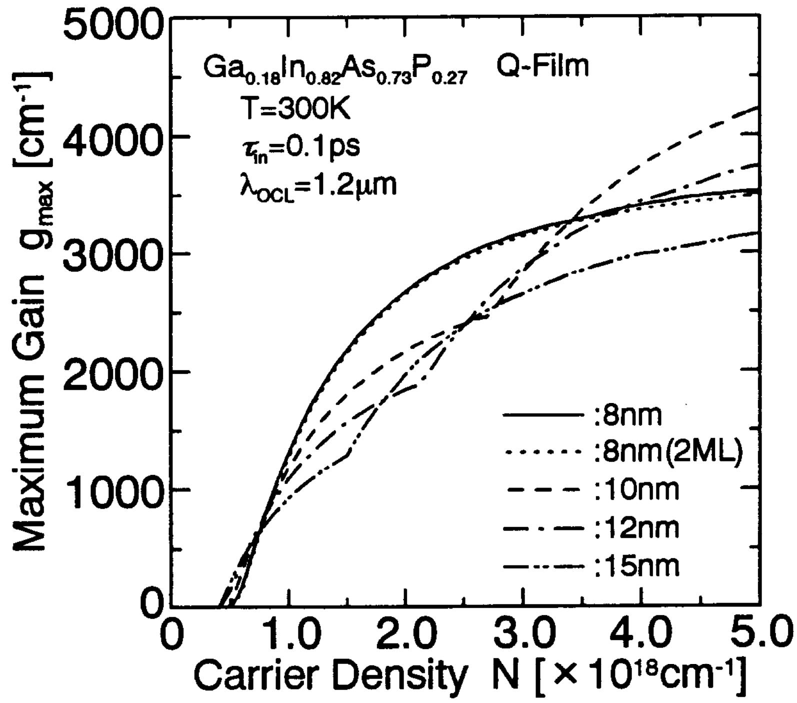

Fig. 2.2 the injection carrier density N dependence of maximum gain g_{max} for Q-Film; W_y=8nm, 10nm, 12nm, and 15nm.

Therefore, it is assumed that the thickness of Q-Wires is constant and that only the width of Q-Wire is fluctuating. The Gaussian distribution is assumed for the size along x-direction[2-15]. The optical gain is obtained by simply adding each spectra of different-size Q-Wires with the same injection carrier density. Figure 2.3 shows, for example, the material gain spectra of Q-Wire structures at T=300K as a parameter of the size fluctuation ΔW; from ΔW=0nm to 3nm. The calculations for strained Q-

Wire are done similar to ref.[2-12], that is, the barrier layers at the upper and lower sides of the wire are assumed to lattice-match one to the substrate, and those of the left and right sides are assumed to mismatch with the same amount as the active layer, i.e., lattice-match to the strained active layer, to apply the biaxial strain effect. The parameters which are used in the calculation (Luttinger parameters[2-16]) are evaluated by linear interpolation between the related binaries[2-17]. The thickness and width of Q-Wire are 8nm and 10nm, respectively. When the size fluctuation ΔW is large, the gain peak is reduced and the spectral width broadens. In case of ΔW=3nm, the gain peak is reduced to 68% of that with ΔW=0nm and the full maximum half width (FWHM) above 0cm^{-1} broadens to about 1.7 times wider than that with ΔW=0nm. Therefore, high uniformity of Q-Wire structures are necessary to realize high performance of Q-Wire lasers. The size fluctuation should be reduced within 1nm, which the peak gain is down to 91% and FWHM is spread of 13%, when the wire size is 10nm.

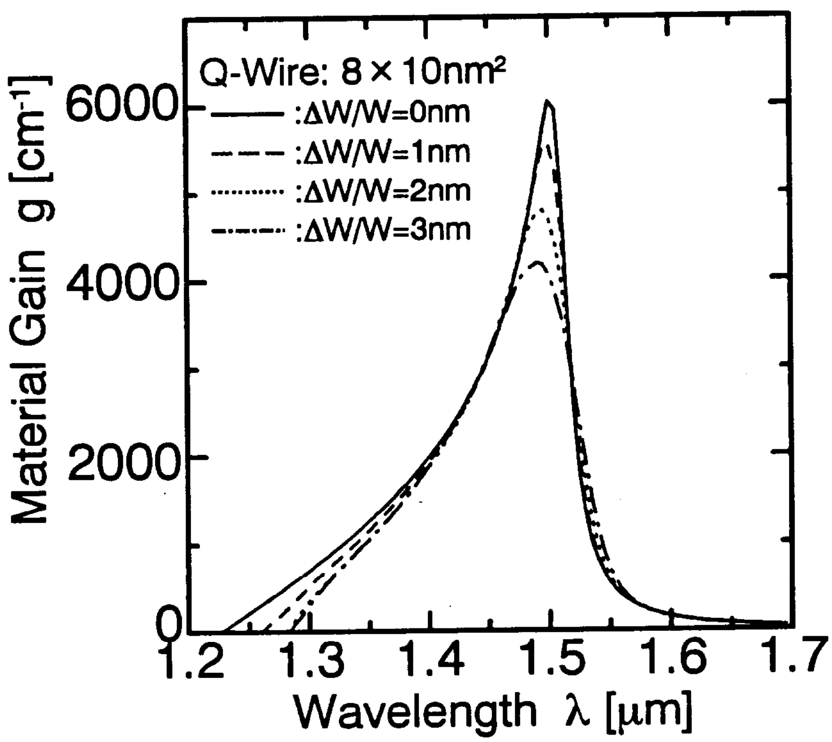

Fig. 2.3 Gain spectra of Q-Wire structures (W_x=10nm and W_y=8nm). The size fluctuation is ΔW=0nm to 3nm.

Figure 2.4 shows the injection carrier density N dependence of maximum gain g_{max} (g-n curve, in short) for Q-Wire at T=300K, which the thickness is (a) 8nm and (b) 10nm. The width of Q-Wire is 10nm and 20nm in both Figs. The other parameters are the same as in Fig. 2.2. In Fig. 2.4(a), the g-n curves of Q-Film with the size fluctuation of 0nm and 0.6nm(2ML), which are negligibly small fluctuations, are shown. The gain peak of both kinds of Q-wires are not shifted to higher subbands. In this case, the maximum gain of the Q-Wire with W_x=10nm is larger than that of the one with W_x=20nm. However the influence of size fluctuation is also larger in the case of W_x=10nm because of larger emission energy broadening with the narrower Q-Wire. The maximum gain and differential gain are drastically reduced in the case of W_x=10nm. On the other hand, those of W_x=20nm are slightly under the influence of the size fluctuation. The differential gain of 10nm-wide Q-Wire with ΔW=2nm is similar to that of 20nm-wide Q-Wire below g_{max} of 1500cm^{-1}. When the size fluctuation is ΔW=3nm these are almost same at g_{max} < 2500cm^{-1}.

In case of W_y=10nm in Fig. 2.4(b), the peak gain of Q-Wires shift to higher subbands with an increase in injected carrier density due to the influence of the quantized energy levels of Q-Film. As can be seen, the maximum gain and differential gain are also much more reduced in the case of W_x=10nm than those of W_x=20nm, but the reduction of the ratio is small compared with W_x=10nm. When the injected carrier density is less than 3×10^{18}cm^{-3}, the maximum gain at ground level of 10-nm-wide Q-Wire is larger than that of 20-nm-wide Q-Wire with ΔW =0-1nm. However, the differential gain of both Q-Wires are almost same as that in ΔW=2nm, and furthermore, that of the 10-nm-wide Q-Wire becomes a little smaller than that of 20-nm-wide Q-Wire.

Then the wire width dependence of maximum gain is calculated considering the size fluctuation effect and is shown in Fig. 2.5 (a) at T=300K and (b) at T=90K. The injected carrier density is 3×10^{18}cm^{-3} at T=300K and 1×10^{18}cm^{-3} at T=90K. The intraband relaxation time is assumed to be 0.1ps at both temperatures. At T=300K, the width to obtain maximum gain is about 8nm (7-10nm) with no size fluctuation.

However the width to obtain maximum gain becomes larger and the maximum gain is reduced with an increase in the size fluctuation. With ΔW=1nm, the maximum gain g_{max} is reduced to 92% compared with no fluctuation and the width to obtain maximum gain $W_{g_{max}}$ is about 10nm (8-12nm). In case of ΔW=2nm, g_{max} is reduced to 80% and $W_{g_{max}}$ is about 12nm (10-16nm), and in case of ΔW=3nm, g_{max} is reduced to 73% and $W_{g_{max}}$ is about 14nm (12-18nm). It is noted that the size fluctuation effect is negligible if the wire width is larger than 22nm. The tendency of size fluctuation effect is similar at T=90K. However the influence of size fluctuation is smaller compared with that at T=300K. This is because energy broadening due to thermal energy becomes small at low temperatures.

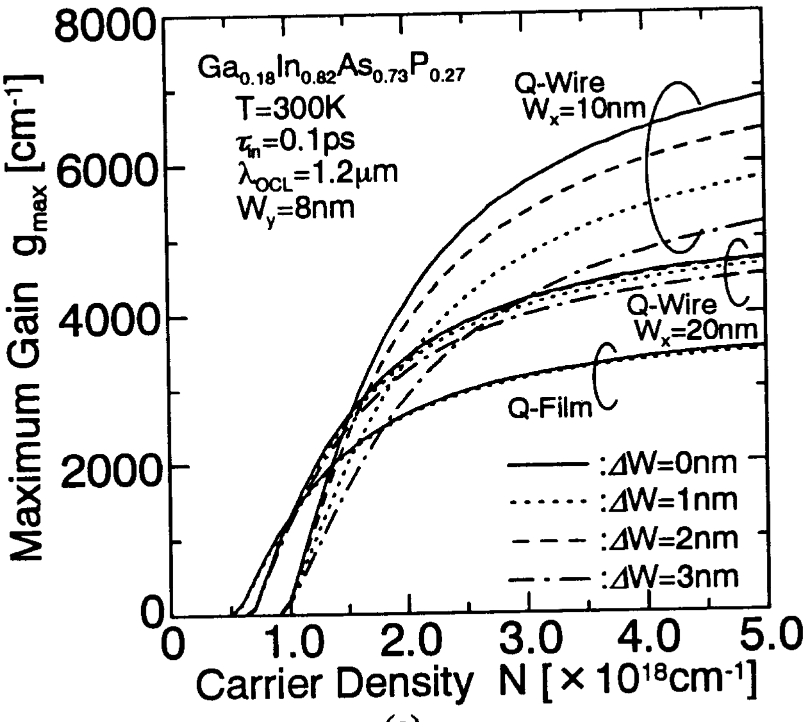

(a)

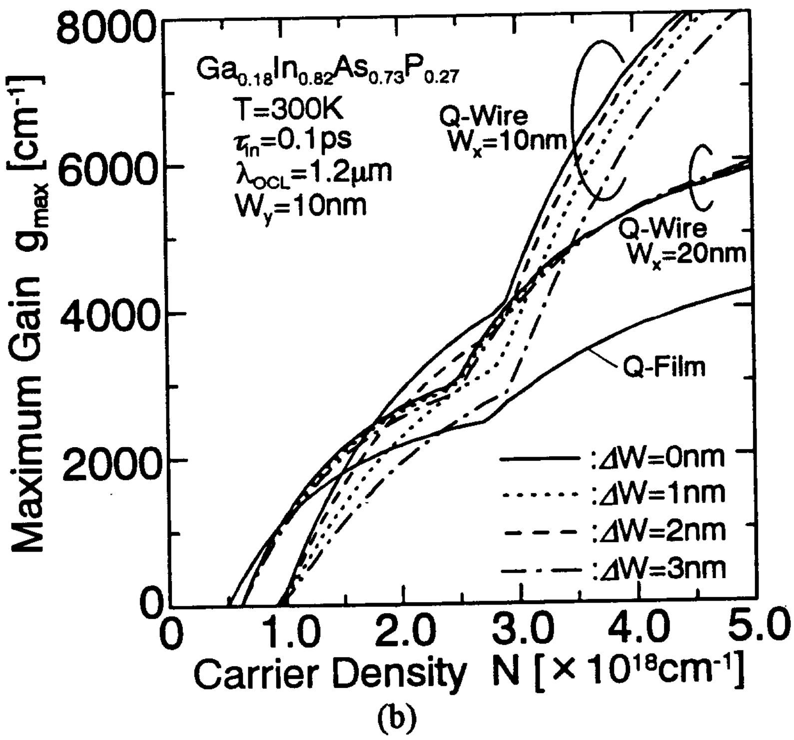

(b)

Fig. 2.4 Injection carrier density dependence of maximum gain for Q-Wire with the width of 10nm and 20nm, and the thickness is (a) 8nm and (b) 10nm.

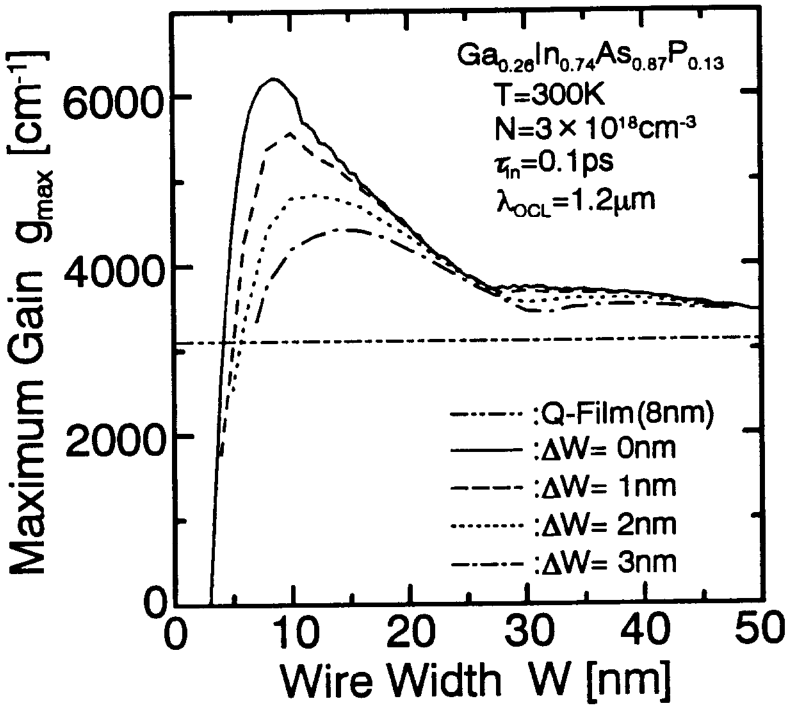

(a) T=300K

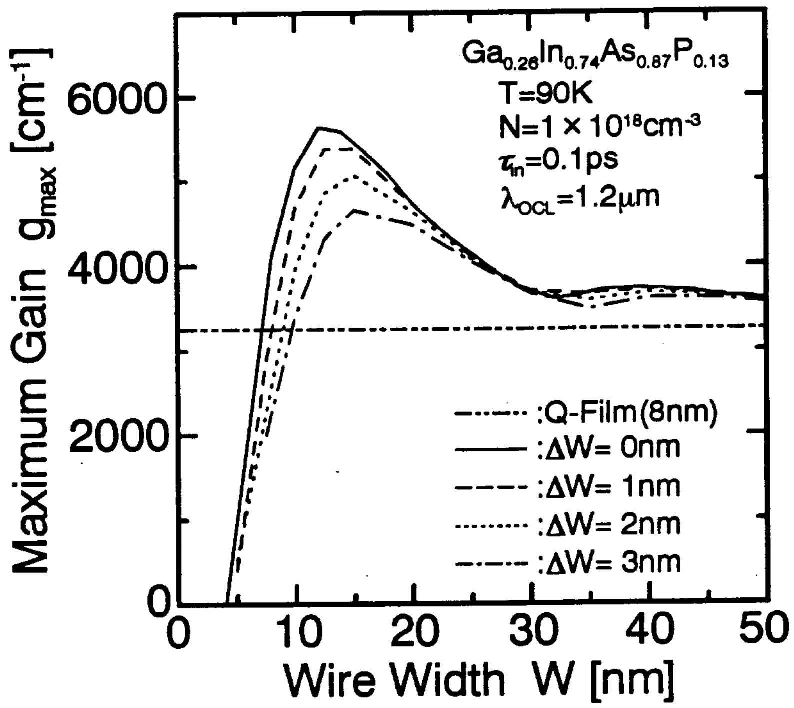

(b) T=90K

Fig. 2.5 Wire width dependence of maximum gain with ΔW=0nm to 3nm, at (a) T=300K and (b) T=90K.

2.3 Requirement to optical confinement factor and size fluctuation

Wet chemical etching is a low damage process because it uses chemical reactions. However, the shape of an etched material strongly depends on crystal orientations, which are usually mesa-shaped. As a result, the optical gain of multi-stacked Q-Wire lasers decreases and broadens due to the large size fluctuation of Q-wires in the vertical direction. Therefore, single-layer Q-Wire structures are required to reduce the size of fluctuation. In this case, the Q-Wire laser is strongly dependent on the in-plane space filling factor, i.e., the optical confinement factor of active region. So it is important to estimate the optical confinement factor in order to realize high-performance operation of Q-Wire lasers, that is, to overcome Q-Film lasers, considering the size fluctuation of the Q-Wires. At low temperatures, because the energy broadening due to thermal excitation and optical losses due to nonradiative recombination are reduced, it is relatively easier to obtain high performance of single-layer Q-Wire lasers. It is possible to realize high performance of single-layer Q-Wire lasers at room temperature under the condition of low cavity loss structures, such as long-cavity structure or high reflective (HR) coating of facets. Firstly, the requirement to the optical confinement factor for single-quantum-well (SQW or Q-Film, in short) laser is estimated, then that for the Q-Wire laser is calculated considering the size fluctuation of the width of Q-Wire structures.

2.3.1 Threshold Current of Single Quantum Well laser

The optical confinement factor of the active region ξ_{Film} for Q-Film laser and ξ_{Wire} for Q-Wire laser can be expressed as

$$\xi_{Film} = \xi_0 W_y, \tag{2.8}$$

$$\xi_{Wire} = (n \cdot \rho)\xi_0 W_y, \tag{2.9}$$

$$\rho = \frac{W_x}{\Lambda}, \tag{2.10}$$

where W_x or W_y is the size of the quantum-wire along the *x*- or *y*-direction as shown in

Fig. 2.1, Λ is the period of the quantum-wire along the x-direction, ρ is the in-plane space filling factor of Q-Wire, ξ_0 is the optical confinement factor of single quantum-well (film) in unit thickness, and n is the number of the Q-Film sheets along the vertical direction[2-18].

The threshold condition can be given by

$$\xi_s \cdot g_{th} = \alpha \qquad (s = Film\ or\ Wire) \tag{2.11}$$

$$= \alpha_{WG} + \frac{1}{L} ln \frac{1}{R}, \tag{2.12}$$

where g_{th}, α, α_{WG}, L, and R are the threshold gain in Q-Film or Q-Wire, the total cavity loss, the waveguide loss, cavity length, and facet reflectivity, respectively. Threshold current density J_{th} can be given by

$$J_{th} = eW_y B_{eff} N_{th}^2, \tag{2.13}$$

where e, B_{eff}, and N_{th} are the electron charge, the effective spontaneous recombination coefficient、threshold carrier density in the well, respectively. In this calculation, the value of B_{eff} is used to be 1.5×10^{-10}cm^3/s[2-19]. Figure 2.6 shows threshold current density J_{th} of Q-Film laser as a function of total loss α at T=300K. The material of active region is compressively-strained (1%-CS) $Ga_{0.18}In_{0.82}As_{0.73}P_{0.27}$. The thickness W_y is 8, 10, 12, and 15nm, respectively and three kinds of optical confinement factor ξ_0 is used, i.e., (a) ξ_0=0.1%/nm, (b) 0.15%/nm, and (c) 0.2%/nm in Fig. 2.6. The intraband relaxation time of all cases is assumed to be 0.1ps in the calculation of threshold carrier density N_{th}. In the case of W_y=8nm, the size fluctuation of thickness is considered, which is assumed to be $\pm$0.6nm (2 mono layer (ML)), but the increase in J_{th} is enough small to ignore the influence of size fluctuation. Therefore the size fluctuation of thickness is not considered in this analysis. At the total loss α below 20cm^{-1}, for instance, when we assume the waveguide loss α_{WG} to be 10cm^{-1}, the cavity length L is about 1mm, J_{th} of thinner QW laser is lower than that of the thicker one due to the small active region, that is, volume effect. However α becomes larger, the J_{th} of the thicker one becomes lower due to larger optical confinement factor ξ_{Film}, i.e., optical confinement effect. In the case of W_y=8nm, J_{th} rapidly increases above 20cm^{-1} with ξ_0=0.1%/nm and above 30cm^{-1} with ξ_0=0.15%/nm due to gain saturation as a result of the low optical confinement factor. When the optical confinement factor becomes larger in unit thickness, that is, ξ_0=0.2%/nm, the gain saturation can be suppressed. The volume effect is stronger to reduce J_{th} at α <40cm^{-1}. The J_{th} of all kinds of lasers are almost the same at the total loss below 30cm^{-1}, which are independent of the thickness, i.e. the optical confinement factor. Thus, in case of low optical confinement factor, the total loss should be reduced under the condition of low cavity-loss structures, such as long-cavity structures or high reflective (HR) coating of facets.

The optical confinement factor dependencies of threshold current density are shown in Fig. 2.7, as a parameter of total loss α; (a) 10cm^{-1}, (b) 20cm^{-1}, (c) 30cm^{-1}, (d) 40cm^{-1}, and (e) 50cm^{-1}. In the case of ξ_0=0.15%/nm and ξ_0=0.2%/nm, the J_{th} of all kinds of lasers are constant at α<20cm^{-1}. That is almost proportional to the optical confinement factor with ξ_0=0.1%/nm at α<20cm^{-1}, in which the volume effect is dominant compared with the optical confinement effect. However J_{th} of the thicker Q-Film laser becomes lower than that of thinner one, that is, the optical confinement effect becomes dominant compared with the volume effect at α=30cm^{-1} due to gain saturation. Above 40cm^{-1} the optical confinement effect is much stronger. At α=50cm^{-1}, there is no volume effect and a rapid increase in J_{th} can be suppressed by the optical confinement effect in case of ξ_0=0.2%/nm. All the calculation results mentioned above are summarized in Fig. 2-8 (closed marks). Another compressively strained material, $Ga_{0.26}In_{0.74}As_{0.87}P_{0.13}$ indicates the similar tendency (open marks). Although there has to be trade-off between the volume effect and the optical confinement effect, broadly speaking, the larger optical confinement reduces the threshold current density, which is independent of the thickness of the quantum well. J_{th} is strongly dependent on the optical confinement factor of a single quantum well in unit thickness ξ_0. In the case of ξ_0=0.1%/nm, J_{th} increases rapidly with increase in the total loss. Especially, J_{th} increases rapidly at α< 30cm^{-1} in case of ξ_0=0.1%/nm (see a solid line in Fig. 2-8), and at $\alpha < 50\text{cm}^{-1}$ in case of ξ_0=0.15%/nm (dashed line).

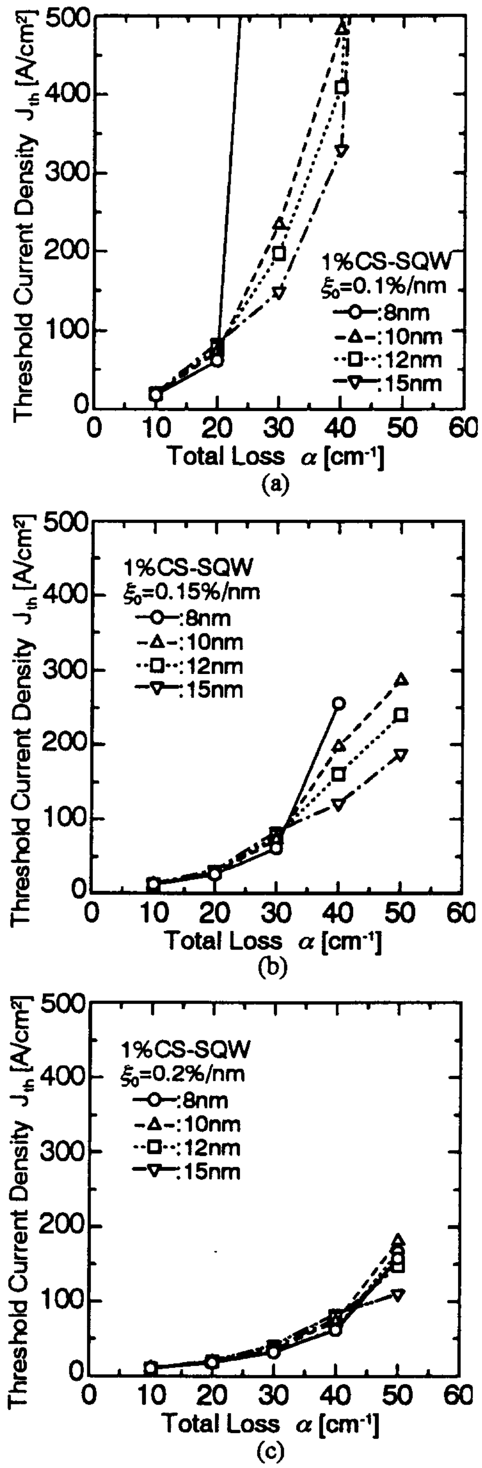

Fig. 2.6 Threshold current density of Q-Film laser as a function of total loss α at T=300K. The thickness is 8, 10, 12, and 15nm, respectively and three kinds of optical confinement factor ξ_0 is used, i.e., (a) ξ_0=0.1%/nm, (b) 0.15%/nm, and (c) 0.2%/nm.

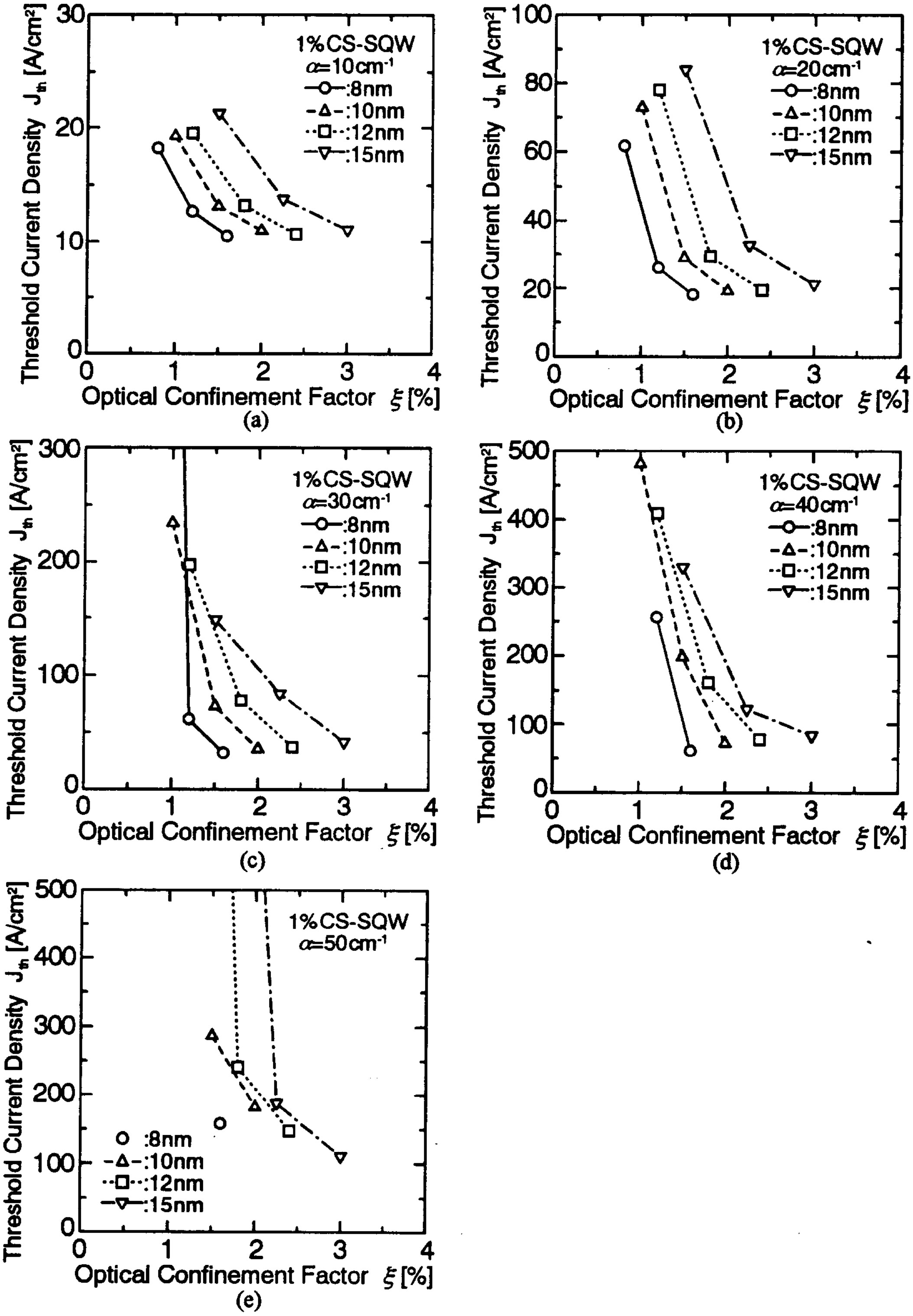

Fig.2.7 Optical confinement factor dependencies of threshold current density as a parameter of total loss α;
(a) 10cm^{-1}, (b) 20cm^{-1}, (c) 30cm^{-1}, (d) 40cm^{-1}, and (e) 50cm^{-1}.

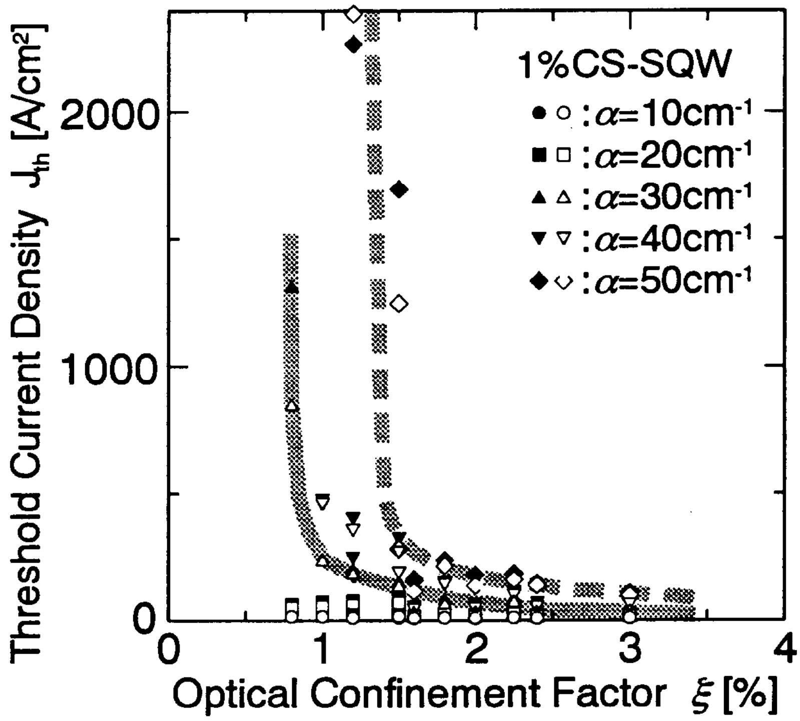

Fig. 2.8 Optical confinement factor dependencies of threshold current density as a parameter of total loss α from 10-50 cm^{-1}. Closed marks show J_{th} of $Ga_{0.18}In_{0.27}As_{0.73}P_{0.27}$ and open marks shows J_{th} of $Ga_{0.26}In_{0.74}As_{0.87}P_{0.13}$, respectively. Both materials indicate similar tendency.

2.3.2 Threshold Current of Quantum-Wire laser

In the case of Q-Wire lasers, the arrays of potential wells should be uniform in size and shape so that inhomogeneous broadening effects would not degrade the effects of quantum confinement. Since the volume of the Q-Wire structure is smaller than that of Q-Film, i.e. smaller optical high optical confinement factor, the reduction of optical gain and differential gain due to size fluctuation should be avoided in order to obtain lower threshold current operation. Therefore, it is important to estimate the effective size of the Q-Wire, considering the size fluctuation of the Q-Wire structure and the optical confinement factor. Figure 2.9 shows the threshold current density J_{th} dependent on the in-plane space filling factor ρ for a parameter of the size fluctuation of Q-Wire structure ΔW. The thickness of all of the Q-Wires calculated here is constant of 8nm and the size fluctuation of thickness is neglected because the optical gain peak of 8nm-thick Q-Film does not shift from ground level to higher subband and the calculation is simplified. The width of Q-Wire W is 10nm and 20nm, respectively, and various conditions are assumed, that is, (a) W=10nm, ξ_0=0.1%/nm, and α=10cm^{-1}, (b) W=10nm, ξ_0=0.1%/nm, and α=20cm^{-1}, (c) W=20nm, ξ_0=0.1%/nm, and α=10cm^{-1}, (d) W=20nm, ξ_0=0.1%/nm, and α=20cm^{-1}, (e) W=10nm, ξ_0=0.15%/nm, and α=10cm^{-1}, and (f) W=10nm, ξ_0=0.15%/nm, and α=20cm^{-1}, respectively. As can be seen, J_{th} becomes minimal at a certain value of ρ, and this increases with an increase of ΔW and also with the increase of α. Very low-threshold current density operation with W=10nm can be attained when the total cavity loss is small, but it increases with increase in total loss and the influence of size fluctuation is enhanced. When the size fluctuation is small, J_{th} of 10nm-wide Q-Wire is lower than that of 20nm-wide Q-Wire at α=20cm^{-1}. If the optical confinement factor of a single quantum well in unit thickness becomes larger, J_{th} is reduced and the size fluctuation effect is also reduced (see Fig. 2.9 (e) and (f)).

Figures 2.10-2.13 show the wire width dependence of threshold current density at T=300K as a parameter of size fluctuation; for α=10cm^{-1} in Fig. 2.10, α=20cm^{-1} in Fig. 2.11, α=30cm^{-1} in Fig. 2.12, and α=40-50cm^{-1} in Fig. 2.13. The space filling

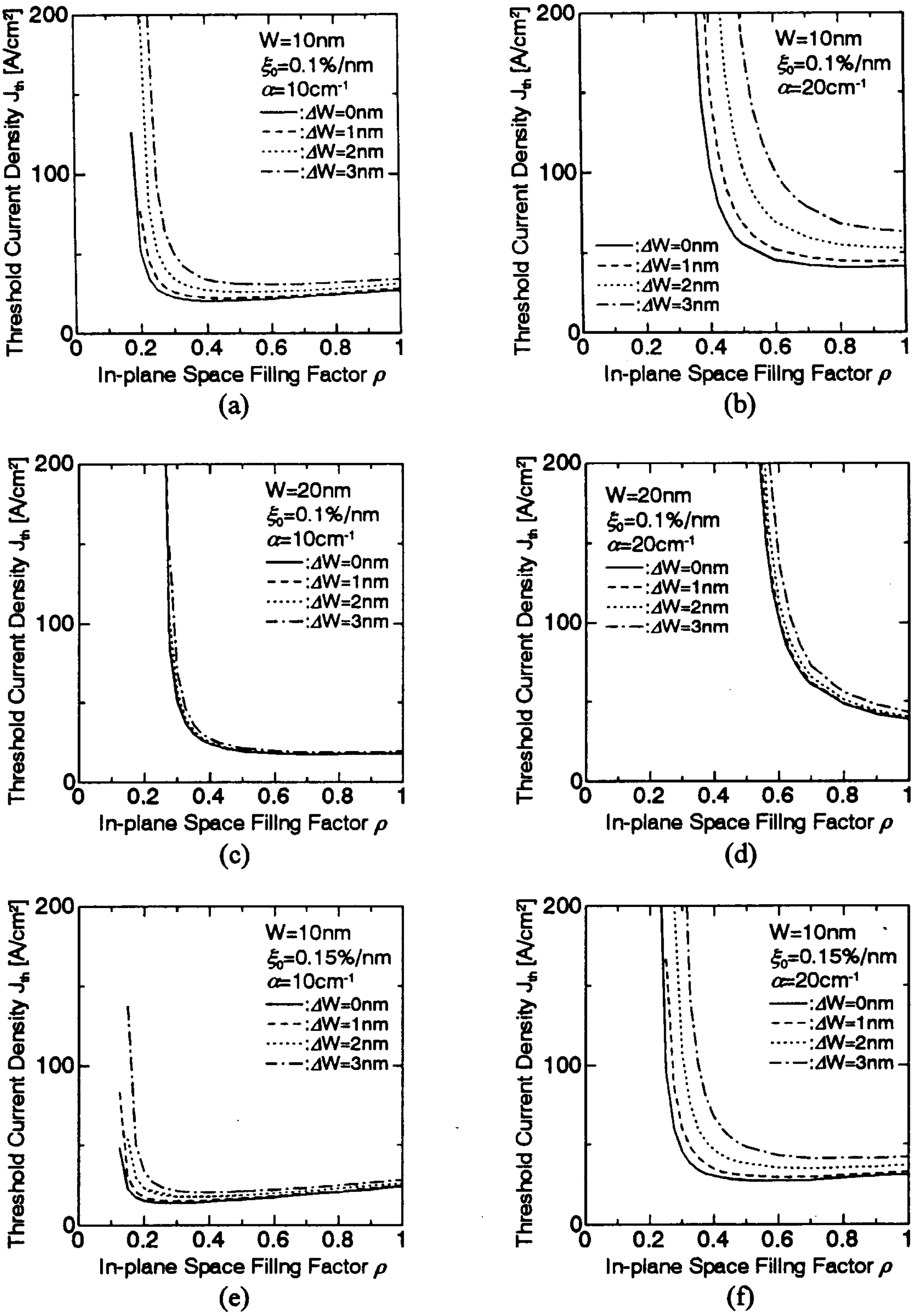

Fig. 2.9 Threshold current density J_{th} dependent on the in-plane space filling factor ρ for a parameter of the size fluctuation of Q-Wire structure ΔW.

factor ρ and the optical confinement factor of unit thickness are assumed to be ρ=0.3, 0.5, 0.7 and 1.0, and ξ_0=0.1%/nm and 0.15%/nm, respectively. In Fig.2.10 (a), in case of low ξ_{Wire}, the wire width to obtain minimum threshold current density is about 10nm due to a strong lateral confinement effect. However when the in-plane filling factor becomes larger, J_{th} is constant and independent of wire width. At low total loss, the volume effect is more dominant than the quantum effect. At α=10cm^{-1}, ρ of 0.5 is better to obtain low J_{th}. The wire width dependence of J_{th} is similar under similar optical confinement factors, such as ξ_{Wire}=0.36% (b) and 0.4% (c), 0.6% (d) and 0.56% (e), and 0.84% (f) and 0.8% (g). The increase in J_{th} due to size fluctuation is negligibly small at W>25nm. When the ξ_{Wire} is larger than 0.36%, the wire width to obtain low threshold current density is estimated to be 20nm considering the size fluctuation. When the total loss is 20cm^{-1}, which corresponds to the cavity length of about 1mm, J_{th} seems to decrease with an increase in the optical confinement factor. The minimal threshold current density can be obtained with W=10-20nm. J_{th} is minimum with W=20nm for ξ_{Wire}>0.8% and with W=10nm for ξ_{Wire}<0.8%. However when the size fluctuation is large, 20nm-wide Q-Wire is better even if ρ=0.5. The wire width dependence of J_{th} is also similar under similar optical confinement factors. In case of α=30cm^{-1}, minimal J_{th} is obtained with W=10nm for ξ_{Wire}<0.8% and with W=20nm for ξ_{Wire}>0.8% due to small size fluctuation. When the total loss is 40-50cm^{-1}, the lasing operation cannot be obtained with ξ_{Wire}<0.8%. A relatively low threshold current operation will be obtained for 10-20nm wide Q-Wire, even though the loss is as large as 50cm^{-1}, only the multi-stacked Q-Wire is necessary for ρ=1. It should be noted that the threshold current density of 8nm-thick Q-Film laser rapidly increased at α>30cm^{-1} for ξ_0 =0.1%/nm, and at α>40cm^{-1} for ξ_0 =0.15%/nm.

At low temperatures, as the total cavity loss becomes small, it will be relatively easier to obtain high performance of single-layer Q-Wire lasers. Figure 2.14 shows the wire width dependence of threshold current density at T=90K as a parameter of size fluctuation with various conditions; (a) α=10cm^{-1} and ρ=0.3, (b) α=10cm^{-1} and ρ=0.5, (c) α=10cm^{-1} and ρ=0.7, (d) α=10cm^{-1} and ρ=1.0, (e) α=20cm^{-1} and ρ=0.5,

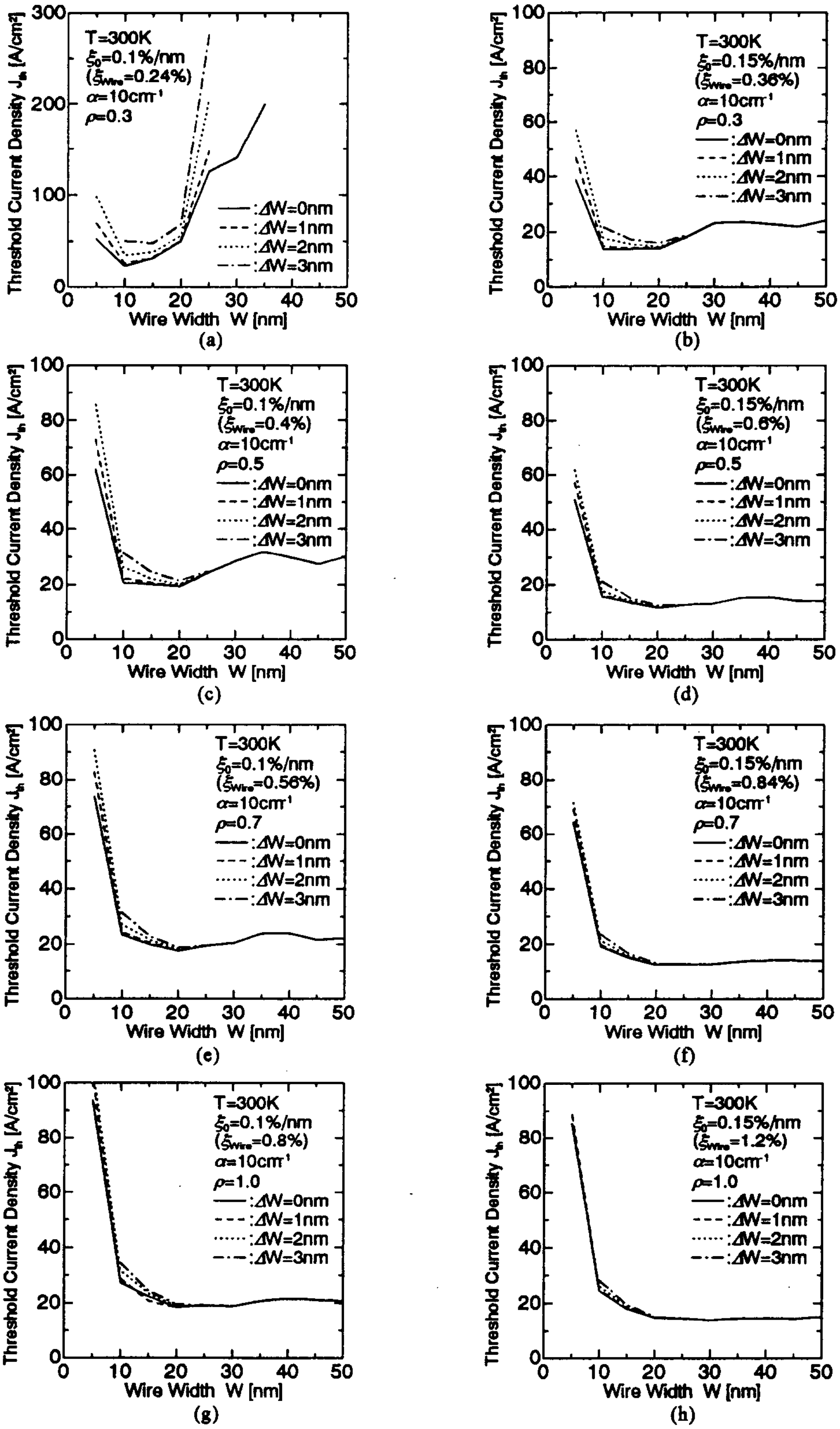

Fig. 2.10 Wire width dependence of threshold current density at T=300K at α=10cm^{-1}.

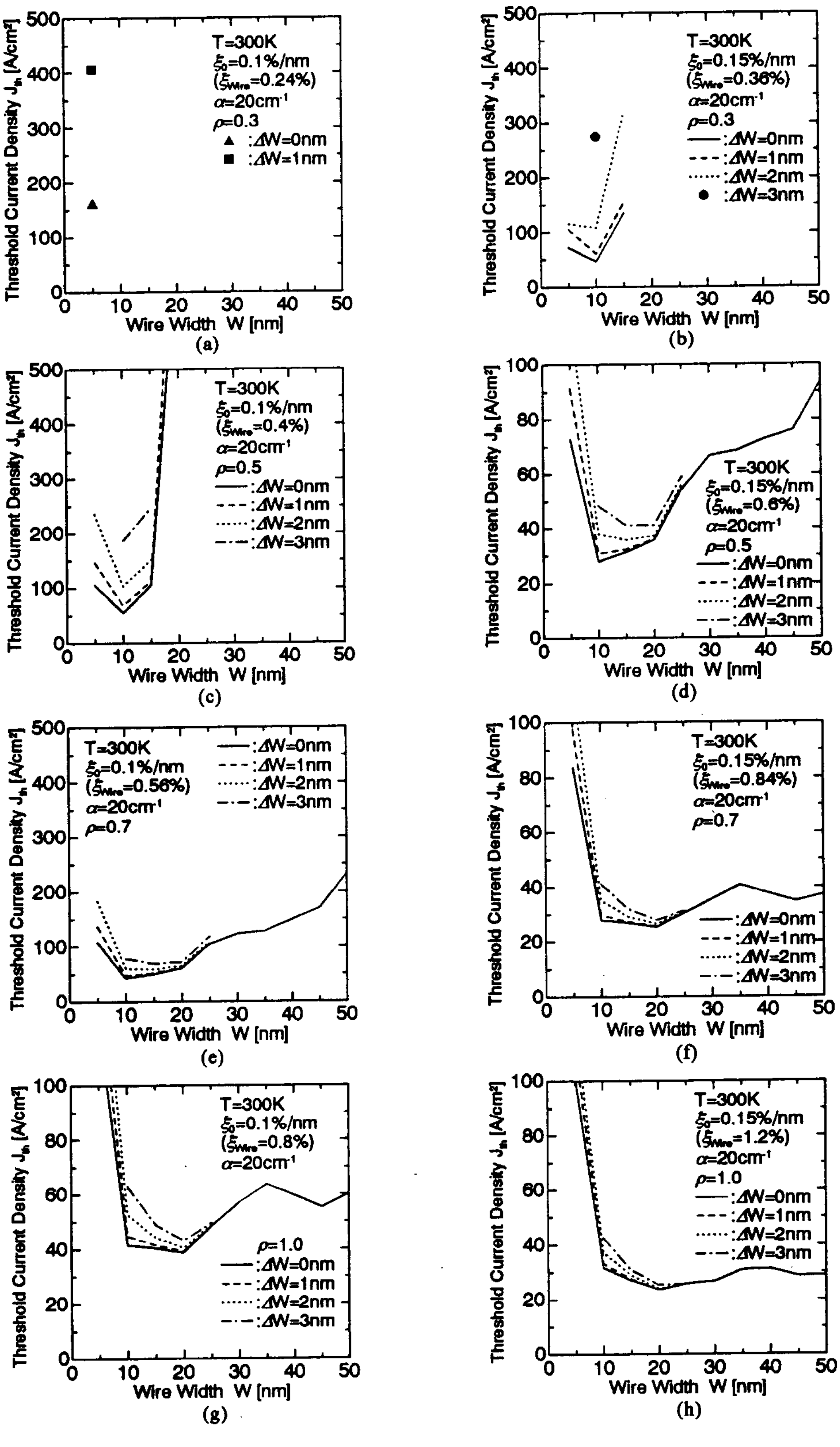

Fig. 2.11 Wire width dependence of threshold current density at T=300K at α=20cm^{-1}.

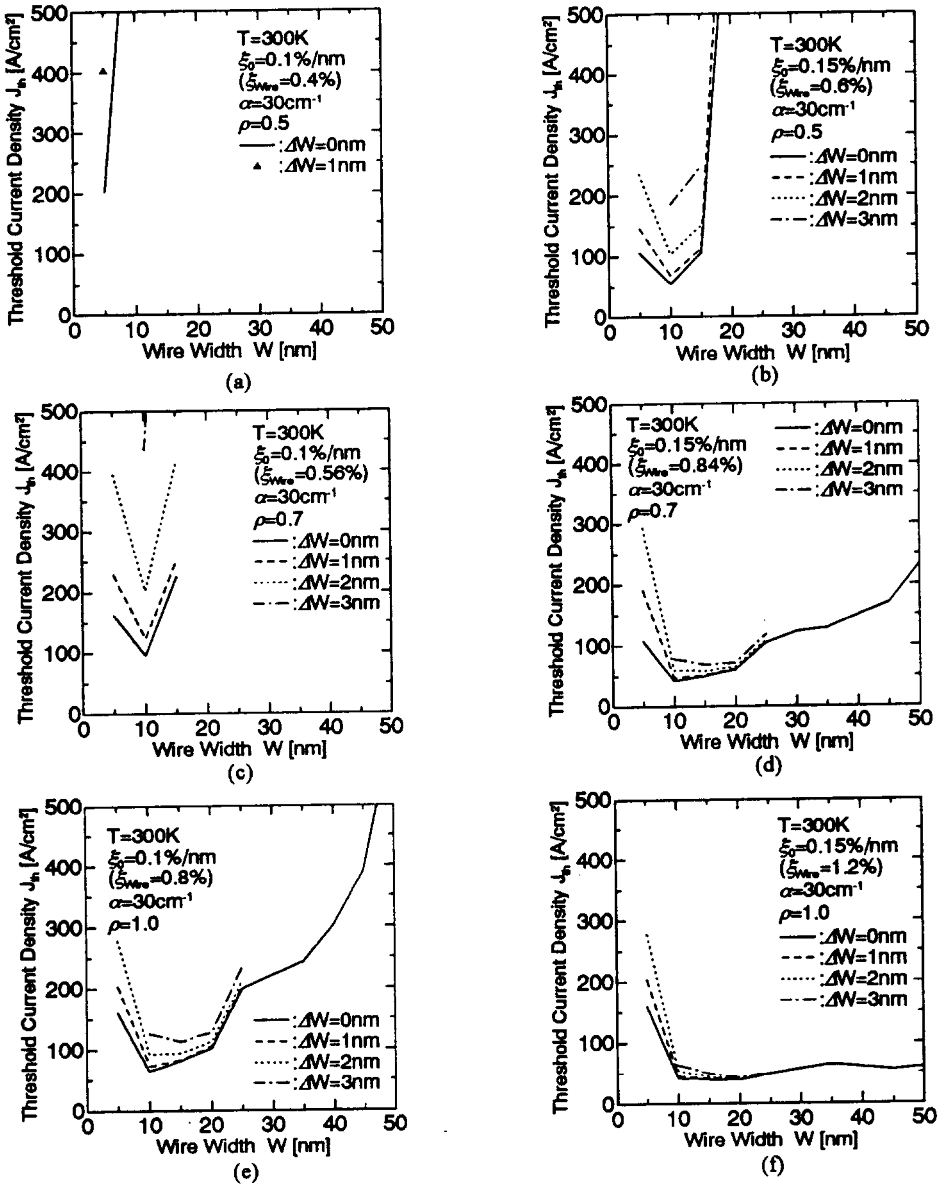

Fig. 2.12 Wire width dependence of threshold current density at T=300K at α=30cm^{-1}.

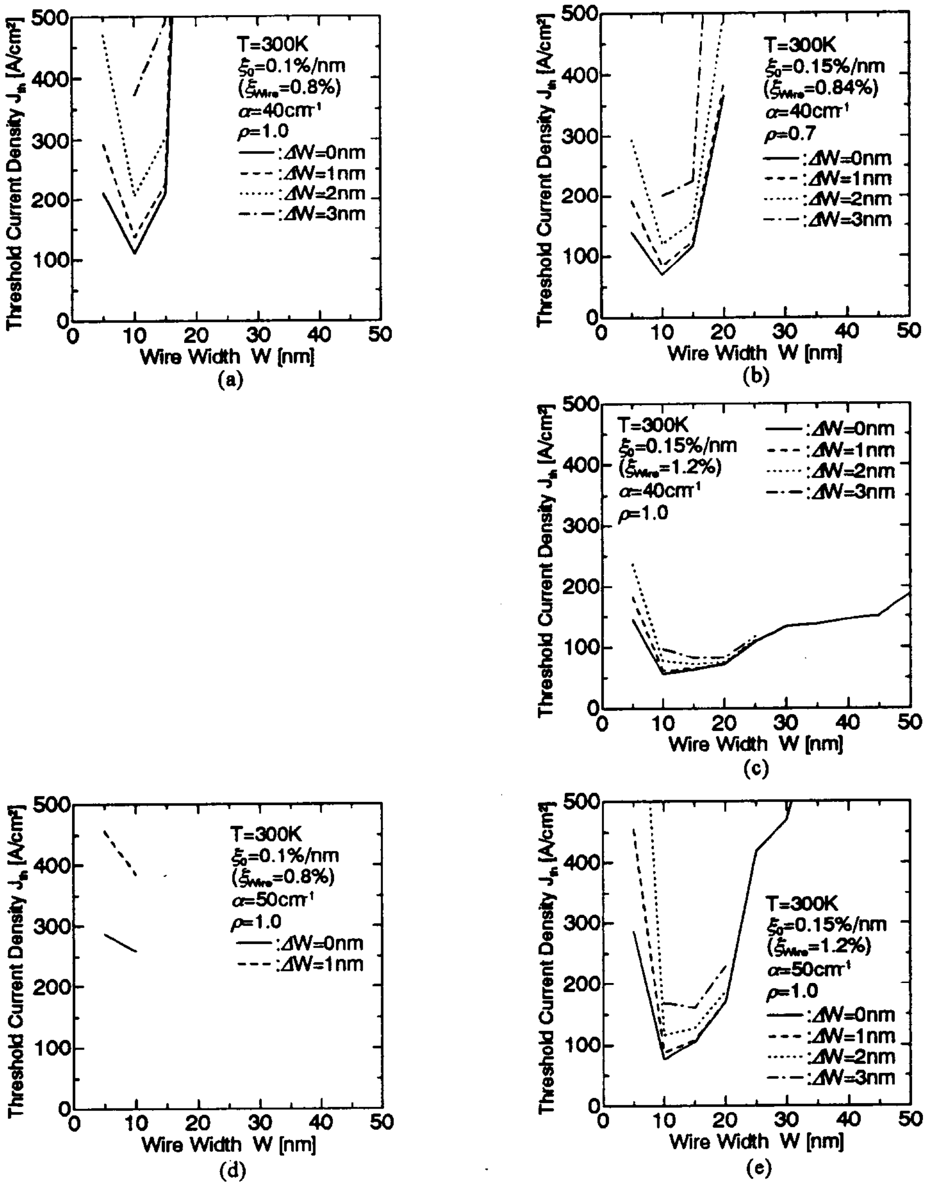

Fig. 2.13 Wire width dependence of threshold current density at T=300K at α=40-50cm^{-1}.

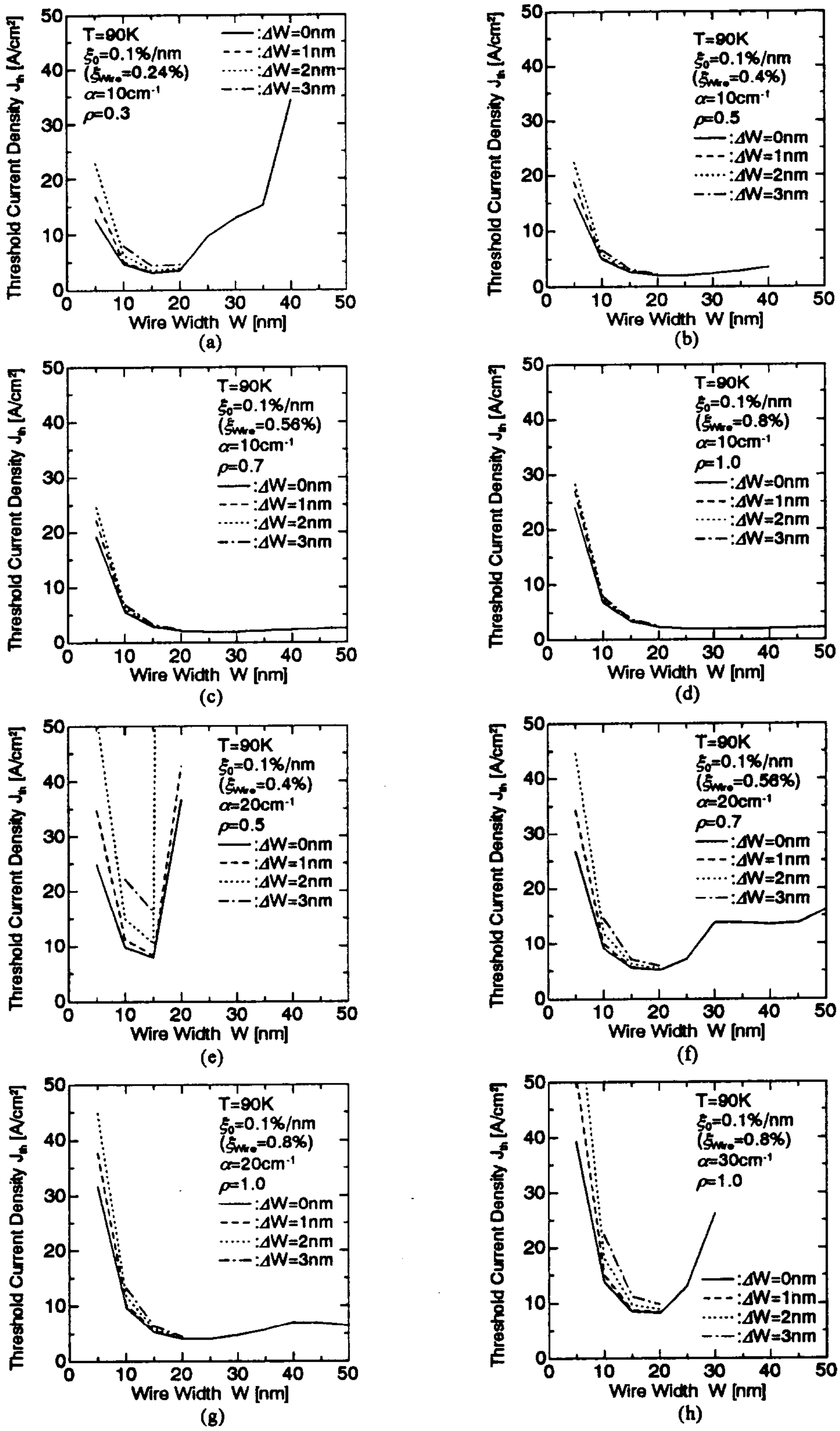

Fig. 2.14 Wire width dependence of threshold current density at T=90K at α=10-30cm^{-1}.

(f) α=20cm^{-1} and ρ=0.7, (g) α=20cm^{-1} and ρ=1.0, and (h) α=30cm^{-1} and ρ=1.0. The ξ_0 of all cases is 0.1%/nm. As can be seen, the tendency is similar to that at T=300K, but the wire size obtaining the minimum J_{th} is a little wider, i.e. 15-20nm, and the increase in J_{th} seems to be suppressed. In summary, high performance of single-layer Q-Wire laser can be operated at the total cavity loss of less than 30cm^{-1}.

Then the threshold current of Q-Wire lasers is compared with that of Q-Film lasers. Normalized threshold current $I_{th,Wire}/I_{th,Film}$ can be given by

$$\frac{I_{th,Wire}}{I_{th,Film}} = \frac{eV_{a,Wire}B_{eff}N_{th,Wire}^2}{eV_{a,Film}B_{eff}N_{th,Film}^2} \tag{2.14}$$

$$= \frac{J_{th,Wire}\cdot(n\cdot\rho)}{J_{th,Film}} \tag{2.15}$$

where $V_{a,Wire}$ or $V_{a,Film}$ is the volume of active region of Q-Wire or Q-Film, respectively. In this analysis, it is assumed that all carriers inject in the active region. Figure 2.15 shows the optical confinement factor dependence of a normalized threshold current $I_{th,Wire}/I_{th,Film}$ considering the size fluctuation of Q-Wire width. The wire width of 20nm is assumed and the periods of Q-Wire Λ are assumed to be 70nm, 50nm, 40nm, and 30nm, respectively. The optical confinement factors of SQW in unit thickness are ξ_0=0.1%/nm, ξ_0=0.15%/nm, and ξ_0=0.2%/nm, respectively. The influence of size fluctuation is small and the in-plane space filling factor obtaining minimum normalized threshold current is estimated to be 0.4-0.5 in the case of ξ_0=0.1%/nm. In ref. [2-20], the optimal space filling factor to obtain a minimum threshold current was reported to be 0.8 i.e., ξ_{Wire}=0.8%, for $Ga_{0.47}In_{0.53}As$/InP Q-Wire laser at a=10cm^{-1}. Our results seem to be about half that in ref. [2-20]. This is attributed to a higher differential gain of compressively-strained material than that of lattice-matched one. In case of W=10nm, the optical confinement factor dependence of normalized threshold current is shown in Fig. 2.16. The periods of Q-Wire Λ are assumed to be 70nm, 50nm, 40nm, 30nm, and 20nm, respectively. The increasing ratio of normalized threshold current due to size fluctuation is larger than that in case of W=20nm. However when the total cavity loss is smaller than 20cm^{-1}, lower $I_{th,Wire}$ can be obtained with ΔW=3nm. The larger total loss α becomes, the larger in-plane space-filling factor is, i.e. a larger optical confinement factor should be necessary. The minimal in-plane space filling factor of Q-Wire lasers to obtain lower J_{th} than that of Q-Film laser are listed in Table 2.1 for W=20nm and Table 2.2 for W=10nm, respectively. Figure 2.17 shows the optical confinement factor dependence of normalized threshold currents of a 20nm-wide Q-Wire as a parameter of α, which are plotted for ξ_0=0.1%/nm, 0.15%/nm, and 0.2%/nm. The tendency is similar to that of SQW as shown in Fig. 2.7, i.e., normalized threshold current density is constant and independent of the optical confinement factor at low loss conditions. In Fig. 2.17(d), the data for W=10nm are also plotted as a comparison. In case of α=50cm^{-1}, I_{th} of the 20nm-wide Q-Wire cannot be lower than that of Q-Film, but it will be expected I_{th} of 10nm-wide Q-Wire laser is half that of Q-Film by means of suppressing the size fluctuation within 2nm. At low temperatures, as the total cavity loss becomes small, it will be relatively easier to obtain high performance of single-layer Q-Wire lasers. Figure 2.18 shows the optical confinement factor dependence of normalized threshold currents at T=90K for (a) W=20nm and (b) W=10nm, respectively. There are assumed to be α=10cm^{-1} and 20cm^{-1}, and ξ_0=0.1%/nm. The tendency is similar to that at room temperature. At low temperatures, better lasing properties do not seem to be expected in the case of W=10nm. However in the case of W=20nm, it can be obtained half that of Q-Film laser when the in-plane space filing factor is 0.4 to 0.5.

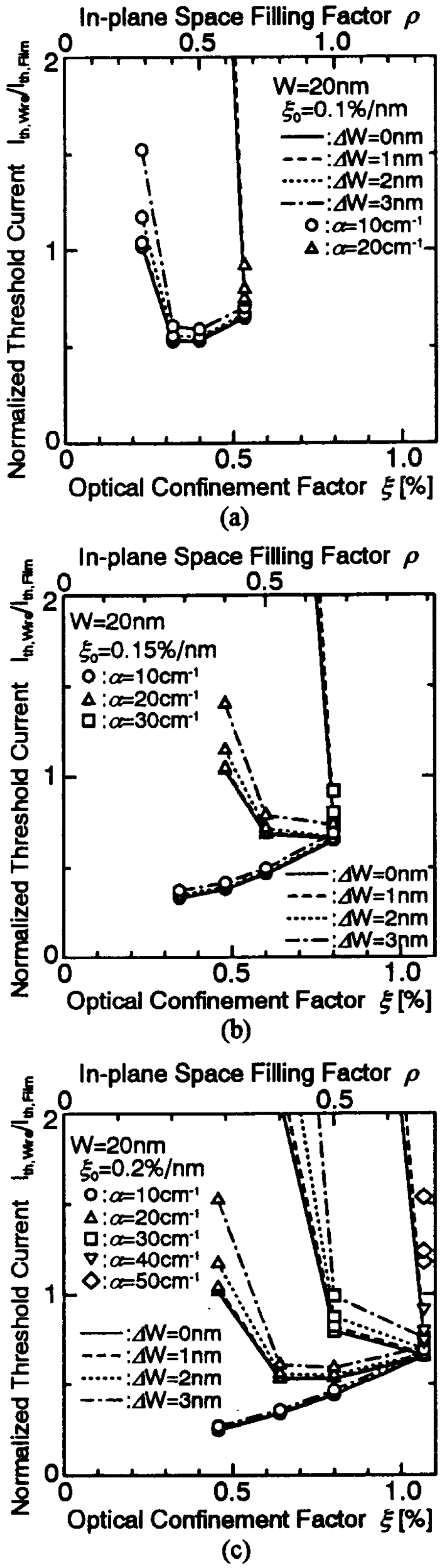

Fig. 2.15 The optical confinement factor dependence of a normalized threshold current with W=20nm considering the size fluctuation.

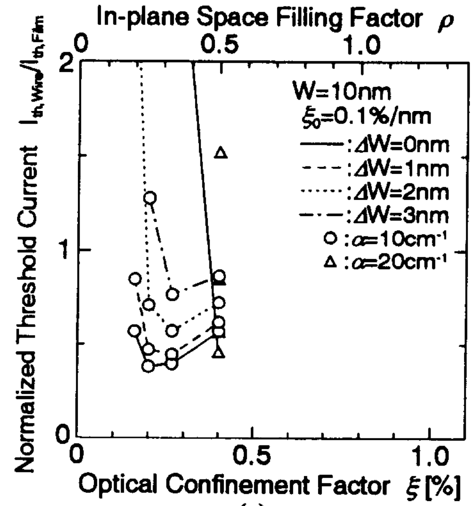

(a)

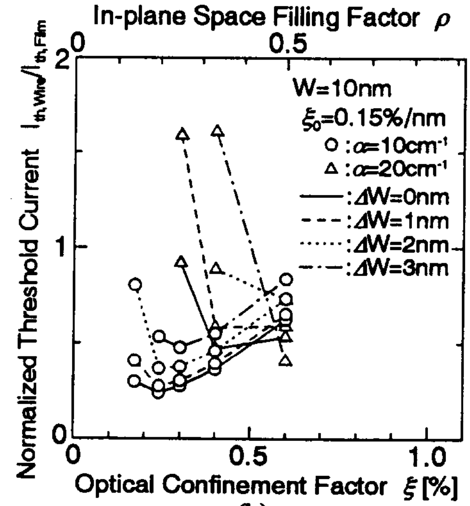

(b)

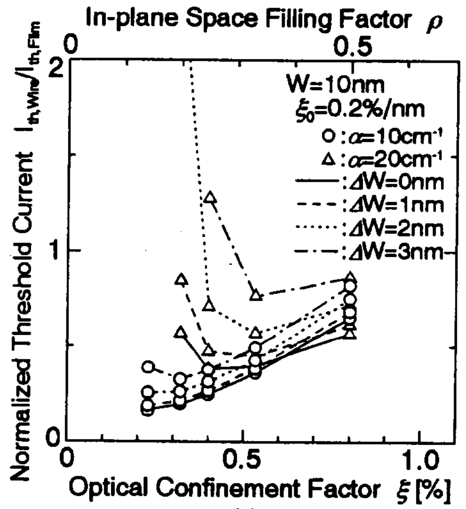

(c)

Fig. 2.16 The optical confinement factor dependence of a normalized threshold current with W=10nm considering the size fluctuation.

Table 2.1 Minimal in-plane space filling factor of Q-Wire lasers to obtain lower J_{th} than that of Q-Film laser for W=20nm.

ξ_0	α=10cm^{-1}			α=20cm^{-1}			α=30cm^{-1}			α=40cm^{-1}			α=50cm^{-1}		
	ρ	Λ	ξ_{Wire}	ρ	Λ	ξ_{Wire}	ρ	Λ	ξ_{Wire}	ρ	Λ	ξ_{Wire}	ρ	Λ	ξ_{Wire}
0.1%/nm	0.5	40	0.4	0.67	30	0.53	—	—	—	—	—	—	—	—	—
0.15%/nm	0.29	70	0.34	0.5	40	0.6	0.67	30	0.8	—	—	—	—	—	—
0.2%/nm	0.29	70	0.46	0.4	50	0.64	0.67	30	1.07	0.67	30	1.07	—	—	—

Table 2.2 Minimal in-plane space filling factor of Q-Wire lasers to obtain lower J_{th} than that of Q-Film laser for W=10nm.

ξ_0	α=10cm^{-1}			α=20cm^{-1}			α=30cm^{-1}			α=40cm^{-1}			α=50cm^{-1}		
	ρ	Λ	ξ_{Wire}	ρ	Λ	ξ_{Wire}	ρ	Λ	ξ_{Wire}	ρ	Λ	ξ_{Wire}	ρ	Λ	ξ_{Wire}
0.1%/nm	0.33	30	0.27	0.5	20	0.4	—	—	—	—	—	—	—	—	—
0.15%/nm	0.2	50	0.24	0.33	30	0.4	0.5	20	0.6	—	—	—	—	—	—
0.2%/nm	0.2	50	0.32	0.33	30	0.53	0.5	20	0.8	0.5	20	0.8	0.5	20	0.8

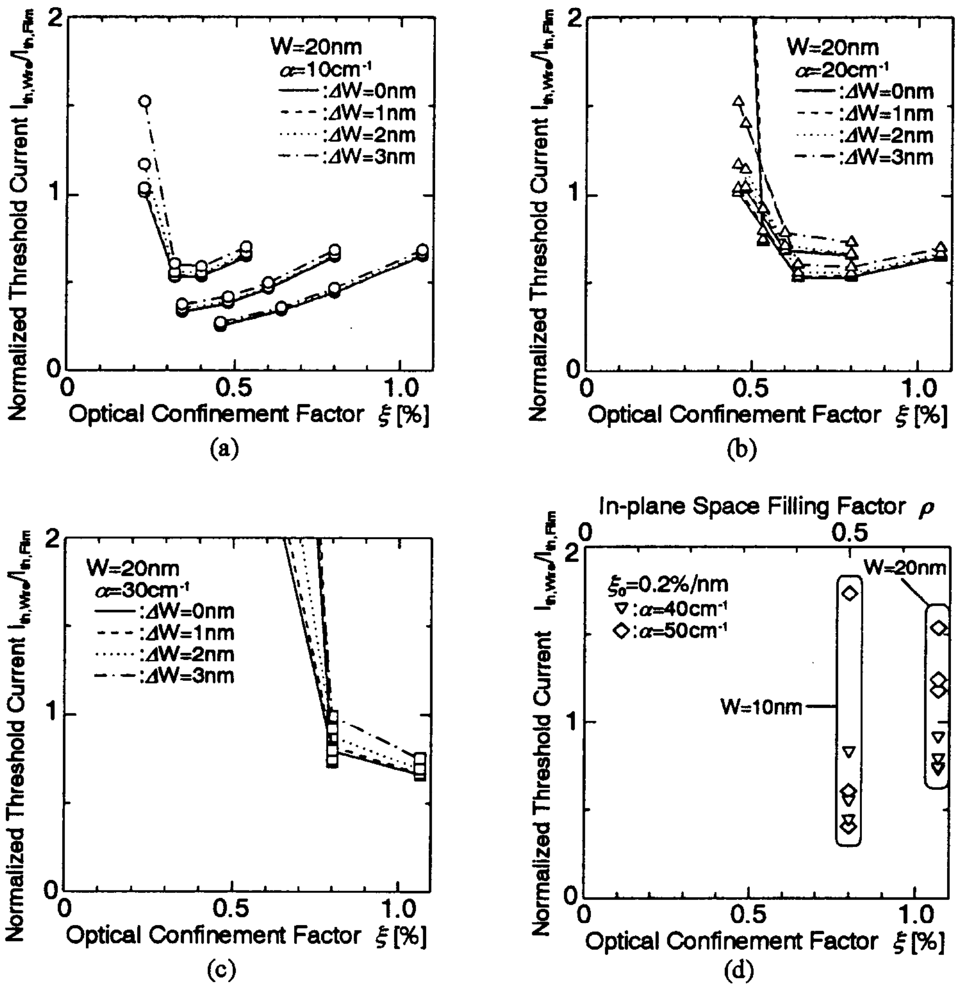

Fig. 2.17 The optical confinement factor dependence of a normalized threshold current with W=20nm as a parameter of the total cavity loss.

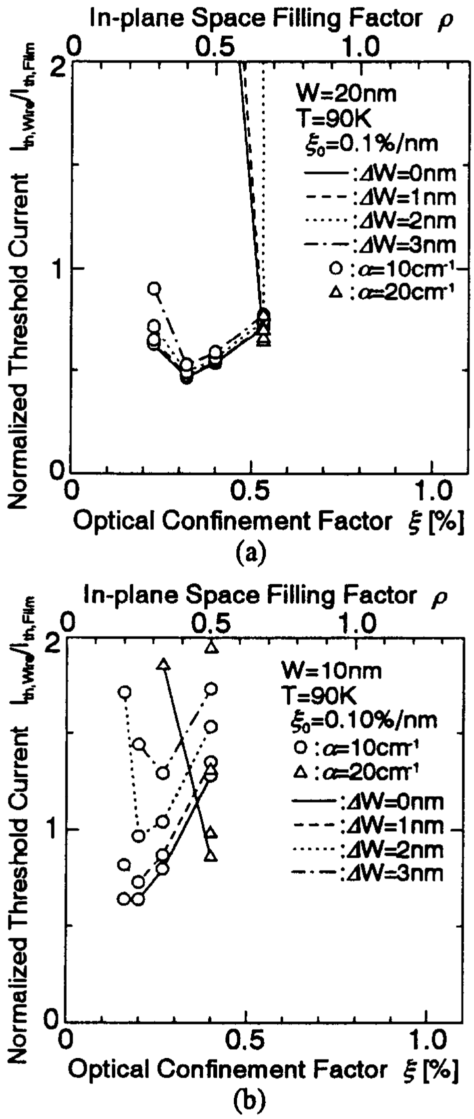

Fig. 2.18 The optical confinement factor dependence of normalized threshold currents at T=90K for (a) W=20nm and (b) W=10nm.

2.4 Conclusion

The most effective size of the Q-Wire was estimated from the point of material gain and threshold current density, considering the size fluctuation of Q-Wire structure and the optical confinement factor. At T=300K, the width to obtain maximum gain is about 8nm (7-10nm) with no size fluctuation. However the width to obtain maximum gain becomes larger and the maximum gain is reduced with an increase in the size fluctuation, and the size fluctuation effect is negligible if the wire width is larger than 22nm. The tendency of the size fluctuation effect is similar at T=90K but the influence of size fluctuation is smaller compared with that at T=300K. This is because energy broadening due to thermal energy becomes small at low temperature.

From the point of threshold current, the minimum threshold current density can be obtained with the wire width of 10-20nm. It is possible to realize high performance of single-layer Q-Wire lasers at room temperature under the condition of low cavity loss structures, such as a long-cavity structure or a high reflective (HR) coating of facets. At low temperatures, as the energy broadening due to thermal excitation and optical losses due to nonradiative recombination is reduced, it is relatively easier to obtain high performance of single-layer Q-Wire lasers. In the case of W=20nm, the threshold current of Q-Wire laser is estimated to be half that of Q-Film laser when the in-plane space filing factor of Q-Wire is 0.4 to 0.5.

References

[2-1] K. Kudo, Y. Nagashima, S. Tamura, S. Arai, Y. Huang and Y. Suematsu, "$Ga_{0.66}In_{0.34}As$/GaInAsP/InP tensile-strained single-quantum-well lasers with 70-nm period wire active region," ***IEEE. Photon. Technol. Lett.***, vol.5, no.8, pp.864-867, Aug. 1993.

[2-2] K. C. Shin, S. Arai, Y. Nagashima, K. Kudo, and S. Tamura, "Temperature dependences of $Ga_{0.66}In_{0.34}As$ /InP tensile-strained quasi-quantum-wire laser fabricated by wet chemical etching and 2-step OMVPE growth," ***IEEE. Photon. Technol. Lett.***, vol.7, no.4, pp.345-347, Apr. 1995.

[2-3] H. Zarem, K. Vahala, and A. Yariv, "Gain spectra of quantum wires with inhomogeneous broadening," ***IEEE. J. Quantum Electron.***, vol.QE-25, no.4, pp.705-712, Apr. 1989.

[2-4] P. J. A. Thijs, L. F. Tiemeijer, P. I. Kindersma, J. J. M. Binsma, and T. Van Dongen, "High-performance 1.5μm wavelength InGaAs-InGaAsP strained quantum well lasers and amplifiers," ***IEEE J. Quantum Electron.***, vol.27, no.6, pp.1426-1439, Jun. 1991.

[2-5] P. J. A. Thijs, J. J. M. Binsma, L. F. Tiemeijer and T. van Dongen, "Submilliamp threshold current (0.62mA at 0℃) and high output power (220mW) 1.5μm tensile strained InGaAs single quantum well lasers," ***Electron. Lett.***, vol.28, no.9, pp.829-830, Apr. 1992.

[2-6] M. P. C. M. Krijn, G. W. 't Hooft, M. J. B. Boermans, P. J. A. Thijs, T. van Dongen, J. J. M. Binsma, L. F. Tiemeijer and C. J. van der Poel, "Improved performance of compressively as well as tensile strained quantum-well lasers," ***Appl. Phys. Lett.***, vol.61, no.15, pp.1772-1774, Oct. 1992.

[2-7] M. Asada and Y. Suematsu, "Density-matrix theory of semiconductor lasers with relaxation broadening model –Gain and gain-suppression in semiconductor lasers," ***IEEE J. Quantum Electron.***, vol.QE-21, no.5, pp.434-442, May 1985.

[2-8] M. Yamada, H. Ishiguro and H. Nagato, "Estimation of the intra-band relaxation time in undoped AlGaAs injection laser," ***Jpn. J. Appl. Phys.***, vol.19, no.1, pp.135-142, Jan. 1980.

[2-9] M. Asada, A. Kameyama and Y. Suematsu, "Gain and intervalence band absorption in quantum-well lasers," ***IEEE J. Quantum Electron.***, vol.QE-20, no.7, pp.745-753, Jul. 1984.

[2-10] M. Asada, Y. Miyamoto and Y. Suematsu, "Theoretical gain of quantum-well wire lasers," ***Jpn. J. Appl. Phys.***, vol.24, no.2, pp.L95-L97, Feb. 1985.

[2-11] M. Asada, Y. Miyamoto, and Y. Suematsu, "Gain and the threshold current of three-dimensional quantum-box lasers," ***IEEE J. Quantum Electron.***, vol.QE-22, no.9, pp.1915-1921, Sept. 1986.

[2-12] S. Ueno, Y. Miyake, and M. Asada, "Advantage of strained quantum wire lasers," ***Jpn. J. Appl. Phys.***, vol.31, pt.1, no.2A, pp.286-287, Feb. 1992.

[2-13] A. R. Adams, "Band-structure engineering for low-threshold high-efficiency semiconductor lasers," ***Electron. Lett.***, vol.22, no.5, pp.249-250, Feb. 1986.

[2-14] E. Yablonobitch and E.O. Kane, "Reduction of lasing threshold current density by the lowering of valence band effective mass," ***IEEE J. Lightwave Technol.***, vol.LT-4, no.5, pp.504-506, May 1986.

[2-15] H. Hirayama and M. Asada, "Reduction of size fluctuation effect in GaInAs/GaInAsP quantum-box lasers using tensile strained active region," ***IEEE 14th Int. Semiconductor Laser Conf.***, P4, Hawaii, pp.89-90, Sep. 1994.

[2-16] J. M. Luttinger and W. Kohn, "Motion of electrons and holes in perturbed periodic fields," ***Phys. Rev.*** vol.97, no.4, pp.869-883, Feb. 1955.

[2-17] S. Adachi, "Material parameters of $In_{1-x}Ga_xAs_yP_{1-y}$ and related binaries," J. Appl. Phys., vol.53, no.12, pp.8775-8792, Dec. 1982.

[2-18] Y. Miyake, H. Hirayama, K. Kudo, S. Tamura, S. Arai, M. Asada, Y. Miyamoto and Y. Suematsu, "Room-Temperature Operation of GaInAs/GaInAsP/InP SCH lasers with quantum-wire size active region," ***IEEE. J. Quantum Electron.***, vol.QE-29, no.6, pp.2123-2133, Jun. 1993.

[2-19] K. Stubkjaer, M. Asada, S. Arai and Y. Suematsu, "Spontaneous recombination, gain and refractive index variation for 1.6μm wavelength InGaAsP/InP lasers," ***Jpn. J. Appl. Phys.***, vol.20, no.8, pp.1499-1505, Aug. 1981.

[2-20] Y. Nambu and K. Asakawa, "Theoretical analysis of optimal conditions in quantum structure semiconductor lasers for low threshold current," ***Appl. Phys. Lett.***, vol.67, no.11, pp.1509-1511, Sep. 1995.

Chapter 3

Fabrication of Quantum-Wire Lasers

3.1 Introduction.. 71
3.2 Crystal Growth Technique... 72
3.2.1 Organometallic Vapor Phase Epitaxy..................... 72
3.2.2 GaInAsP Compressively-Strained Quantum-Well........ 75
3.3 Measurement of Size Fluctuation of Quantum-Wire Structure..... 81
3.3.1 Measurement of Size Fluctuation of EB Pattern.......... 81
3.2.2 Reduction of Size Fluctuation.............................. 83
3.4 Fabrication Process of Quantum-Wire laser......................... 87
3.5 Conclusion.. 96
References.. 97

3.1 Introduction

A FABRICATION technique using electron beam (EB) lithography and etching followed by an embedded growth with organometallic vapor phase epitaxy (OMVPE) is an effective one to fabricate the quantum-wire (Q-Wire) or quantum-box (Q-Box) lasers for long-wavelength emission as mentioned in chapter 1[3-1]-[3-3], though numerous works have been reported on the fabrication of such devices with low-dimensional quantum structures[3-1]-[3-9]. As it is also a better technique for the position and size controllability of Q-Wire and Q-Box structures, it is suitable for use in production of distributed feedback (DFB) lasers consisting of a Q-Wire or

Q-Box active region[3-10]-[3-12]. In order to realize high performance operation of Q-Wire (-Box) lasers, it is important to control size fluctuation within 10% (20%)[3-13]-[3-15]. In this chapter, the fabrication process of Q-Wire lasers is described, including the crystal growth technique using OMVPE. The size uniformity of a Q-Wire pattern formed by EB lithography was also investigated.

3.2 Crystal Growth Technique

3.2.1 Organometallic Vapor Phase Epitaxy

In this study, the OMVPE system with a horizontal reactor (HR3246, Nippon Sanso) was used for the growth of initial wafers, whose photograph is shown in Fig. 3.1. The reactor never exposed to the air in case of loading wafers because this had a preparation chamber. The epitaxial growth was done on a carbon susceptor coated with SiC under the condition of the growth temperature T_g=600℃ heated by RF coil and the low pressure of 76Torr with the substrate rotation (12rpm). Trimethyl Indium (TMI), two lines of Triethyl Gallium (TEG), and Trimehtyl Aluminum (TMA) can be used as the group-III sources. By the use of a gas concentration monitoring system (Epison III) for TMI, the reproduction of the growth condition can be much improved. The super PH_3 (100%), and two kinds of AsH_3; one is the super AsH_3 (100%) and the other is the diluted AsH_3 (1%) in H_2, can be used as the group-V sources. Therefore the GaInAs(P) layers at the bandgap wavelength between 1.0μm and 1.65μm can be grown. Tertiarybutylphosphine (TBP) can be also used as the group-V source to enhance the vapor pressure of phosphorus[3-16],[3-17]. Dimetyl Zinc (DMZn) and Disilane (Si_2H_6) are employed as p- and n-type dopant, respectively, which the dopant concentration can be controlled more than two orders by using two types of mass flow controller (MFC). The H_2 carrier gas was used with the flow rate of 17slm including the side-flow to improve the growth uniformity, and the velocity of which at the position of the substrate in reactor is about 50cm/sec. This gas-flow velocity with quick run-vent switching systems.enable to make a sharp interfaces of grown GaInAsP multiple quantum wells (MQWs).

The vapor pressure P_x (x=TMI, TEG, TMA, and TBP) at the temperature T K is given by

$$log_{10} P_{TMI} = 10.52 - 3014/T, \quad (3.1)$$

$$log_{10} P_{TEG} = 8.234 - 2222/T, \quad (3.2)$$

$$log_{10} P_{TMA} = 8.999 - 2361.2/T, \quad (3.3)$$

$$log_{10} P_{TBP} = 7.586 - 1539/T. \quad (3.4)$$

In the OMVPE growth, the temperatures of TMI, TEG, TMA, and TBP are 32℃, 25℃, 20℃, and 30℃, respectively. Mole flow rates I_x (x=TMI, TEG, and TMA) can be described as

$$I_x = \frac{P_x}{P_{bubbler}} I_{carrier}, \quad (3.5)$$

where $P_{bubbler}$ and $I_{carrier}$ are the pressure in the bubbler and the H_2 carrier gas flow rate to the each bubbler, respectively. $P_{bubbler}$ for all the bubblers is 760Torr. Using low pressure conditions, the direct supply of TBP is possible.

The bandgap energy E_g and lattice constant a of quaternary $Ga_xIn_{1-x}As_yP_{1-y}$ is given by

$$\begin{aligned} E_g &= 1.35 + 0.672x - 1.091y + 0.758x^2 + 0.101y^2 \\ &+ 0.111xy - 0.580x^2y - 0.159xy^2 + 0.268x^2y^2 \end{aligned}, \quad (3.6)$$

and

$$a = 5.8687 - 0.4176x + 0.1896y + 0.125xy, \quad (3.7)$$

respectively. Our OMVPE system can be grow one 2-inch wafer. The in-plane uniformity of thickness is about ±1.63% for InP and ±2.93% for $Ga_{0.47}In_{0.53}As$, respectively, the distribution of the composition is ±0.045% for $Ga_{0.47}In_{0.53}As$ and ±0.09% for GaInAsP emitting at 1.55μm, and in-plane uniformity of the emitting wavelength of GaInAsP (λ_g=1.55μm) is within 12nm as shown in Fig. 3.2.

Figure 3.3 shows the emitting wavelength of lattice-matched GaInAsP to InP as the function of the composition ratio in solid, As/P for V-group and Ga/In for III-group,

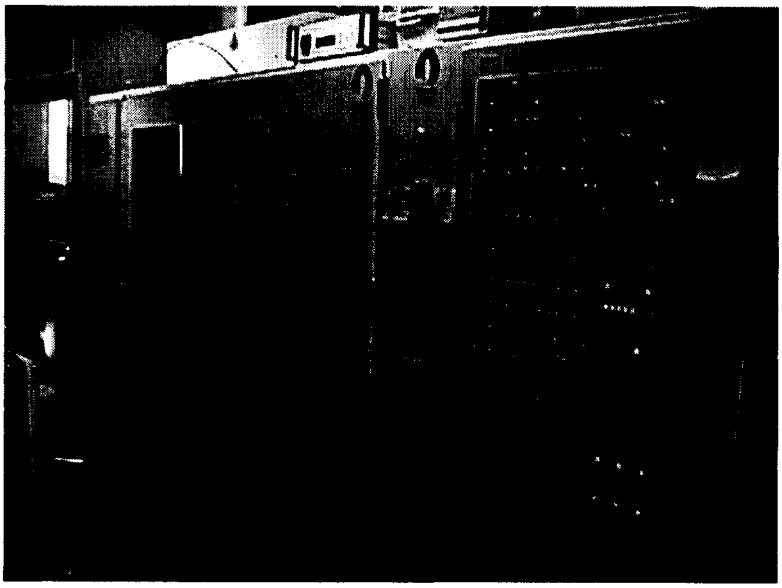

Fig. 3.1 Photograph of OMVPE system

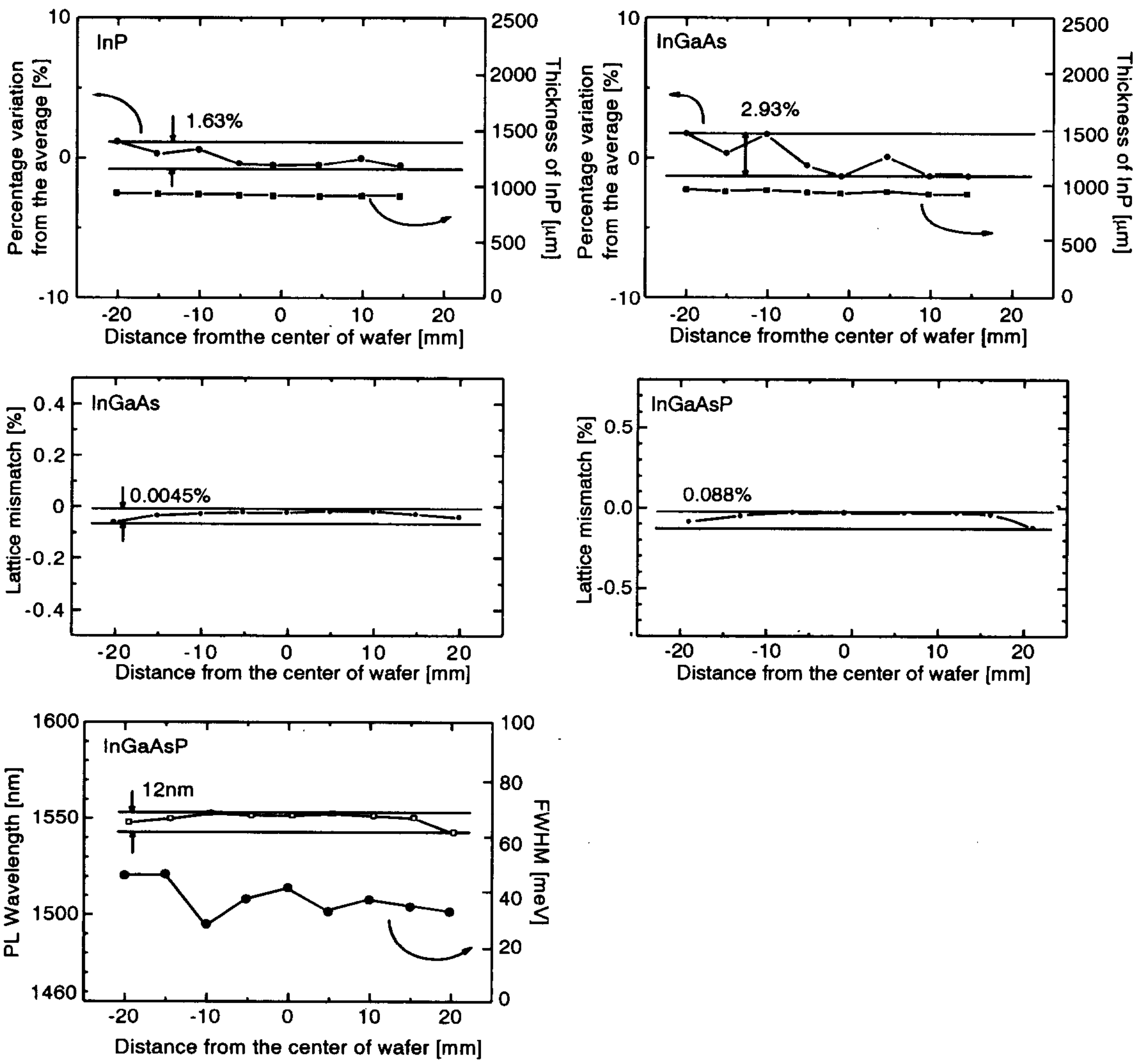

Fig. 3.2 The in-plane uniformity of OMVPE growth.

respectively. The open circles are the experimental results and the solid lines are the calculation results using the eqs. (3.6) and (3.7). As can be seen, the experimental results agreed well with the theoretical curve for both groups.

Figure 3.4 shows (a) the experimentally found relation between Ga and In content in solid and the flow rate of carrier gas for TEG and TMI, and (b) that between As and P in solid and the flow rates of AsH_3 and PH_3, respectively. The dashed line shows the fitting line by least squares. As can be seen, the relation between solid and vapor is almost linear for both groups. The simple relations between Ga/In and TEG/TMI, and between As/P and AsH_3/PH_3 of our OMVPE system can be expressed by

$$\left(\frac{Ga}{In}\right) = 0.02624 + 1.598\left(\frac{TEG}{TMI}\right), \tag{3.8}$$

and

$$\left(\frac{As}{P}\right) = 0.03927 + 52.90\left(\frac{AsH_3}{PH_3}\right). \tag{3.9}$$

In the case of $Al_{0.48}In_{0.52}As$, which is lattice-matched to InP, the relation between Al/In and TMA/TMI is shown in Fig. 3.5 and compared with that between Ga/In and TEG/TMI. The ratio of Al/In to TMA/TMI was higher than that of Ga/In to TEG/TMI. This is considered to be due to the dimer of TMA, i.e., $(TMA)_2$.

3.2.2 GaInAsP Compressively-Strained Quantum-Well

In order to realize high performance operation of long-wavelength Q-Wire lasers fabricated by EB lithography and wet chemical etching followed by OMVPE embedding growth, it is necessary to prepare the relatively thick initial Q-Film layer with compressively strained material. In the case of tensile-strained material, it is difficult to fabricate the Q-Wire lasers emitting at more than 1.5μm using GaInAs material[3-2],[3-3]. Furthermore, as the band discontinuity in the conduction band is small[3-15], it is feared that it will result in poor temperature characteristics. The compressively-strained quaternary GaInAsP seems to be an easier way to design and fabricate the relatively thick single-layer Q-Film emitting at 1.5-1.6μm than with ternary GaInAs material[3-1],[3-18]. In the case of $Ga_{0.22}In_{0.78}As_{0.80}P_{0.20}$, whose strain is about 1% CS, the flow rate of the sources can be obtained from the experimental relation between solids and vapors as shown in Fig. 3.4. The black points in Fig.3.4 shows the results in this case.

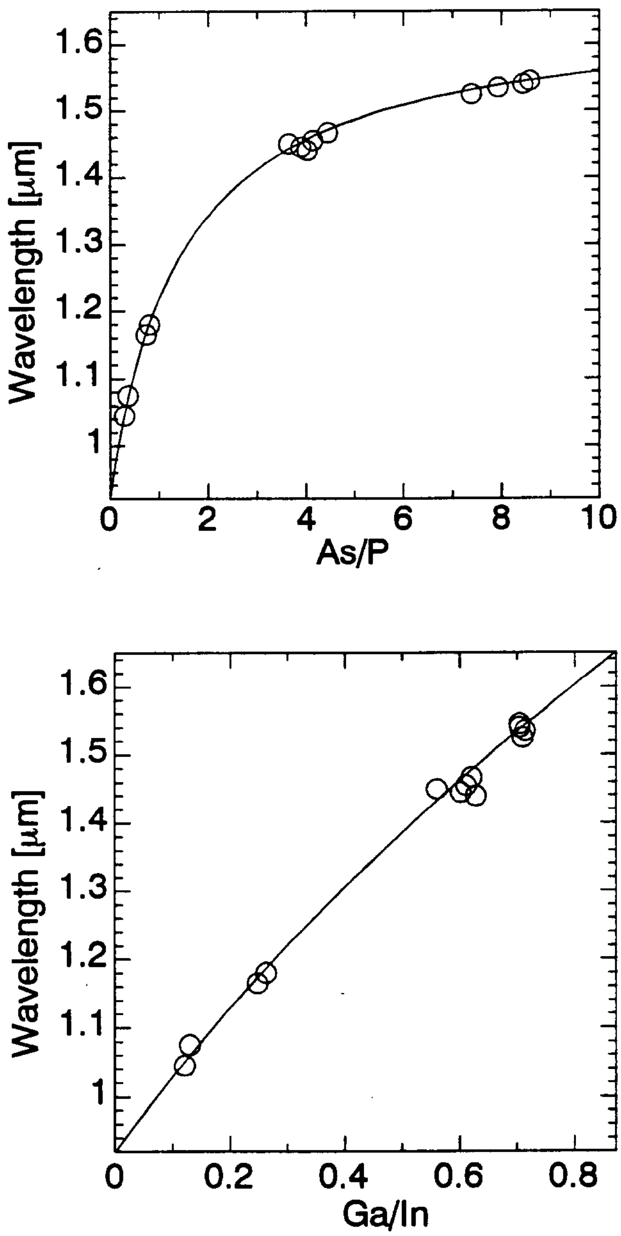

Fig. 3.3 The emitting wavelength of lattice-matched GaInAsP as the function of the composition ratio in solid, As/P for V-group and Ga/In for III-group.

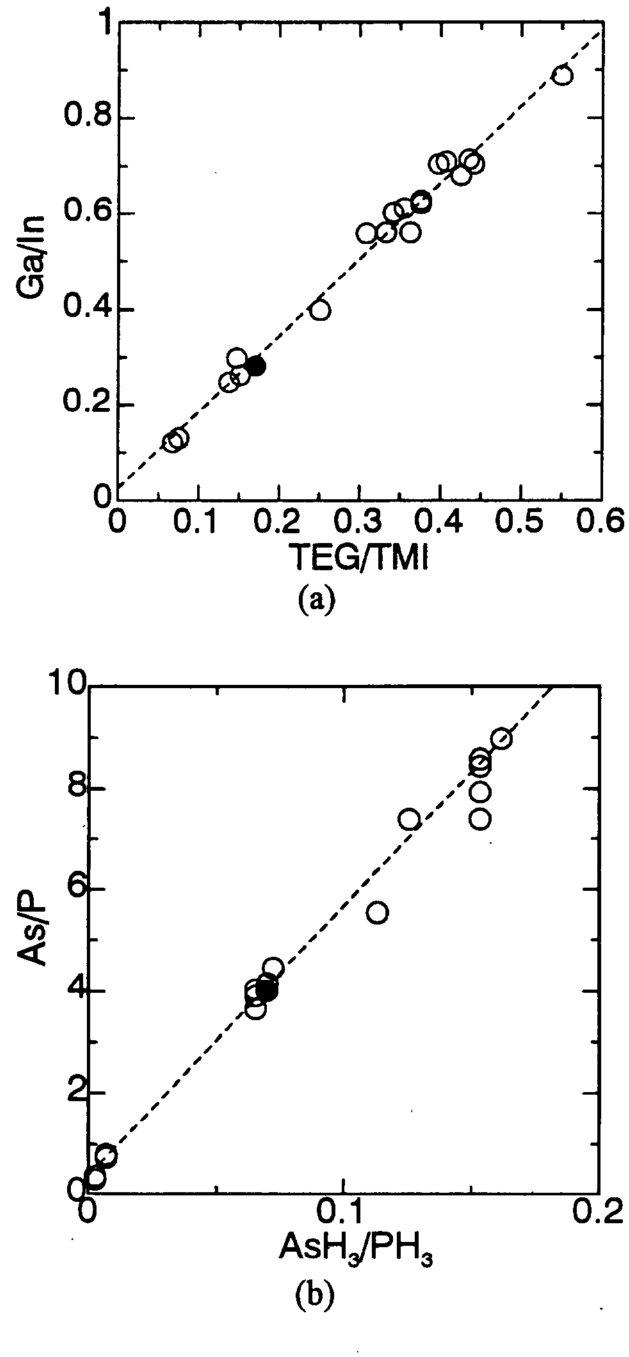

Fig. 3.4 The lattice conditions between (a) Ga/In and TEG/TMI, and (b) As/P and AsH_3 and PH_3, respectively.
The dashed lines are the fitting lines by least squared.

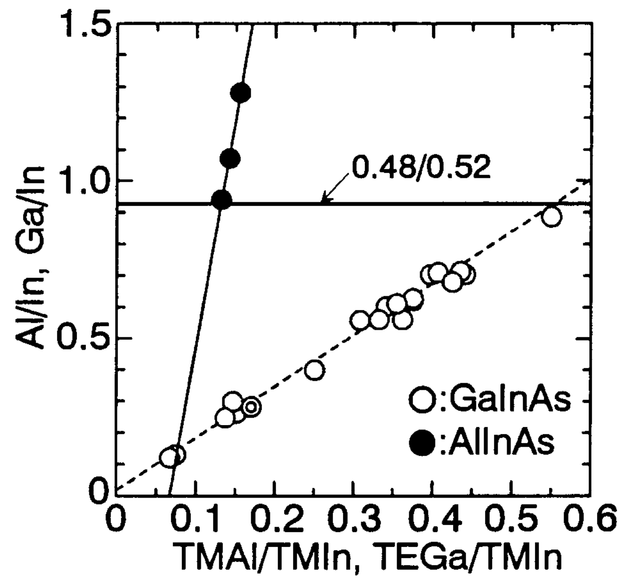

Fig. 3.5 Lattice condition of Al and In in the OMVPE system and compared with that of Ga and In.

Figure 3.6 shows the strain dependence of the full width half maximum (FWHM), the intensity, and the peak wavelength of photoluminescence (PL). When the strain was about 0.9% by the calculation, the narrowest FWHM and the highest PL intensity were obtained with the Q-Film thickness of 8nm, that PL spectrum was shown in Fig. 3.7. However with the thickness of 10-11nm, which is shown by the open marks in Fig. 3.7, the PL peak wavelength was largely shifted to the longer wavelength and the FWHM was broadened to 52meV. This is considered to be beyond the critical thickness. Adjusting the flow rate of TEG, the 10nm-thick single Q-Film was obtained with the FWHM of 39meV.

To check the growth conditions, 10nm-thick $Ga_{0.22}In_{0.78}As_{0.80}P_{0.20}$ single quantum-well mesa-striped lasers with one-step OCL (optical confinement layer) were fabricated on a p-InP substrate. Fundamental lasing properties, i.e., the cavity length dependence of the threshold current density and the differential quantum efficiency at room temperature under pulse conditions were measured.

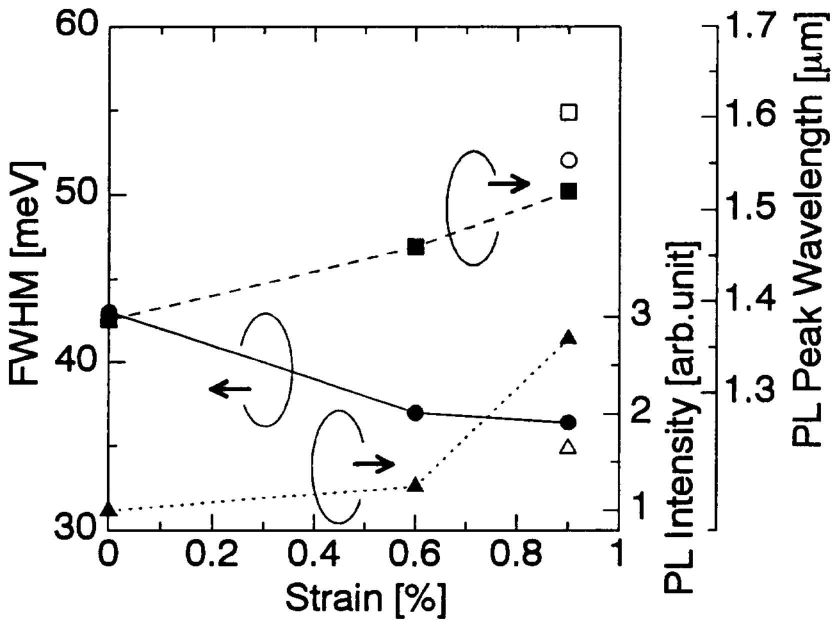

Fig. 3.6 Strain dependence of the FWHM, intensity and peak wavelength of PL.

Figure 3.8 shows the square root of threshold current density J_{th} of these three types of lasers as a function of the reciprocal cavity length $1/L$. The stripe width W_s of the lasers was 12μm. The lowest J_{th} was obtained to be 290A/cm^2 at L=2.3mm, which was comparable with that of GRIN-SCH (grated-index separate-confinement-heterostructure) lasers[3-19]. However the sudden increase of J_{th} was observed for L<650 μm, as shown in Fig. 3.8. This is attributed to gain saturation due to the low optical confinement factor of single quantum-well lasers. By fitting only in a linear gain region (L>1mm), the transparent current density J_0 was estimated to be about 100 A/cm^2.

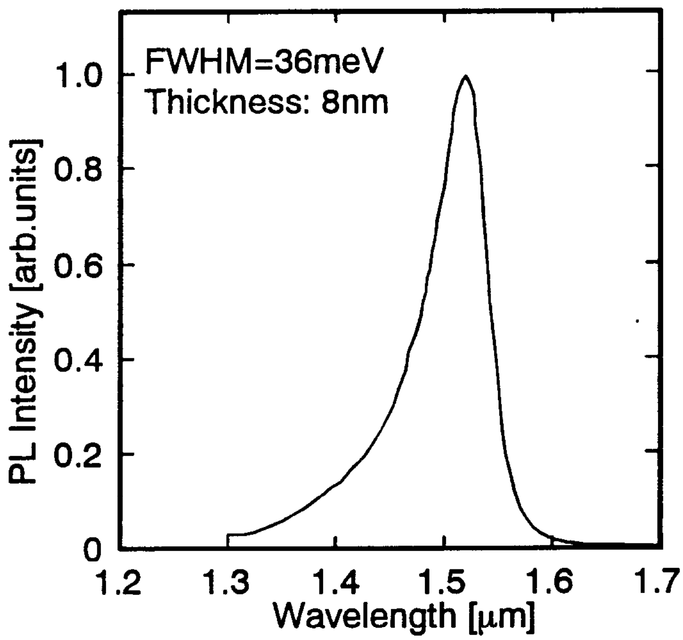

Fig. 3.7 PL spectrum of compressively strained single quantum well.

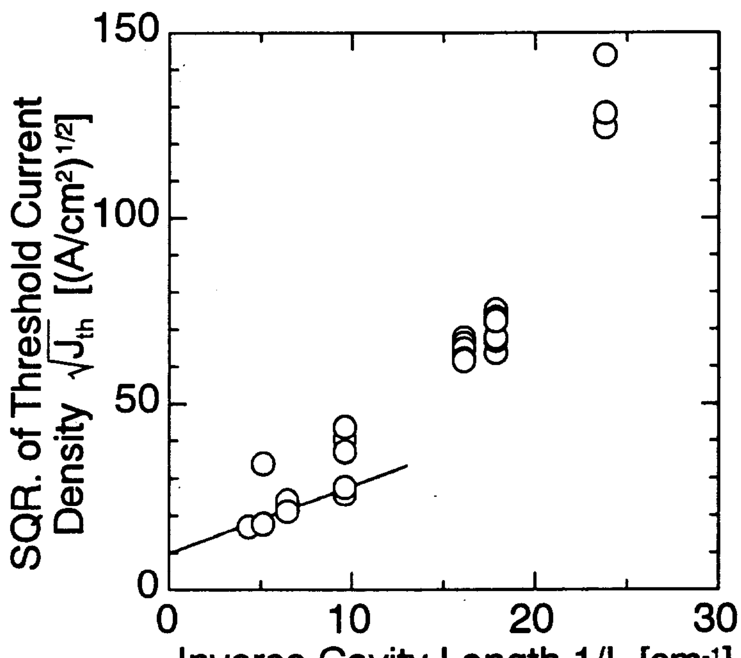

Fig. 3.8 Cavity length dependence of threshold current density of CS-SQW laser.

3.3 Measurement of Size Fluctuation of Quantum-Wire Structure

3.3.1 Measurement of Size Fluctuation of EB Pattern

For high performance operation of semiconductor lasers consisting of a Q-Wire active region, it is essential to realize high density and highly uniform Q-Wire structures in a relatively wide area because tens of thousands of Q-Wires are needed in a typical laser structure with a cavity length of several hundred micron-meters. Since there is an advantage in selecting size, material composition, and degree of strain of the Q-Wires, we have used EB lithography and an etching technique followed by an embedding growth using OMVPE[3-2],[3-20], but the size uniformity of such Q-Wire structures has not been studied as of yet. In the other fabrication methods, the size fluctuation of $\pm$3.8nm for the average wire size of 9.2nm by strain-induced lateral-layer ordering (SI-LO) of binary superlattices[3-8], and that of $\pm$4.8nm for the average dot size of 20nm by strain-induced self-organized SI-SO[3-21] growth which was reduced by higher growth temperature to that of $\pm$1.2nm for the average dot size of 50nm, were reported. Furthermore, for lasing properties multi-mode-like operation[3-22] and negative characteristic temperature[3-23] of the Quantum-Dot (Q-Dot) lasers by SI-SO were observed at a low temperature range, which were attributed to the size fluctuation of Q-Dots.

In this section, the size fluctuations of densely arranged wire patterns of EB resist and GaInAsP/InP etched structures were analyzed.

Several line patterns with various periods (Λ) were formed by JBX-5FE EBX system (JEOL) with various line dose conditions on ZEP-520 positive type EB resist[3-24] coated on 20nm thick SiO_2 deposited on InP substrate, and each pattern consisted of 300 lines with a length of 90μm. The resist was spun to a thickness of 30nm and prebaked at 180℃ for 20 minutes. After exposure, samples were developed in MIBK:IPA (1:3) solution for 45 seconds, followed by being rinsed in IPA for 15 seconds. Figures 3.9 (a) and (b) show, for example, the histogram of the line width at the center portion (for 100 wires) of a 50nm periodic pattern obtained with a dose condition of 0.8nC/cm and its SEM view, respectively. The line width was

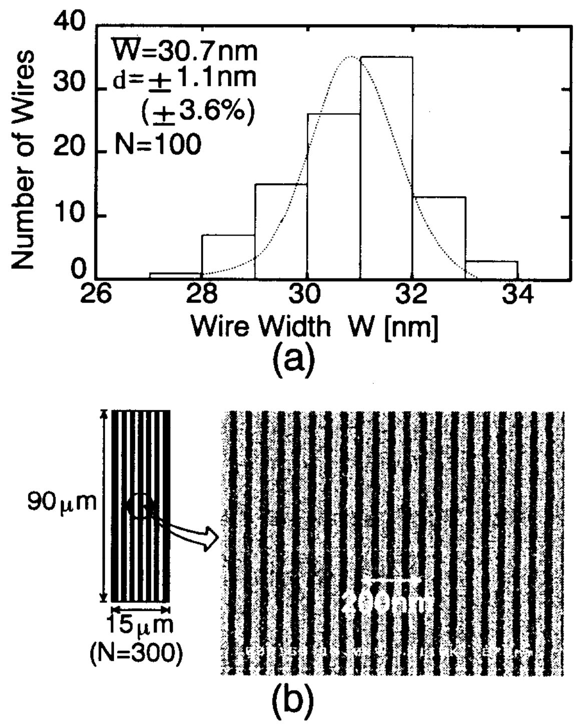

Fig. 3.9 (a) Histogram of the line width at the center portion (for 100 wires) of a 50nm periodic pattern obtained with a dose condition of 0.8nC/cm and (b) its SEM image, respectively. The average size of the line pattern was 30.7nm and the standard deviation was ±1.1nm (3.6%).

measured by a high resolution SEM (Hitachi S-5000) after sputtering thin Au/Pd film on the sample for high contrast. The average size of the line pattern of 30.7nm and its standard deviation of ±1.1nm (3.6%) was obtained for these 100 wires. The width fluctuation of a single line was also measured and its standard deviation, excluding the 5μm-long edge portions, was ±1.5nm (4.9%); however, for 300 wires, the line width at the center portion was slightly narrower than that at the edge due to the proximity effect of electrons, especially the backward scattering of electrons. The average size of the line pattern of 32.4nm and its standard deviation of approximately ±2.7nm (8.2%) was obtained for 300 wires.

3.3.2 Reduction of Size Fluctuation

The nominal beam spot size of the EBX system is 5nm at a maximum acceleration voltage of 50kV. However, for an exposure of periodic line patterns, the proximity effect due to forward/backward scattering from resist and wafer limits the line width. In order to reduce the size fluctuation of the line width between at the center portion and those at the edge, it is necessary to correct the dose profile for the proximity effect. At first, the line exposure distributions were measured so as to give an electron range at each dose due to the forward/backward electron scattering. Energy E which is given to the resist is shown by the product of dose D and a distribution function $f(x)$,

$$E(x) = K \cdot D \cdot f(x) \tag{4.10}$$

Here x is the distance from the beam incident point and K is a coefficient. The distribution function $f(x)$ is given as follows[3-25],

$$f(x) = A\,exp\left\{-\left(\frac{x}{\alpha}\right)^2\right\} + B\,exp\left\{-\left(\frac{x}{\beta}\right)^2\right\} + C\,exp\left\{-\left(\frac{x}{\gamma}\right)\right\} \tag{4.11}$$

which can be experimentally estimated by fitting the line exposure distributions[3-26]. Using this function, the dose profile for the correction of the proximity effect was estimated. Figure 3.10 shows the line width distribution of 300 wires obtained with (a) a constant dose condition of 0.8nC/cm and (b) a corrected dose profile from 0.8 (at the center portion) to 1.42nC/cm (at the edge portion). As can be seen in Fig. 3.10(b), the size fluctuation was reduced and the average size of the line pattern of 25.5nm and its standard deviation of $\pm$1.4nm (5.5%) was obtained, which was almost half the value of that without the dose profile correction.

Next, we measured the wire width after a wet chemical etching process. The sample wafer consists of a GaInAsP (λ_{PL}=1.2μm, 200nm thick) barrier layer, compressively-strained (1%-CS) GaInAsP quantum-well (λ_{PL}=1.56μm, 8nm thick), GaInAsP (λ_{PL}=1.2μm, 4nm thick) barrier layer and 4nm thick InP top layer grown on (100) p-InP substrate. In order to fabricate a quantum-wire structure, we used 40ppm (volume ratio) Br-methanol, and the line pattern was made along the $<01\bar{1}>$

direction so as to form mesa structures with relatively smooth sidewall surfaces by using orientation dependent chemical etching. Figure 3.11 shows the wire width distribution of 300 wires with (a) a constant dose condition of 0.8nC/cm and (b) a corrected dose profile from 0.8 (at the center portion) to 1.42nC/cm (at the edge portion). The standard deviation was reduced from ±3.8nm to ±2.9nm (9%) by the proximity effect correction. Since a size fluctuation of approximately ±1nm is required for high performance operation of quantum-wire lasers with the wire width of around 10nm[3-13],[3-14], further improvements are required.

Recently, the reason for the linewidth fluctuation of the resist pattern was reported due to the granular structure of the ZEP-520 resist film, of which the diameter was more than 30nm[3-27]. When the narrower wire patterns are fabricated, one candidate to reduce the size fluctuation may be to use another resist which has small granular structures[3-28].

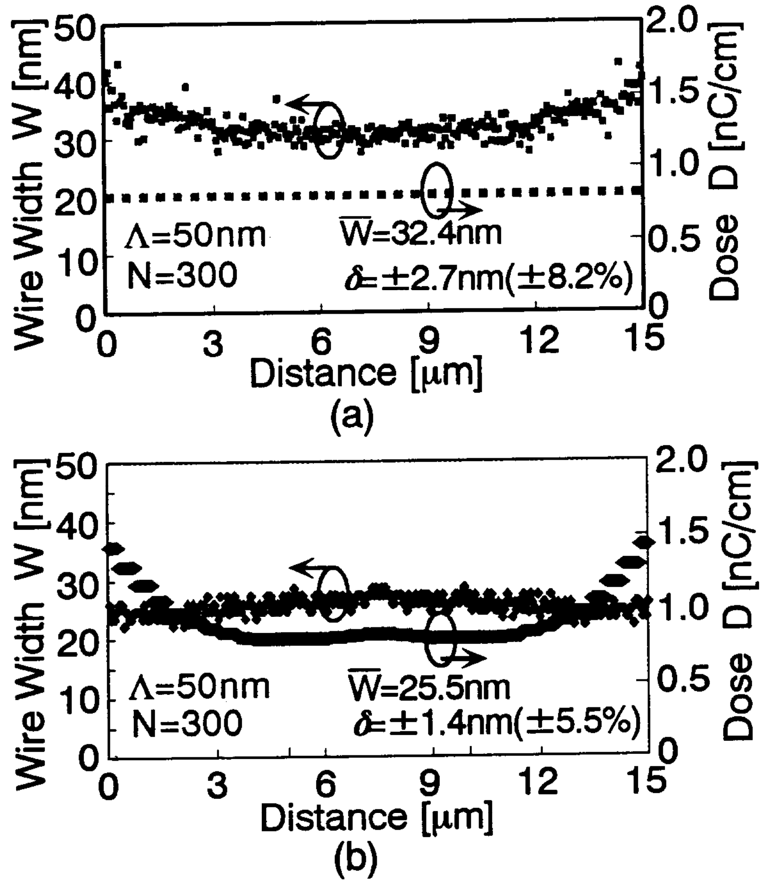

Fig. 3.10 A line width distribution of 300 line patterns with (a) a constant dose condition of 0.8nC/cm and (b) with a corrected dose profile from 0.8 (at the center portion) to 1.42nC/cm (at the edge portion).
The size fluctuation of the resist pattern could be reduced from 2.7nm to 1.4nm by proximity effect correction.

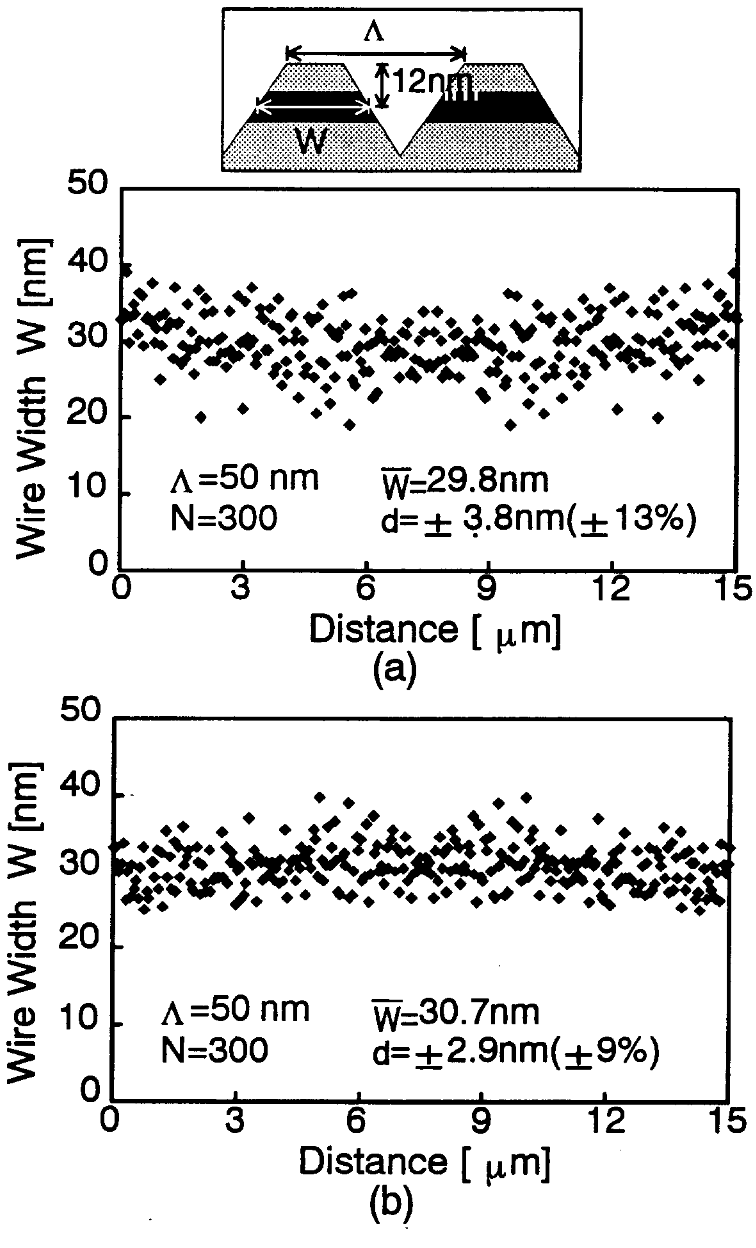

Fig. 3.11 A wire width distribution of 300 wires with (a) a constant dose condition of 0.8nC/cm and (b) a corrected dose profile from 0.8 (at the center portion) to 1.42nC/cm (at the edge portion) after wet chemical etching.
The size fluctuation of the GaInAsP wire structure could be reduced from 3.8nm to 2.9nm by proximity effect correction.

3.4 Fabrication Process of Quantum-Wire Laser

The fabrication process of long-wavelength GaInAsP/InP compressively-strained Q-Wire lasers, using EB lithography and wet chemical etching followed by OMVPE embedding growth, is shown in Fig. 3.12. This process is similar to those of the previous works, however, due to low optical confinement factor ξ of the active region, and poor size uniformity of these Q-Wire structures, higher performance over quantum-film (Q-Film) lasers fabricated from the initial quantum-well structures was not obtained within the investigated temperature range T between 150K and 300K[3-1]-[3-3].

To solve this problem, we adopted a relatively thick compressively-strained (1% CS) quantum-well (10nm thick, ξ=1.3% for the quantum-film, λ_{PL}=1.576μm) structure as an initial wafer for quantum-wire structure, and a thin quantum-film layer (1% CS, 5nm thick, ξ=0.6%, λ_{PL}=1.512μm) was introduced to enhance the optical confinement factor and to partially support optical gain when the wire size becomes very narrow and the gain peak wavelength shifts close to the gain peak of quantum-film structure. The following fabrication sequences are used.

(a) Preparation of double heterostructure (DH) by OMVPE growth
(b) Formation of Q-Wire pattern by EB lithography on SiO_2 mask layer
(c) Formation of SiO_2 etching mask by CF_4 reactive ion etching (RIE)
(d) Fabrication of Q-Wire structures
(e) OMVPE regrowth on the Q-Wire structures
(f) Formation of the mesa-striped laser

<u>(a) Preparation of double heterostructure (DH) by OMVPE growth</u>

First, an initial wafer was prepared on a p-InP substrate (Fig.3.12(a)) by OMVPE[3-29]. It consists of the following layers:

(1) p-InP first buffer layer (Zn-doped, $N_A=5\times10^{17}cm^{-3}$, 0.5μm thick)

(2) p-InP second buffer layer (Zn-doped, $N_A=2\times10^{17}cm^{-3}$, 1.5μm thick)

(3) GaInAsP lower three-step optical confinement layer (OCL)
(un-doped, λ_g=1.0～1.2μm, 90nm thick)

(4) $Ga_{0.18}In_{0.82}As_{0.73}P_{0.27}$ CS-QW layer (un-doped, 5nm thick, 1% strain)

(5) GaInAsP barrier layer (un-doped, λ_g=1.2μm, 12nm thick)

(6) $Ga_{0.18}In_{0.82}As_{0.73}P_{0.27}$ CS-QW active layer (un-doped, 10nm thick, 1% strain)

(7) GaInAsP barrier layer (un-doped, λ_g=1.2μm, 5nm thick)

(8) InP top layer (un-doped, 5nm thick).

The band profile and PL spectrum of the initial wafer are shown in Fig. 3.13.

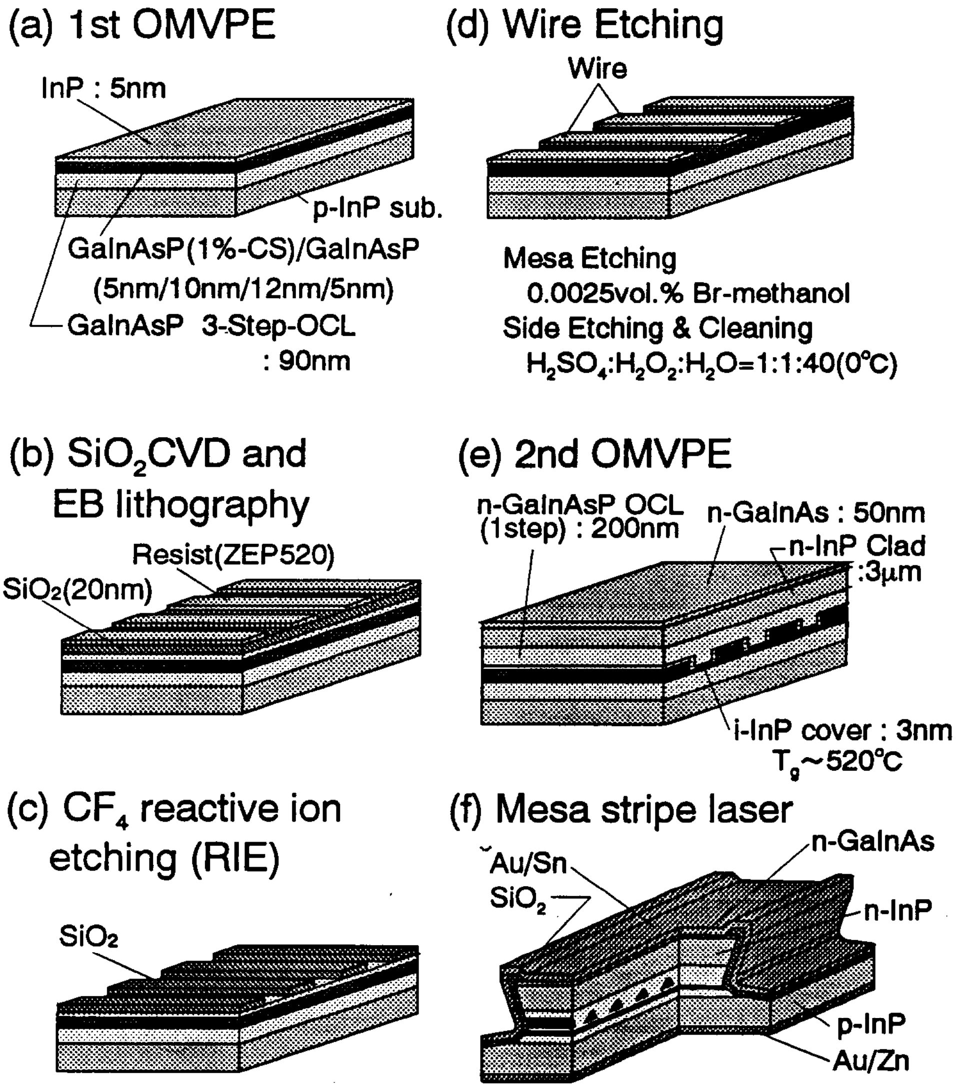

Fig. 3.12 Fabrication process.

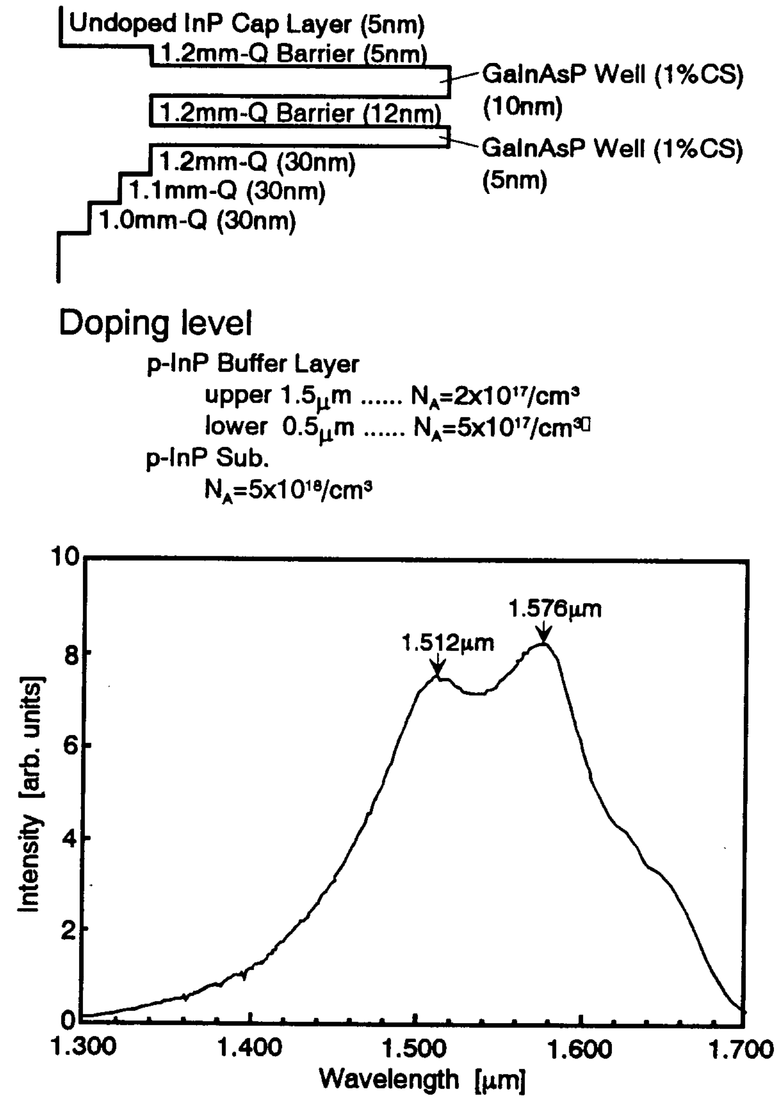

Fig. 3.13 The band profile and PL spectrum of the initial wafer.

<u>(b) Formation of Q-Wire pattern by EB lithography on SiO_2 mask</u>

To fabricate the Q-Wire structure by wet chemical etching with Br-methanol solution, the thin SiO_2 layer was deposited on the wafer as an etching mask. Then the Q-Wire resist pattern was fabricated by EB lithography. This process is described as follows:

1) Cleaning of the initial wafer by acetone (boiling at 150℃ for 5 min., three times), methanol (boiling at 180℃ for 5 min., three times), and pure H_2O.

2) By using thermal CVD, SiO_2 was deposited at 320℃ on the wafer to the

thickness of about 20nm. The InP cap layer was to protect the surface of the thin GaInAsP barrier layer and moreover, better adhesion of SiO_2 on the InP layer was obtained than that on the GaInAsP layer.

3) Fabrication of the EB resist pattern (see the previous section). There were two kinds of Q-Wire patterns fabricated; one was with the period of 50nm and the other was with the period of 70nm, as shown in Fig. 3.14. In actual samples used for the fabrication of Q-Wire lasers, 40μm long periodic line patterns were formed with an interval of 300μm so as to make a stripe laser structure at the center portion of the pattern. The line pattern was made along $<01\bar{1}>$ direction so as to form mesa structures with relatively smooth side wall surfaces by Br-methanol etchant.

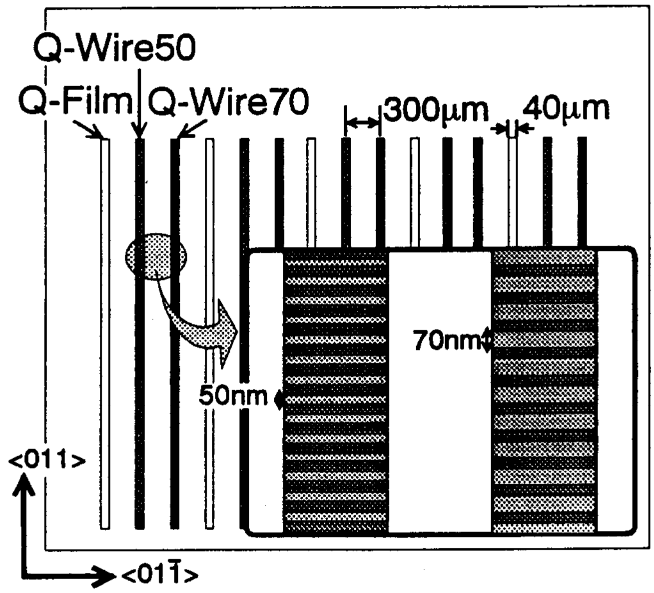

Fig. 3.14 EB pattern used for the fabrication of the Q-wire lasers.

<u>(c) Formation of SiO_2 etching mask by CF_4 reactive ion etching</u>

To fabricate SiO_2 mask, CF_4 reactive ion etching (RIE) was used for the purpose of the reduction of the size fluctuation. This process is described as follows:

1) First, the resist patterns were transferred to the SiO_2 layer under the conditions shown in Table 3.1. It is noted that the etching time is strongly dependent on the

thickness of the SiO_2 layer, that should be confirmed using the dummy samples fabricated on the same wafer. In case of the thickness of 20nm, the etching time is about 1min.

Table 3.1 The conditions for SiO_2 mask.

Resist	ZEP520
Gas	CF_4 1sccm
RF Power	20W(200W range)
Etching Pressure	3.5×10^{-2}mbar
Back Ground	5×10^{-3}mbar

2) Covering the Q-Wire SiO_2 pattern by OMR photoresist to protect the etching of the Q-Wire patterns at the next marker fabrication.
3) The marker was fabricated using 1% (volume ratio) Br-methanol after reducing the rest of SiO_2 using 1% BHF for few seconds.
4) Removal of the photoresist using OMR remover. (boiling at 200℃ until the OMR is reduced, the boiling time is typically within 2 min. to prevent the etching of the semiconductor by OMR remover)
5) Cleaning of the sample by acetone (boiling at 150℃ for 5min, four times), and methanol (boiling at 180℃ for 5 min., three times) to reduce the OMR remover.
6) Finally, plasma O_2 ashing was done for the scum and bridge of ZEP resist, of which the conditions are shown in Table 3.2.

Table 3.2 The conditions of O_2 ashing.

Resist	ZEP520
Gas	O_2 3sccm
RF Power	20W(200W range)
Etching Pressure	4.0×10^{-2}mbar
Back Ground	5×10^{-3}mbar

(d) Fabrication of Q-Wire structures

To fabricate the Q-Wire structures, the two types of etchant were used. This process described as follows;

1) Cleaning of the initial wafer by acetone (boiling at 150℃ for 5 min., three times), methanol (boiling at 180℃ for 5 min., three times), and pure H_2O.
2) The rest of the SiO_2 was removed using 1% BHF for a few seconds.
3) 40ppm (volume ratio) Br-methanol was used for mesa-etching for 6 sec. Figure

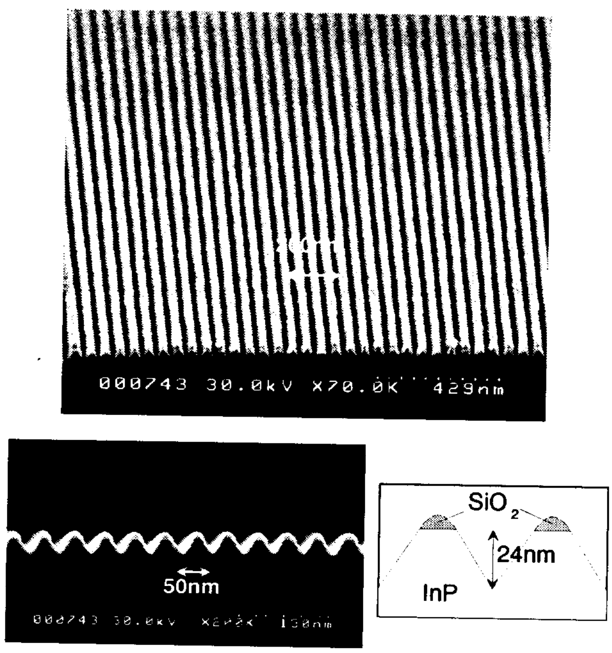

Fig. 3.15 SEM views of 50nm-periodic patterns of InP after mesa-etching.

3.15 shows , for example, the SEM views of 50nm-periodic patterns of InP after mesa-etching.

4) H_2SO_4:H_2O_2:H_2O=1:1:40 (0℃) was used to etch As-rich GaInAsP compound so as to squeeze the wire width and eliminate (111)A. The total etching depth was about 30nm.
5) The SiO_2 etching mask was removed by 7% BHF for 1 min.

(e) OMVPE regrowth on the Q-Wire structures

In a regrowth process, another OMVPE system (TEL-SAMCO) was used, which was fundamentally similar system to that mentioned in §3.2. After removing the SiO_2 mask, n-GaInAsP OCL (λ_g=1.2μm, 200nm thick, $N_D=1\times10^{18}cm^{-3}$), n-InP cladding layer (3μm thick, $N_D=1\times10^{18}cm^{-3}$), and n-GaInAs contact layer (50nm thick, $N_D=5\times10^{18}cm^{-3}$) were grown using the OMVPE (Fig.12(e)). In the beginning of the embedding growth, a thin (3nm thick) InP cover layer was grown first (at 520-528℃) after a preheating process in hydrogen atmosphere at 350℃ for 30min in order to reduce the non-radiative recombination or optical loss at the regrowth interface[3-30]. The time schedule diagram of substrate temperature and the material gas flow used in the regrowth process are shown in Fig. 3.16. The cross sectional SEM views of two kinds of Q-Wire structures are shown in Fig. 3.17; one is that with a wire width ($\overline{W}$) of 20nm for a period (Λ) of 50nm (Q-Wire20, in short), and the other is that with a 25nm-wide wire for Λ=70nm (Q-Wire25). As can be seen, the embedded Q-Wire was typically mesa-shaped and the wire width was defined as that at the center depth.

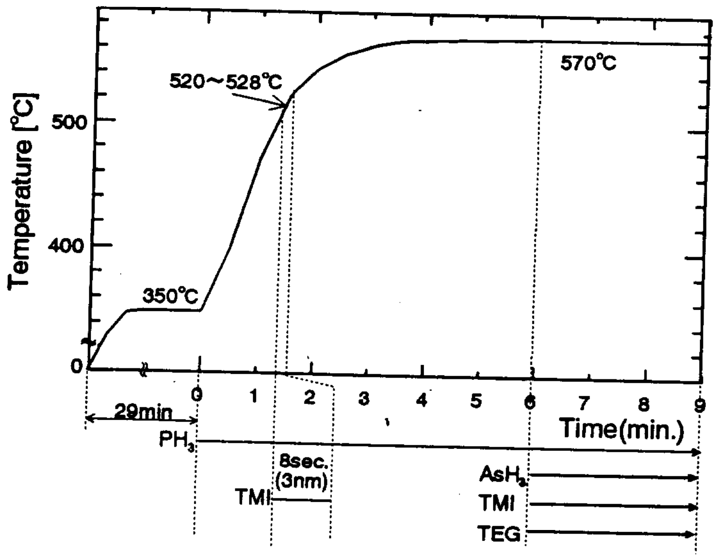

Fig. 3.16 The time schedule diagram of substrate temperature and the material gas flow used in the regrowth process.

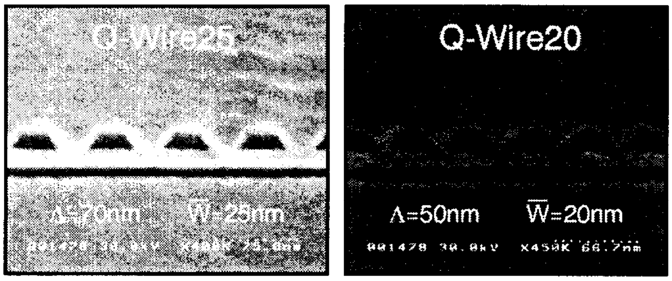

Fig.3.17 Cross sectional SEM views of Q-Wires.

<u>(f)Formation of the mesa-striped laser</u>

By using conventional process of photolithography (AZ1400-17 resist, positive type), SiO_2 (0.1μm thick) stripe masks with 20μm width were formed along <011> crystal axis, which was perpendicular to the Q-Wire direction so as to obtain higher optical gain for TE mode due to anisotropic polarization property inherent to Q-wire structures[3-31]. The reverse mesa stripe was formed by 0.3% (volume ratio) Br-methanol to make the active region width of 15μm at a center portion of the Q-Wire pattern (40μm wide) so as to select an area with better size uniformity. After the formation of reverse mesa, the SiO_2 insulating layer with the thickness of 0.3μm was deposited. It is noted that, when the thickness of the SiO_2 insulating layer is 0.1μm, it is possible for the injection current to go through this layer from a pin hole or something. Then the window of the electrode was formed by the photolithography (OMR resist, negative type) with the window width of 8μm. Finally, After polishing the substrate side of the wafer to a thickness of around 100μm, electrodes were formed by using Au/Zn for p- and Au/Sn for n- sides, respectively (Fig.3.12(f)). The schematic structure of the Q-Wire laser and the band profile with a cross sectional SEM are shown in Fig. 3.18.

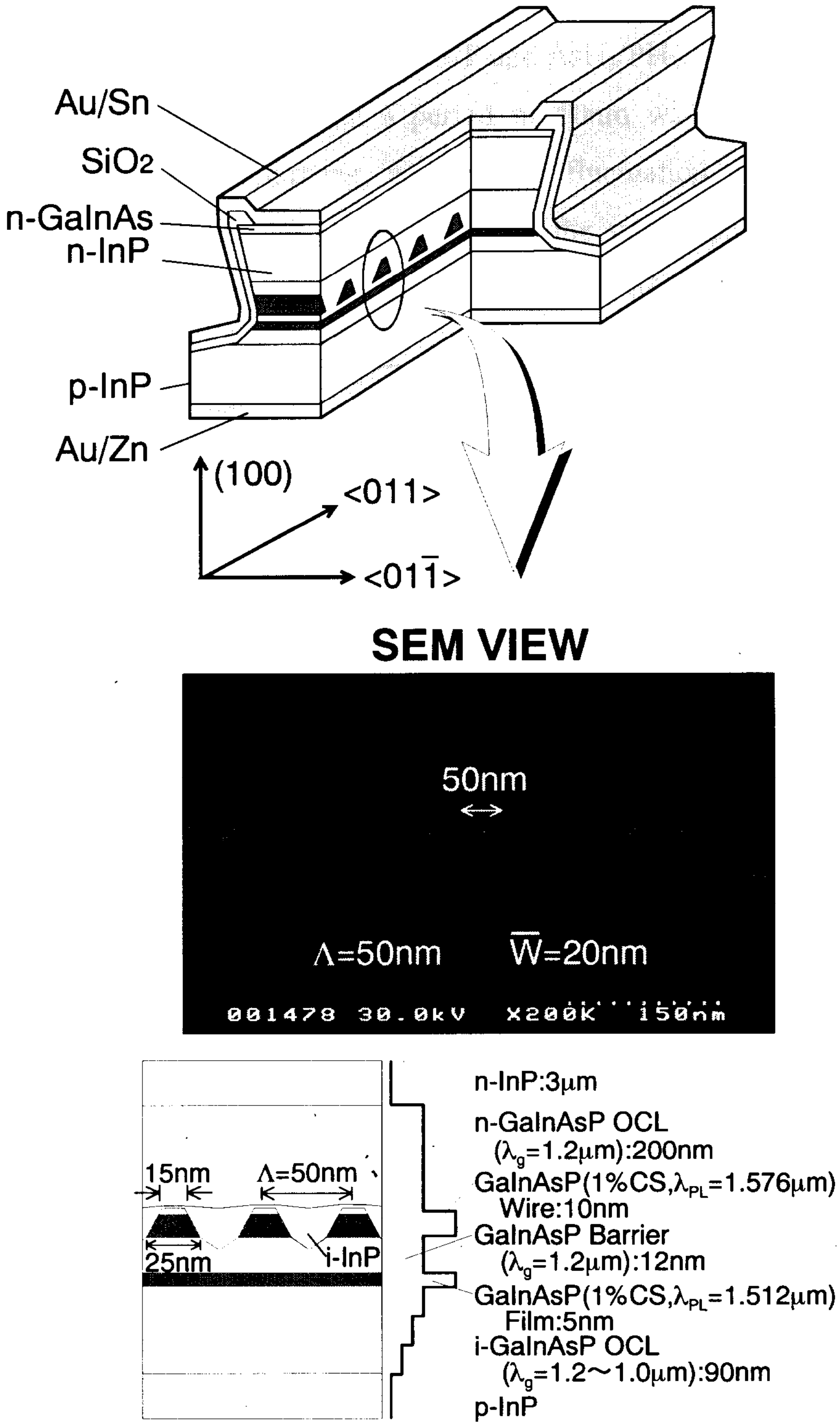

Fig. 3.18 The schematic structure and band profile of Q-Wire laser.

3.5 Conclusion

The fabrication process of Q-Wire lasers is described including the crystal growth technique using OMVPE. It was found that our OMVPE system has simple relations between Ga/In and TEG/TMI, and between As/P and AsH_3/PH_3.

GaInAsP fine wire structure with a period of 50nm was fabricated using EB lithography and wet chemical etching, and its size fluctuation was analyzed. By correcting the dose profile for the proximity effect, the size fluctuation of the resist pattern was reduced from ±2.7nm to ±1.4nm and that of GaInAsP wire structure was reduced from ±3.8nm to ±2.9nm, respectively, for a typical wire width of 30nm.

Two kinds of high density Q-Wire structures were fabricated for high performance operation of Q-Wire lasers; one had the wire size of 20nm with a period of 50nm, and the other had that of 25nm with a period of 70nm, respectively.

References

[3-1] Y. Miyake, H. Hirayama, K. Kudo, S. Tamura, S. Arai, M. Asada, Y. Miyamoto and Y. Suematsu, "Room-Temperature Operation of GaInAs/GaInAsP/InP SCH lasers with quantum-wire size active region," *IEEE. J. Quantum Electron.*, vol.QE-29, no.6, pp.2123-2133, Jun. 1993.

[3-2] K. Kudo, Y. Nagashima, S. Tamura, S. Arai, Y. Huang and Y. Suematsu, "$Ga_{0.66}In_{0.34}As$/GaInAsP/InP tensile-strained single-quantum-well lasers with 70-nm period wire active region," *IEEE. Photon. Technol. Lett.*, vol.5, no.8, pp.864-867, Aug. 1993.

[3-3] K. C. Shin, S. Arai, Y. Nagashima, K. Kudo, and S. Tamura, "Temperature dependences of $Ga_{0.66}In_{0.34}As$ /InP tensile-strained quasi-quantum-wire laser fabricated by wet chemical etching and 2-step OMVPE growth," *IEEE. Photon. Technol. Lett.*, vol.7, no.4, pp.345-347, Apr. 1995.

[3-4] E. Kapon, S. Simhony, R. Bhat, and D. M. Hwang, "Single quantum wire semiconductor lasers," *Appl. Phys. Lett.*, vol.55, no.25, pp.2715-2717, Dec. 1989.

[3-5] S. Tiwari, G. D. Pettit, K. R. Milkove, F. Legoues, R. J. Davis and J. M. Woodall, "High efficiency and low threshold current strained V-groove quantum-wire lasers," *Appl. Phys. Lett.*, vol.64, no.26, pp.3536-3538, Jun. 1994.

[3-6] U. A. Griesinger, H. Schweizer, V. Härle, F. Barth, B. Höhing, B. Klepser, and F. Scholz "Dry-Etched Wire Distributed Feedback Laser," *IEEE Photon. Technol. Lett.*, vol.7, no.9, pp.953-955, Sep. 1995.

[3-7] S. T. Chou, K. Y. Cheng, L. J. Chou and K. C. Hsieh, "$Ga_xIn_{1-x}As$ multiple-quantum-wire lasers grown by the strain-induced lateral-layer ordering process," *Appl. Phys. Lett.*, vol.66, no.17, pp.2220-2222, Apr. 1995.

[3-8] J. Yoshida, K. Kishino, A. Kikuchi and I. Nomura, "Continuous-wave (CW) operation of GaInP-AlGaInP visible compressively strained multiple quantum-wire (CS-MQWR) lasers," *IEEE J. Selected Topics in Quantum Electron.*, vol.1, no.2, pp.173-182, Jun. 1995.

[3-9] J. Temmyo, E. Kuramochi, M. Sugo, T. Nishiya, R. Nötzel, and T. Tamamura, "Strained InGaAs quantum disk laser with nanoscale active region fabricated with self-organization on GaAs (311)B substrate," *Electron. Lett.*, vol.31, no.3, pp.209-211, Feb. 1995.

[3-10] A. Orth, H. Zull, J. P. Reithmaier and A. Forchel, "GaInAs/GaAs quantum wire laser structures with strong gain coupling defined by reactive ion etching," *Electron. Lett.*, vol.31, no.6, pp.457-458, Mar. 1995.

[3-11] . P. Reithmaier, A. Orth, J. Müller and A. Forchel, "First order gratings for gain coupled GaInAsP DFB-lasers made by maskless focused ion beam patterning," *IEEE 7th Int. Conf. on Indium Phosphide and Related Materials (IPRM'95)*, ThP53, Sapporo, pp.569-572, May 1995.

[3-12] U. A. Griesinger, H. Schweizer, S. Kronmüller, D. Ottenwälder, F. Scholz, and M. H. Pilkun, "Realization of dot DFB lasers," *IEEE. Photon. Technol. Lett.*, vol.8, no.5, pp.587-589, May 1996

[3-13] K. J. Vahala, "Quantum box fabrication tolerance and size limits in semiconductors and their effect on optical gain," *IEEE J. Quantum Electron.*, vol.24, no.3, pp.523-530, Mar. 1988.

[3-14] H. Zarem, K. Vahala, and A. Yariv, "Gain spectra of quantum wires with inhomogeneous broadening," ***IEEE. J. Quantum Electron.***, vol.QE-25, no.4, pp.705-712, Apr. 1989.

[3-15] H. Hirayama and M. Asada, "Reduction of size fluctuation effect in GaInAs/GaInAsP quantum-box lasers using tensile strained active region," ***IEEE 14th Int. Semiconductor Laser Conf.***, P4, Hawaii, pp.89-90, Sep. 1994.

[3-16] H. Ochimizu, T. Kikkawa, S. Kuroda, K. Kasai and J. Komeno, "Large-area MOVPE growth of an n-InGaP/InGaAs/GaAs HEMT structure using TBP," ***Int. Conf. on Solid State Devices and Materials (SSDM'93)***, D-8-5, pp.1068-1070, Makuhari, Sep. 1993.

[3-17] J. Komeno, "Metalorganic vapor phase epitaxy using organic group V precursors," ***J. Cryst. Growth***, vol.145, pp.468-472, 1994.

[3-18] K. Kudo, Y. Miyake, H. Hirayama, S. Tamura, S. Arai and Y. Suematsu, "Room temperature CW operation of $Ga_{0.3}In_{0.7}As$/GaInAsP/InP strained MQW lasers with wire active region," ***IEEE. Photon. Technol. Lett.***, vol.4, no.10, pp.1089-1092, Oct. 1992.

[3-19] N. Yamamoto, K. Yokoyama, T. Yamanaka and M. Yamamoto, "Design and fabrication of low-threshold 1.55-μm grated-index separate-confinement-heterostructure strained InGaAsP single-quantum-well laser diodes," ***IEEE J. Quantum Electron.***, vol.33, no.7, pp.1141-1148, Jul. 1997.

[3-20] T. Kojima, M. Tamura, K. C. Shin, S. Tamura and S. Arai, "Temperature dependences of GaInAsP/InP compressively-strained quantum-wire lasers fabricated by EB-lithography and 2-step OMVPE growth," ***IEEE 8th Int. Conf. on Indium Phosphide and Related Materials (IPRM'96)***, ThA1-5, Schwäbisch Gmünd, pp.731-734, Apr. 1996.

[3-21] H. Saito, K. Nishi and S. Sugou, "High uniform InAs quantum dot under high-temperature growth phase," ***Nat. Conv. Res. of Japan Soc. Appl. Phys.***, 17p-YG-2, Higashi-hiroshima, p.1254, Sep. 1998.

[3-22] H. Shoji, Y. Nakata, K. Mukai, Y. Sugiyama, M. Sugawara, N. Yokoyama and H. Ishikawa, "Lasing characteristics of self-formed quantum dot lasers with multistacked dot layer," ***IEEE J. Selected Topics in Quantum Electron.***, vol.3, no.2, pp.188-195, Apr. 1997.

[3-23] A. E. Zhukov, V. M. Ustinov, A. Yu. Egorov, A. R. Kovsh, A. F. Tsatsul'nikov, N. N. Lendentsov, S. V. Zaitsev, N. Yu. Gordeev, P. S. Kop'ez, and Z. I. Alferov, "Negative characteristic temperature of InGaAs quantum dot injection laser," ***Jpn. J. Appl. Phys.***, vol.36, pt.1, no.6B, pp.4216-4218, Jun. 1997.

[3-24] T. Nishida, M. Notomi, R. Iga and T. Tamamura, "Quantum wire fabrication by e-beam lithography using high-resolution and high-sensitivity e-beam resist ZEP-520," ***Jpn. J. Appl. Phys.***, vol.31, no.7, pp.4508-4514, Dec. 1992.

[3-25] C. Dix, P. G. Flavin, P. Hendy and M. E. Jones, "0.1μ scale lithography using a conventional electron beam system," ***J. Vac. Sci. Technol. B***, vol.3, no.1, Jan/Feb 1985.

[3-26] E. Inamura, Y. Miyamoto, S. Tamura, T. Takasugi and K. Furuya, "Wet chemical etching for ultrafine periodic structure: rectangular InP corrugations of 70nm pitch and 100nm depth," ***Jpn. J. Appl. Phys.***, vol.28, no.10, pp.2193-3196, Oct. 1989.

[3-27] T. Yamaguchi, H. Namatsu, M. Nagase, K. Yamazaki and K. Kurihara, "Nanometer-scale linewidth fluctuations caused by polymer aggregates in resist films," ***Appl. Phys. Lett.***, vol.71, no.16, pp.2388-2390, Oct. 1997.

[3-28] H. Namatsu, Y. Takahashi, K. Yamazaki, T. Yamaguchi, M. Nagase and K. Kurihara, "Three-dimensional siloxane resist for the formation of nanopatterns with minimum linewidth fluctuations," *J. Vac. Sci. Technol. B*, vol.16, no.1, pp.69-76, Jan/Feb 1998.

[3-29] Y. Miyake, H. Hirayama, J. I. Shim, S. Arai and Y. Miyamoto, "Threshold current reduction of GaInAs/GaInAsP/InP SCH quantum-well lasers with wire-like active region by using p-type substrates," *IEEE. Photon. Technol. Lett.*, vol.4, no.9, pp.964-966, Sep. 1992.

[3-30] Y. Miyake, H. Hirayama, S. Arai, Y. Miyamoto and Y. Suematsu, "Room temperature operation of GaInAs-GaInAsP-InP SCH multiquantum-film laser with narrow wire-like active region," *IEEE. Photon. Technol. Lett.*, vol.3, no.3, pp.191-192, Mar. 1991.

[3-31] M. Asada, Y. Miyamoto and Y. Suematsu, "Theoretical gain of quantum-well wire lasers," *Jpn. J. Appl. Phys.*, vol.24, no.2, pp.L95-L97, Feb. 1985.

Chapter 4

Photoluminescence Properties of Quantum-Wire Structures

4.1 Introduction... 100
4.2 Polarization Dependence... 101
4.3 Temperature Dependence... 111
4.4 Conclusion.. 113
References.. 114

4.1 Introduction

SEVERAL advantages of semiconductor lasers consisting of low-dimensional quantum structures, such as low threshold current and high efficiency operation, temperature insensitive operation, and narrow linewidth operation[4-1]-[4-4], are expected. Quantum wire (Q-Wire) structures, with their constrained density of states and active volume, are expected to show large nonlinear effects in electronic and optical processes[4-5]. A room temperature CW operation of GaInAsP/InP Q-Wire lasers fabricated by an electron beam lithography (EBL) and an etching technique followed by an embedding growth using organo-metallic vapor phase epitaxy (OMVPE) was reported[4-6],[4-7], where a small blue shift of the emission wavelength was observed, however clear evidence of the lateral quantum confinement effect was not reported. The anisotropy of the dipole moment in Q-Wire structures can give rise to higher gain for light polarized along the wire (i.e. light propagation perpendicular to the wire); gain anisotropy ratio of ~2 was predicted for rectangular wires[4-8].

In this chapter, anisotropic polarization properties of photoluminescence (PL) from both lattice-matched (LM) and compressively-strained (CS) GaInAsP/InP Q-Wire structures fabricated by the above method are studied, which is the same structure as long-wavelength Q-Wire lasers. Furthermore the temperature dependence of PL was also measured.

4.2 Polarization Dependence

Anisotropic polarization property of Q-Wire structures is a clearly indicative evidence of the lateral quantum confinement. The fabrication process employed here was almost the same as that in the previous chapter, except for the structure of the embedding layers. Since the purpose of this study is focused on the polarization properties of PL from the top surface, only a thin InP layer (100nm thick, undoped) was grown on patterned and etched samples.

Figure 4.1 (a) shows a schematic diagram of a LM-GaInAsP/InP Q-Wire structure, which was fabricated on a wafer consisting of a 10nm thick $Ga_{0.41}In_{0.59}As_{0.89}P_{0.11}$ quantum-film (Q-Film) grown on a (100) p-InP substrate with an area of 1mm × 1mm. After depositing a thin SiO_2 (20nm thick) mask layer, the wire pattern was formed by JBX-5FE EBX system using ZEP-520 resist (30nm thick) with a line dose condition of 0.8nC/cm. Two patterns of different wire periods (Λ=50nm, 70nm) were fabricated on the wafer. The wire width of the EB resist was separately measured by Hitachi S-5000 SEM, it was about 30nm ± 1.4nm (standard deviation) for the sample with Λ=50nm and the standard deviation was almost doubled after transferring the pattern into the wafer by a reactive ion etching (RIE) with CF_4 gas followed by a wet chemical etching with 40ppm (volume ratio) Br-methanol for mesa-etching and with H_2SO_4:H_2O_2:H_2O =1:1:10 (0-1℃) for side etching of the active region.

After removing the SiO_2 mask by a BHF solution, a 100nm thick InP layer was grown on the entire surface of the sample by a low-pressure (LP) OMVPE system, where a thin (3nm) InP was grown at the temperature of 530℃ (40℃ lower than the temperature for the initial wafer growth) so as to suppress a decomposition of phosphorus from the surface and then the rest InP was grown at 570℃. The flatness of the overgrown surface was almost the same quality as one-step growth. Thus, the

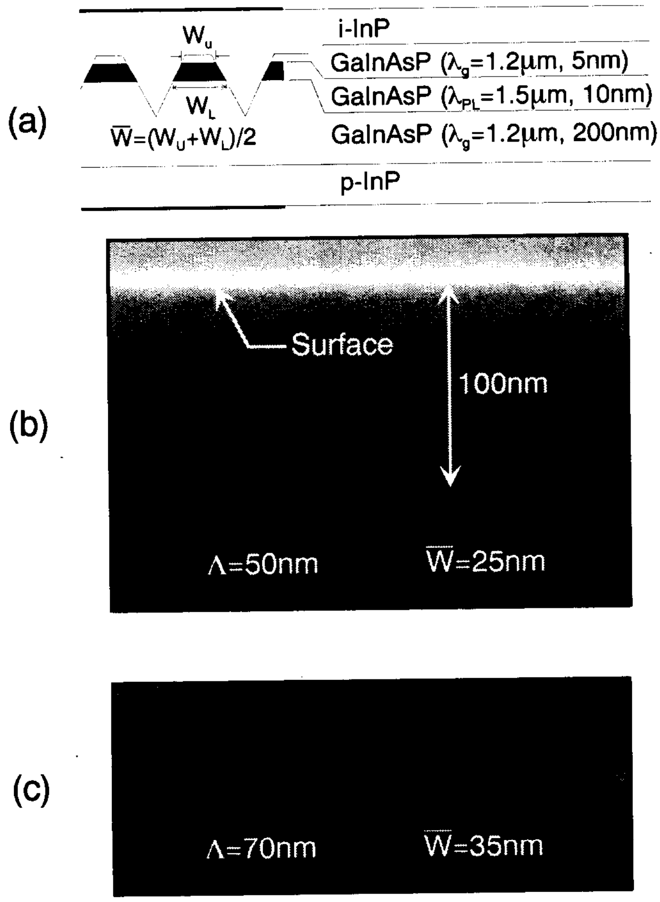

Fig. 4.1 (a) The schematic diagram of a LM-GaInAsP Q-Wire structure. (b) and (c) shows cross sectional SEM views of GaInAsP/InP Q-wire structures; (b) Λ=50nm, $\overline{W} = 25nm$, and (c) Λ=70nm, $\overline{W} = 35nm$.

polarization of the PL was not caused by a grating effect. Figure 4.1 (b) and (c) show cross sectional SEM views of GaInAsP/InP Q-Wire structures with the period of 50nm and 70nm, respectively. As can be seen, the embedded GaInAsP Q-Wire was typical mesa-shaped for both samples and the wire width at the center depth was 25nm and 35nm for the period of 50nm and 70nm, respectively.

Figure 4.2 shows a schematic diagram of the set-up used in this PL measurement. A sample was excited by a Nd-YAG laser (λ=1.064μm, 20mW output) through a chopper and the PL signal was collected from the top surface by a Ge photodetector through a polarizer and a monochromator. The Q-Wire was made along $\langle 01\bar{1}\rangle$ direction in all samples prepared this time and the angle θ was defined for the intersecting angle of this direction and the parallel direction of the polarizer.

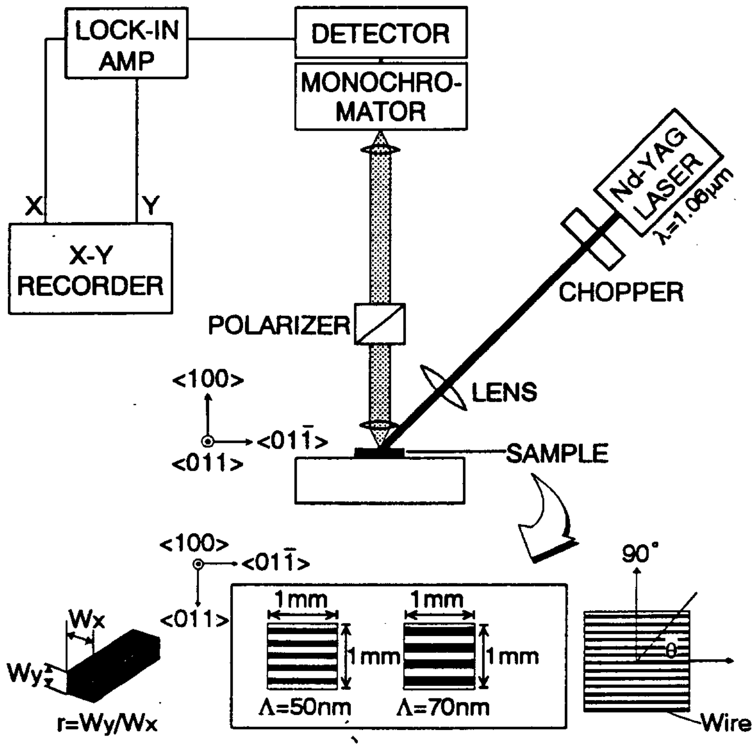

Fig. 4.2 A schematic diagram of the set up for PL measurement. The direction of Q-Wire was <011> and *r* was the aspect ratio Wy/Wx of the Q-Wire.

Figure 4.3 shows PL spectra for the LM-Q-Wire and the LM-Q-Film at room temperature for different polarizations. The solid lines are the spectra at θ=0 degree which is parallel to the direction of the quantum wire (along $<01\bar{1}>$), and the dashed lines are the spectra at θ=90 degree which is perpendicular to the quantum wire (along <011>). As can be seen, both PL spectra were about the same for the LM-Q-Film sample and the spectrum (both the profile and the peak intensity) was almost constant between θ=0 degree and θ=90 degree. On the other hand, in case of the Q-Wire samples, the PL spectra were almost the same but the PL intensity was maximum at θ=0 degree and was minimum at θ=90 degree. This difference can be attributed to the lateral quantum confinement effect, which causes an anisotropic behavior of the dipole moment.

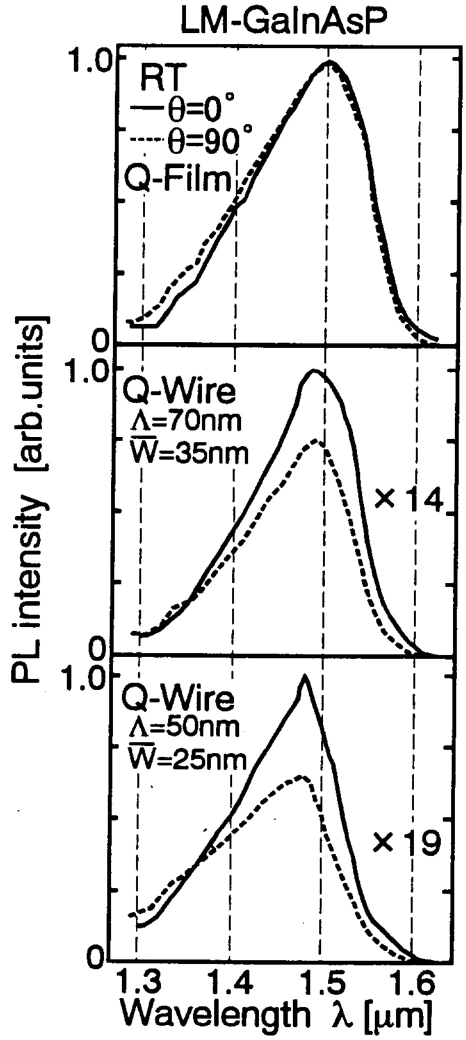

Fig. 4.3 PL spectra for the LM-Q-Wire and the LM-Q-Film at room temperature for different polarizations. The solid lines are at θ=0 degree and the dashed lines are at θ=90 degree.

The optical transition strength is given as follows[4-9];

$$|M_T|_V^2 = a \cdot |M|^2 . \tag{4.1}$$

Here M is momentum matrix elements and $|M|^2$ determines the transition probability between the conduction band Bloch function and the basis functions, where as $|M_T|_V^2$ determines the matrix element between the conduction band Bloch function and the valence band Bloch functions. For heavy hole band, a is given by

$$a = 1 - |\vec{k} \cdot \vec{e}|^2 . \tag{4.2}$$

where $\vec{k}$ is the unit vector directed along electron wave vector, and $\vec{e}$ is the unit vector of the electric field polarization. Near the band edge in quantum-confined structures, the $\vec{k}$ vectors are quantized along certain directions. In case of the quantum-wire structure, the density of state function in k space is described as $\rho(k) = (1/\pi) \cdot (1/W_x \cdot W_y)$, where W_x and W_y are the wire width and the well thickness of the Q-Wire, respectively. So $\vec{k}$ vector for band edge state is

$$\vec{k} = \left(\frac{r}{\sqrt{1+r^2}}, \frac{1}{\sqrt{1+r^2}}, 0 \right), \tag{4.3}$$

obtained by assuming $\vec{k} \propto 1/W_x, 1/W_y$, and r is the aspect ratio W_y/W_x of the Q-Wire. In addition, when the electric vector is rotated in the plane of the Q-Wire, the optical anisotropy is expected in case of heavy hole band[4-10]. Therefore the optical transition strength a for TE polarization considering the direction of the luminescence from the top surface is

$$a = 1 - \frac{r^2}{1+r^2} sin^2 \theta , \tag{4.4}$$

where θ is the angle between the wire-axis and electric field. The smaller r becomes, the coupling coefficient becomes like Q-Film's. On the other hand, the large r becomes, the lateral confinement becomes strong.

Figure 4.4 shows the PL intensity of the LM-Q-Wire and LM-Q-Film samples as a function of the angle θ, where the PL intensity at each measured point was normalized by the intensity at θ=0 degree. While the normalized PL intensity is constant in case of the Q-Film, we observed a significant decrease of the PL intensity with increasing θ for the LM-Q-Wire samples. Dashed lines indicate show the calculated value of the optical transition strength from eq. (4.4). The r=0.29 corresponds to W_x=35nm and W_y=10nm, while r=0.4 corresponds to W_x=25nm. In both cases, measured polarization dependences were much stronger than theoretical curves. Since the eq. (4.4) is obtained from a rough approximation, quantitative discussion can not be done here. But observed polarization anisotropy, which can be characterized by the ratio *I(θ=90 degree)/I(θ=0 degree)*, was 0.77 for 35nm-wide LM-Q-Wire and 0.65 for 25nm LM-Q-Wire structures.

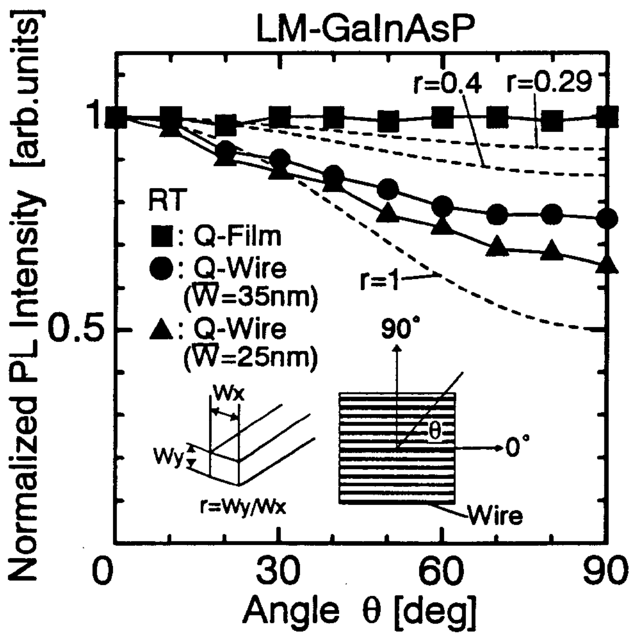

Fig. 4.4 The polarization dependence of the PL intensity of the LM-Q-Wire and LM-Q-Film structures.

The degree of polarization, *[I(θ=0 degree)-I(θ=0 degree)]/[I(θ=0degree)+I(θ=90 degree)]* of the PL was 0.13 in case of 35nm-wide LM-Q-Wire and 0.21 for 25nm LM-Q-Wire structures. It is relatively small compared with the other reports[4-11]-

[4-13]. However, it is reasonable because the width of Q-Wire was relatively wide and our results do not include both composition modulation effect and electric-field modulation effect. In addition, the energy separation may not be sufficient due to the measurement at room temperature.

A similar structure was also fabricated by using 1%-CS $Ga_{0.18}In_{0.82}As_{0.73}P_{0.27}$/InP Q-Film (10nm thick) as an initial wafer on a (100) p-InP substrate, which was the same initial wafer as that for long-wavelength Q-Wire lasers. Figure 4.5 shows the cross sectional SEM view and the band profile of the CS-Q-Wire structure. The fabrication method was similar to that of LM samples, where only a pattern with the period of 70nm was prepared and the width at the center depth was 35nm.

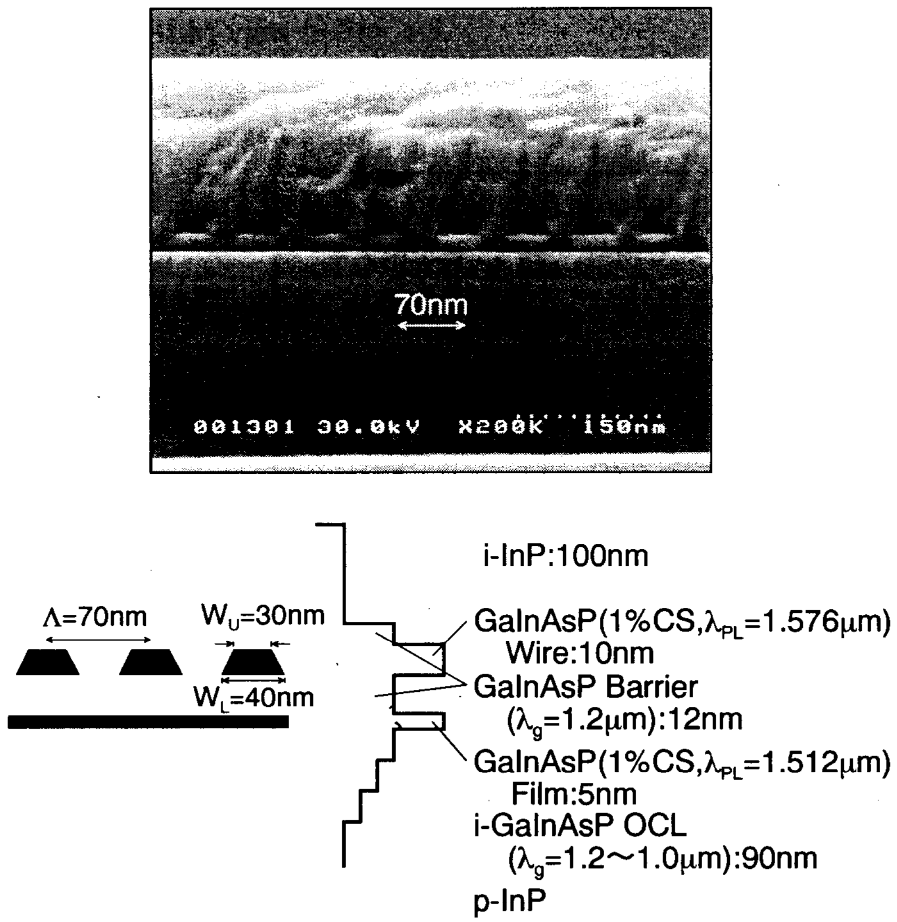

Fig. 4.5 The cross sectional SEM view and the band profile of the CS Q-Wire structure.

Figure 4.6 shows the polarization properties of the PL spectrum of the Q-Wire and the Q-Film structure at room temperature. Solid-line arrow marks at 1.51μm indicate the peak of the lower quantum-film and the dashed-line arrow marks at 1.64μm indicate the peak due to an As-rich layer, formed during the growth of the initial wafer. This layer was considered to be located above the upper quantum-film layer, because the intensity was reduced in case of Q-Wire s spectrum. The FWHM at θ=0 degree and at θ=90 degree for the Q-Wire were 43meV and 58meV, respectively, and that of the Q-Film was constant, i.e., 57meV. The difference of them was dependent on polarization, because at θ=0 degree the contribution of the lower quantum film peak to the FWHM of the Q-Wire is small. The energy value of blue shift for the Q-Wire was estimated to be about 8meV, which is a reasonable value compared with the quantum-wire size of SEM view in Fig. 4.5.

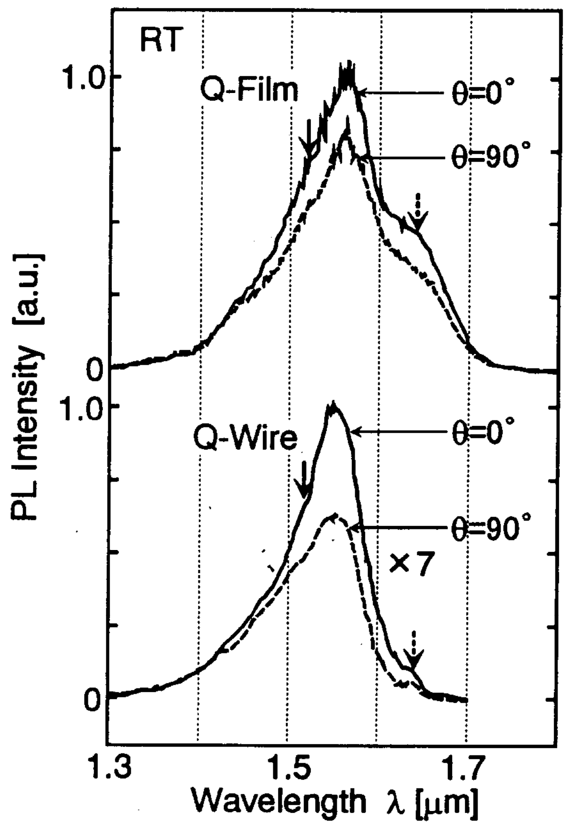

Fig. 4.6 Polarization properties of the PL spectrum of CS-Q-Wire structures compared with CS-Q-Film at room temperature.

Figure 4.7 shows the polarization dependence of the PL intensity of the CS-Q-Wire and the CS-Q-Film structures. As can be seen, a quite strange polarization dependence was observed in the CS-Q-Film sample, i.e. the normalized PL intensity took a maximum value at around θ=20 degree and a minimum at around θ=80 degree. The reason for this is not fully understood yet, but it may be attributed to a step formation or a lateral ordering due to strain[4-14]. The polarization anisotropy, i.e. I(θ=90 degree)/I(θ=0 degree), was 0.87 for the CS-Q-Film and was 0.63 for the CS-Q-Wire with the wire width of $\overline{W}$=35nm. Hence the relative factor of the polarization anisotropy was 0.63/0.87=0.72, which was a little smaller than that (0.77) of the LM-Q-Wire sample with the same size. This result indicates that the lateral quantum effect in the CS-Q-Wire is stronger than LM-Q-Wire, in other words, an effective mass of heavy hole band in the CS-Q-Film is smaller than that in the LM-Q-Film. Dashed lines show the theoretical curves from eq. (4.4) for reference.

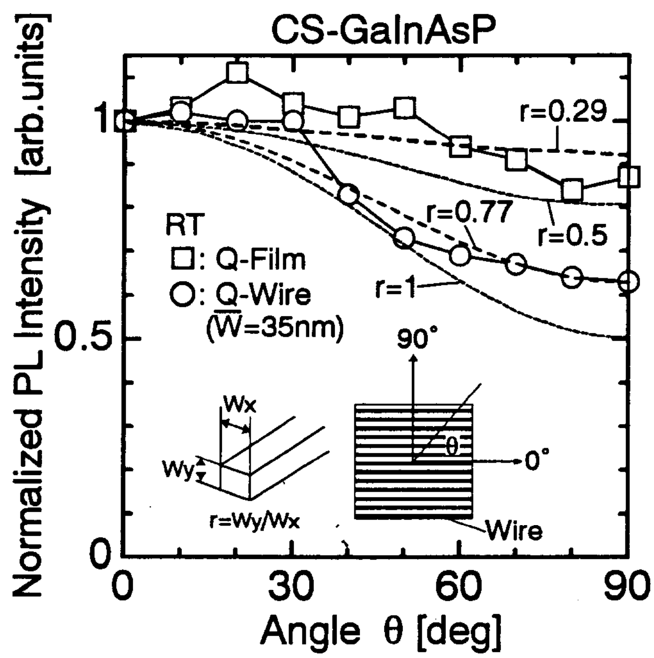

Fig. 4.7 The polarization dependence of the PL intensity of the CS-Q-Wire and CS-Q-Film structures.

When the Q-Wire structures were not embedded, i.e. etched, or embedded by the Tensile-Strained (TS) layer, the anisotropic polarization properties of Q-Wires were enhanced. Figure 4.8 shows the polarization dependence of the PL intensity at room temperature, and the polarization anisotropy, i.e. I(θ=90 degree)/I(θ=0 degree), was shown in Table 4.1. That of the LM-Q-Wire and LM-Q-Film(in Fig. 5.4), and of CS-Q-Wire embedded by the LM (InP) layer (in Fig. 4.7) were also shown as reference. The width of all the Q-Wires was $\overline{W}$=35nm. The reason for the enhanced polarization anisotropy was the composition modulation effect[4-12] for the Q-Wire embedded by the TS layer, of which the composition was $Ga_{0.22}In_{0.78}As_{0.16}P_{0.84}$ obtained by high-resolution x-ray diffraction measurement[4-15],[4-16], and due to the electric-field modulation effect as a result of anisotropic refractive index[4-17]. Especially, in the case of the as etched Q-Wire, I(θ=90 degree)/I(θ=0 degree) was 0.22, that is, the degree of polarization, [I(θ=0 degree)-I(θ=0 degree)]/[I(θ=0 degree)+I(θ=90 degree)] was 0.64, which was slightly larger than that in ref. [4-13]. This is attributed to the stronger lateral quantum effect in the CS-Q-Wire than that in the LM-Q-Wire.

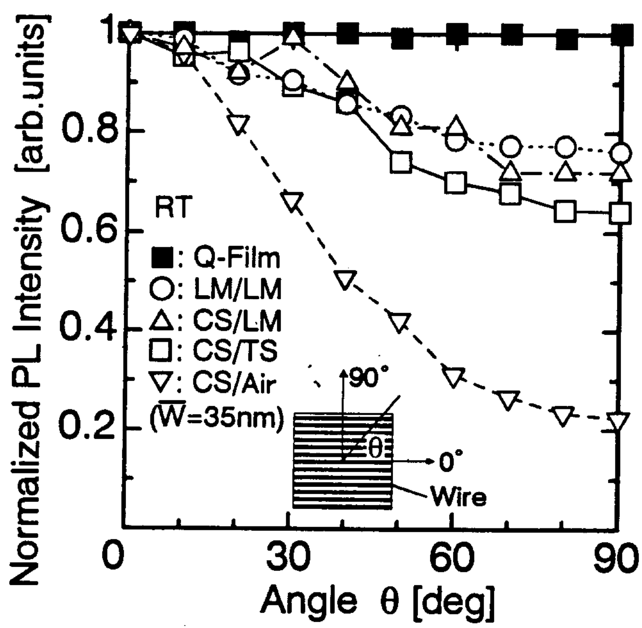

Fig. 4.8 The polarization dependence of the PL intensity of the Q-Wire with a various embedded layer.

Table 4.1 The degree of polarization of the Q-Wires at room temperature.

		Active	Regrown	I(θ=90°)/I(θ=0°)
Q-Film	■	LM	LM	1.0
Q-Wire ($\overline{W}$=35nm)	○	LM	LM	0.77
	△	CS	LM	0.72
	□	CS	TS	0.64
	▽	CS	Air	0.22

4.3 Temperature Dependence

The temperature dependence of the PL signal of the Q-Wire, which was the CS-Q-Wire embedded by InP as shown in Fig. 4.5, was also measured. Figure 4.9 shows the temperature dependence of the PL intensity of the Q-Wire and the Q-Film, normalized by the intensity of the Q-Wire at T=90K. Although the intensity of the Q-Wire was only about 14% of that of the Q-Film at room temperature, it became 80% at 90K. Considering the space-filling factor of the Q-Wire structure, which is 0.5, the PL intensity from the Q-Wire was 1.6 times larger than that from the Q-Film. The reason for this may be an efficient carrier capture in the Q-Wire structure in a relatively low temperature range. However the steep decline in the PL intensity of the Q-Wire suggests an increase in nonradiative recombination velocity at the regrowth interface. The sidewall recombination velocity of the Q-Wire was estimated from PL measurements by assuming that the PL intensity depends linearly on the carrier density normalized by the radiative carrier lifetime in the active region[4-18]. The product of the sidewall recombination velocity S and carrier lifetime τ, i.e., $S\cdot\tau$ can be given by

$$\frac{I_{Wire}/\rho}{I_{Film}}=\frac{1}{1+\dfrac{2\cdot S\cdot\tau}{W-W_d}}, \qquad (4.5)$$

where I_{Wire} and I_{Film} denote the PL intensity from the Q-Wire structure and that from the initial Q-Film structure, respectively. Here ρ is the in-plane space filling factor and W_d is the width of a so-called dead layer formed on both sides of the Q-Wire sidewalls. Assuming W_d=0, the $S \cdot \tau$ was estimated to be 56nm at room temperature and 0.6nm at T=200K. Thus, the nonradiative recombination velocity at the regrowth interface can be negligibly small at temperatures below T=200K.

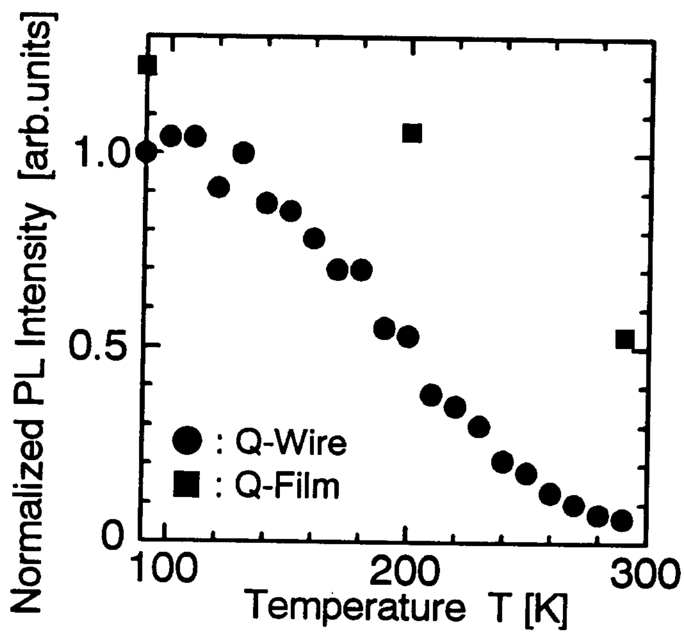

Fig. 4.9 The temperature dependence of the PL intensity of the Q-Wire and the Q-Film, normalized by the intensity of the Q-Wire at T=90K.

Figure 4.10 shows temperature dependencies of PL peak wavelengths of the Q-Wire and the Q-Film samples. The temperature coefficient of the PL peak wavelength of the Q-Wire was 0.5 nm/deg and was almost the same as that of the Q-Film. The energy blue shift for the Q-Wire sample is estimated to be about 8 meV, which is a reasonable value for the wire width of 35 nm.

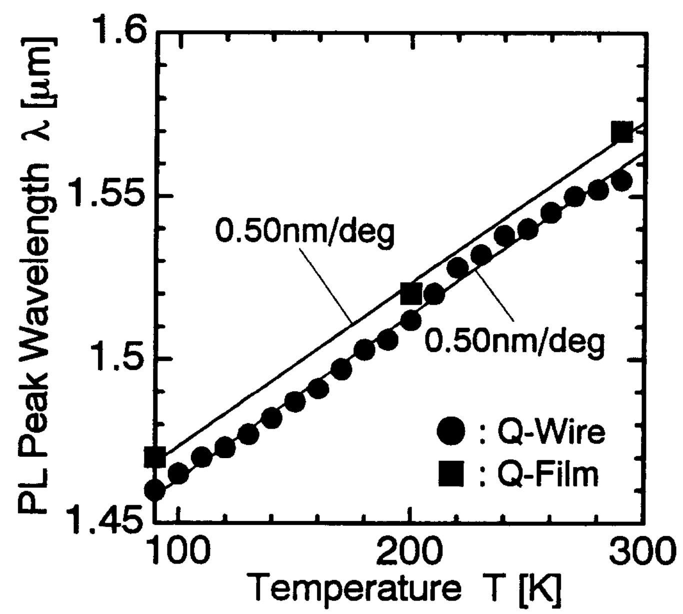

Fig. 4.10 The temperature dependencies of PL peak wavelengths of the Q-Wire and the Q-Film samples.

4.4 Conclusion

In conclusion, anisotropic polarization properties of PL intensity from GaInAsP/InP quantum-wire structures fabricated by an electron beam lithography and OMVPE regrowth were measured and it was experimentally confirmed that the polarization anisotropy becomes stronger in a narrow quantum-wire structure. A compressively-strained quantum-wire structure showed stronger polarization anisotropy compared to a lattice-matched one with the same size. The polarization dependence was enhanced due to a composition modulation effect and an electric-field modulation effect because of an anisotropic refractive index

From the temperature dependence of the PL signal, nonradiative recombination velocity at the regrowth interface of the Q-Wire can be negligibly small at temperatures below T=200K.

References

[4-1] Y. Arakawa and H. Sakaki, "Multidimensional quantum well laser and temperature dependence of its threshold current," *Appl. Phys. Lett.*, vol.40, no.11, pp.939-941, June 1982.

[4-2] M. Asada, Y. Miyamoto, and Y. Suematsu, "Gain and the threshold current of three-dimensional quantum-box lasers," *IEEE J. Quantum Electron.*, vol.QE-22, no.9, pp.1915-1921, Sept. 1986.

[4-3] Y. Arakawa and A. Yariv, "Quantum well lasers-gain, spectra, dynamics," *IEEE J. Quantum Electron.*, vol.QE-22, no.9, pp.1887-1899, Sep. 1986.

[4-4] Y. Miyake and M. Asada, "Spectral characteristics of linewidth enhancement factor α of multidimensional quantum wells," *Jpn. J. Appl. Phys.*, vol.28, no.7, pp.1280-1281, July 1989.

[4-5] H. Ando, H. Oohashi and H. Kanbe, "Carrier-induced optical nonlinear effects in semiconductor quantum well wire structure," *J. Appl. Phys.*, vol.70, no.11, pp.7024-7032, Dec. 1991.

[4-6] Y. Miyake, H. Hirayama, K. Kudo, S. Tamura, S. Arai, M. Asada, Y. Miyamoto and Y. Suematsu, "Room-Temperature Operation of GaInAs/GaInAsP/InP SCH lasers with quantum-wire size active region," *IEEE. J. Quantum Electron.*, vol.QE-29, no.6, pp.2123-2133, Jun. 1993.

[4-7] K. Kudo, Y. Nagashima, S. Tamura, S. Arai, Y. Huang and Y. Suematsu, "$Ga_{0.66}In_{0.34}As$/GaInAsP/InP tensile-strained single-quantum-well lasers with 70-nm period wire active region," *IEEE. Photon. Technol. Lett.*, vol.5, no.8, pp.864-867, Aug. 1993.

[4-8] M. Asada, Y. Miyamoto and Y. Suematsu, "Theoretical gain of quantum-well wire lasers," *Jpn. J. Appl. Phys.*, vol.24, no.2, pp.L95-L97, Feb. 1985.

[4-9] S. W. Corzine, R. H. Yan and L. A. Coldren, "Optical gain in III-V bulk and quantum well semiconductors," *Quantum Well Lasers*, ed. P. S. Zory *(Academic Press, New York, 1993)* Chap.1.

[4-10] M. Tsuchiya, J. M. Gaines, R. H. Yan, R. J. Simes, P. O. Holtz, L. A. Coldren, and P. M. Petroff, "Optical anisotropy in a quantum-well-wire array with two-dimensional quantum confinement," *Phys. Rev. Lett.*, vol.62, no.4, pp.466-469, Jan. 1989.

[4-11] S. T. Chou, K. Y. Cheng, L. J. Chou and K. C. Hsieh, "$Ga_xIn_{1-x}As$ multiple-quantum-wire lasers grown by the strain-induced lateral-layer ordering process," *Appl. Phys. Lett.*, vol.66, no.17, pp.2220-2222, Apr. 1995.

[4-12] P. J. Pearah, E. M. Stellini, A. C. Chen, A. M. Moy, K. C. Hsieh and K. Y. Cheng, "Strained $Ga_xIn_{1-x}P$ multiple quantum wire light emitting diodes: A luminescence polarization study," *Appl. Phys. Lett.*, vol.62, no.7, pp.729-731, Feb. 1993.

[4-13] P. Ils, C. Gréus and A. Forchel, "Linear polarization of photoluminescence emission and absorption in quantum-well wire structures: Experiment and theory," *Phys. Rev. B*, vol.51, no.7, pp.4272-4277, Feb. 1995.

[4-14] B. Lakshmi, B. J. Robinson and D. T. Cassidy, "[001] Interface anisotropy using degree of polarization," *IEEE 8th Int. Conf. on Indium Phosphide and Related Materials (IPRM'96)*, MA1-4, Schwäbisch Gmünd, pp.27-30, Apr. 1996.

[4-15] B. Jenichen, H. T. Grahn, T. Kojima and S. Arai, "Lateral periodicity and elastic stress relaxation in GaInAsP quantum wires on InP investigated by x-ray diffractometry," ***J. Appl. Phys.***, vol.83, no.11, pp.5810-5813, Jun. 1998.

[4-16] B. Jenichen, G. Paris, H. T. Grahn, D. Luebbert, T. Baumbach, T. Kojima, S. Arai and A. Mazuelas, "Stress relaxation in $Ga_{0.22}In_{0.78}As_{0.80}P_{0.20}$ quantum wires on InP investigated by high-resolution x-ray diffractometry," ***The 5th Int. Symposium on Quantum Effect Electron.***, 7, pp.26-31, Meguro, October 1998.

[4-17] U. Bockelmann, "Polarization-dependent optical-wave fields in grating structures," ***Europhys. Lett.***, vol.16, no.6, pp.601-606, Oct. 1991.

[4-18] M. Tamura, T. Ando, N. Nunoya, S. Tamura, S. Arai and G. U. Bacher, "Estimation of sidewall nonradiative recombination in GaInAsP/InP wire structures fabricated by low energy electron-cyclotron-resonance reactive-ion-beam-etching," ***Jpn. J. Appl. Phys.***, vol.37, pt.1, no.6A, pp.3576-3584, Jun. 1998.

Chapter 5

Lasing Properties of Quantum-Wire lasers

5.1 Introduction 116
5.2 I-L Characteristics 117
5.3 Cavity Length Dependence 120
5.4 Temperature Dependence 123
5.4.1 Threshold Current and Lasing Wavelength 123
5.4.2 Differential Quantum Efficiency 126
5.4.3 Internal Quantum Efficiency 131
5.4 Quantum-Wire DFB Lasers 142
5.5 Conclusion 146
References 148

5.1 Introduction

HIGH-PERFORMANCE operation of semiconductor lasers is expected by introducing either quantum-wire (Q-Wire) or quantum-box (Q-Box) structure as an active region because of a higher medium gain due to the elimination of carriers for unwanted energy levels[5-1]-[5-4]. In this chapter, the fundamental properties of 1.5μm wavelength compressively strained (CS) GaInAsP/InP single-quantum-well lasers with Q-Wire as the active region, fabricated by 2-step OMVPE growth, EB lithography and wet chemical etching, which the fabrication process is described in

Chapter 3 in detail. The temperature dependencies of threshold current, differential quantum efficiency and spontaneous emission efficiency of Q-Wire lasers are compared with those of Q-Film lasers prepared on the same wafer. Furthermore, the internal quantum efficiency of Q-Wire lasers was evaluated from the cavity length dependence of the differential quantum efficiency. Fundamental lasing properties of Q-Wire DFB lasers are also shown in the next section.

5.2 I-L Characteristics

Figure 5.1 shows (a) the cross sectional SEM view and (b) bandprofile of the Q-Wire laser (Q-Wre25, in short). As can be seen, the embedded GaInAsP Q-Wire was of a typical mesa-shape and the nominal wire width at the center depth $\overline{W}$ (W_U=20nm, W_L=35nm) was about 25nm. Figure 5.2 shows typical I-L characteristics of Q-Wire25 and Q-Film lasers with cleaved facets (a) at room temperature and (b) at 90K under pulsed condition. The cavity length L and the stripe width W_s of these lasers were 1050μm and 15.5μm, respectively. At room temperature, threshold current I_{th} of the Q-Wire25 laser was 390mA and was much higher than that of the Q-Film laser, but it rapidly decreased by lowering the temperature, and became lower than that of the Q-Film laser. As can be seen in Fig. 5.2(b), not only the lower threshold current but also the higher differential quantum efficiency operation of the Q-Wire laser was

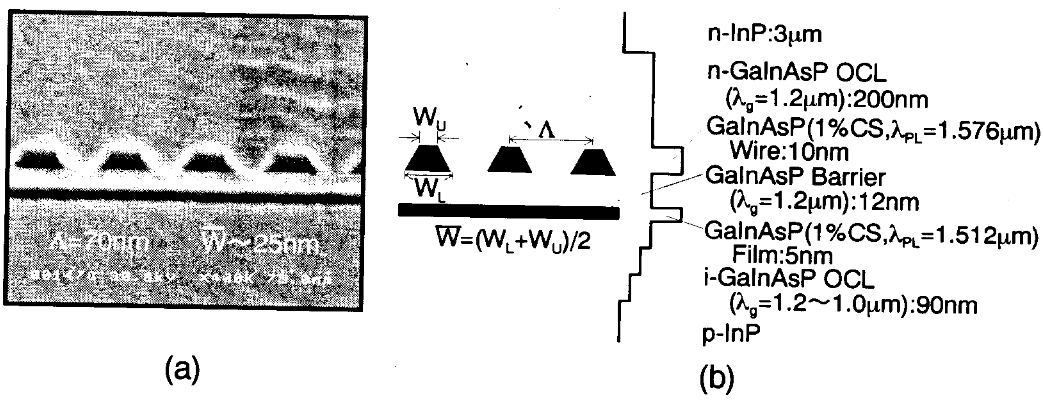

Fig. 5.1 (a) Cross-sectional SEM view and (b) band profile of Q-Wire25 laser. Λ=70nm and $\overline{W}$ =25nm.

obtained. At T=90K, threshold current density J_{th} of the Q-Wire laser was 34A/cm^2 (I_{th}=5.5mA) which was almost half that of the Q-Film laser (J_{th}=68A/cm^2 and I_{th}=11mA). Under continuous wave (CW) condition at T=90K, threshold current of the Q-Wire laser was 6mA (J_{th}=37A/cm^2) and that of the Q-Film laser was 12mA (J_{th}=74A/cm^2).

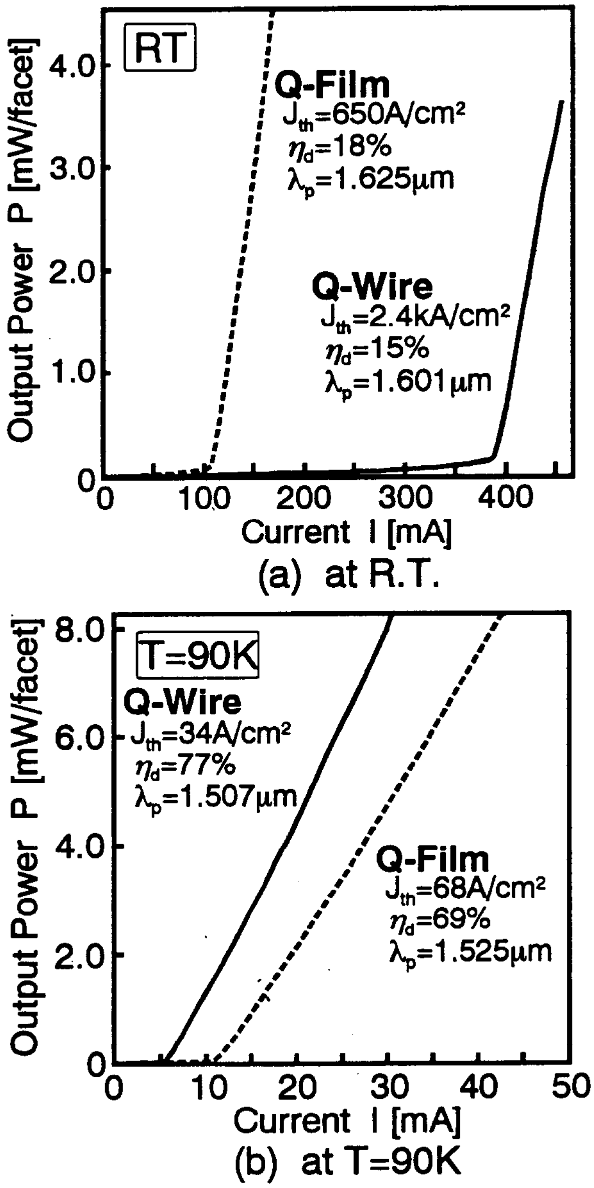

Fig. 5.2 I-L characteristics of Q-Wire (solid line) and Q-Film (dashed line) lasers (a) at room temperature and (b) at 90K. The cavity length and the stripe width of these lasers are 1050μm and 15.5μm, respectively.

Figure 5.3(a) shows the I-L characteristics of the 50-nm-period ($\overline{W}$ ~20 nm) Q-Wire laser (Q-Wire20) at T=90 K, which the cross sectional SEM view and bandprofile of Q-Wire20 are shown in Fig. 3.18. The cavity length L and the stripe width W_s of the laser were 400 μm and 15.5 μm, respectively. The threshold current (density) I_{th} (J_{th}) was 6.5mA (105A/cm^2) under pulsed conditions. The differential quantum efficiency η_d of 86% was obtained by measuring the slope of the I-L curve from 1-3mW. Under CW conditions at T=90K, the threshold current of the Q-Wire20 laser was obtained to be 4mA (J_{th}=38.5A/cm^2) with L=670μm as shown in Fig. 5.3(b).

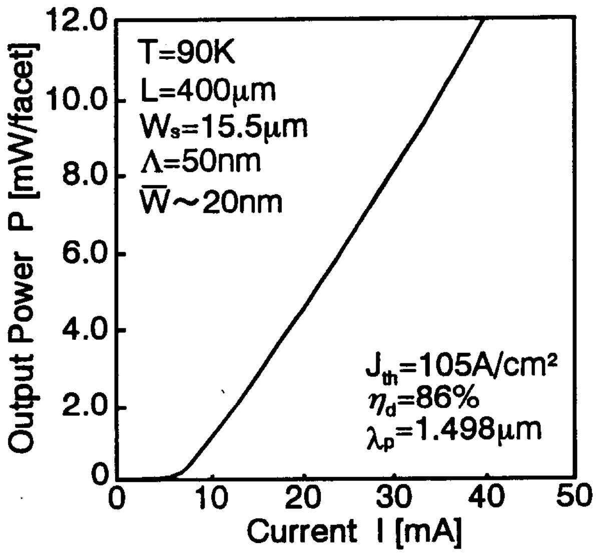

(a)

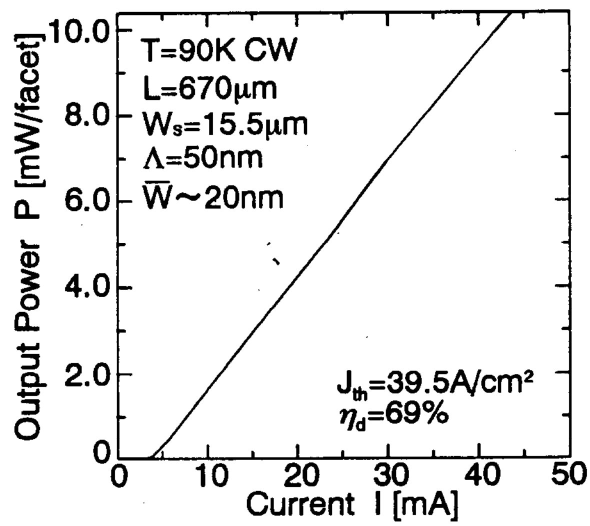

(b)

Fig. 5.3 I-L characteristics of Q-Wire20 laser with (a) L=400μm under pulse condition and (b) L=670μm under CW condition at T=90K.

5.3 Cavity Length Dependence

Then cavity length dependences of the differential quantum efficiency η_d and threshold current density J_{th} were measured at T=90 K. The data of other cavity lengths of Q-Wire20 lasers are listed in Table 5.1. The reciprocal differential quantum efficiency can be given by[5-5]

$$\frac{1}{\eta_d} = \frac{1}{\eta_i}\left\{1 + \frac{\alpha_{WG} L}{ln(1/R)}\right\}, \tag{5.1}$$

$$\alpha_{WG} = \xi \cdot \alpha_{ac} + (1-\xi)\alpha_{ex}, \tag{5.2}$$

where η_i is an internal quantum efficiency, α_{WG}, α_{ac} and α_{ex} are the waveguide loss, the loss in the active region and that in cladding region, respectively. R is the facet reflectivity, and ξ is the optical confinement factor of the active region. Figure 5.4(a) shows the inverse differential quantum efficiency $1/\eta_d$ of Q-Wire20 lasers as a function of the cavity length L (indicated by open squares □). Data points for the Q-Wire25 and the initial Q-Film laser are also indicated by triangles (△) and circles (○), respectively. The in-plane space filling factor ρ and the optical confinement factor ξ of the Q-Wire20 and Q-Wire25 lasers were 0.4 and 0.51%, and 0.36 and 0.46%, respectively, compared with ξ=1.27% for the Q-Film laser. As can be seen in Fig. 5.4(a), η_i was estimated to be almost 1.0, hence the carrier leakage is negligibly small at T=90 K. From the slope of $1/\eta_d$, the waveguide loss was determined to be α_{WG}~4.5 cm^{-1}, when R was assumed to be 0.33. In the case of Q-Wire25 and Q-Film lasers, α_{WG} was similarly estimated to be 3 cm^{-1} and 5 cm^{-1}, respectively by assuming η_i=1.0 at around this temperature. From eq. (5.2), α_{ac}~50 cm^{-1} and α_{ex}~ 3-4 cm^{-1} was obtained, which was similar to that in ref. [5-6].

Figure 5.4(b) shows the square root of threshold current density[5-7],[5-8] of these three types of lasers as a function of the reciprocal cavity length $1/L$. Recently, Ustinov et al. reported 1.9-μm-wavelength InAs/InGaAs/InP quantum-dot (InAs Q-Dot) lasers by self-organization growth[5-9], and J_{th} of this Q-Dot laser is also plotted as a reference. The optical confinement factor ξ of InAs Q-Dot laser was estimated to be 0.36% as in ref. [5-5]. In the case of Q-Wire25 with L=1050 μm, J_{th}=34 A/cm^2 (I_{th}=5.5mA) was obtained, which was almost half that of the Q-Film laser with L=1050 μm, and furthermore, η_d=77% of the Q-Wire25 was a little higher than that of the Q-Film laser (η_d=69%). However the sudden increase of J_{th} was observed for L<400 μm, as shown in Fig. 5.4(b). J_{th} of Q-Wire20 lasers also seems to increase at L=400 μm. This tendency was also reported for the InAs Q-Dot laser, that is, the steep increase in J_{th} was also observed when the cavity length was shorter than 240 μm. This is attributed to gain saturation due to the low optical confinement factor of Q-Wire/Q-Dot lasers[5-10],[5-11]. By fitting only in a linear gain region (L>600 μm), the transparent current density J_0 was estimated to be about 15 A/cm^2 for Q-Wire lasers (solid line) and 37 A/cm^2 for Q-Film lasers (dashed line). The product of the J_0 of the Q-Film laser (37 A/cm^2) and the space filling factor ρ of the Q-Wire lasers is J_0=14.8 A/cm^2 for Q-Wire20 and is J_0= 13.4 A/cm^2 for Q-Wire25, hence the leakage current of these Q-Wire lasers is negligibly small.

Table 5.1 Lasing properties of Q-Wire20 at T=90K.

L [μm]	I_{th} [mA]	J_{th} [A/cm^2]	η_d [%]
1020	6.0	38	61
670	4.0	39	69
400	6.5	105	86

Then we estimated material gain $g_{mat.}$ from the relationship that threshold modal gain is equal to the overall losses. Figure 5.5 shows the material gain as a function of current density normalized by the space filling factor ρ. As observed, differential material gain $\Delta g_{mat.} / \Delta(J/\rho)$ and maximum material gain of both Q-Wire lasers were approximately 1.7 times larger than those of the Q-Film laser while normalized transparent current density (J_0/ρ) was almost the same for all these lasers. From a theoretical point of view, the discrepancies between gains and parameters of the Q-Wire and the Q-Film lasers seem to be too large for the size fluctuation of ±2.9 nm of

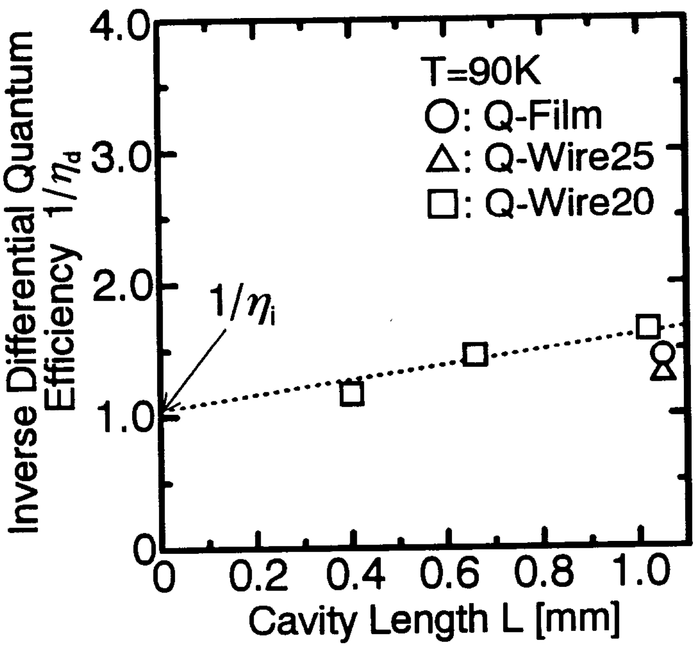

(a)

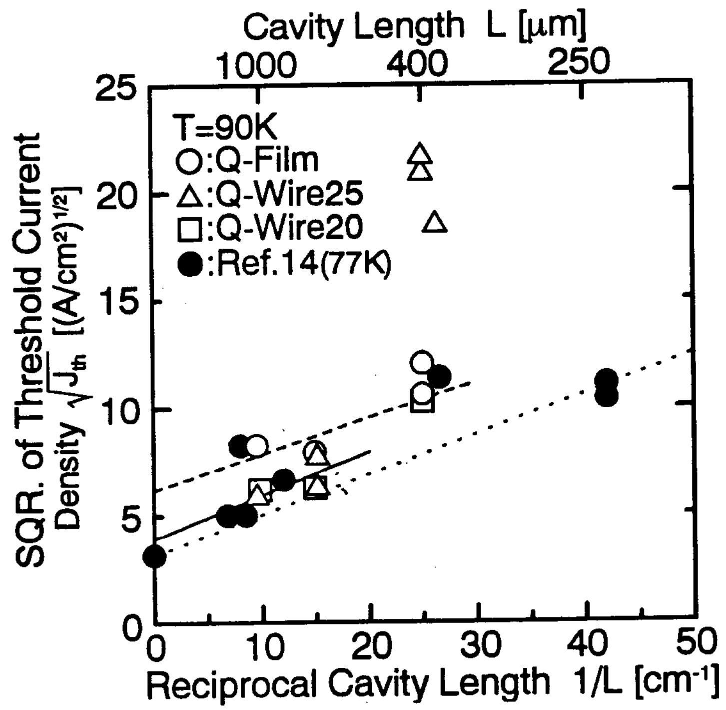

(b)

Fig. 5.4 Cavity length dependence of (a) inverse differential quantum efficiency and (b) square root of threshold current density.

the Q-Wire structure fabricated by the same process (see in chapter3). However the material gain spectrum of Q-Wire lasers was observed to be slightly narrower than that of a Q-Film laser even at a material gain level of around 1000 cm^{-1}, this fact indicates that the intraband relaxation time in the Q-Wire laser is longer than that in the Q-Film laser, which is described in the next chapter. For better comparison with theoretical material gain on injection carrier density, measurements of carrier lifetime should be carried out in future investigations.

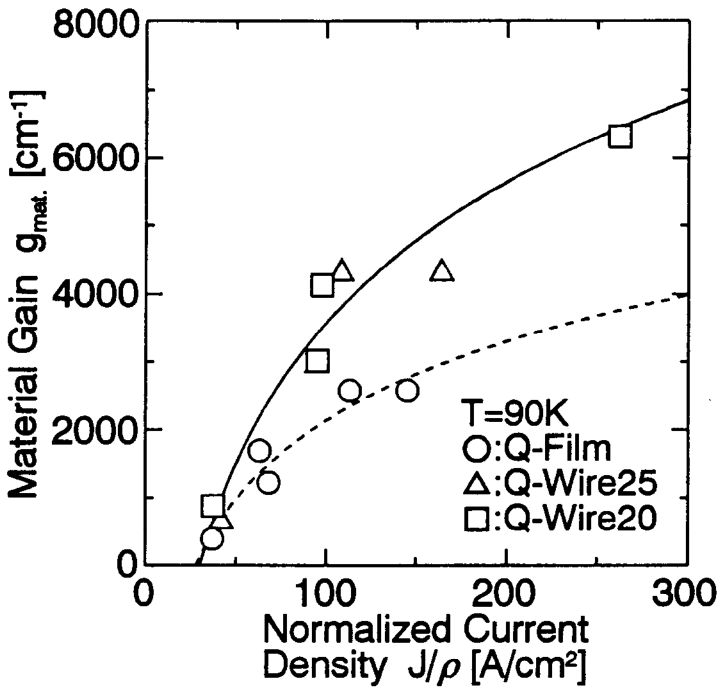

Fig. 5.5 Material gain as a function of current density normalized by in-plane space filling factor ρ.

5.4 Temperature Dependence

5.4.1 Threshold Current and Lasing Wavelength

Temperature dependences of lasing properties of Q-Wire lasers with 70nm periodic wires (Q-Wire25), i.e. threshold current, lasing wavelength and external differential quantum efficiency, were measured and compared with those of Q-Film lasers fabricated on the same wafer.

Figure 5.6 shows the temperature dependence of threshold current density of these two lasers under pulsed condition. Even though the threshold current of the Q-Wire laser was about four times greater than that of the Q-Film laser at room temperature, it rapidly decreased with a decrease in the temperature, and becomes lower than the Q-Film laser at T<170K. The characteristic temperature of the threshold current of the Q-Wire laser was T_0=137K for T<150K and T_0=37K for T>150K, which was poorer than that of the Q-Film laser in contrary to the theoretical prediction of low-dimensional quantum-well lasers[5-1]. The reason for this experimental result is considered to be attributed to too small optical confinement factor ξ of the active region as well as temperature dependent non-radiative recombination at the regrowth interface, which will be discussed in the next port (§ 5.4.2). In case of Q-Dot laser, the T_0 started to decrease at T=170K with cleaved facets and at T=200K with HR coated facets[5-12].

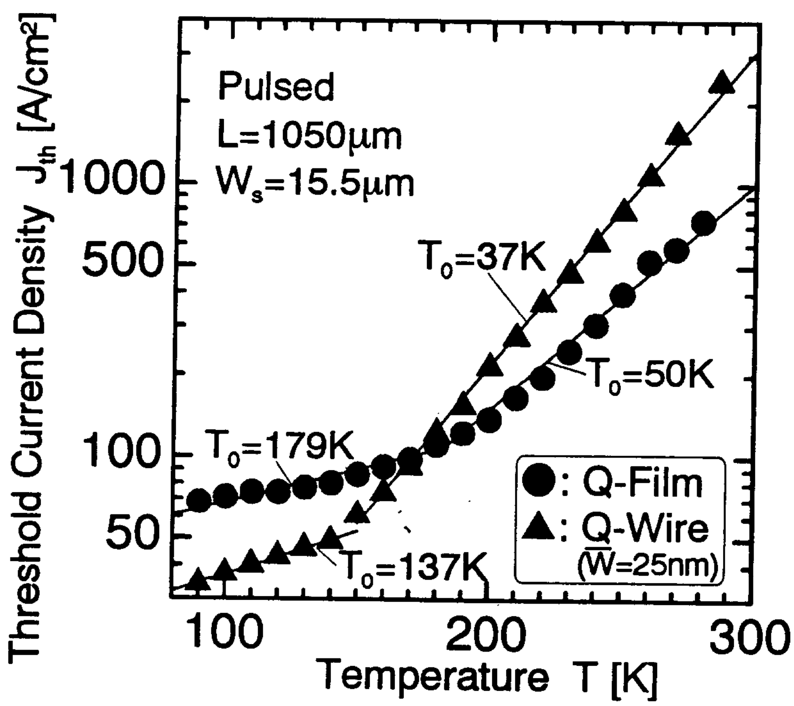

Fig. 5.6 Temperature dependence of threshold current density of Q-Wire and Q-Film lasers under pulsed condition.

Figure 5.7 shows the temperature dependence of the lasing wavelength of these two lasers measured at I=1.1I_{th}. Since the stripe width of these lasers was much wider than transverse single-mode conditions, temperature dependence the lasing wavelength showed a little large mode jump at certain temperatures. An incremental temperature coefficients $\Delta\lambda/\Delta T$ of the lasing wavelength of the Q-Film laser was obtained by the least square method to be 0.56nm/deg, while that of the Q-wire laser was 0.51nm/deg. These values were similar to temperature coefficients of PL peak wavelengths as shown in Fig. 4.10. Lasing wavelength of the Q-Wire laser was 1.601μm and that of the Q-Film laser was 1.625μm at room temperature, hence the energy blue shift in the Q-Wire laser was estimated to be about 11meV. Similarly the energy blue shift was estimated to be around 9-10meV at 90-140K. This value was in good agreement with that from theoretical one (15meV) with the wire width of 25nm when an effective mass of heavy-hole band along vertical (epitaxial-layer) direction was assumed to be $m^*_{hh\perp} = 0.37m_0$ (m_0: electron mass).

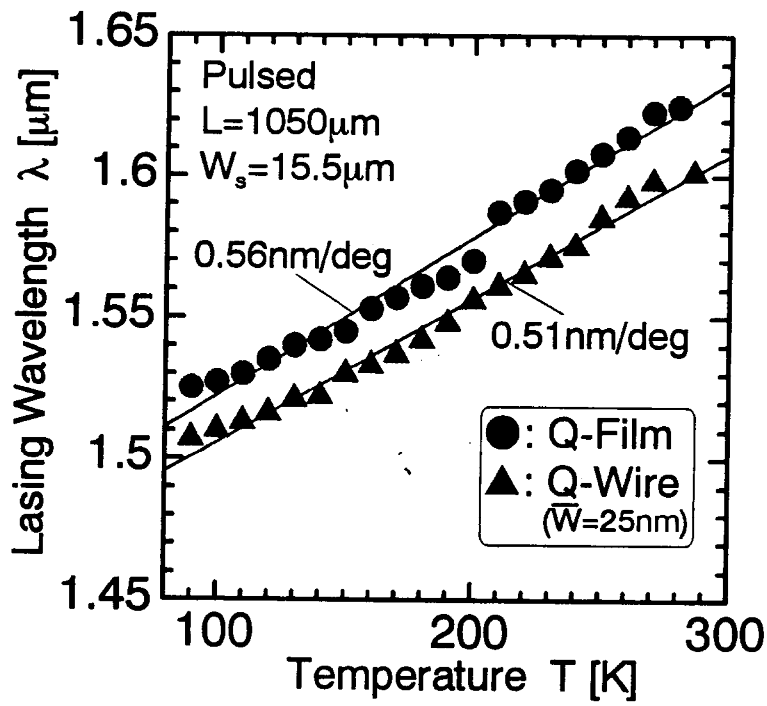

Fig. 5.7 Temperature dependence of the lasing wavelength of Q-Wire and Q-Film lasers.

From experimental results shown in Figs. 5.6 and 5.7, superior lasing properties of the Q-Wire laser was considered to be attributed to inherent optical property of low-dimensional structures and/or smaller volume of the active region (volume effect). Hence we measured spontaneous emission spectrum of the Q-Wire laser and compared with that of the Q-Film laser at T=100K. Figure 5.8 shows edge emitted spontaneous emission spectra at various CW injection current levels. These spectra were almost the same, but the tail of shorter wavelength side (i.e. higher energy side) slightly broadened at higher injection current. The full width at half maximum (FWHM) of the emission spectrum of the Q-Wire laser was about 10meV at I=1mA (J=6.2A/cm^2), and was almost the same as that of the Q-Film laser (FWHM=10~11meV), hence the lower threshold current operation of the Q-Wire laser can be considered to be due to the volume effect. The narrower FWHM of 1meV at T=2K was reported for GaInAs Q-Dot arrays fabricated by EB-lithography and etching[5-13]. A red shift of the peak wavelength of the spontaneous emission compared with the lasing wavelength under pulsed condition may be attributed to temperature rise due to CW injection current because the laser chip was mounted epi-side-up on a small copper block without bonding.

5.4.2 Differential Quantum Efficiency

Temperature dependences of differential quantum efficiency η_d of Q-Wire and Q-Film lasers were also measured and results are shown in Fig. 5.9. As can be seen, the differential quantum efficiency η_d of Q-Wire laser rapidly reduced at temperature above 200K and became lower than that of Q-Film laser at T>230K. The reason for poor performance (lower η_d and higher I_{th}) of the Q-Wire laser at around room temperature may be due to larger fraction of non-radiative recombination caused by carrier overflow over hetero-barriers and temperature dependent surface (interface) recombinations at regrowth interfaces. Actually the slope efficiency of spontaneous emission below the threshold of the Q-Wire laser was about 50% that of the Q-Film laser at room temperature. Another reason is too small optical confinement factor ξ which causes carrier leakage to OCL[5-14],[5-15] and leads to increase in threshold carrier density.

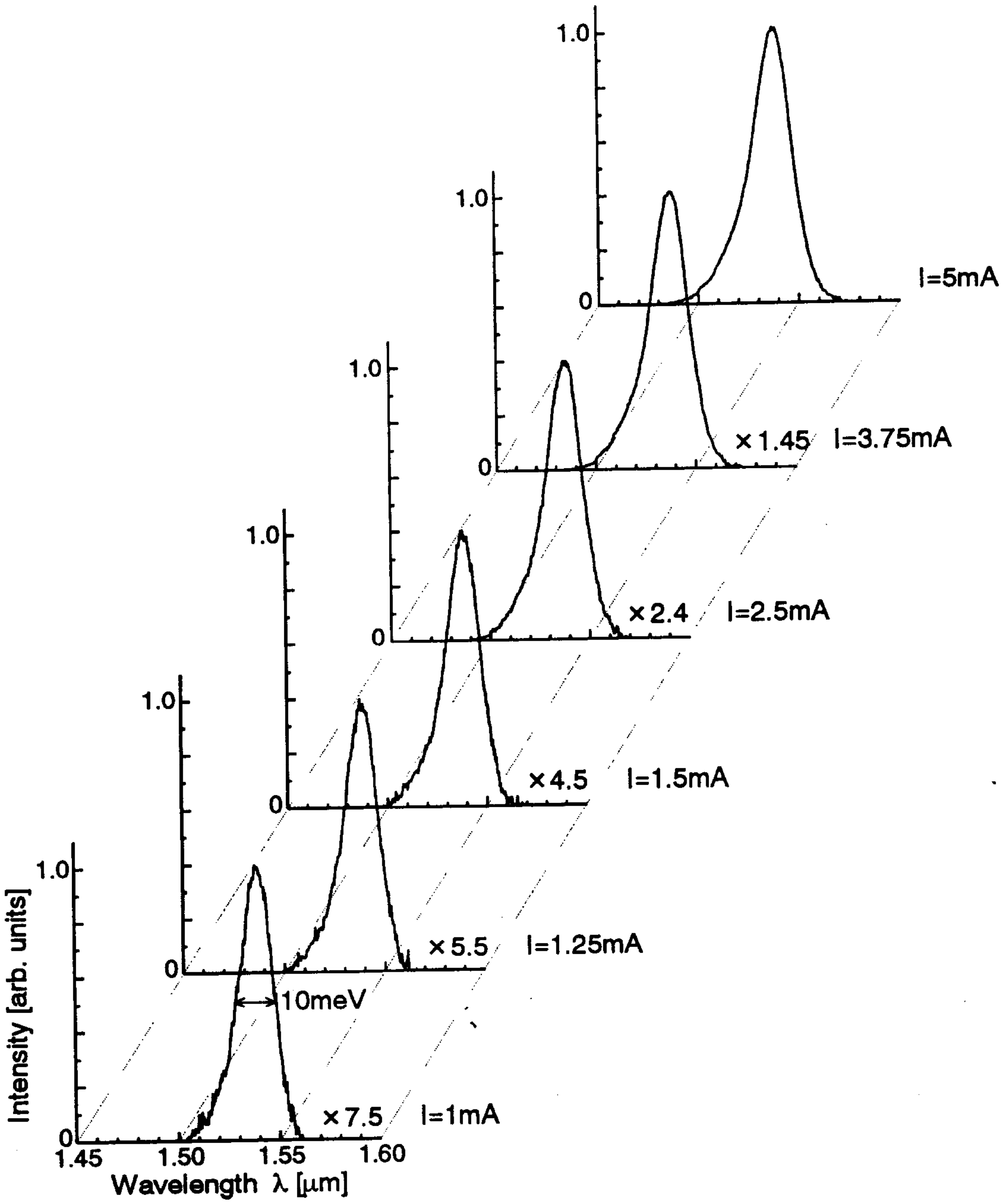

Fig. 5.8 Spontaneous emission spectra of Q-Wire laser from 1mA to 5mA under CW condition at T=100K. FWHM at I=1mA is 10meV.

Actually the optical confinement factor of the Q-Film laser is calculated to be ξ_{Film}=1.27%, while that of the Q-Wire laser is only $\xi_{Film} \cdot \rho$=1.27·(25/70)=0.46%, where ρ is an in-plane space filling factor of the Q-Wire structure. Lasing properties of the Q-Wire and the Q-Film lasers shown in Figs. 5.6-5.9 are summarized in Table5.2.

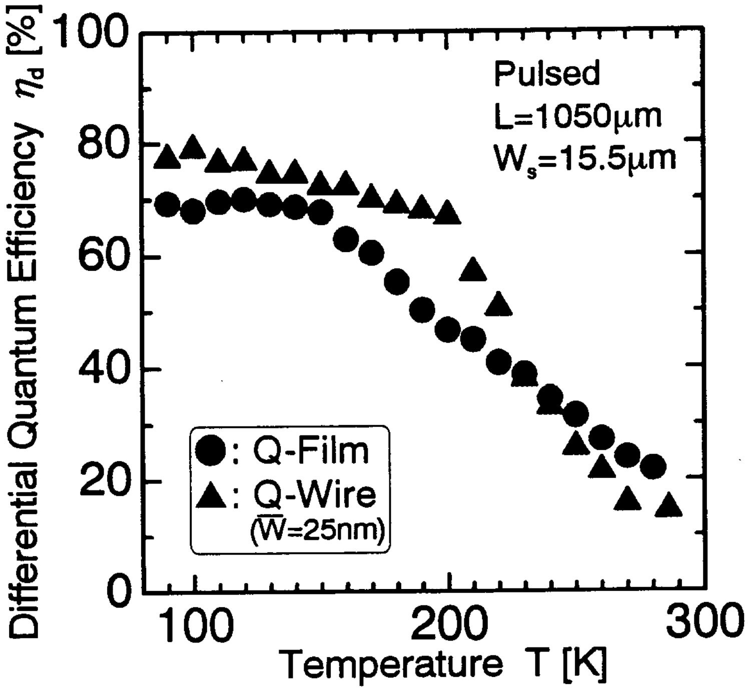

Fig. 5.9 Temperature dependence of differential quantum efficiency of Q-Wire and Q-Film lasers.

Table 5.2 Lasing properties of Q-Wire25 and Q-Film lasers.

	L[μm]	Ws[μm]	Λ[nm]	$\overline{W}$[nm]	ρ	ξ [%]	R.T.			90K			$\Delta\lambda/\Delta T$
							I_{th} [mA]	J_{th}[A/cm^2]	η_d [%]	I_{th} [mA]	J_{th}[A/cm^2]	η_d [%]	[nm/deg]
Q-Wire25	1050	15.5	70	25	0.36	0.46	390	2400	15	5.5	34	77	0.51
Q-Film	1050	15.5	—	—	1.0	1.27	105	650	18	11	68	69	0.56

In order to investigate the reason for poor performance of the Q-Wire laser at around room temperature, we measured temperature dependences of spontaneous emission efficiency of Q-Wire and Q-Film lasers. Figure 5.10 shows temperature dependence of spontaneous emission efficiency of them normalized at T=90K. Since the spontaneous emission efficiency η_{spon} can be given by,

$$\eta_{spon} = \tau_s / \tau_R \text{,} \tag{5.3}$$

$$1/\tau_s = 1/\tau_R + 1/\tau_{NR} \text{,} \tag{5.4}$$

where τ_R and τ_{NR} are lifetimes for radiative and non-radiative recombination processes, and τ_s is the carrier lifetime[5-16], the rapid decrease in η_{spon} can be considered to be due to a rapid decrease in τ_{NR} with respect to τ_R. Actually the rapid decrease in η_{spon} became noticeable at 20～30K lower than the temperature where η_d decreased rapidly. Since measurements were done at the same injection current of 3mA for Q-Wire and Q-Film lasers, the carrier overflow to OCL in the Q-Wire laser is considered to be as same as that in the Q-Film laser. Hence the rapid decrease in η_{spon} of the Q-Wire laser at around room temperature was considered to be attributed to carrier-trap to non-radiative recombination centers at around regrowth interface dominantly. Further measurements of carrier lifetimes and their dependences on temperature and carrier density will be required to clarify the mechanism.

The reason for this poor differential quantum efficiency of the Q-Wire laser at around room temperature may be due to increase in optical absorption loss, such as intervalence band absorption[5-5],[5-17] in OCLs because higher threshold carrier density due to smaller optical confinement factor of the active region leads to carrier leakage to OCLs.

From the spontaneous emission efficiency, the product of the surface recombination velocity beside the wires S and the carrier life time τ, $S \cdot \tau$ can be estimated[5-18]. Spontaneous emission efficiency $\eta_{spon,wire}$ of a laser with a wire-like active region normalized by that of an initial quantum-well film laser can be written as

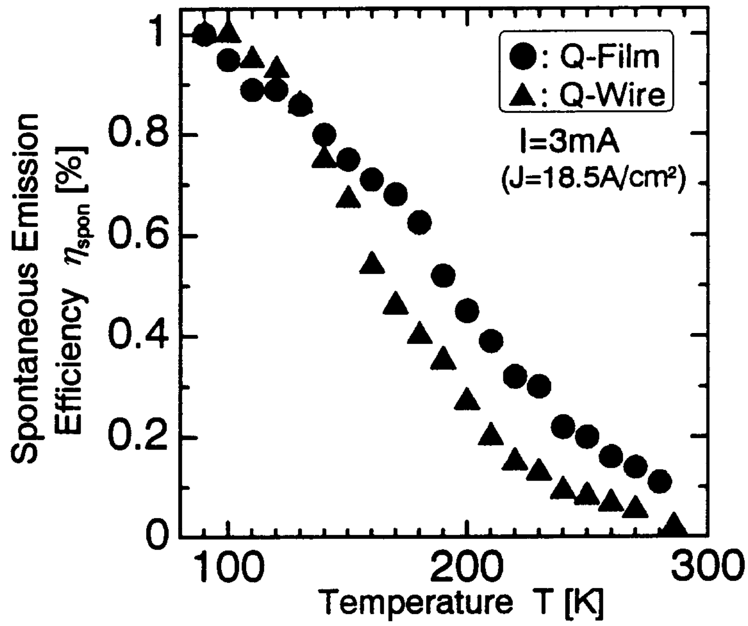

Fig. 5.10 Temperature dependence of spontaneous emission efficiency of Q-Wire and Q-Film lasers at injection current of 3mA.

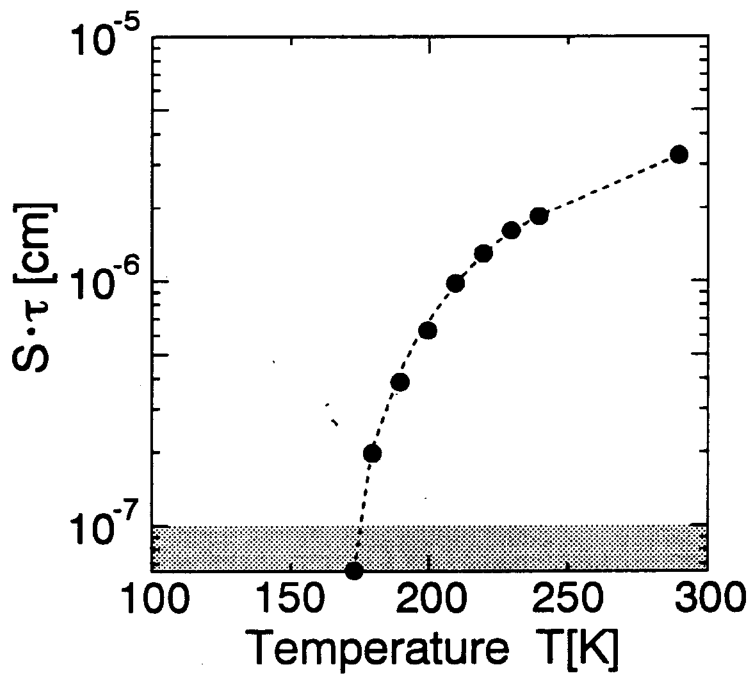

Fig. 5.11 Temperature dependence of the product of the surface recombination velocity beside the wires and the carrier life time $S \cdot \tau$.

$$\frac{\eta_{spon,wire}}{\eta_{spon,film}} = \frac{1}{1+\dfrac{2S\cdot\tau}{W-2W_d}}, \qquad (5.5)$$

which equation is similar to that in case of photoluminescence as shown in eq. (4-5). Normalized spontaneous emission efficiency $\eta_{spon,wire}/\eta_{spon,film}$ can give much accurate measurement of the nonradiative recombination process compared with that estimated from threshold current density[5-18]. Figure 5.11 shows the temperature dependence of the product of the surface recombination velocity beside the wires and the carrier life time $S\cdot\tau$. At room temperature, the $S\cdot\tau$ was estimated to be about 30nm, but it rapidly decreased by lowering the temperature, and became lower than 1nm at T<180K. This result was similar to that from the PL. Thus, the nonradiative recombination velocity at the regrowth interface can be negligibly small at the temperature below ~200K.

5.4.3 Internal Quantum Efficiency

Figure 5.12 shows the temperature dependencies of three kinds of the lasers with different cavity lengths. The characteristic temperature T_0 ($J_{th}(T)=J_{th0}\exp(T/T_0)$) of threshold current of the Q-Wire25 samples was found to be very sensitive to the cavity length, whereas that of the Q-Wire20 samples was not so sensitive. The poorer characteristic temperature of the Q-Wire25 was attributed to an increase in threshold material gain due to a lower optical confinement factor, while T_0 of the Q-Wire20 is larger because of a slightly larger optical confinement factor[5-20]. Further improvement can be expected by adopting narrower wires without sacrificing the space filling factor. The characteristic temperature T_0 and the optical confinement factor of these lasers are summarized in Table 5.3 and 5.4, respectively.

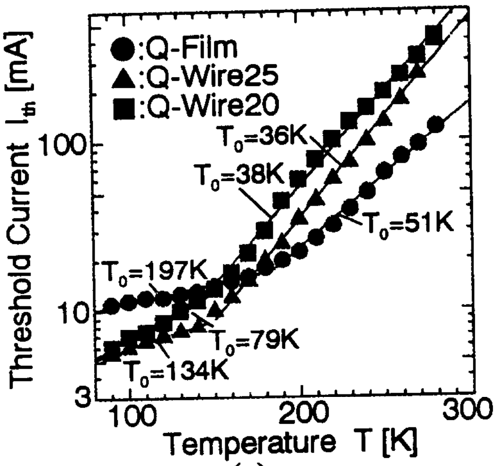

(a)

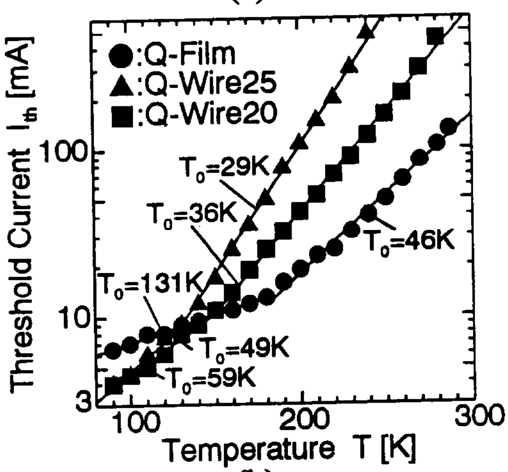

(b)

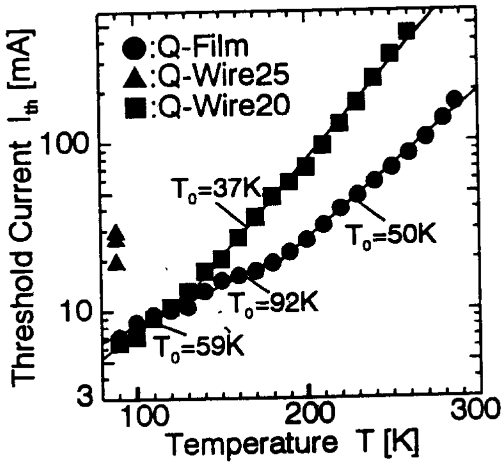

(c)

Fig. 5.12 Temperature dependencies of the threshold current of the three kinds of lasers with the Cavity length of (a) 1mm, (b) 670μm, and (c) 400μm, respectively.

Table 5.3 Summary of characteristic temperature T_0.

	Q-Film		Q-Wire25		Q-Wire20	
	T_0(L.T.)	T_0(H.T.)	T_0(L.T.)	T_0(H.T.)	T_0(L.T.)	T_0(H.T.)
L=1000μm	197	51	134	36	79	38
L=660μm	131	46	49	29	59	36
L=400μm	92	50	——	——	59	37

Table 5.4 Summary of optical confinement factor ξ and in-plane space filling factor ρ.

	ρ	ξ [%]
Q-Film	1.0	1.27
Q-Wire25	0.36	0.46
Q-Wire20	0.40	0.51

Figure 5.13 shows the cavity length dependence of the threshold current density J_{th} of Q-Wire lasers and a comparison with the Q-Film laser at room temperature. As can be seen, the transparent current density J_0 of the Q-Wire lasers was about 660A/cm^2. Thus the J_{th} of the Q-Wire laser can be reduced with the low cavity loss structure, such as a long cavity or HR coating. On the other hand, the J_0 of the Q-Film laser was about 140 A/cm^2, which is a little higher than that of CS-SQW laser by one-step growth as shown in Chapter 3.

Figure 5.14 shows the temperature dependence of the transparent current density J_0 and the threshold current density J_{th} of the Q-Wire20 and the Q-Film lasers. Filled marks correspond to J_0 and open marks correspond to J_{th}, respectively, for the cavity length of 1 mm. J_0 of the Q-Wire20 laser was lower than that of the Q-Film laser at a temperature below 150 K, and J_{th} was lower at T<190 K. However, J_0 rapidly

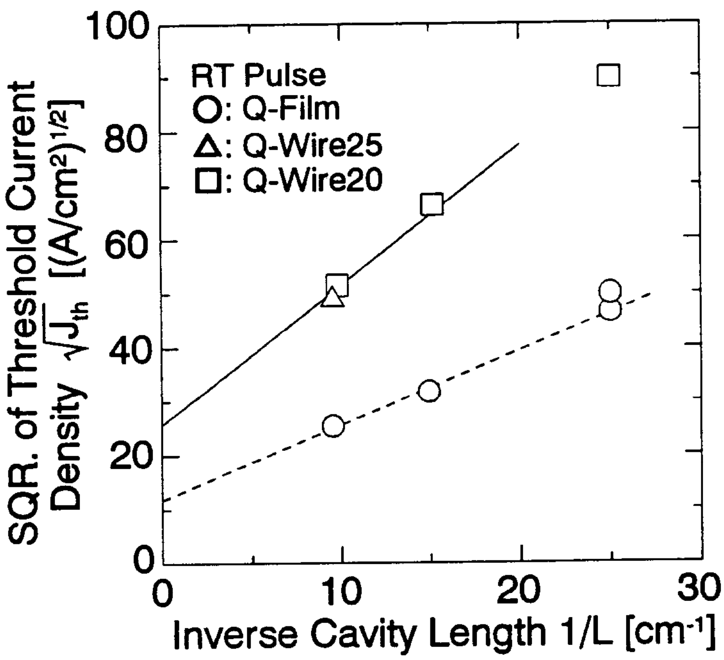

Fig. 5.13 Cavity length dependence of threshold current density of Q-Wire lasers compared with that of Q-Film lasers.

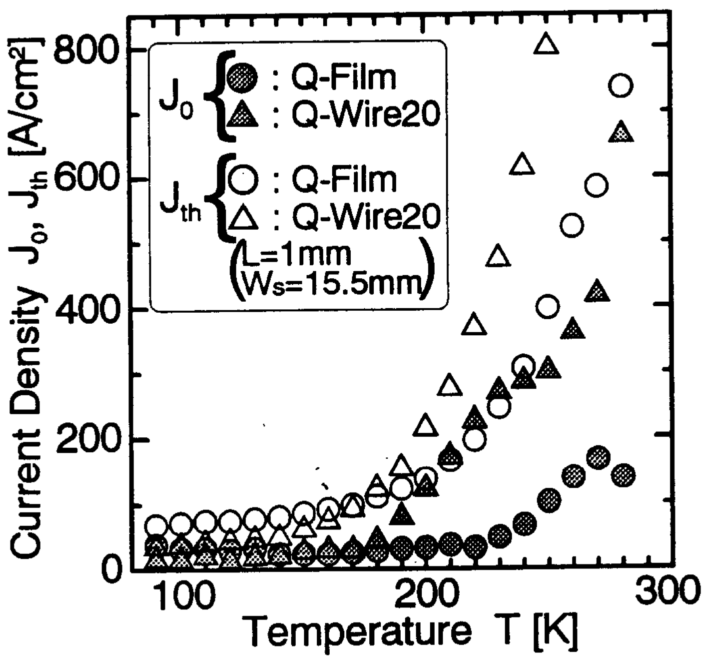

Fig. 5.14 Temperature dependence of transparent current density and threshold current density of Q-Wire20 and Q-Film lasers.

increased at T>230 K for the Q-Film and at T>190 K for the Q-Wire20 laser, and the incremental slope $\Delta J_0/\Delta T$ of the Q-Wire20 laser was 1.5 times higher than that of the Q-Film laser. The J_{th} of both lasers also rapidly increased as well as the J_0. The increase in J_{th} seems to be related to the increase in J_0[5-20].

By measuring the temperature dependence of the differential quantum efficiency of these Q-Wire lasers, we obtained the temperature dependence of the internal quantum efficiency η_i and the waveguide loss α_{WG} of the Q-Wire20 laser, as shown in Fig. 5.15. As can be seen, $\eta_i \sim 1.0$ was evaluated at T<200 K. Since η_i above threshold conditions is defined as the ratio of the increase in the number of generated photons to the increase in the number of injected electrons, a rapid decrease of η_i at T>200 K can be attributed to temperature-dependent non-radiative recombination[5-21], such as carrier overflow or carrier leakage beside the wires[5-22]. The increase in J_0 corresponds to the decrease in η_i.

Temperature dependence of spontaneous emission efficiency (slope efficiency below threshold) was measured and a steep decrease with an increase in temperature at around T>200 K was observed as mentioned in the previous section, which corresponds to a rapid increase in threshold current. This may also be attributed to non-radiative recombination around the regrowth interface, therefore, the growth temperature and regrowth process to overcome this problem are still under investigation.

α_{WG} also increased rapidly with the temperature, which can be largely attributed to the inter-valence band absorption and free carrier absorption [5-23]-[5-24] in GaInAsP OCLs, because of the small optical confinement factor of the active layer.

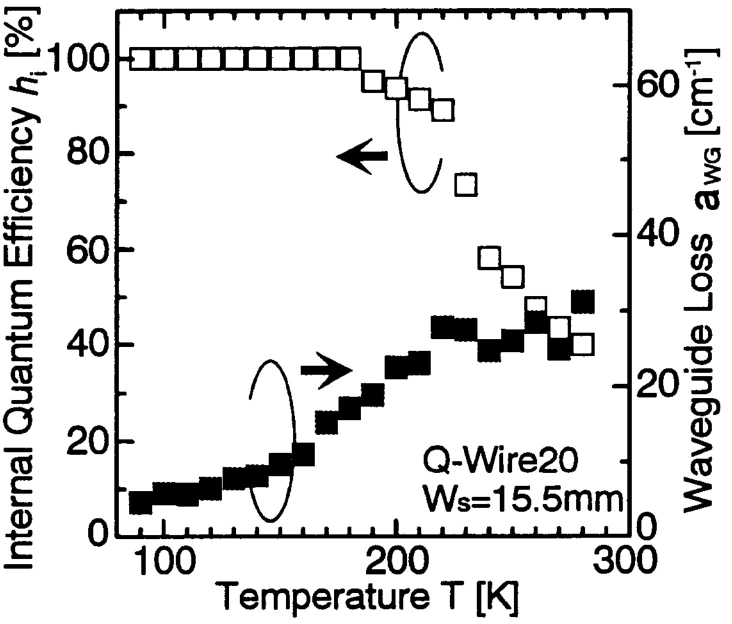

Fig. 5.15 Temperature dependence of internal quantum efficiency and waveguide loss of Q-Wire20 laser.

It can explain to some extent the further reduction of the threshold current density of the Q-wire lasers[5-25]. Two reasons for poorer characteristic temperature of the threshold current of the Q-Wire lasers than the Q-Film laser were considered; one was non-radiative recombination at the regrowth interface and the other was carrier overflow or leakage beside the wires. The threshold current density can be given by[5-26],

$$J_{th} = \frac{edB_{eff}N_{th}^2}{\eta_i \eta_{spon}}; \qquad (5.6)$$

If we can obtain higher η_i and η_{spon}, at room temperature, that is, the same as those of the Q-Film laser, J_{th} of the Q-Wire lasers would be drastically reduced. From the measurement of η_{spon}, one can see that only 50% of carriers compared with those of the Q-Film laser take part in radiative recombination. If it is simply assumed that the spontaneous emission efficiency decreases due to the non-radiative recombination and the internal quantum efficiency decreases due to the carrier leakage, we can separate the two reasons increasing the threshold current density of the Q-Wire lasers. The η_i of the Q-Film laser was assumed to be 90% at T>240K, and 100% at T<230K because that of 5MQW laser fabricated by the same process was 90% at room temperature[5-18] and a rapid increase in J_{th} of the Q-Film laser was observed at T>230K as shown in Fig.5.14. For example, only 50% of carriers participate in radiative recombination and only about 44(=40/90)% of them take part in stimulated emission, as compared with the Q-Film laser. Thus, only about 22% of the applied current is used to reach the threshold in the case of the Q-Wire laser. Figure 5.16 shows the temperature dependence of the net threshold current density of the Q-Wire laser (in case of the Q-Wire25 with L~1mm as shown in Fig. 5.6). The region above the dot line shows the increasing J_{th} due to carrier leakage and that below the dot line shows the increasing J_{th} due to non-radiative recombination. As can be seen, the reason for the increasing J_{th} due to non-radiative recombination at the regrowth interface was more dominant than that due to carrier overflow or leakage beside the wires. If the same η_i and η_{spon}, as those of the Q-Film laser can be obtained, T_0 of the Q-Wire laser is expected to be 82K

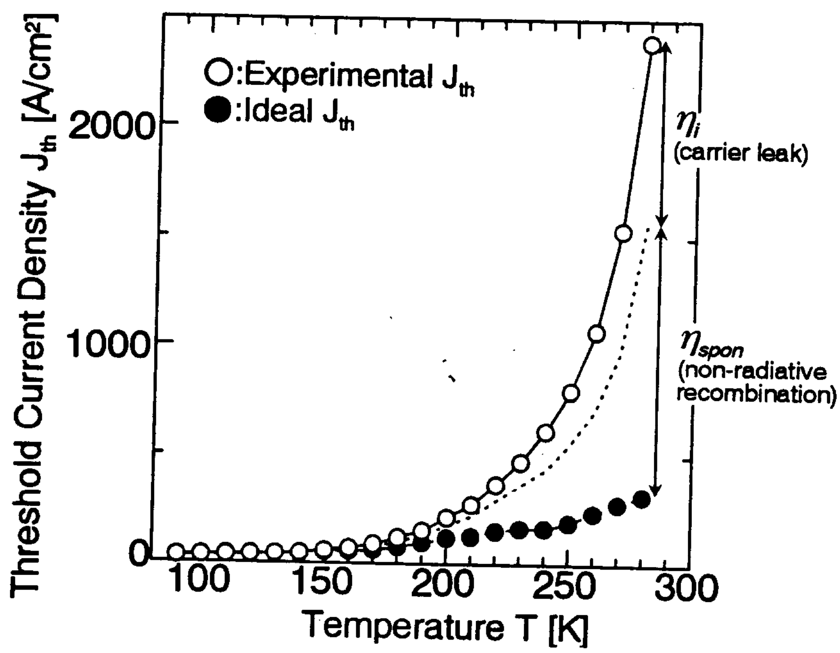

Fig. 5.16 Comparison of the temperature dependence of the threshold current density of Q-Wire laser between ideal and experimental results

at T>200K.

Figure 5.17 shows the temperature dependence of the lasing wavelength of Q-Wire20 lasers and the Q-Film laser. Temperature coefficients of the lasing wavelength of these lasers were almost the same, namely 0.5 nm/deg, which was similar to that of Q-Wire25 as shown in Fig. 5.7. In order to estimate the fundamental energy level shift due to the lateral quantum size effect, several effects, such as the band filling, the bandgap shrinkage[5-27] and the strain relaxation[5-13] at the regrowth interface should be taken into account. In this study, we assumed that these effects were almost the same and negligible, since the injected current density normalized by the space filling factor of both lasers were almost the same, i.e., 95(=38/0.4)A/cm^2 (L=1020 μm) for the Q-Wire20 laser and 68 A/cm^2 (L=1050 μm) for the Q-Film laser. Actually the electro-luminescence (EL) peak at a bias level of $0.1I_{th}$ at T=100 K was almost the same as the lasing wavelength (photon energy was less than 1 meV). The blue shift energy for the Q-Wire20 to the Q-Film lasers was estimated at 90 K so as to eliminate the band-filling effect at around room temperature and was about 15 meV, which was in good agreement with the theoretical value (20 meV) for the wire width of 20 nm when the effective masses of heavy-hole bands along the vertical (epitaxial-layer) and the in-plane direction were assumed to be $m^*_{hh\perp} = 0.37m_0$ (m_0: electron mass) and $m^*_{hh//} = 0.052m_0$[5-28], respectively. A large discrepancy in the temperature coefficients of the Q-Wire20 with L=670 μm and L=400 μm at around room temperature may be attributed to the band-filling effect due to higher threshold carrier density. In the case of L=400 μm, a mode jump was observed at around T=240 K, which can be regarded as emission from the higher-order subbands due to band filling and also due to increasing thermal excitation[5- 29], or emission from the 5-nm-thick Q-Film layer grown below the 10-nm-thick active Q-Film layer as shown in Fig. 3.18.

Figure 5.18 shows the wire width dependence of the blue shift energy for the Q-Wire to the Q-Film laser. The solid line is the calculated energy shift of the fundamental level and the dash line is that of the second level. In this calculation, it was assumed that the active layer was $Ga_{0.18}In_{0.82}As_{0.73}P_{0.27}$ and the bandgap wavelength of the barrier layer was 1.2μm. The difference of the transition energy between the 5-nm-thick Q-Film layer and the 10-nm-thick active Q-Film layer was estimated at about 50meV. When the wire width becomes about 10nm, the optical gain peak of the Q-Wire can be fitted to that of the 5-nm-thick Q-Film layer. The closed circles show the experimental results of the blue shift energy estimated from the lasing wavelength and the open circle shows that estimated from the PL peak wavelength as shown in Fig. 4.10. The error bars indicate the wire width from the mesa-top to the mesa-bottom and the circles mean the average size. By changing the duration of wet-etching process, a narrower Q-Wire structure laser was fabricated. The average size of the Q-Wire structure was 15nm (12nm at mesa top and 18nm at mesa bottom) with a period of 70nm. The blue shift energy was estimated to be 20meV at T=90K. The blue shift energy of the Q-Wire structure dependent on the wire width W in the conduction band and the valence band are also shown in Fig. 5.19 (a) and (b), respectively. The parameters were the same as those in Fig. 5.18. When the energy separation between the ground (fundamental) level and the second level is necessary to be more than 30meV in the conduction band, the wire width should be 5nm $< W <$25nm. On the other hand, the energy separation between them is in sufficient because the thickness of the initial Q-Film active layer is relatively thick (10nm). However, in the case of 10nm $< W <$ 25nm, the energy separation can be obtained to be more than 20meV.

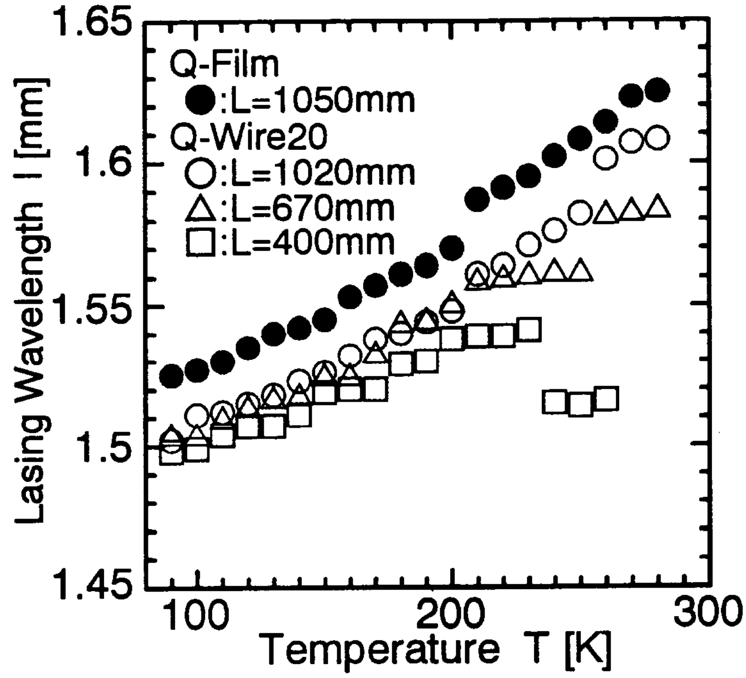

Fig. 5.17 Temperature dependence of lasing wavelength of Q-Wire20 lasers with various cavity lengths.

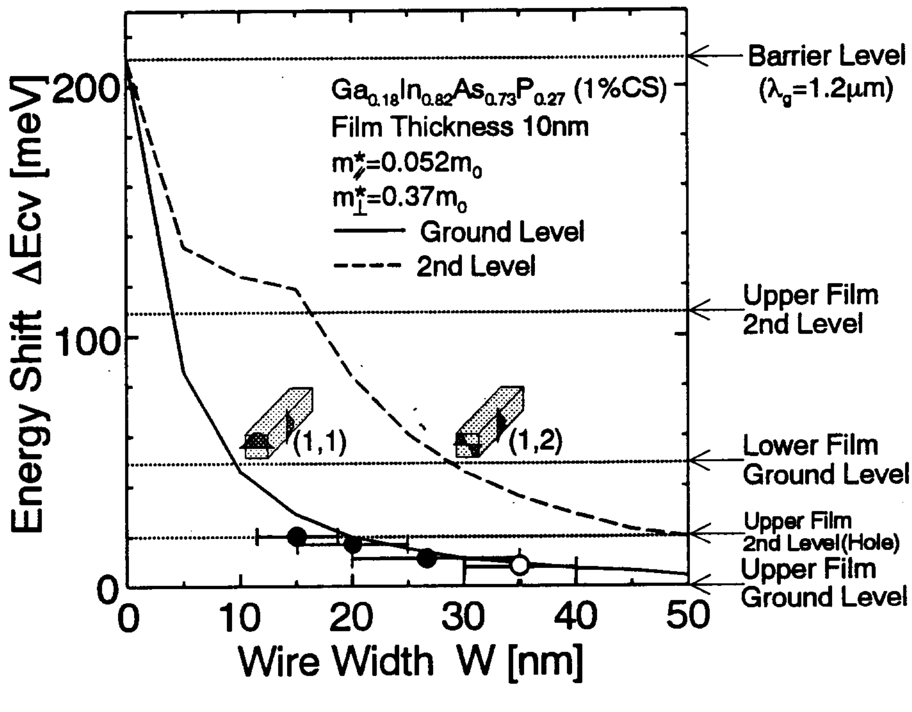

Fig. 5.18 The wire width dependence of the blue shift energy for the Q-Wire to the Q-Film structure.

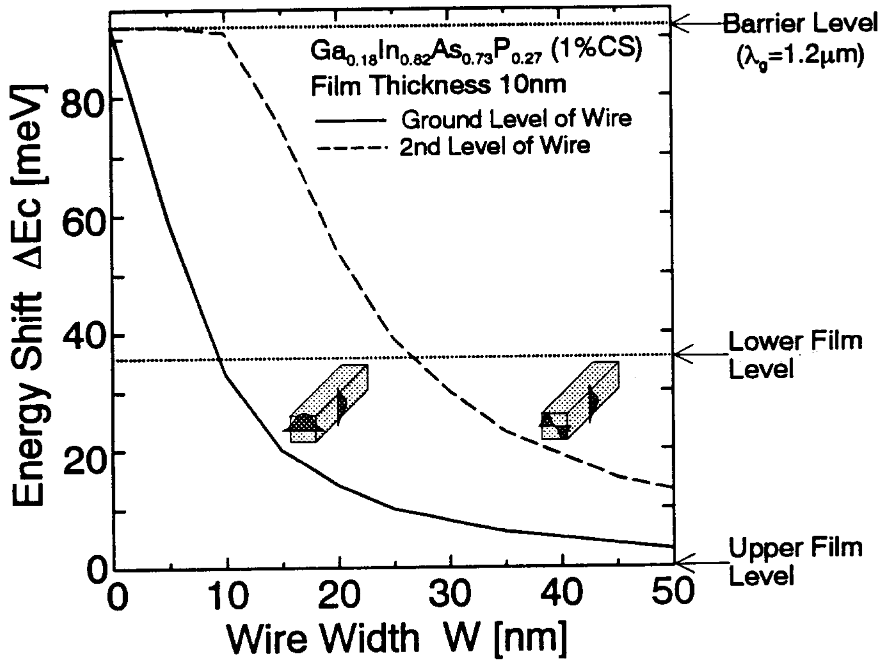

(a)

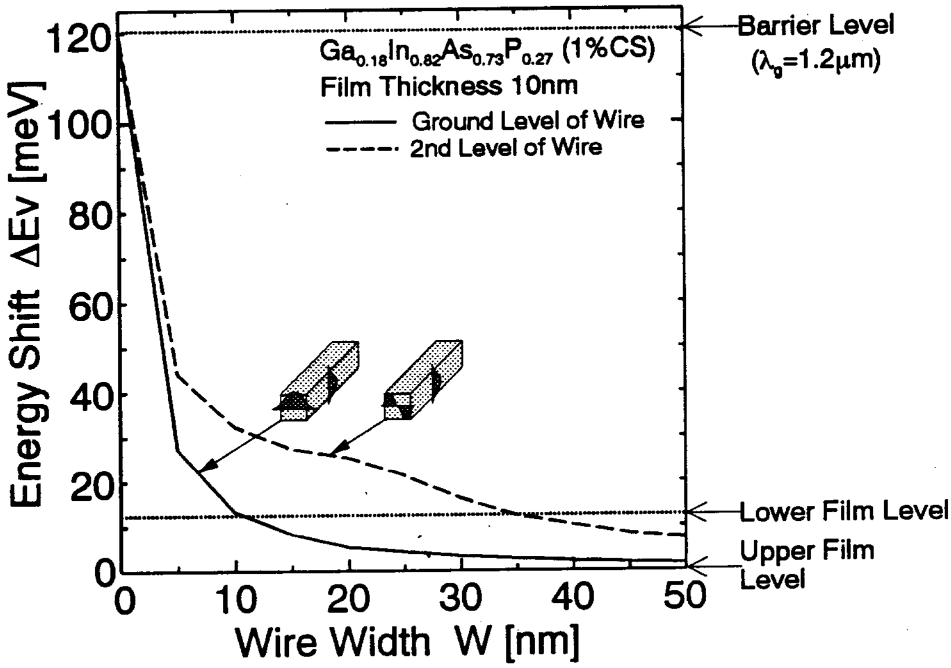

(b)

Fig. 5.19 The wire width dependence of the blue shift energy of the Q-Wire structure; (a) in the conduction band and (b) in the valence band.

5.4 Quantum-Wire DFB Lasers

Since our fabrication method of Q-Wire lasers can be applied to realize partially gain-coupled (complex-coupled) DFB lasers[5-30]-[5-33] with Q-Wire active region which is considered to be very attractive for low threshold and narrow linewidth operation if advantages of the cavity and the gain medium are effectively utilized, we fabricated three different patterns using EB-lithography, i.e. Q-Wire lasers, Q-Wire DFB lasers, and initial Q-Film lasers on the same wafer as shown in Fig. 5.20(a). The Q-Wire laser consisted of a 70nm periodic pattern and the Q-Wire DFB laser consisted of two Q-Wires separated by 70nm with an interval of 240nm. Cross sectional SEM views of these lasers are also shown in Fig. 5.20(b) and (c). As can be seen, the size of the Q-Wire laser is 15nm (top) and 28nm (bottom), and the Q-Wire DFB laser consists of two 20-30nm-width wires.

Figure 5.21 shows (a) the I-L curves and (b) electro-luminescence at threshold of the three kinds of lasers at room temperature. The I_{th} of the Q-Wire DFB laser was about half of that of the Q-Wire laser. This is attributed to higher reflectivity of the DFB grating, despite of poor optical confinement factor of the Q-Wire DFB laser, ξ=0.26%. In Fig. 5.21(b), the Q-Wire DFB laser was emitting at 1.54μm, which is the Bragg wavelength and shifted from the gain peak of 1.58μm. The Q-Wire and Q-Film, lasers were emitting at the gain peak, at 1.58μm of the Q-Wire laser and at 1.62μm of the Q-Film laser, respectively.

Figure 5.22 shows temperature dependence of threshold current for these three lasers under pulsed condition. The cavity length L and the stripe width W_s of these lasers were 860μm and 15μm, respectively. Even though threshold current of the Q-Wire and Q-Wire DFB lasers was 5～10 times higher than that of the Q-Film laser at room temperature, it rapidly decreased with the decrease in the temperature, and became lower than the Q-Film laser at T<193K. At T=98K, threshold current density of the Q-Wire laser was 43A/cm^2 (I_{th}=5.5mA) which was almost half the value of the Q-Film laser (J_{th}=85A/cm^2 and I_{th}=11mA). The Q-Wire DFB laser showed a similar temperature dependence, and its threshold current density was 54A/cm^2 (I_{th}=7mA) at

98K.

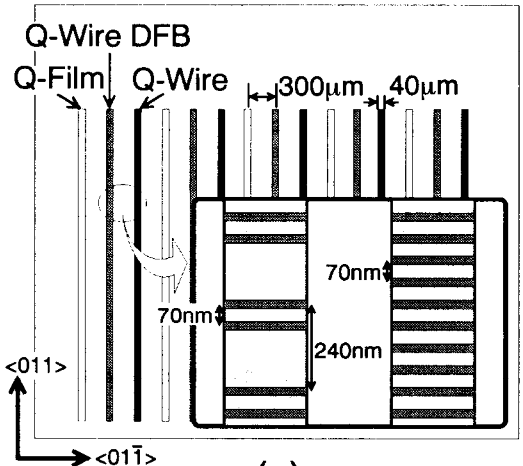

(a)

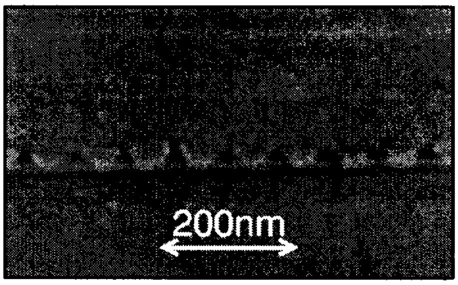

(b)

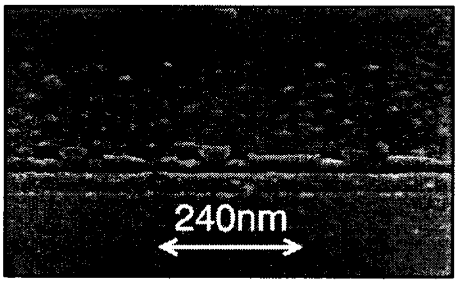

(c)

Fig. 5.20 (a) EB pattern used for the fabrication of Q-Wire, Q-Wire DFB and Q-Film lasers on the same wafer, and cross-sectional SEM views of two kinds of quantum-wire lasers; (b) a Q-Wire and (c) a Q-Wire DFB laser. The direction of quantum wires was $< 01\bar{1} >$.

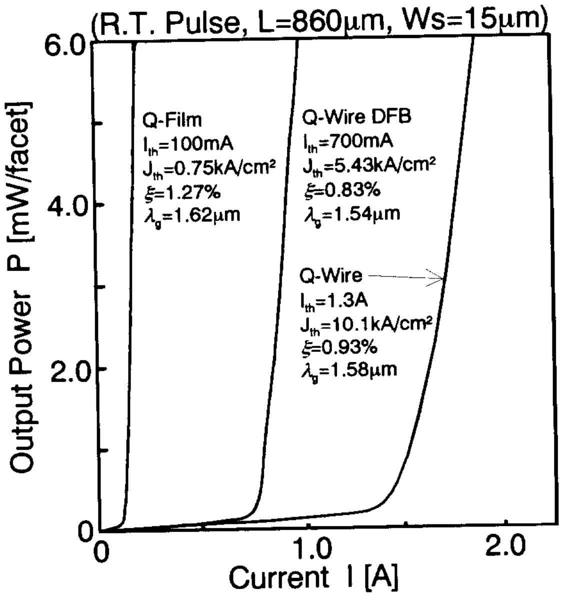

(a)

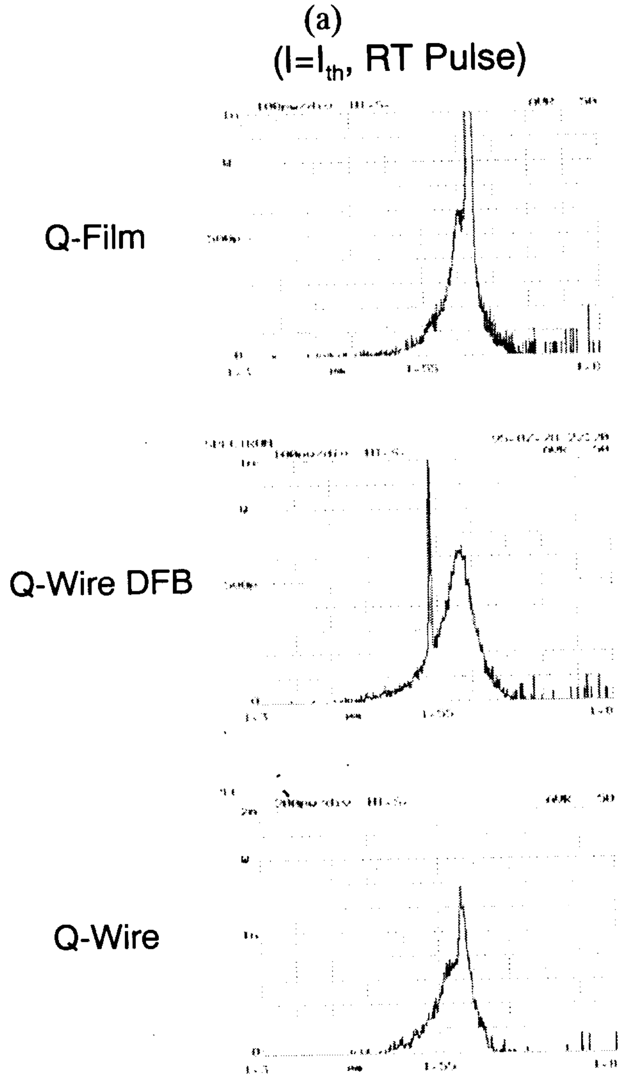

(b)

Fig. 5.21 (a) the I-L curves and (b) electro-luminescence at the threshold of the three kinds of lasers at room temperature.

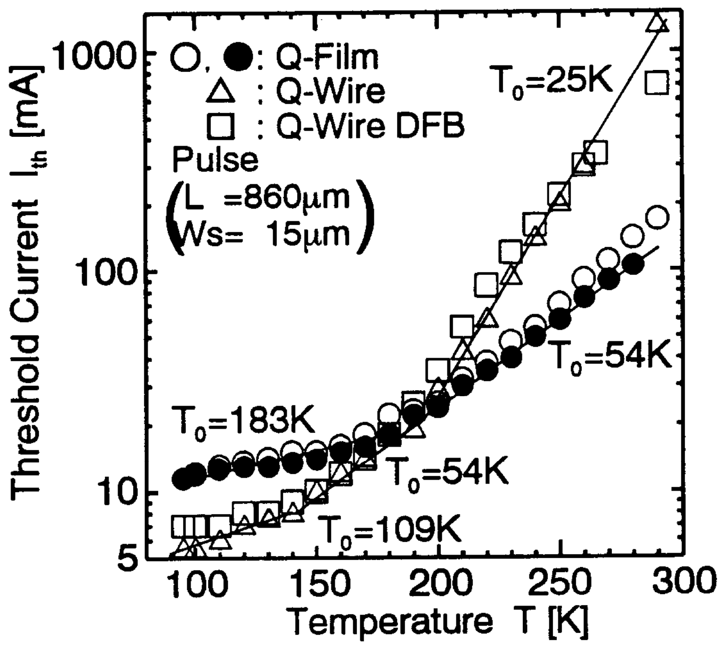

Fig. 5.22 Temperature dependence of threshold current of Q-Wire, Q-Wire DFB and Q-Film lasers under pulsed condition. The cavity length and the stripe width of these lasers are 860μm and 15μm, respectively.

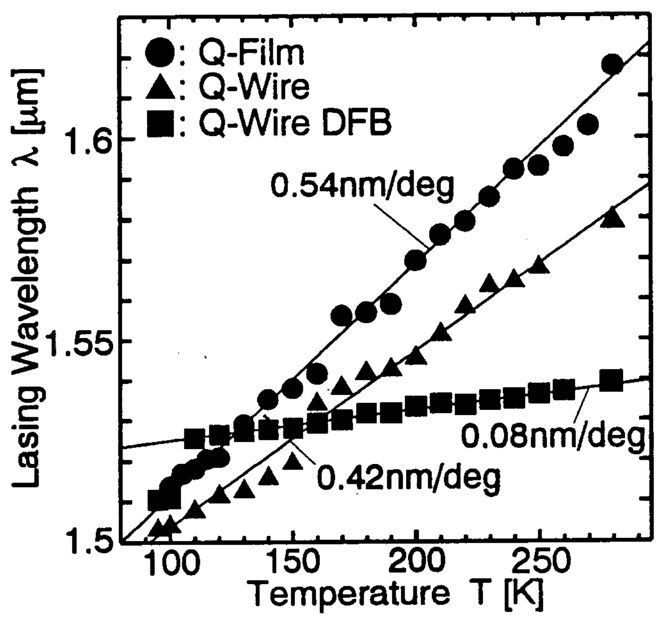

Fig. 5.23 Temperature dependence of lasing wavelength of Q-Wire, Q-Wire DFB and Q-Film lasers. The solid lines show the temperature coefficients of lasing wavelength of these lasers.

Figure 5.23 shows temperature dependence of lasing wavelength of these three lasers. The temperature coefficient of the Q-Wire DFB laser was about 0.08nm/deg and single wavelength operation was confirmed within the investigated temperature range. At around room temperature the detuning (difference between the lasing wavelength and the gain peak wavelength) was observed to be about 40nm, this fact indicates the possibility of high performance DFB lasers with Q-Wire active region when problems of before mentioned temperature dependences are overcome. A large discrepancy between the temperature coefficients of lasing wavelength of the Q-Wire laser (0.42nm/K) and the Q-Film laser may be attributed to also band filling effect due to high threshold carrier density of the Q-Wire laser at around room temperature. Lasing properties of these three lasers are summarized in Table 5.5.

Table 5.5 Lasing properties of Q-Wire, Q-Wire DFB and Q-Film lasers.

				R.T.		98K		$\Delta\lambda/\Delta T$
	L[μm]	W_s[μm]	ξ [%]	I_{th} [mA]	J_{th}[kA/cm^2]	I_{th} [mA]	J_{th}[A/cm^2]	[nm/deg]
Q-Wire	860	15	0.42	1300	10.1	5.5	43	0.42
Q-Wire DFB	860	15	0.26	700	5.4	7.0	54	0.08
Q-Film	860	15	1.27	100	0.75	11	85	0.54

5.5 Conclusion

We measured fundamental lasing properties, especially temperature dependencies of lasing properties of 1.5μm wavelength GaInAsP/InP Compressively-Strained Quantum-Wire lasers with the nominal wire width of 20nm and 25nm fabricated by electron beam lithography and 2-step OMVPE growth, and compared with the results those of Quantum-Film lasers prepared on the same wafer. As the result, we obtained, for the first time, a lower threshold current and a higher differential quantum efficiency operation of a Q-Wire laser over the Q-Film laser at a temperature below T<200K. At T=90K, threshold current density of the Q-Wire laser as low as 34A/cm^2 and the differential quantum efficiency as high as 77% were obtained. Furthermore the internal quantum efficiency was evaluated to be 1.0 at *T*<200K from measurements of the temperature dependence of differential quantum efficiency of different cavity length samples. We also confirmed the possibility of a complex-coupled DFB laser consisting of Q-Wire active region as the grating structure.

References

[5-1] Y. Arakawa and H. Sakaki, "Multidimensional quantum well laser and temperature dependence of its threshold current," *Appl. Phys. Lett.*, vol.40, no.11, pp.939-941, June 1982.

[5-2] M. Asada, Y. Miyamoto, and Y. Suematsu, "Gain and the threshold current of three-dimensional quantum-box lasers," *IEEE J. Quantum Electron.*, vol.QE-22, no.9, pp.1915-1921, Sept. 1986.

[5-3] Y. Arakawa and A. Yariv, "Quantum well lasers-gain, spectra, dynamics," *IEEE J. Quantum Electron.*, vol.QE-22, no.9, pp.1887-1899, Sep. 1986.

[5-4] Y. Miyake and M. Asada, "Spectral characteristics of linewidth enhancement factor α of multidimensional quantum wells," *Jpn. J. Appl. Phys.*, vol.28, no.7, pp.1280-1281, July 1989.

[5-5] A. R. Adams, M. Asada, Y. Suematsu and S. Arai, "The temperature dependence of the efficiency and threshold current of $In_{1-x}Ga_xAs_yP_{1-y}$ lasers related to intervalence band absorption," *Jpn. J. Appl. Phys.*, vol.19, no.10, pp.L621-L624, Oct. 1980.

[5-6] M. Asada, A. R. Adams, K. E. Stubkjaer, Y. Suematsu, Y. Itaya and S. Arai, "The temperature dependence of the threshold current of GaInAsP/InP DH lasers," *IEEE J. Quantum Electron.*, vol.QE-17, no.5, pp.611-619, May 1981.

[5-7] K. Stubkjaer, M. Asada, S. Arai and Y. Suematsu, "Spontaneous recombination, gain and refractive index variation for 1.6μm wavelength InGaAsP/InP lasers," *Jpn. J. Appl. Phys.*, vol.20, no.8, pp.1499-1505, Aug. 1981.

[5-8] S. J. Sweeney, A. F. Phillips, A. R. Adams, E. P. O'Reilly and P. J. A. Thijs, "The effect of temperature dependent processes on the performance of 1.5-μm compressively strained InGaAs(P) MQW semiconductor diode lasers," *IEEE Photon. Technol. Lett.*, vol.10, no.8, pp.1076-1078, Aug. 1998.

[5-9] V. M. Ustinov, A. E. Zhukov, A. Yu. Egorov, A. R. Kovsh, S. V. Zaitsev, N. Yu. Gordeev, V. I. Kopchatov, N. N. Lendentsov, A. F. Tsatsul'nikov, B. V. Volovik, P. S. Kop'ez, Z. I. Alferov, S. S. Ruvimov, Z. Liliental-Weber and D. Bimberg, "Low threshold quantum dot injection laser emitting at 1.9μm," *Electron. Lett.*, vol.34, no.7, pp.670-672, April, 1998.

[5-10] N. Kirstaedter, O. G. Schmidt, N. N. Ledentsov, D. Bimberg, V. M. Ustinov, A. Yu. Egorov, A. E. Zhukov, M. V. Maximov, P. S. Kop'ev and Zh. I. Alferov, "Gain and differential gain of single layer InAs/GaAs quantum dot injection lasers," *Appl. Phys. Lett.*, vol.69, no.9, pp.1226-1228, Aug. 1996.

[5-11] M. Grundmann, D. Bimberg, "Gain and threshold of quantum dot lasers: Theory and comparison to experiments," *Jpn. J. Appl. Phys.*, vol.36, pt.1, no.6B, pp.4181-4187, Jun. 1997.

[5-12] H. Shoji, Y. Nakata, K. Mukai, Y. Sugiyama, M. Sugawara, N. Yokoyama and H. Ishikawa, "Lasing characteristics of self-formed quantum dot lasers with multistacked dot layer," *IEEE J. Selected Topics in Quantum Electron.*, vol.3, no.2, pp.188-195, Apr. 1997.

[5-13] K. H. Wang, A. Pecher, E. Höfling and A. Forchel, "Low voltage electron-beam lithography based InGaAs/GaAs quantum dot arrays with 1meV luminescence linewidths," *J. Vac. Sci. Technol. B*, vol.15, no.6, pp.2829-2831, Nov/Dec 1997.

[5-14] S. Yamakoshi, T. Sanada, O. Wada, I. Umebu and T. Sakurai, "Direct observation of electron leakage in InGaAsP/InP double heterostructure," *Appl. Phys. Lett.*, vol.40, no.2, pp.144-146, Jan. 1982.

[5-15] L. C. Chiu and A. Yariv, "Comments on the nature on electron leakage in InGaAsP/InP double heterostructure," ***Jpn. J. Appl. Phys.***, vol.21, no.5, pp.L305-L306, May 1982.

[5-16] M. Asada and Y. Suematsu, "Measurement of spontaneous emission efficiency and nonradiative recombinations in 1.58-μm wavelength GaInAsP/InP crystals," ***Appl. Phys. Lett.***, vol.41, no.4, pp.353-355, Aug. 1982.

[5-17] M. Asada and Y. Suematsu, "The effects of loss and nonradiative recombination on the temperature dependence of threshold current in 1.5-1.6μm GaInAsP/InP lasers," ***IEEE J. Quantum Electron.***, vol.QE-19, no.6, pp.917-923, Jun. 1983.

[5-18] M. Tamura, T. Kojima, T. Ando, N. Nunoya, S. Tamura and S. Arai, "Estimation of sidewall recombination in GaInAsP/InP narrow quantum-well wire lasers fabricated by wet chemical etching and 2-step OMVPE growth," to be published in ***Jpn. J. Appl. Phys.***, (vol.37, pt.1, no.12, Dec. 1998.)

[5-19] S. V. Zaitsev, N. Yu. Gordeev, Yu. M. Shernniakov, V. M. Ustinov, A. E. Zhukov, A. Yu. Egorov, M. V. Maximov, P. S. Kop'ez, Zh. I. Alferov, N. N. Lendentsov, N. Kirstaedter, and D. Bimberg "Radiation characteristics of injection lasers based on vertically coupled quantum dots," ***Superlattices and Microstructures***, vol.21, no.4, pp.559-564, 1997.

[5-20] T. Higashi, T. Yamamoto, S. Ogita and M. Kobayashi, "Experimental analysis of characteristic temperature in quantum-well semiconductor lasers," ***IEEE J. Selected Topics in Quantum Electron.***, vol.3, no.2, pp.513-521, Apr. 1997.

[5-21] M. Asada, "Rate-equation analysis of semiconductor lasers," ***Handbook of Semiconductor Lasers and Photonic Integrated Circuits***, ed. Y. Suematsu and A. R. Adams ***(Chapman & Hall, London, 1994)*** Chap.7.

[5-22] L. V. Asryan and R. A. Suris, "Temperature dependence of the threshold current density of a quantum dot laser," ***IEEE J. Quantum Electron.***, vol.34, no.5, pp.841-850, May 1998.

[5-23] H. C. Casey, Jr. and P. L. Carter, "Variation of intervalence band absorption with hole concentration in p-type InP," ***Appl. Phys. Lett.***, vol.44, no.1, pp.82-83, Jan. 1984.

[5-24] M. Asada, A. Kameyama and Y. Suematsu, "Gain and intervalence band absorption in quantum-well lasers," ***IEEE J. Quantum Electron.***, vol.QE-20, no.7, pp.745-753, Jul. 1984.

[5-25] S. V. Zaitsev, N. Yu. Gordeev, V. I. Kopchatov, V. M. Ustinov, A. E. Zhukov, A. Yu. Egorov, N. N. Lendentsov, M. V. Maximov, P. S. Kop'ez, A. O. Kosogov and Z. I. Alferov, "Vertically coupled quantum dot lasers: First device oriented structures with high internal quantum efficiency, " ***Jpn. J. Appl. Phys.***, vol.36, pt.1, no.6B, pp.4219-4220, Jun. 1997.

[5-26] M. Asada, "Handotai to hikari-ritoku (Semiconductor and optical gain)," ***Handotai re-za (Semiconductor Lasers)***, ed. K. Iga ***(Ohmsha, Tokyo, 1994)*** Chap.3 [in Japanese].

[5-27] S. H. Park, J. I. Shim, K. Kudo, M. Asada and S. Arai, "Band gap shrinkage in GaInAs/GaInAsP/InP multi-quantum well lasers," ***J. Appl. Phys.***, vol.72, no.1, pp.279-281, Jul. 1992.

[5-28] S. Ueno, Y. Miyake, and M. Asada, "Advantage of strained quantum wire lasers," ***Jpn. J. Appl. Phys.***, vol.31, pt.1, no.2A, pp.286-287, Feb. 1992.

[5-29] H. Shoji, Y. Nakata, K. Mukai, Y. Sugiyama, M. Sugawara, N. Yokoyama and H. Ishikawa, "Temperature dependent lasing characteristics of multi-stacked quantum dot lasers," ***Appl. Phys. Lett.***, vol.71, no.2, pp.193-195, Jul. 1997.

[5-30] K. Kudo, J. I. Shim, K. Komori and S. Arai, "Reduction of effective linewidth enhancement factor α_{eff} of DFB lasers with complex coupling coefficients," ***IEEE Photon. Technol. Lett.***, vol.4, no.6, pp.531-534, Jun. 1992.

[5-31] A. Orth, H. Zull, J. P. Reithmaier and A. Forchel, "GaInAs/GaAs quantum wire laser structures with strong gain coupling defined by reactive ion etching," ***Electron. Lett.***, vol.31, no.6, pp.457-458, Mar. 1995.

[5-32] U. A. Griesinger, H. Schweizer, V. Härle, F. Barth, B. Höhing, B. Klepser, and F. Scholz "Dry-Etched Wire Distributed Feedback Laser," ***IEEE Photon. Technol. Lett.***, vol.7, no.9, pp.953-955, Sep. 1995.

[5-33] U. A. Griesinger, H. Schweizer, S. Kronmüller, D. Ottenwälder, F. Scholz, and M. H. Pilkun, "Realization of dot DFB lasers," ***IEEE. Photon. Technol. Lett.***, vol.8, no.5, pp.587-589, May 1996.

Chapter 6

Optical Gain Properties of Quantum-Wire Lasers

6.1 Introduction.. 151
6.2 Measurement of Optical Gain 152
6.3 Comparison to Theoretical Analysis.................................. 159
6.3.1 Gain Spectrum... 159
6.3.2 Intraband Relaxation Time... 161
6.3.3 Differential Gain... 165
6.4 Conclusion.. 170
References.. 171

6.1 Introduction

SEMICONDUCTOR lasers can be operated at a high level of performance due to narrow gain spectrum feature by introducing quantum-wire (box) structures as an active region[6-1]-[6-3]. Operation at very low threshold current[6-4]-[6-6] and the anisotropic polarization properties of quantum-wire (Q-Wire) lasers[6-7],[6-8], such as an electro-luminescence (EL) spectrum and threshold current which are dependent on stripe direction with regard to the Q-Wire, were observed. In a previous study, we fabricated long wavelength GaInAs(P)/InP Q-Wire lasers by using electron-beam (EB) lithography and two-step organometallic vapor phase epitaxy (OMVPE)[6-5], and investigated the temperature dependences of lasing properties[6-9],[6-10]. Even though the width of the quantum-wire was relatively large (20～35 nm), a clear anisotropic polarization property was observed in photoluminescence (PL) intensity[6-11] as mentioned in chapter 4. Superior lasing properties such as a lower threshold current and higher differential quantum efficiency as compared to quantum-film (Q-Film) lasers fabricated on the same wafer were obtained in temperature ranges up to around T=200K[6-10] as mentioned in chapter 5, but it was unclear if the origin of these properties can be attributed to only the volume of the active medium and/or to the lateral quantum-confinement effect inherent in the Q-Wire structures, i.e. a narrow gain spectral.

In this chapter, the measurements of the gain spectral characteristics of 1.5 μm wavelength GaInAsP/InP Q-Wire lasers in comparison with those of Q-Film laser fabricated on the same wafer by use of EB lithography and OMVPE regrowth process will be discussed.

6.2 Measurement of Optical Gain

The gain spectra of three different types of samples on the same wafer were measured: a Q-Wire laser with a wire width ($\overline{W}$) of 20 nm for a period (Λ) of 50 nm (Q-Wire20, in short), a Q-Wire laser with a 25 nm-wide wire for Λ=70 nm (Q-Wire25), and an initial quantum-film laser (Q-Film). The cavity length of all lasers investigated here was 1 mm. The schematic structure and the cross sectional SEM views of Q-Wire20 and Q-Wire25 are shown in Fig. 3.17 in chapter 3. The Q-Wire structure was fabricated on a wafer consisting of a 10nm thick $Ga_{0.18}In_{0.82}As_{0.73}P_{0.27}$ compressively-strained (1%-CS) single-quantum-well grown on a (100) p-InP substrate by making a 50 nm and 70 nm-period line pattern along the $<01\overline{1}>$ direction, which was perpendicular to the direction of the cavity. The lower thin GaInAsP layer (5 nm thick) was inserted to support the optical confinement but the optical gain. The wire pattern was formed by a JBX-6000FS EBX system using ZEP-520 resist (30 nm thick, including C_{60} 5%wt.[6-12]) with a line dose condition of 0.6 nC/cm. After transferring the pattern onto the wafer using a SiO_2 etching mask, the mask was removed and the Q-Wire structure was embedded by a thin (3 nm) InP layer, a 200 nm thick n-GaInAsP optical confinement layer (OCL), a 3 μm thick n-InP cladding layer, and a 50 nm thick n-GaInAs contact layer. The thin InP layer was grown only for obtaining better regrown interface which resulted in smooth surface of the GaInAsP OCL, and the contribution of this InP layer to the optical confinement factor of the active region is negligibly small. Finally, 14μm wide mesa-structure stripe lasers were fabricated. The fabrication process is described in chapter 3 in more detail.

The gain spectrum was obtained by the Hakki-Paoli method, where the depth of the Fabry-Perot fringes of the spontaneous emission spectrum were measured[6-13]-[6-15]. The modal gain coefficient was obtained by

$$g_{mod.} = \xi \cdot g_{mat.} - \alpha = \frac{1}{L} ln \frac{1}{R} + \frac{1}{L} ln \frac{\sqrt{r}-1}{\sqrt{r}+1}, \qquad (6.1)$$

where ξ is an optical confinement factor of an active region, $g_{mat.}$ is the material gain, α is the waveguide loss, L is the cavity length, R is the power reflectivity of the facet mirror, and r is the peak to valley ratio of the Fabry-Perot mode resonance. Figure 6.1 shows the experimental setup for gain spectrum measurement. A sample was put

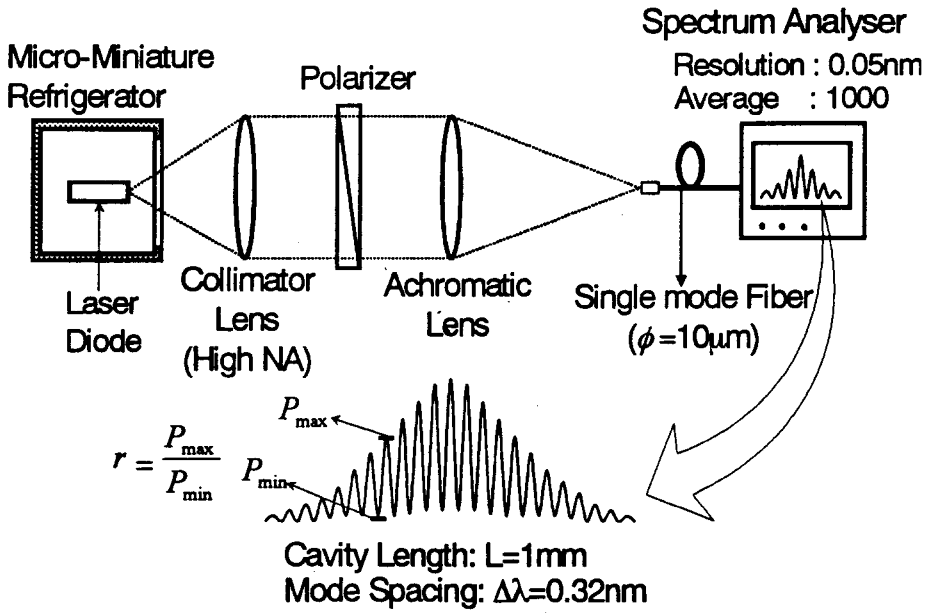

Fig. 6.1 Gain spectrum measurement system

into a Micro-Miniature Refrigerator. Light output was incident into the single mode fiber by two lenses and a polarizer was put between them. The spontaneous emission spectrum below the threshold was measured by a spectrum analyzer with a resolution of 0.05 nm and data averaging times of 1000.

Threshold current (density) I_{th} (J_{th}), the nominal active region width ($\overline{W}$), the in-plane space filling factors (ρ) and the optical confinement factor of active region (ξ) of the measured samples are listed in Table 6.1. All the measurements were done under continuous wave (CW) condition at T=100 K. Figure 6.2 shows, for example, spontaneous emission spectra of these lasers below threshold.

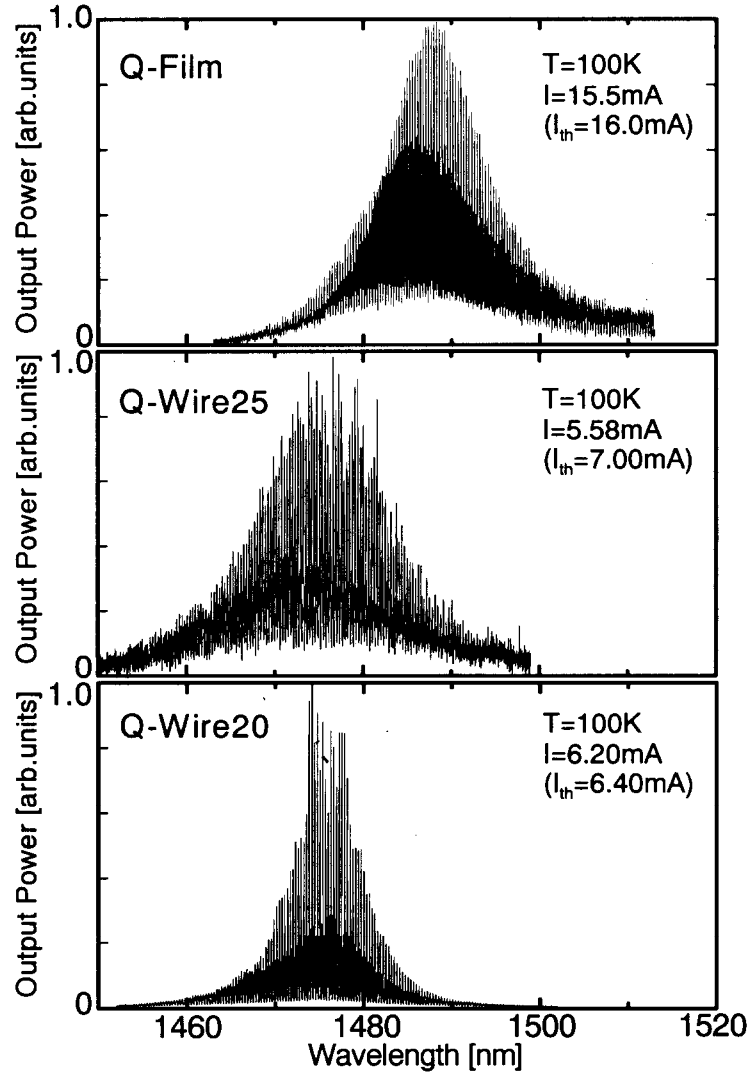

Fig. 6.2 Spontaneous emission spectrum.

In each spectrum, the subpeaks were nominally observed in the main peaks that corresponded to different transverse modes due to the oversized stripe width for single transverse mode operation. Both the longitudinal mode spacing of the main peaks and that of the subpeaks were 0.32 nm. Due to the subpeaks of higher transverse mode, we used the lowest value of the valleys and the highest value of peaks in each longitudinal mode spacing to obtain *r*, then obtained the modal gain spectrum using eq.(6.1).

Figure 6.3 shows, for example, the measured modal gain spectrum at various injection current levels for the Q-Wire20 laser. The modal gain spectrum was similar to those of the Q-Wire25 and Q-Film lasers. Since the spectral resolution was

Table 6.1 Lasing properties at T=100K (CW condition).

	Λ [nm]	$\bar{W}$ [nm]	ρ ($\bar{W}/\Lambda$)	I_{th} [mA]	J_{th} [A/cm^2]	ξ [%]
Q-Wire20	50	20	0.40	6.4	46	0.51
Q-Wire25	70	25	0.36	7.0	50	0.46
Q-Film	——	——	1.0	16.0	114	1.27

(L=1mm, W_s=14μm)

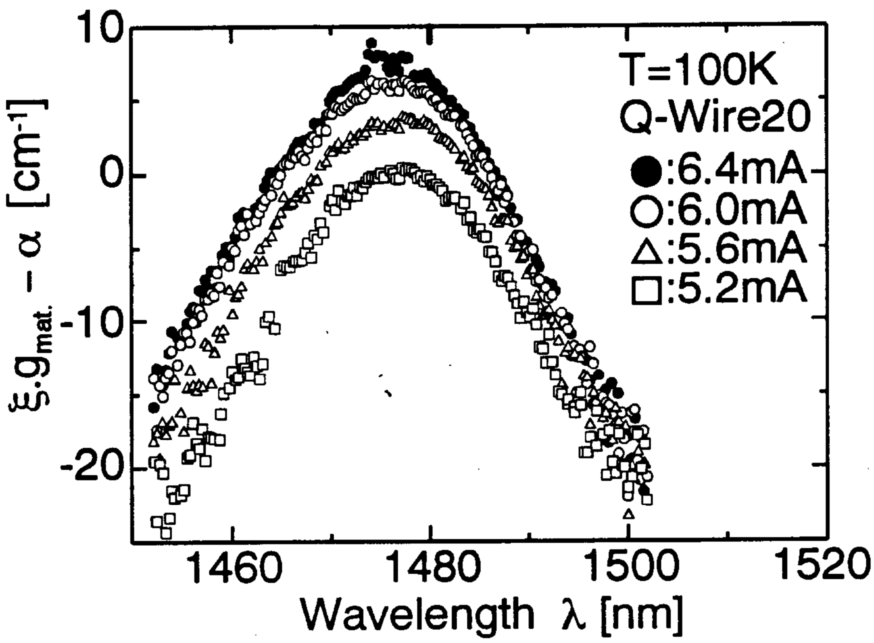

Fig. 6.3 Modal gain spectra at various injection current levels of Q-Wire20 laser. □:I=5.2mA, △:I=5.6mA, O:I=6.0mA, and ●:I(I_{th})=6.4mA.

relatively poor (0.05 nm) for the resonant spacing of 0.32 nm, measured data may include larger inaccuracy in lower gain region where the modal gain is less than −10 cm^{-1}.

From the modal gain spectrum, the material gain spectrum was obtained by using the relationship given by,

$$g_{mat.} = (g_{mod.} + \alpha)/\xi, \qquad (6.2)$$

where the waveguide loss α and the internal quantum efficiency η_i were obtained from the cavity length dependence of an inverse of the differential quantum efficiency, and were about 5 cm^{-1} and η_i=1.0 for the Q-Wire20 samples, when the power reflectivity of the facet mirror R was assumed to be 0.33, as discussed in Chapter 5. For the other two kinds of samples, α was obtained to be 3 cm^{-1} for the Q-Wire25 laser and 5 cm^{-1} the Q-Film laser, respectively. Figure 6.4 shows the obtained material gain spectra of the three kinds of lasers, where the injection current level was properly chosen in each sample so as to compare the gain spectral width for the peak gain which was adjusted to 800∼1000cm^{-1}. The injection current density which was normalized

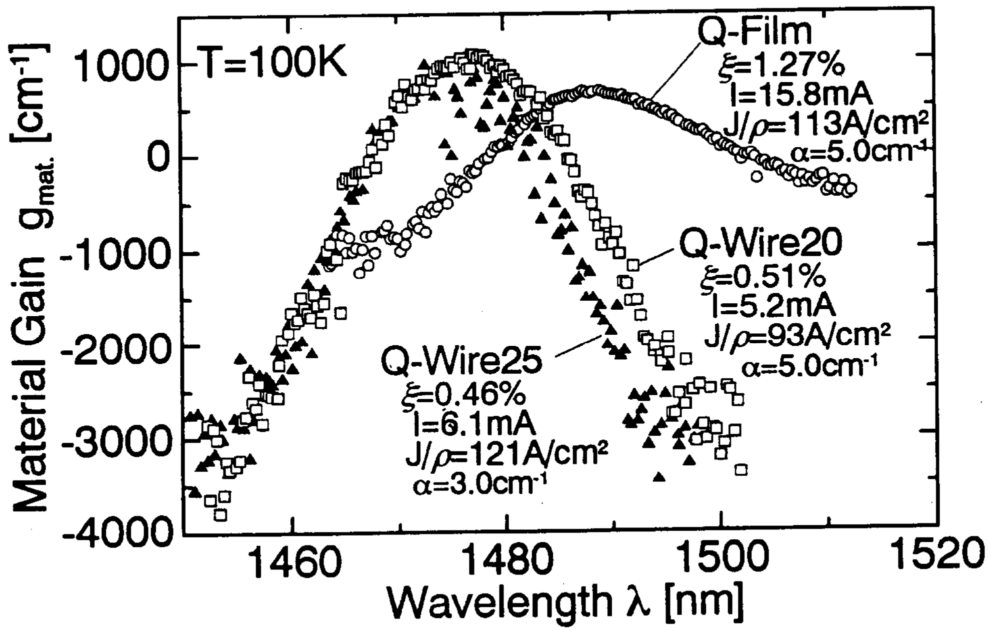

Fig. 6.4 Material gain spectra of three kinds of lasers at a peak gain around 800∼1000cm^{-1}. □:Q-Wire20, I=5.2mA, ▲:Q-Wire25, I=6.12mA, and ○:Q-Film, I=15.8mA.

by the in-plane space filling factor of the Q-Wire ($\rho=\overline{W}/\Lambda$) was 93 A/cm^2 for Q-Wire20, 121 A/cm^2 for Q-Wire25, and 113 A/cm^2 for the Q-Film lasers. The leakage current or non-radiative recombination in Q-Wire samples is considered to be negligible at this temperature.

The experimental results showed that the spectra of the Q-Wire lasers were narrower than that of the Q-Film laser. The spectral width at a material gain of 0 cm^{-1} was 10.8 meV for Q-Wire20, 9.7 meV for Q-Wire25, and 14 meV for Q-Film, respectively.

Figure 6.5 (a) shows the measured peak modal gain $g_{mod.}$ as a function of injection current I. From the least square fitting method, the slope gain ($\partial g_{mod.}/\partial I$) was obtained to be 9.0 cm^{-1}mA^{-1} for both Q-Wire lasers and be 7.8 cm^{-1}mA^{-1} for the Q-Film laser. Though the difference between these values is very small, it can be considered to be reflecting narrower gain spectral property of the Q-Wire lasers since the optical confinement factor of the active region of our Q-Wire lasers is regarded as proportional to the in-plane space filling factor ρ.

In order to evaluate the lateral quantum confinement effect in Q-Wire lasers the differential gain should be compared after measuring carrier lifetime, but it could not be done this time. From measurements of temperature dependencies of our samples, we found that the spontaneous emission efficiency was almost the same and an internal quantum efficiency was almost unity in these three kinds of lasers at around T=100K as mentioned in chapter 5. Hence we assumed that non-radiative recombination was negligible and the carrier lifetime was the same at the same normalized injection current density J/ρ and tried to plot the relation between material gain and the normalized injection current density J/ρ. By putting the values of ρ and α into eq. (6.2), the peak material gain $g_{mat.}$ as a function of the injection current density J normalized by ρ was obtained as shown in Fig. 6.5(b). As can be seen, the transparent current density of Q-Wire20 was about 20% lower than that of Q-Wire25 and Q-Film while the slope gain (against the normalized injection current density) of Q-Wire lasers was about 1.2 times higher than that of the Q-Film laser. Since the

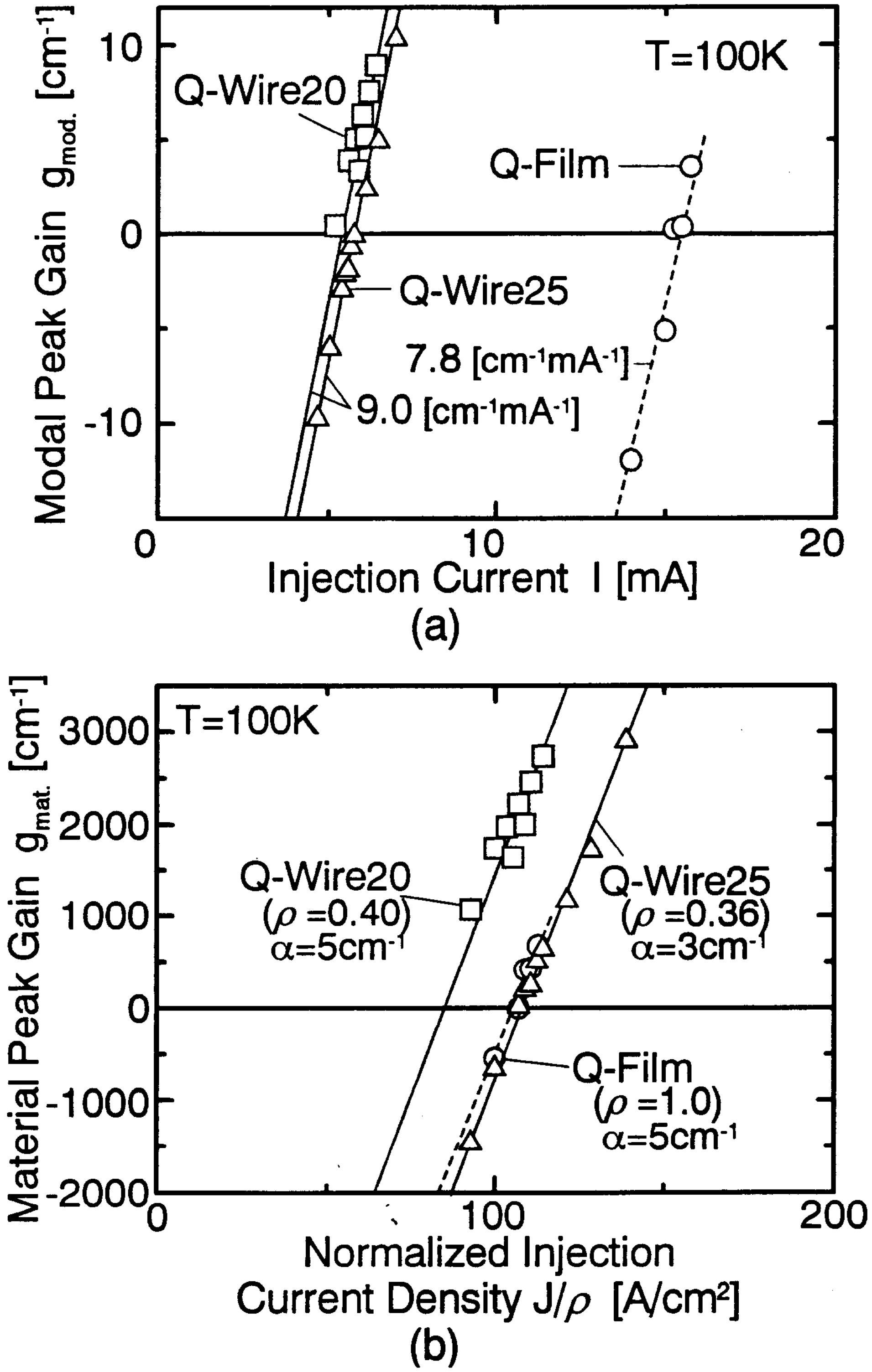

Fig. 6.5 (a) Peak modal gain as a function of injection current, and (b) peak material gain as a function of normalized injection current density.
□:Q-Wire20, △:Q-Wire25, and ○:Q-Film.

transparent carrier density of an ideal Q-Wire laser is theoretically expected to be higher than that of a Q-Film laser, our result indicates that an actual/or an effective wire width of our Q-Wire lasers may be slightly narrower than that measured from cross sectional SEM view. For comparison of differential gain between Q-Wire and Q-Film lasers the carrier lifetime measurements should be done in future.

6.3 Comparison to Theoretical Analysis

6.3.1 Gain Spectrum

Figure 6.6 shows the comparison of the material gain spectra of (a) experimental and (b) calculation results at T=100K. The linear gain coefficient is given by

$$g(\omega)=\frac{\omega}{n_r}\sqrt{\frac{\mu_0}{\varepsilon_0}}\int_{E_g}^{\infty}\left\langle R_{ch}^2\right\rangle\cdot g_{ch}(E_{ch})\cdot\{f_c-f_v\}\cdot\frac{\hbar/\tau_{in}}{(E_{ch}-\hbar\omega)^2+(\hbar/\tau_{in})^2}dE_{ch}, \quad (6.3)$$

where the subscripts c and h denote the conduction and valence band, respectively, $\hbar$ is the Plank's constant, ω is the angular frequency of input light, ε_0 and μ_0 are permittivity and permeability in the vacuum, τ_{in} is the intraband electron relaxation time, n_r is the refractive index without dispersion, and $\left\langle R_{ch}^2\right\rangle$ is the matrix element of transition dipole moment. The Fermi functions in the conduction and the valence band are f_c and f_v, respectively. The $g_{ch}(E_{ch})$ is the effective density of states. While the tail of the calculated gain spectrum was asymptotic to 0cm^{-1}, that of the experimental gain spectrum of the Q-Wire lasers was reduced to -1000cm^{-1} due to the limit of the gain approximation method given by eq. (6.1); the modal gain therefore becomes a negative infinite when peak to valley ratio r approaches 1. Therefore, we compared it at around the peak of the gain spectrum. The calculation results were fitted for the experimental results above 0 cm^{-1} by changing the number of injected carriers N and the intraband relaxation time τ_{in}. The fitting parameters N and τ_{in} are listed in Table 6.2. The difference in the spectral shape between the Q-Wire and Q-Film lasers was observed at the long wavelength side of the gain peak, i.e. the slope in

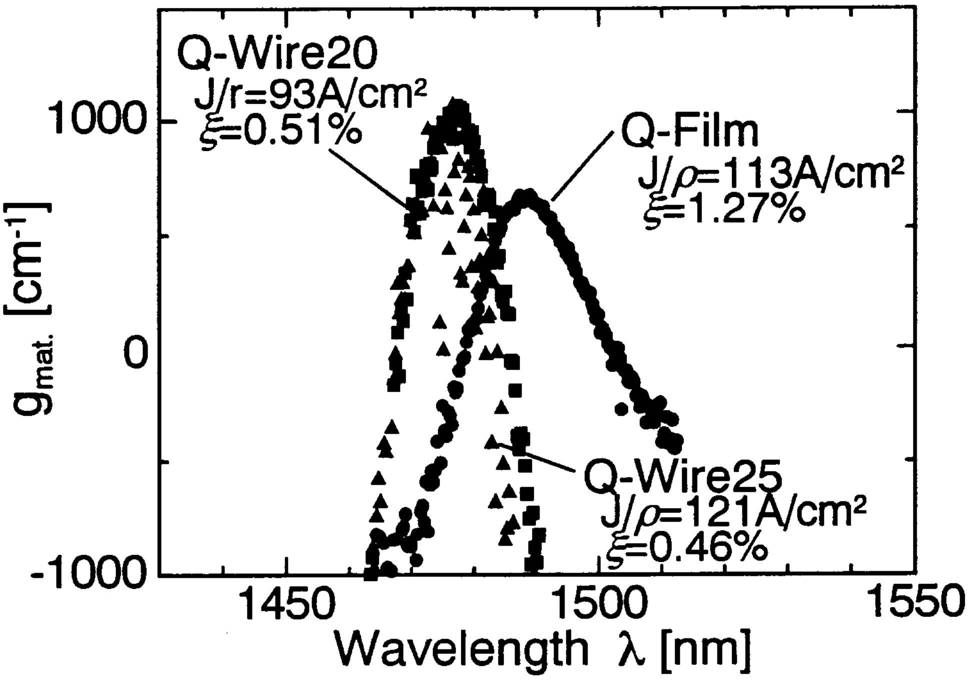

(a)

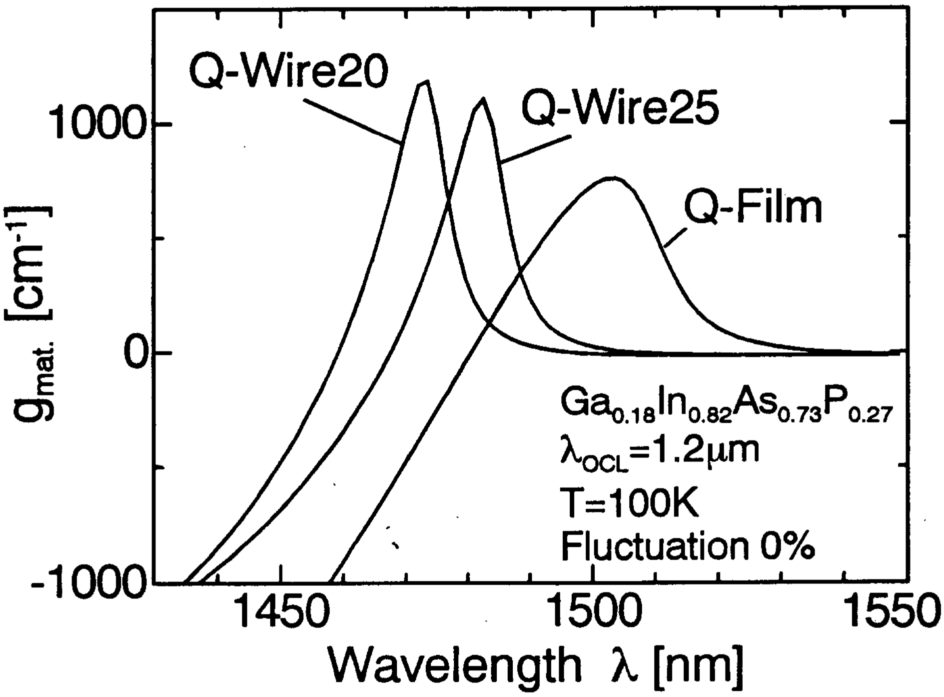

(b)

Fig. 6.6 Material gain spectrum of (a) experimental and (b) calculation.

the long wavelength side of the Q-Wire samples was steeper than that of the Q-Film sample. These features qualitatively agree with theoretical gain spectra of the Q-Wire and Q-Film lasers as can be seen in Fig. 6.6. The narrow gain spectra of Q-Wire lasers can be attributed to the density of states of the Q-Wire structures and/or to the larger (~1.5 times) intraband relaxation time in the Q-Wire structures than that in the Q-Film structure. When comparing the gain spectra of Q-Wire25 and Q-Wire20, the spectrum of Q-Wire20 is a little broad; this might be due to the size fluctuation of the wire width.

Table 6.2 Fitting parameters.

	τ_{in} [psec]	N [cm^{-3}]
Q-Film	0.2	2.1×10^{17}
Q-Wire25	0.3	2.2×10^{17}
Q-Wire20	0.3	2.5×10^{17}

6.3.2 Intraband Relaxation Time

In the previous section, the difference of the intraband relaxation time between the Q-Wire lasers and the Q-Film laser was observed. The intraband relaxation is introduced as a result of electron-electron and electron-hole scatterings and the magnitude of the band tail depends on the value of the intraband relaxation time[6-16]. Thus in this section, we will discuss the intraband relaxation time τ_{in} dependence of the material gain and determine the τ_{in} of the Q-Wire and Q-Film lasers at the temperature about 100K, considering the size fluctuation of the Q-Wire[6-17]. Figure 6.7 shows the calculation results of the intraband relaxation time dependence of the material gain at T=90K; (a) at τ_{in}<3ps and (b) at τ_{in}<0.5ps. The size fluctuation of the Q-Wire width ΔW was assumed to be 2.9nm, which was obtained from the measurement as shown in Chapter 3. In this case, the ratio of the size fluctuation is about 30% for a 10nm-wide Q-Wire, 20% for a 15nm-wide Q-Wire, 15% for a 20nm-wide Q-Wire, and 10% for a 30nm-wide Q-Wire. Open marks show the results with no size fluctuation, and closed marks show those with ΔW=2.9nm. The thickness was assumed to be constant (no size fluctuation). While the material peak gain $g_{mat.}$ of the Q-Film was proportional to the intraband relaxation time, that of all the Q-Wires was saturated at a certain intraband relaxation time at τ_{in} <3psec. As shown in Fig. 6.7(b), if the Q-Wire has no size fluctuation, the maximum $g_{mat.}$ is expected with the wire width W of 10nm. However, when there is ΔW=2.9nm, the maximum $g_{mat.}$ can be obtained with the wire width of 20nm. In the case of W=15nm, the material peak gain is drastically reduced due to the size fluctuation.

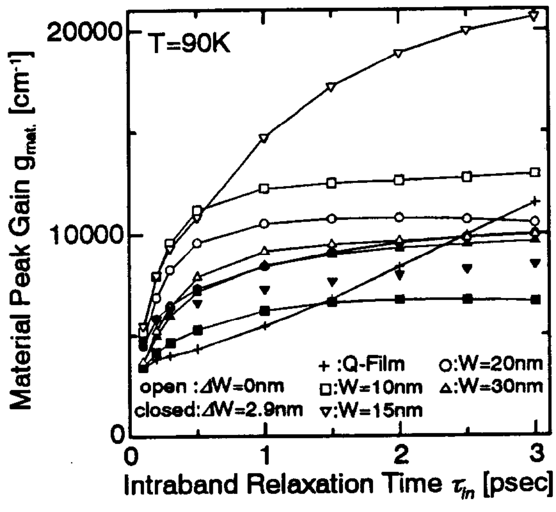

(a)

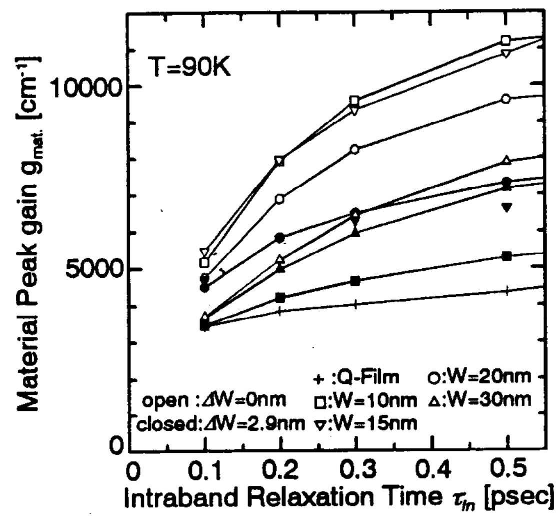

(b)

Fig. 6.7 The calculation results of the intraband relaxation time dependence of the material gain at T=90K; (a) at τ_{in}<3ps and (b) at τ_{in}<0.5ps.

The difference in the spectral shape between the Q-Wire and Q-Film lasers was observed at the long wavelength side of the gain peak, i.e. the slope in the long wavelength side of the Q-Wire samples was steeper than that of the Q-Film sample as shown in Fig. 6.5. This may be attributed to the difference of the intraband relaxation time between the Q-Wire lasers and the Q-Film laser. Here we will determine them from the slope in the long wavelength side by comparing the calculation results. In the spectrum of both the experimental and the calculated results, the slope was defined as the tangent line at the half maximum above $0cm^{-1}$. Figure 6.8 shows the slope in the long wavelength side $\Delta g_{mat.}/\Delta\lambda$ as a function of the material peak gain $g_{mat.}$ for (a) Q-Wire20, (b) Q-Wire25, and (c) Q-Film lasers. The solid lines show the calculation results with no size fluctuation, the dashed lines show those with ΔW=2.9nm and the dots show the experimental results. In Fig. 6.8(a), the experimental results of the Q-Wire20 laser seem to fit the dashed line of τ_{in}=0.4ps. In the case of the Q-Wire25 laser, the experimental results seem to fit the solid line of τ_{in}=0.2ps, however the τ_{in} of the Q-Wire25 laser can be considered to be 0.3-0.4ps considering the size fluctuation, which is similar to that of the Q-Wire20 laser. On the other hand, the experimental results of the Q-Film laser seem to fit the line of τ_{in}=0.2ps, as shown in Fig. 6.8(c). Thus, the reason for the steeper slope of the long wavelength side of the Q-Wire samples than that of the Q-Film sample can be due to the larger (~twice) intraband relaxation time in the Q-Wire structures than that in the Q-Film structure.

During lasing, the density of electrons in the conduction band is depressed at the energy level corresponding to the emitting wavelength. The intraband relaxation time τ_{in} is the recovering time of the depressed distribution to flow electron from the other levels. When τ_{in} is small the depressed distribution becomes wide and shallow, on the contrary, when τ_{in} is large the depressed distribution becomes narrow and deep. At room temperature, τ_{in} is 0.1ps[6-16],[6-18],[6-19], and that is 1.5 times longer at T=100K in case of bulk[6-16]. The τ_{in} of the Q-Film laser at T=100K can be longer than that of the bulk because of the narrower density of state. At low temperatures, the energy broadening due to thermal excitation becomes small, and the narrower

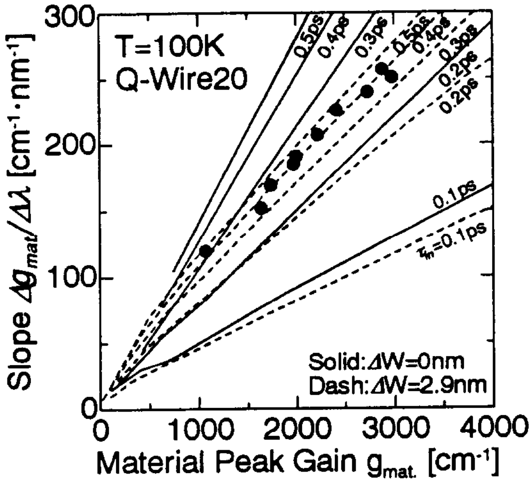

(a)

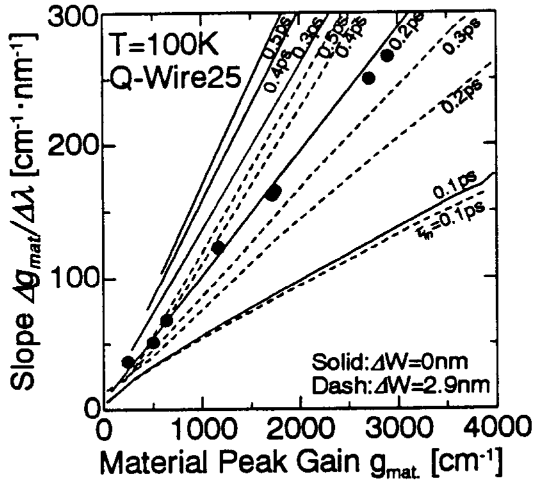

(b)

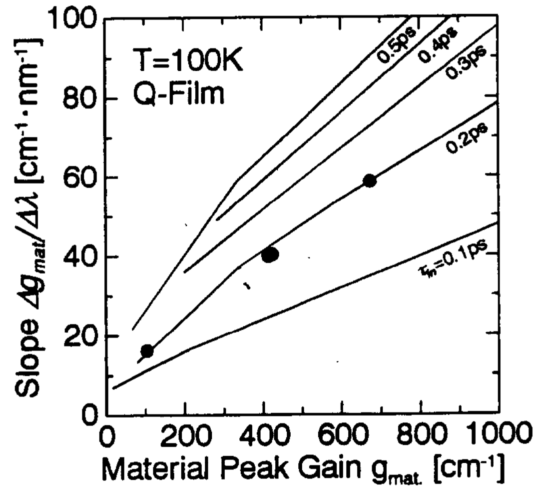

(c)

Fig. 6.8 The slope in the long wavelength side $\Delta g_{mat.}/\Delta\lambda$ as a function of the material peak gain $g_{mat.}$ for (a) Q-Wire20, (b) Q-Wire25, and (c) Q-Film lasers.

density of the state and larger separation of energy levels of the Q-Wire than those of the Q-Film resulted in the longer intraband relaxation time. In case of Q-Box laser, the τ_{in} is possible to be much longer than that of Q-Wire or Q-Film laser. Actually, the lasing occurred at many wavelengths at the same time from many quantum dots with different sizes and composition at T=60K[6-20]. Very slow carrier relaxation of 100ps of the Q-Dot structure was reported from the measurement of photoluminescence and time-resolved photoluminescence[6-21].

From the relation between the full width at half maximum (FWHM) of the material gain spectrum and the material gain peak, the intraband relaxation time of the Q-Wire lasers is estimated to be also 0.4ps. Figure 6.9 shows the comparison of the gain spectra of the Q-Wire laser between (a) experimental and (b) theoretical results. In Fig. 6.9(b), the spectrum of Q-Wire20 is a little broad due to the size fluctuation of the wire width.

6.3.3 Differential Gain

In chapter 5, we discussed the differential material gain as a function of current density $\Delta g_{mat.} / \Delta(J/\rho)$ of the Q-Wire laser was higher than that of the Q-Film laser (see Fig. 5.5), however, for better comparison with theoretical material gain on injection carrier density, we estimate the carrier lifetime and compare with that of Q-Film laser.

Comparing the experimental results of the material gain as a function of injection current $g(J/\rho)$ with the calculated results of the material gain as a function of injected carriers $g(N)$, the two functions are plotted together and share the same abscissa (abscissa =gain) but different ordinates (ordinates =N or J)[6-22]. The carrier lifetime is determined from the plot of N versus J in the following manner. The differential carrier lifetime is described as

$$\frac{\partial R}{\partial N} = \frac{1}{\tau}, \qquad (6.4)$$

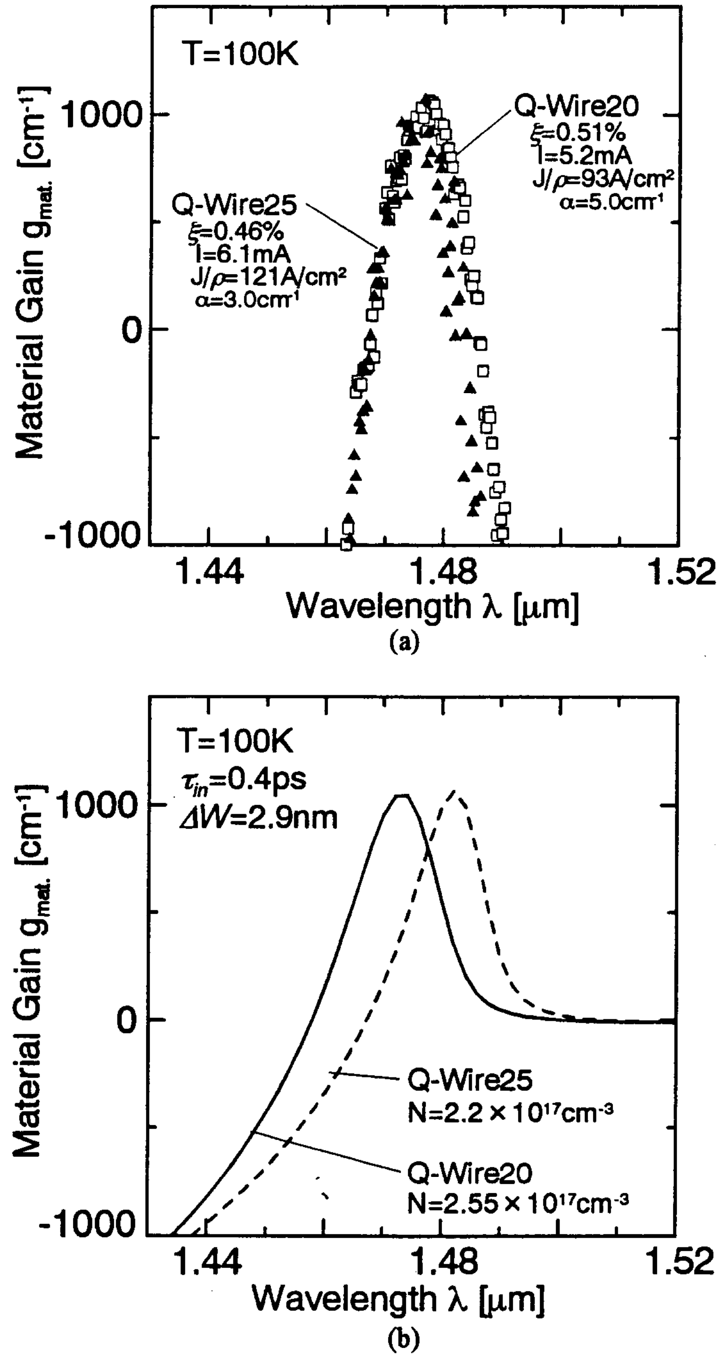

Fig. 6.9 The comparison of the gain spectra of the Q-Wire laser between (a) experimental and (b) theoretical results.

where R is the total recombination rate. The injected current density must be proportional to the total recombination rate as

$$J \equiv \frac{R \times e}{\eta_i}, \tag{6.5}$$

where e is the electronic charge, and η_i is an internal quantum efficiency. Differentiating eq. (6.5), with respect to N, assuming constant η_i, and using eq. (6.4) we find

$$\frac{\partial N}{\partial J} = \tau \times \frac{\eta_i}{e}. \tag{6.6}$$

Equation (6.6) indicates that the local slope is given by τ. From chapter 5, we obtained $\eta_i = 1$ at T=90K. Figure 6.10 shows the injected carrier density as a function of current density normalized by space filling factor J/ρ. As can be seen, the slope of all of the lasers were almost the same, that is, the lifetimes of all lasers were the same.

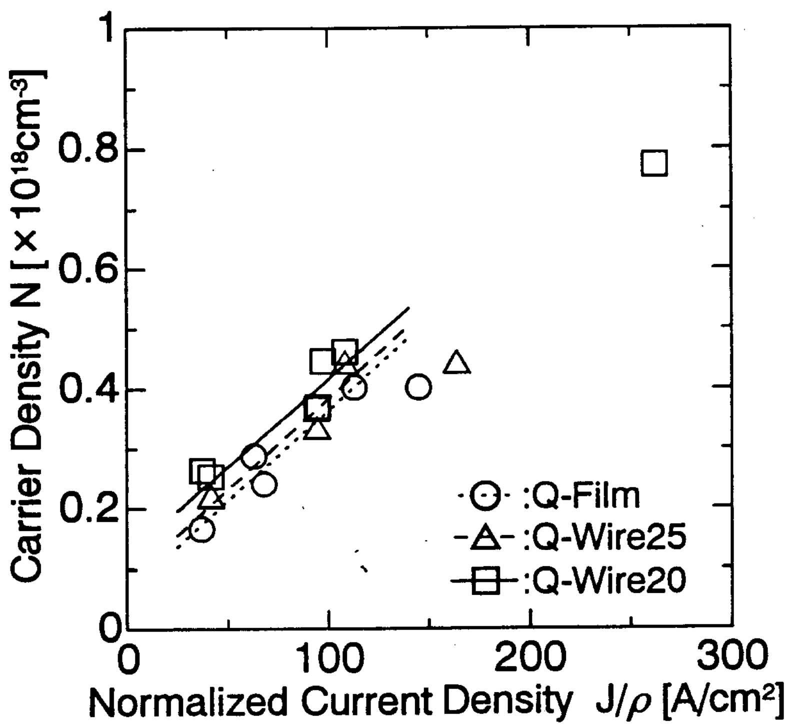

Fig. 6.10 The injected carrier density as a function of current density normalized by space filling factor J/ρ. The slope indicates the lifetime.

Figure 6.11 shows the material gain as a function of the injected carrier density (a) at $N<5\times10^{18}cm^{-3}$ and (b) $N<1\times10^{18}cm^{-3}$. The lines are the calculated results and the plotted marks are the experimental results. As can be seen, the differential gain on the injected carrier density of the Q-Wire lasers were higher than that of the Q-Film laser at T=90K.

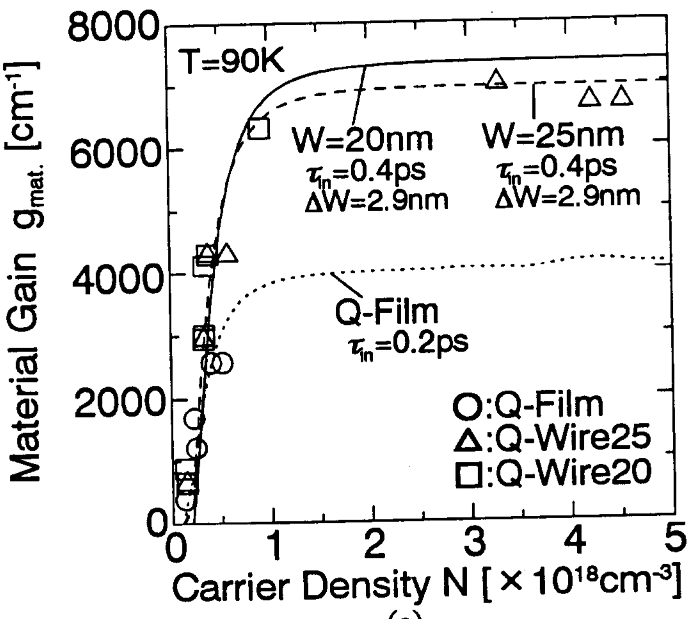

(a)

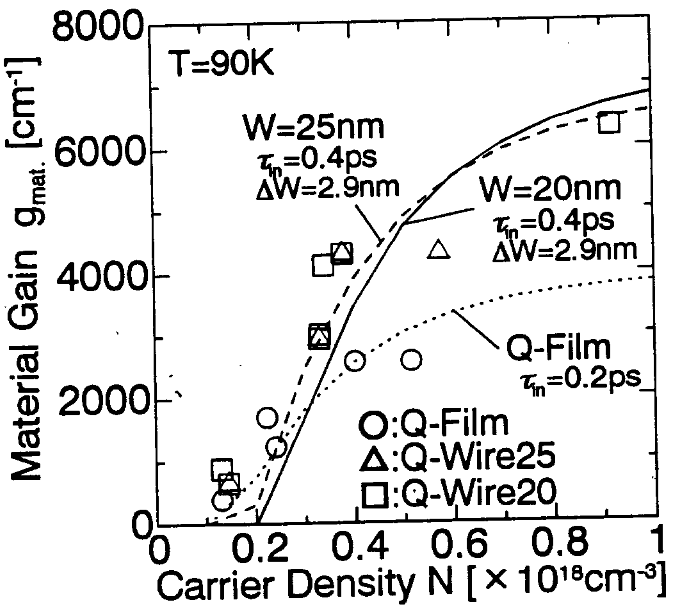

(b)

Fig. 6.11 The material gain as a function of injected carrier density; (a) at $N<5\times10^{18}cm^{-3}$ and (b) $N<1\times10^{18}cm^{-3}$.

Finally, in Fig. 6.12, we show the wire width dependence of the maximum gain considering the size fluctuation of ΔW=0-3nm at T=90K as a parameter of τ_{in}; (a) τ_{in}=0.1ps, (b) τ_{in}=0.2ps, (c) τ_{in}=0.3ps, and (d) τ_{in}=0.4ps. The painted circle at W=50nm shows the g_{max} of the Q-Film. The injected carrier density is $1\times10^{18}cm^{-1}$, which is almost maximum value as shown in Fig. 6.11(a). In all of τ_{in}, the width obtaining maximum gain is 10-12nm, when there is no size fluctuation. However the more the size fluctuation increases, the width obtaining maximum gain becomes

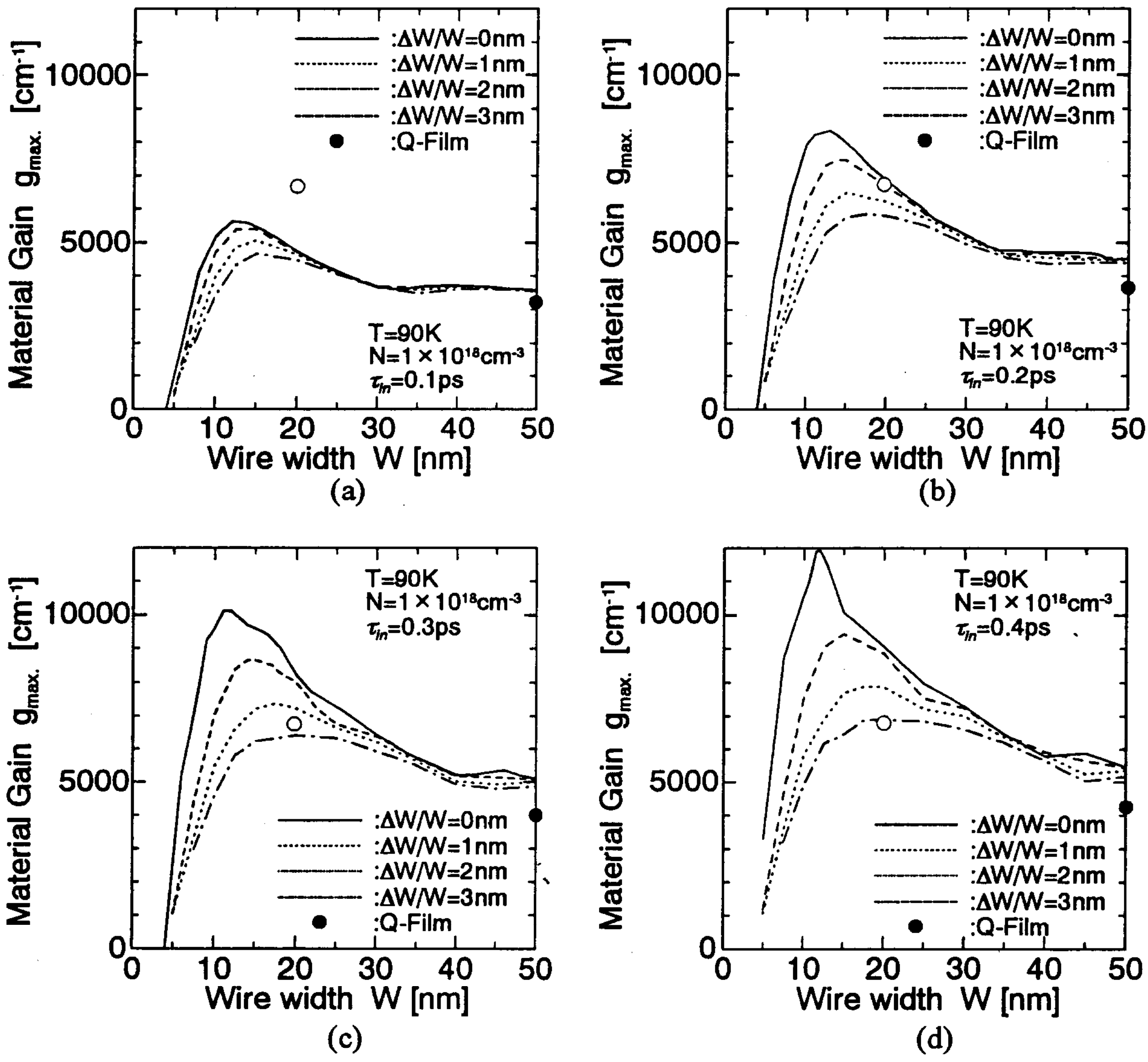

Fig. 6.12 The wire width dependence of the maximum gain considering the size fluctuation of ΔW=0-3nm at T=90K as a parameter of τ_{in}; (a) τ_{in}=0.1ps, (b) τ_{in}=0.2ps, (c) τ_{in}=0.3ps, and (d) τ_{in}=0.4ps.

larger, and this tendency becomes remarkable with an increase in the τ_{in}. The open circle shows the experimental result as shown in Fig. 6.11. In τ_{in}=0.1ps, the calculated maximum gain is lower than the experimental result even with no size fluctuation. In τ_{in}=0.3ps and τ_{in}=0.4ps, the width obtaining maximum gain is theoretically about 20nm with the size fluctuation of 3nm, and the experimental result seems to agree with the theoretical limit.

6.4 Conclusion

In conclusion, the gain spectra of 1.5 μm wavelength GaInAsP/InP quantum-wire lasers ($\overline{W}$=20, 25 nm) were measured at T=100 K and were compared with quantum-film lasers prepared on the same wafer. It was found for the first time that the material gain spectrum of quantum-wire lasers was narrower than that of the quantum-film laser.

Comparing the experimental results with the calculated results, the intraband relaxation time of the Q-Wire lasers seemed to be longer (~twice) than that of the Q-Film laser. The carrier lifetimes of the Q-Wire lasers and the Q-Film lasers were almost the same, that is, the differential gain of the Q-Wire lasers were higher than that of the Q-Film lasers.

When the size fluctuation is 3nm, the wire width obtaining the maximum gain is theoretically about 20nm, and our experimental result seems to agree with the theoretical limit.

References

[6-1] Y. Arakawa and H. Sakaki, "Multidimensional quantum well laser and temperature dependence of its threshold current," *Appl. Phys. Lett.*, vol.40, no.11, pp.939-941, June 1982.

[6-2] M. Asada, Y. Miyamoto, and Y. Suematsu, "Gain and the threshold current of three-dimensional quantum-box lasers," *IEEE J. Quantum Electron.*, vol.QE-22, no.9, pp.1915-1921, Sept. 1986.

[6-3] Y. Miyake and M. Asada, "Spectral characteristics of linewidth enhancement factor α of multidimensional quantum wells," *Jpn. J. Appl. Phys.*, vol.28, no.7, pp.1280-1281, July 1989.

[6-4] E. Kapon, S. Simhony, R. Bhat and D. M. Hwang, "Single quantum wire semiconductor lasers," *Appl. Phys. Lett.*, vol.55, no.26, pp2715-2717, Dec. 1989.

[6-5] K. Kudo, Y. Nagashima, S. Tamura, S. Arai, Y. Huang, and Y. Suematsu, "$Ga_{0.66}In_{0.34}As$/GaInAsP/InP Tensile-Strained Single-Quantum-Well Lasers with 70-nm Period Wire Active Region," *IEEE Photon Technol. Lett.*, vol.5, no.8, pp.864-867, Aug. 1993.

[6-6] S. Tiwari, G. D. Pettit, K. R. Milkove, F. Legoues, R. J. Davis and J. M. Woodall, "High efficiency and low threshold current strained V-groove quantum-wire lasers," *Appl. Phys. Lett.*, vol.64, no.26, pp.3536-3538, Jun. 1994.

[6-7] S. T. Chou, K. Y. Cheng, L. J. Chou and K. C. Hsieh, "$Ga_xIn_{1-x}As$ multiple-quantum-wire lasers grown by the strain-induced lateral-layer ordering process," *Appl. Phys. Lett.*, vol.66, no.17, pp.2220-2222, Apr. 1995.

[6-8] J. Yoshida, K. Kishino, A. Kikuchi and I. Nomura, "Continuous-Wave (CW) operation of GaInP-AlGaInP visible compressively strained multiple quantum-wire (CS-MQWR) lasers," *IEEE J. Selected Topics in Quantum Electron.* vol.1, pp.173-182, Jun. 1995.

[6-9] K. C. Shin, S. Arai, Y. Nagashima, K. Kudo and S. Tamura, "Temperature Dependences of $Ga_{0.66}In_{0.34}As$ /InP Tensile-Strained Quasi-Quantum-Wire Laser Fabricated by Wet Chemical Etching and 2-step OMVPE Growth," *IEEE Photon Technol. Lett.*, vol.7, no.4, pp.345-347, Apr. 1995.

[6-10] T. Kojima, M. Tamura, K. C. Shin, S. Tamura and S. Arai, "Temperature dependences of GaInAsP/InP compressively-strained quantum-wire lasers fabricated by EB-lithography and 2-step OMVPE growth," *IEEE 8th Int. Conf. on Indium Phosphide and Related Materials (IPRM'96)*, ThA1-5, Schwäbisch Gmünd, pp.731-734, Apr. 1996.

[6-11] T. Kojima, S. Arai and G. U. Bacher, "Anisotropic polarization properties of photoluminescence from GaInAsP/InP quantum -wire structures fabricated by two-step organometallic vapor phase epitaxy growth," *Jpn. J. Appl. Phys.*, vol.37, Pt.2, no.1A/B, pp.L46-L49, Jan. 1998.

[6-12] T. Ishii, H. Nozawa and T. Tamamura, "Nanocomposite resist system," *Appl. Phys. Lett.*, vol.70, no.9, pp.1110-1112, Mar. 1997.

[6-13] T. L. Paoli and B. W. Hakki, "cw degradation at 300°K of GaAs double- heterostructure junction lasers. I,. Emission spectra," *J. Appl. Phys.*, vol.44, no.9, pp.4108-4112, Sep. 1973.

[6-14] B. W. Hakki and T. L. Paoli, "cw degradation at 300°K of GaAs double-heterostructure junction lasers. II,. Electronic gain," *J. Appl. Phys.*, vol.44, no.9, pp.4113-4119, Sep. 1973.

[6-15] B. W. Hakki and T. L. Paoli, "Gain spectra in GaAs double- heterostructure junction lasers," *J. Appl. Phys.*, vol.46, no.3, pp.1299-1306, Mar. 1975.

[6-16] M. Yamada, H. Ishiguro and H. Nagato, "Estimation of the intra-band relaxation time in undoped AlGaAs injection laser," *Jpn. J. Appl. Phys.*, vol.19, no.1, pp.135-142, Jan. 1980.

[6-17] H. Zarem, K. Vahala, and A. Yariv, "Gain spectra of quantum wires with inhomogeneous broadening," *IEEE. J. Quantum Electron.*, vol.QE-25, no.4, pp.705-712, Apr. 1989.

[6-18] M. Asada and Y. Suematsu, "Density-matrix theory of semiconductor lasers with relaxation broadening model –Gain and gain-suppression in semiconductor lasers," *IEEE J. Quantum Electron.*, vol.QE-21, no.5, pp.434-442, May 1985.

[6-19] M. Asada, Y. Miyamoto and Y. Suematsu, "Theoretical gain of quantum-well wire lasers," *Jpn. J. Appl. Phys.*, vol.24, no.2, pp.L95-L97, Feb. 1985.

[6-20] H. Shoji, Y. Nakata, K. Mukai, Y. Sugiyama, M. Sugawara, N. Yokoyama and H. Ishikawa, "Lasing characteristics of self-formed quantum dot lasers with multistacked dot layer," *IEEE J. Selected Topics in Quantum Electron.*, vol.3, no.2, pp.188-195, Apr. 1997.

[6-21] K. Mukai and M. Sugawara, "Slow carrier relaxation among sublevels in annealed self-formed InGaAs/GaAs quantum dots," *Jpn. J. Appl. Phys.*, vol.37, pt.1, no.10, pp.5451-5456, Oct. 1998.

[6-22] A. P. Ongstad, G. C. Dente, M. L. Tilton, J. Stohs and D. J. Gallant, "Determination of carrier lifetimes using Hakki-Paoli gain data," *Appl. Phys. Lett.*, vol.72, no.7, pp.836-838, Feb. 1998.

Chapter 7

Approach for Improvement of Temperature Characteristics of Quantum-Wire Lasers

7.1 Introduction 173
7.2 Approach for Improvement of Temperature Characteristics of Quantum-Wire lasers 174
7.2.1 Multiple-Stacked Quantum-Wire Laser Using Dry Etching 174
7.1.2 Introduction of Al-Containing Materials 176
7.2.3 High Optical Confinement Structure Laser 178
7.3 Conclusion 179
References 180

7.1 Introduction

FUNDAMENTAL lasing properties, especially temperature dependencies of GaInAsP/InP 1.5μm-wavelngth quantum-wire (Q-Wire) lasers, fabricated by electron beam (EB) lithography and the wet chemical etching technique followed by organometallic vapor phase epitaxy (OMVPE) embedding growth, were studied in the previous chapters. As a result, better lasing properties of the quantum-wire laser over the quantum-film laser, i.e. lower threshold current and higher differential quantum efficiency operations, were obtained at a temperature below 200K. However, high performance operation of the Q-Wire laser cannot be obtained at room temperature.

In this chapter, some approaches for the improvement of temperature characteristics of quantum-wire lasers will be discussed.

7.2 Approach for Improvement of Temperature Characteristics of Quantum-Wire lasers

7.2.1 Multiple-Stacked Quantum-Wire Laser Using Dry Etching

It is necessary to obtain a high optical confinement factor for the realization of a Q-Wire laser even under large cavity loss conditions, as mentioned in Chapter 2. Wet chemical etching is a low damage process because it uses chemical reactions. However, the shape of an etched material strongly depends on crystal orientation, which is usually mesa-shaped. As a result, the optical gain of multi-stacked Q-Wire lasers decreases and broadens due to the large size fluctuation of Q-wires in the vertical direction. On the other hand, the dry etching is superior to the wet etching from a viewpoint of high density nano-structure fabrication by adopting stacked multi-layers. Recently, GaInAsP wire structures of various sizes were fabricated by EB lithography, CH_4/H_2 reactive ion etching (RIE) and OMVPE embedding growth and their photoluminescence (PL) intensity dependence on the wire width was measured[7-1]. As a result, the product of etched sidewall recombination velocity and carrier lifetime ($S \cdot \tau$) was estimated to be about 30 nm at room temperature, which is comparable with that of wet etching. Using this process, 1.5μm wavelength 5-MQW gain-coupled (GC) distributed feedback (DFB) lasers were fabricated. Figure 7.1 shows the cross sectional SEM view of etched and embedded active layer and its illustration. As can be seen, the uniform, vertical-stacked wire layers were obtained. Figure 7.2 shows I-L characteristic of a GC-DFB laser under pulsed condition. The threshold current was 50mA and threshold current density as low as 660A/cm^2 was obtained. This is the best value for GC-DFB lasers where active layers were completely etched by dry etching.

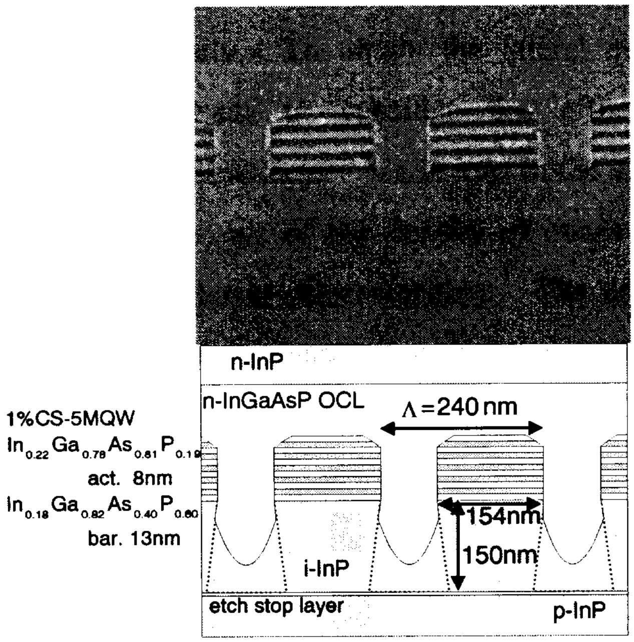

Fig. 7.1 Cross sectional SEM view and schematic of DFB structure.

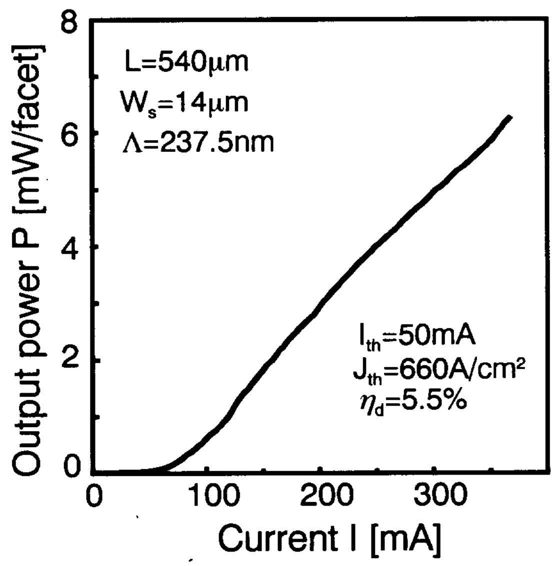

Fig. 7.2 I-L characteristics at room temperature under pulsed condition.

This process is very attractive for the fabrication of multi-stacked Q-Wire laser. As shown in Fig. 2.5(a), the wire width obtaining maximum gain with the size fluctuation of 1nm is estimated to be about 10nm. In this case, the optical confinement factor of the Q-Wire is necessary to be more than 54% of the initial quantum-film (Q-Film) in order to overcome the Q-Film laser. If a 10nm-wide Q-

Wire structures are fabricated with the period of 40nm, more than three stacked Q-Wire structures are necessary as shown in Fig. 7.3. This condition can be added to the present process relatively easily. To obtain the lateral quantum confinement effect sufficiently, it is important to consider the effects of fabricational inhomogeneities on quantum wire structures. Variations in the size of quantum wires will smear some of the sharpness out of the density of states of these structures, reducing some of the benefits of lower dimensionality. The dry etching process is possible to reduce the size fluctuation compared with the wet etching, because of no under-cut or side etching.

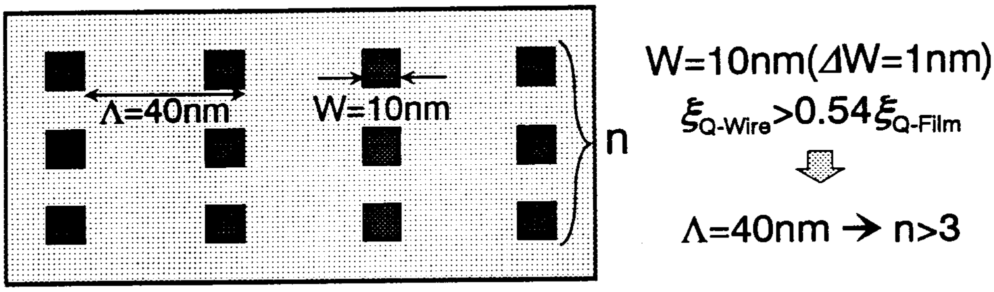

Fig. 7.3 Introducing dry process for Q-Wire fabrication.

7.2.2 Introduction of Al-Containing Materials

As a result of the temperature dependence of the internal quantum efficiency η_i of the Q-Wire laser, a rapid decrease of η_i at T>200 K was observed. One of the reasons for this can be attributed to carrier overflow or carrier leakage beside the wires[7-2],[7-3]. The Al(Ga)InAs material system is an attractive method for the improvement of the characteristic temperature T_0 of long-wavelength semiconductor lasers[7-4],[7-5] by reducing carrier overflow because of a larger band offset (ΔE_c=0.72E_g) than conventional GaInAsP material systems (ΔE_c=0.4E_g). High T_0 of 122K emitting at 1.55μm AlGaInAs 7-multiple quantum-well (7MQW) laser was reported[7-6].

Furthermore, larger optical confinement factor was also obtained in this material system. Figure 7.4 shows the optical confinement factor as a function of optical confinement layer (OCL) thickness. In the case of single-quantum-well (SQW) (10nm thick), high optical confinement factor of 1.7% was obtained using AlGaInAs OCL. Recently compressively-strained GaInAsP SQW lasers with AlGaInAs OCL were fabricated by 2-step OMVPE growth. Figure 7.5 shows the I-L characteristics at room temperature under pulsed conditions. The threshold current density of

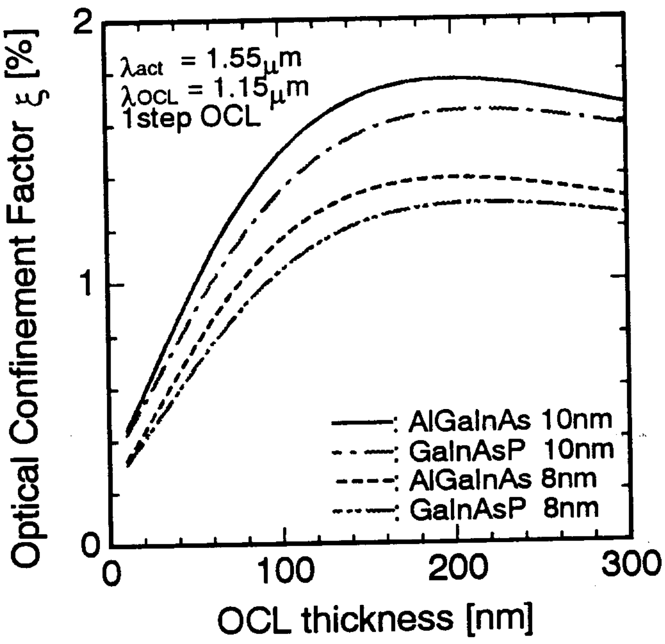

Fig. 7.4 The optical confinement factor as a function of OCL thickness.

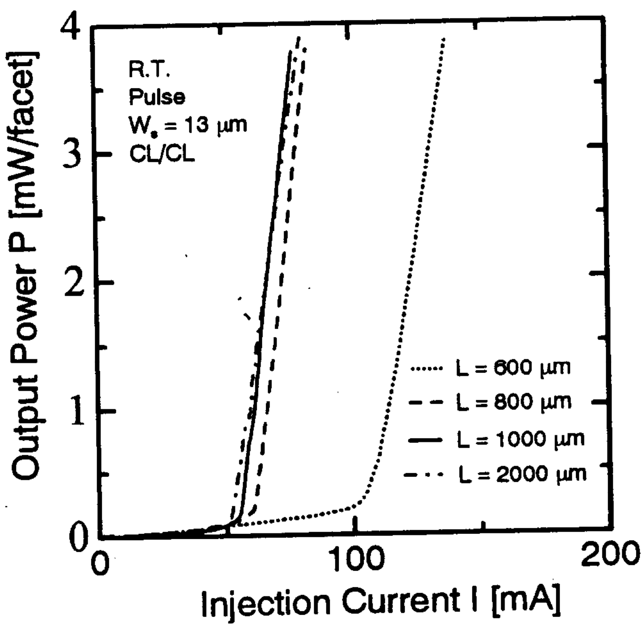

Fig. 7.5 I-L characteristics at room temperature under pulsed condition.

140A/cm^2 and differential quantum efficiency of 31% was obtained with the cavity length of 2mm. It can be beneficial to use this material system for the single layer Q-Wire lasers illustrated in Fig. 7.6 and also multi-stacked Q-Wire lasers because of reducing the carrier over flow and obtaining a higher optical confinement factor.

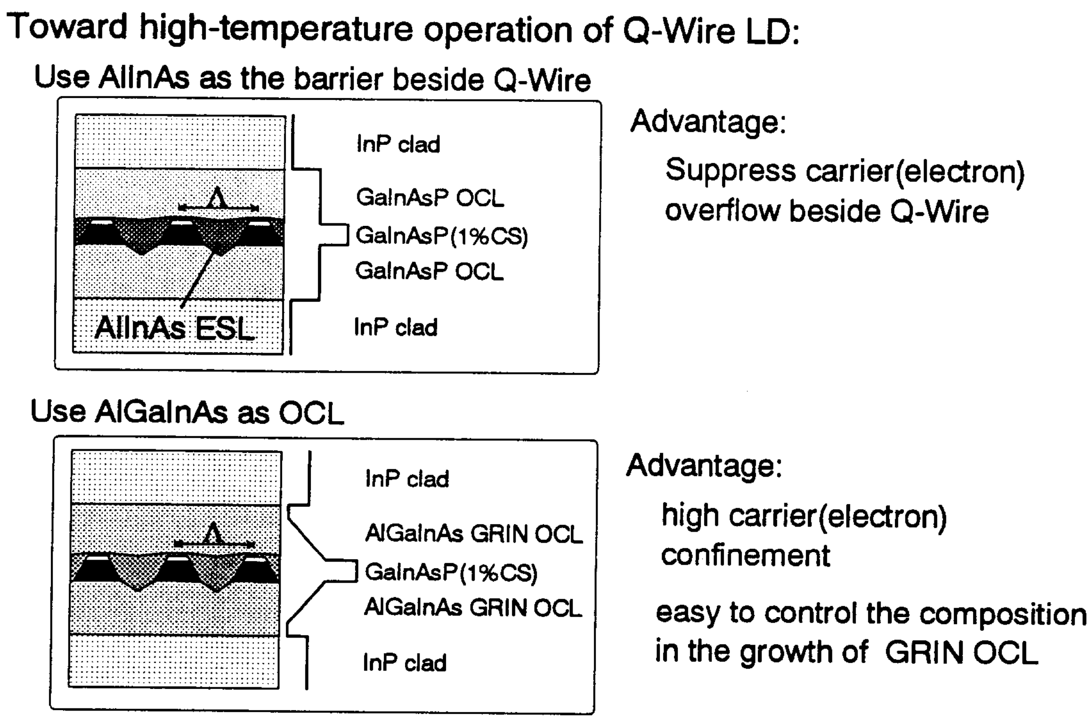

Fig. 7.6 Introducing Al(Ga)InAs system for Q-Wire lasers.

7.2.3 High Optical Confinement Structure Laser

Recently, a novel laser structure having high optical confinement factor was proposed[7-7], that is, a semiconductor core region (GaInAsP/InP) sandwiches with the Benzocyclobutene (BCB)[7-8] as cladding layers, called semiconductor membrane lasers, as shown in Fig. 7.7(a). The optical confinement factor of GaInAsP SQW active layer is expected to be 4.66% due to the large refractive index difference ($\Delta n/n$=54%) as shown in Fig. 7.7(b). Introducing the Q-Wire structure as the active region, a very low threshold current operation of the Q-Wire laser can be expected. In this novel structure, the Q-Wire laser can also tolerate the relatively large-size fluctuation of the Q-Wire size due to the high optical confinement effect as mentioned in Chapter 2.

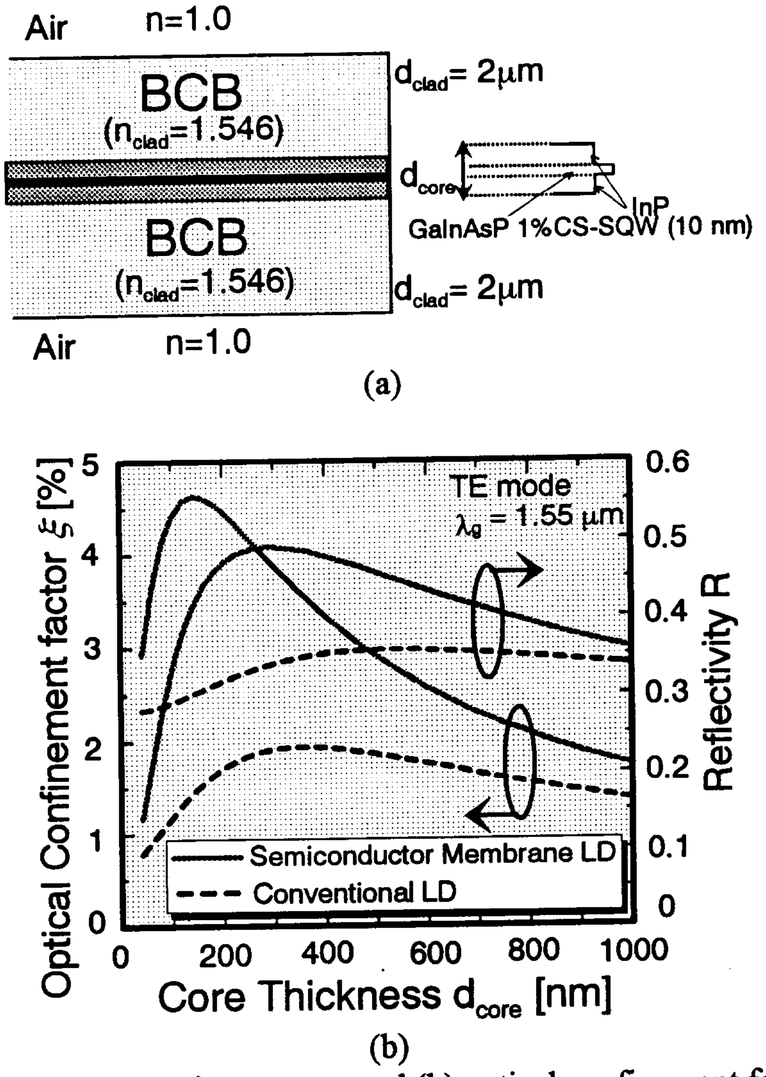

Fig. 7.7 (a) Schematic structure and (b) optical confinement factor of the semiconductor membrane laser.

7.3 Conclusion

Some approaches for the improvement of temperature characteristics of quantum-wire lasers was discussed. With the combination of the dry etching technique and/or the introduction of the AlGaInAs system, it can be relatively easy to obtain high performance operation of quantum-wire lasers at room temperature. A semiconductor membrane type quantum-wire laser is also expected to have an ultimately low threshold current operation.

References

[7-1] N. Nunoya, M. Nakamura, S. Tanaka, H. Yasumoto, I. Fukushi, S. Tamura and S. Arai, "Low Damage GaInAsP/InP Nano-Structures by CH_4/H_2 Reactive Ion Etching and Its Application to Low Threshold Gain-Coupled DFB Lasers," to be submitted in ***IEEE 11th Int. Conf. on Indium Phosphide and Related Materials (IPRM'99)***, May 1999.

[7-2] M. Asada, "Rate-equation analysis of semiconductor lasers," ***Handbook of Semiconductor Lasers and Photonic Integrated Circuits***, ed. Y. Suematsu and A. R. Adams ***(Chapman & Hall, London, 1994)*** Chap.7.

[7-3] L. V. Asryan and R. A. Suris, "Temperature dependence of the threshold current density of a quantum dot laser," ***IEEE J. Quantum Electron.***, vol.34, no.5, pp.841-850, May 1998.

[7-4] C. E. Zah, R. Bhat, B. N. Pathak, F. Favire, W. Lin, M. C. Wang, N. C. Andreadakis, D. M. Hwang, M. A. Koza, T.-P. Lee, Z. Wang, D. Darby, D. Flanders and J. J. Hsieh, "High-performance uncooled 1.3-μm $Al_xGa_yIn_{1-x-y}As$/InP strained-layer quantum-well lasers for subscriber loop applications," ***IEEE J. Quantum Electron.***, vol.30, no.2, pp.511-523, Feb. 1994.

[7-5] C. C. Lin, K. S. Liu, M. C. Wu and H. P. Shiano, "Highly uniform characteristics 12-element 1.5μm strain-compensated AlGaInAs/InP laser arrays with low threshold current and high characteristic temperature," ***Electron. Lett.***, vol.34, no.2, pp.186-187, Jan. 1998.

[7-6] N. Ohnoki, G. Okazaki, F. Koyama and K. Iga, "Record high characteristic temperature (T_0=122K) in 1.55μm AlGaInAs lasers with AlAs/AlInAs multiple quantum barrier," ***IEEE 16th Int. Semicond. Laser Conf. (ISLC 1998)***, PD-9, Nara, pp.19-20, Oct. 1998.

[7-7] M. Madhan Raj, S. Toyoshima, Y. Saka, T. Kojima and S. Arai, "Analysis of threshold current of a high optical confinement semiconductor laser," ***Nat. Conv. Res. of Japan Soc. Appl. Phys.***, 15a-A-19, p.997, Higashi-Hiroshima, Sep. 1998.

[7-8] M. Madhan Raj, K. Numata, S. Toyoshima, S. Peng, Y. Miyamoto and S. Arai, "Application of Benzocyclobutene (BCB) polymer to active opto-electronics devices," ***Nat. Conv. Res. of Japan Soc. Appl. Phys.***, 30a-ZH-9, p.1145, Hachioji, Mar. 1998.

Chapter 8
Conclusions

THE objective of this thesis is to realize high performance operation, i.e. lower threshold and higher efficiency, of a 1.55μm-wavelength quantum-wire (Q-Wire) laser compared with quantum-film (Q-Film) laser using the GaInAsP/InP system.

In Chapter 1, recent progress in the development of Q-Wire and quantum-box/dot (Q-Box) lasers is reviewed with an emphasis on the fabrication technology. The fabrication technology using electron beam (EB) lithography and etching followed by an embedded growth with organometallic vapor phase epitaxy (OMVPE) is one of the most effective methods for 1.55μm-wavelength Q-Wire or Q-Box lasers, which is a better technique for the position and size controllability of Q-Wire and Q-Box structures. Furthermore, this fabrication technique is suitable for use in the production of distributed feedback (DFB) lasers consisting of a Q-Wire or Q-Box active region.

In Chapter 2, the most effective size of the Q-Wire is estimated from the point of material gain and threshold current density, considering the size fluctuation of Q-Wire structure and the optical confinement factor. At T=300K, the width to obtain maximum gain is about 8nm (7-10nm) with no size fluctuation. However, the width to obtain maximum gain becomes larger and the maximum gain is reduced with an increase in the size fluctuation, and the size fluctuation effect is negligible if the wire width is larger than 22nm. The tendency of the size fluctuation effect is similar at T=90K, but the influence of size fluctuation is smaller compared with that at T=300K. This is because energy broadening due to thermal energy becomes small at low temperatures.

Regarding threshold current, minimum threshold current density can be obtained with the wire width of 10-20nm. It is possible to realize high performance of single-layer Q-Wire lasers at room temperature under the condition of low cavity loss structures, such as long-cavity structures or high reflective (HR) coating of facets. At low temperatures, as the energy broadening due to thermal excitation and optical losses due to nonradiative recombination are reduced, it is relatively easier to obtain high performance of single-layer Q-Wire lasers. In the case of W=20nm, the threshold current of Q-Wire laser is estimated to be half that of the Q-Film laser when the in-plane space filling factor of Q-Wire is 0.4 to 0.5.

In Chapter 3, the fabrication process of Q-Wire lasers is described, including the crystal growth technique using OMVPE. It was found that our OMVPE system has proportional relations between Ga/In and TEG/TMI, and between As/P and AsH_3/PH_3.

GaInAsP fine wire structure with a period of 50nm was fabricated using EB lithography and wet chemical etching, and its size fluctuation was analyzed. By correcting the dose profile for the proximity effect, the size fluctuation of the resist pattern was reduced from $\pm$2.7nm to $\pm$1.4nm, and that of GaInAsP wire structure was reduced from $\pm$3.8nm to $\pm$2.9nm, respectively, for a typical wire width of 30nm.

To solve the problems of low optical confinement factor of the active region and poor size uniformity in these Q-Wire structures, a relatively thick compressively-strained (1% CS) quantum-well (10nm thick, ξ=1.3% for the quantum-film, λ_{PL} =1.576μm) structure was adopted as an initial wafer for the quantum-wire structure, and a thin quantum-film layer (1% CS, 5nm thick, ξ=0.6%, λ_{PL}=1.512μm) was introduced to enhance the optical confinement factor and to partially support optical gain when the wire size becomes very narrow and the gain peak wavelength shifts close to the gain peak of the quantum-film structure.

Two kinds of high-density Q-Wire structures were fabricated for high performance operation of Q-Wire lasers; one was the wire size of 20nm with a period of 50nm, and the other's size was 25nm with a period of 70nm.

In Chapter 4, anisotropic polarization properties of photoluminescence (PL) intensity from GaInAsP/InP quantum-wire structures due to the lateral quantum confinement effect, which causes anisotropic behavior of the dipole moment, were observed, and it was experimentally confirmed that the polarization anisotropy becomes stronger in narrow quantum-wire structures. A compressively-strained quantum-wire structure showed stronger polarization anisotropy compared with a lattice-matched one of the same size. The polarization dependence was enhanced due to a composition modulation effect and an electric-field modulation effect because of the anisotropic refractive index

From the temperature dependence of the PL signal, nonradiative recombination velocity at the regrowth interface of the Q-Wire can be negligibly small at temperatures below T=200K.

In Chapter 5, fundamental lasing properties, especially temperature dependencies of lasing properties of 1.5μm wavelength GaInAsP/InP compressively-strained Q-Wire lasers with the nominal wire width of 20nm and 25nm fabricated by EB lithography and 2-step OMVPE growth, and compared with those of Q-Film lasers prepared on the same wafer. As the result, we obtained, for the first time, a lower threshold current and a higher differential quantum efficiency operation of a Q-Wire laser over the Q-Film laser at a temperature below T<200K. At T=90K, threshold current density of the Q-Wire laser as low as $34A/cm^2$ and differential quantum efficiency as high as 77% were obtained, which is the lowest value of the threshold current density within the Q-Wire lasers. Furthermore, the internal quantum efficiency was evaluated to be 1.0 at T<200K from measurements of the temperature dependence of differential quantum efficiency of different cavity length samples. We also confirmed the possibility of a complex-coupled DFB laser consisting of a Q-Wire active region as the grating structure.

In Chapter 6, the gain spectra of 1.5 μm wavelength GaInAsP/InP Q-Wire lasers ($\overline{W}$=20, 25 nm) were measured at T=100 K and were compared with the Q-Film lasers prepared on the same wafer. It was found for the first time that the material gain spectrum of the Q-Wire lasers was narrower than that of the Q-Film laser.

Comparing the experimental results with the calculated results, the intraband relaxation time of the Q-Wire lasers seemed to be longer (~twice) than that of the Q-Film laser. The carrier lifetime of the Q-Wire lasers and the Q-film laser were almost the same, that is, the differential gain on injected carrier density of the Q-Wire lasers can be higher than that of the Q-Film lasers.

When the size fluctuation of the wire structure is assumed to be 3nm, the wire width obtaining the maximum gain is theoretically about 20nm, and our experimental result seems to agree with the theoretical limit.

Finally, in Chapter 7, some approaches for the improvement of the temperature characteristics of Q-Wire lasers were discussed. With the combination of dry and wet etching techniques, and the introduction of the AlGaInAs system, it can be relatively easy to obtain high performance operation of quantum-wire lasers at room temperature. Semiconductor-membrane-type Q-Wire lasers are also expected to have ultimately low threshold current operation at room temperature.

Acknowledgments

The author would like to express his sincere acknowledgement to Professor Shigehisa Arai for his guidance, continuous encouragement throughout this study and daily life guidance, and fruitful discussions.

The author wishes to thank Professor Hiroshi Ishihara, Professor Motoichi Ohtsu, Associate Professor Kazuo Tsutsui and Associate Professor Masahiro Asada for guidance and numerous discussions on this study.

The author would like to thank Associate Professor Yasuyuki Miyamoto for his guidance, especially on the experiments of this study.

The author would like to acknowledge Professor Emeritus Yasuharu Suematsu, Professor Kenichi Iga, Professor Kazuhito Furuya, Associate Professor Fumio Koyama, Associate Professor Masahiro Watanabe and Lecturer Tomoyuki Miyamoto for their encouraging and constructive discussions.

The author would like to thank Professor Hiroshi Kawarada, Professor Sadayuki Ueha, Professor Shigeo Ohtsuki, Professor Mitsumasa Iwamoto, Associate Professor Matsuo Sekine, Associate Professor Eisuke Tokumitsu, Associate Professor Kentaro Nakamura, Associate Professor Sumio Watanabe, Associate Professor Yutaka Majima and the members of the microwave research group for their advice and suggestions to this study.

The author wishes to acknowledge Professor Minoru Yamada of Kanazawa University, Professor Hideo Kawanishi of Kogakuin University, Professor Toshio Kambayashi of Technical University of Nagaoka, Professor Katsumi Kishino of

Sophia University, Professor Yasuo Kokubun of Yokohama National University, Professor Kazunori Moriki of Musashi Institute of Technology, Professor Katsuyuki Utaka of Waseda University, Associate Professor Kazuhiko Shimomura of Sophia University, Associate Professor Toshihiko Baba of Yokohama National University, Lecturer Toru Honda of Kogakuin University, Lecturer Yuji Kuwamura of Kanazawa University and the members of the summer seminar on optical communications for helpful advice and fruitful discussions.

The author would like to thank Dr. Michihiko Suhara for his continuous encouragement and discussions.

The author expresses his sincere thanks to Technical Staff Shigeo Tamura for his fruitful discussions and experimental help on this study.

The author would like to acknowledge Dr. Akihiko Kasukawa (Furukawa Electric) for his technical support and discussions on this study.

The author deeply appreciates the continuous help being rendered by co-workers Dr. Ki-Chul Shin (LG Cable and Machinery, Korea), Dr. Toshiyuki Takizawa (Matsusita Electronics Corp.), Dr. Munehisa Tamura (NTT), Mr. Masatsugu Hotta (Toyota), Mr. Toshio Kimura (Furukawa Electric), Mr. Tsukasa Kakinuma (TBS), Mr. Toshihiko Otake (Matsusita Electric Industrial), Mr. Hirotsugu Kasyo (Toshiba), Mr. Shinji Kurihashi (Mitsubishi Electric), Mr. Machiya Kumazawa (Matsusita Electric Industrial), Mr. Jiro Yoshinaga (NTT), Mr. Toshikazu Ando (NTT), Mr. Naoki Serizawa (NTT Data), Mr. Ryotaro Ubukata (JR East) and Dr. Gerd U. Bacher (Würzburg University, Germany).

The author would like to sincerely thank Mothi Madhan Raj, Mrs. Xue-Ying Jia (Irie Koken), Mr. Hiroyuki Nakaya (Sumitomo Electronic), Messrs. Suguru Tanaka, Nobuhiro Nunoya, Yoshinori Hayafune (Prof. Oda's group), Hideo Yasumoto, Madoka Nakamura, and members of the laser group for their fruitful discussions and experimental help.

The author would like to acknowledge Mr. Junichi Hidaka (Nippon Sanso), Mr. Akinori Ubukata (Nippon Sanso), Dr. Jie Dog (Nippon Sanso), Mr. Toshiki Arai, and members of OMVPE group for their continuous help and discussions.

The author wishes to thank Professor Dr. Holger T. Grahn and Dr. Bernd Jenichen, Paul Drude Institute, Berlin, Germany, for their analysis of the quantum-wire structure using high-resolution x-ray diffractometry.

The author would like to acknowledge Dr. Takashi Suemasu (Tsukuba University), Dr. Hiroo Hongo (NEC), Mr. Nobutaka Kikegawa, Mr. Jun Suzuki (Hitachi), the late Mr. Yoshifumi Kohno, Mr. Wataru Saito, Mr. Nobuya Machida, Mr. Eijiro Kikuno (Sony Disk Technology), Mr. Noriyuki Ohnoki (Prof. Iga's group) and Mr. Takeo Katayama (Prof. Iga's group) for their fruitful discussions and various supports.

The author would like to thank Dr. Kazuhisa Uomi (Hitachi), Dr. Hiroshi Ishikawa (Fujitsu), Dr. Masahiro Aoki (Hitachi), Dr. Hajime Shoji (Fujitsu), Dr. Kenichi Nishi (NEC), Dr. Hajime Fujikura (Hokkaido University), Dr. Koji Kudo (NEC), Mr. Yasumasa Suzaki (NTT), Professor Manfred H. Pilkuhn and Professor Heintz Schweizer of Stuttgart University, Germany, Professor Alfred Forchel of Würzburg University, Germany, Professor Alfred R. Adams of Surrey University, United Kingdom, Professor Dieter Bimberg of Technical University of Berlin and Dr. Sergey V. Zaitsev of A. F. Ioffe Institute of Russian Academy of Sciences, Russia for their helpful comments in the domestic and international conferences.

The author appreciates the kindness and help of the Secretaries, Mrs. Sachiko Itai, Miss Tomomi Nagano, Miss Etsuko Morita, Mrs. Kyoko Kasukawa, Miss Asako Kimura, Miss Ryoko Moriizumi and Miss Yukiko Yabe.

The author thanks all of his colleagues in Prof. Suematsu's group, Prof. Furuya's group, Prof. Arai's group, Assoc. Prof. Asada's group, Assoc. Prof. Miyamoto's group, Assoc. Prof. Watanabe's group and Prof. Iga's group for private advice as well as technical advice.

The author is extremely thankful to Colonel Haruhiko Kataoka of Japan Air Self Defense Force and Professor Koji Toda of National Defense Academy to have an occasion of this study under Professor Shigehisa Arai, and to 1st Development Div., Air Staff office, Japan defense Agency for a lot of support, especially financial support.

Finally, the author deeply thanks his family, his late father, Teruo, who passed last summer, his mother, Emiko, especially his wife, Tomoyo, and his daughter, Miduki.

This work was financially supported by the "Research for the Future" Program (#JSPS-RFTF96P00101) from The Japan Society for the Promotion of Science, and Grant-In-Aids for a Scientific Research Project in a Priority Area "Single Electron Nano-electronics", Fundamental Research B (#10450115), and other assistance through the Research Center for Quantum Effect Electronics from the Ministry of Education, Science, Sports and Culture, Japan.

Publication List

I. Journal Papers

(1) T. Kojima, S. Arai and G. U. Bacher, "Anisotropic polarization properties of photoluminescence from GaInAsP/InP quantum-wire structures fabricated by two-step organometallic vapor phase epitaxy growth," ***Jpn. J. Appl. Phys.***, vol.37, pt.2, no.1A/B, pp.L46-L49, January 1998.

(2) T. Kojima, M. Tamura, H. Nakaya, S. Tanaka, S. Tamura and S. Arai, "GaInAsP/InP compressively strained quantum-wire lasers fabricated by electron beam lithography and 2-step organometallic vapor phase epitaxy," ***Jpn. J. Appl. Phys.***, vol.37, pt.1, no.9A, pp.4792-4800, September 1998.

(3) T. Kojima, S. Tanaka, H. Yasumoto, H. Nakaya, S. Tamura and S. Arai, "Gain spectrum measurement of GaInAsP/InP compressively-strained quantum-wire lasers," ***Jpn. J. Appl. Phys.***, vol.37, pt.2, no.11B, pp.L1386-L1389, November 1998.

(4) T. Kojima, X. Y. Jia, Y. Hayafune, S. Tamura, M. Watanabe and S. Arai, "Size fluctuation of 50nm periodic GaInAsP/InP wire structure by electron beam lithography and wet chemical etching," ***Jpn. J. Appl. Phys.***, vol.37, pt.1, no.11, pp.5961-5962, November 1998.

(5) T. Kojima, H. Nakaya, S. Tanaka, H. Yasumoto, S. Tamura and S. Arai, "Temperature dependence of internal quantum efficiency of 20nm-wide GaInAsP/InP compressively strained quantum-wire lasers," to be published in ***Jpn. J. Appl. Phys.*** (vol.38, pt.1, no.1B, January 1999.)

(6) B. Jenichen, H. T. Grahn, T. Kojima and S. Arai, "Lateral periodicity and elastic stress relaxation in GaInAsP quantum wires on InP investigated by X-ray diffractometry," ***J. Appl. Phys.***, vol.83, no.11, pp.5810-5813, June 1998.

(7) M. Tamura, T. Kojima, T. Ando, N. Nunoya, S. Tamura and S. Arai, " Sidewall recombination velocity in GaInAsP/InP quantum-well lasers with wire-like active region fabricated by wet-chemical etching and organo-metallic vapor-phase-epitaxial regrowth," ***Jpn. J. Appl. Phys.***, vol.37, pt.1, no.12A, pp.6569-6574, December 1998.

II. International Conferences

(1) T. Kojima, M. Tamura K. C. Shin, S. Tamura and S. Arai, "Temperature dependences of GaInAsP/InP compressively-strained quantum-wire lasers fabricated by EB lithography and 2-step OMVPE growth," ***IEEE 8th Int. Conf. on Indium Phosphide and Related Materials (IPRM'96)***, ThA1-5, pp.731-734, Schwäbisch Gmünd (Germany), April 1996.

(2) T. Kojima, M. Tamura, X. Y. Jia, T. Ando, H. Nakaya, S. Tanaka, S. Tamura and S. Arai, "1.5μm GaInAsP/InP compressively-strained quantum-wire lasers fabricated by EB-lithography and wet-chemical etching," ***Int. Symposium on Formation, Physics and Device Application of Quantum Dot Structures (QDS'96)***, Th2-8, p.190, Sapporo, November 1996.

(3) T. Kojima, M. Tamura, X. Y. Jia, H. Nakaya, T. Ando, S. Tanaka, S. Tamura, S. Arai and G. U. Bacher, "Anisotropic polarization properties of GaInAsP/InP compressively-strained quantum-wire structure," ***IEEE 9th Int. Conf. on Indium Phosphide and Related Materials (IPRM'97)***, MD7, pp.226-229, Hyannis (USA), May 1997.

(4) T. Kojima, H. Nakaya, S. Tanaka, S. Tamura and S. Arai, "Evaluation of internal quantum efficiency and waveguide loss of 50nm-period GaInAsP/InP quantum-wire lasers," ***IEEE 10th Int. Conf. on Indium Phosphide and Related Materials (IPRM'98)***, WA2-4, pp.365-368, Tsukuba, May 1998.

(5) T. Kojima, H. Nakaya, S. Tanaka, H. Yasumoto, S. Tamura and S. Arai, "Temperature dependence of internal quantum efficiency of 20nm-wide GaInAsP/InP quantum-wire lasers," ***Int. Symposium on Formation, Physics and Device Application of Quantum Dot Structures (QDS'98)***, Th2-8, p.212, Sapporo, May/June 1998.

(6) M. Tamura, T. Kojima, T. Ando, S. Tamura, N. Nunoya and S. Arai, "Fabrication of GaInAsP/InP multiple-quantum wire structures by Cl_2-ECR dry etching," ***Int. Symposium on Formation, Physics and Device Application of Quantum Dot Structures (QDS'96)***, Th2-10, p.194, Sapporo, November 1996.

(7) H. Nakaya, T. Kojima, S. Tanaka, S. Tamura and S. Arai, "Gain spectral characteristics of GaInAsP/InP quantum-wire lasers," ***IEEE 10th Int. Conf. on Indium Phosphide and Related Materials (IPRM'98)***, TuP-20, pp.591-594, Tsukuba, May 1998.

III. Domestic Conferences

(1) T. Kojima, M. Tamura, K. C. Shin, S. Tamura and S. Arai, "Fabrication of GaInAsP/InP semiconductor lasers with compressively-strained wire structure," 「GaInAsP/InP圧縮歪細線構造を有する半導体レーザの試作」 ***Nat. Conv. Res. of Japan Soc. Appl. Phys.***, 28p-ZA-3, Digest Ⅲ-p.949, Kanazawa, August 1995.

(2) T. Kojima, M. Tamura, K. C. Shin, S. Tamura and S. Arai, "Temperature dependences of GaInAsP/InP compressively-strained quantum-wire lasers," 「GaInAsP/InP圧縮歪量子細線レーザの温度依存性」 *Nat. Conv. Res. of Japan Soc. Appl. Phys.*, 27a-C-11, Digest Ⅲ-p.1044, Asaka, March 1996.

(3) T. Kojima, M. Tamura, S. Tamura, H. Nakaya, S. Tanaka and S. Arai, "Temperature characteristics of GaInAsP/InP compressively-strained quantum-wire lasers," 「GaInAsP/InP圧縮歪量子細線レーザの温度特性」 *Nat. Conv. Res. of Japan Soc. Appl. Phys.*, 8p-KH-11, Digest Ⅲ-p.952, Fukuoka, September 1996.

(4) T. Kojima, X. Y. Jia, H. Nakaya, S. Tanaka, S. Tamura and S. Arai, "Anisotropic polarization properties of PL from GaInAsP/InP quantum-wire structure," 「GaInAsP/InP量子細線構造のPL偏光特性」 *Nat. Conv. Res. of Japan Soc. Appl. Phys.*, 29p-T-15, Digest 0-p.1337, Chiba, March 1997.

(5) T. Kojima, H. Nakaya, S. Tanaka, S. Tamura and S. Arai, "Cavity length dependence of threshold current of GaInAsP/InP quantum-wire lasers," 「GaInAsP/InP量子細線レーザの発振しきい値電流の共振器長依存性」 *Nat. Conv. Res. of Japan Soc. Appl. Phys.*, 2a-ZC-6, Digest Ⅲ-p.1073, Akita, October 1997.

(6) T. Kojima, H. Nakaya, S. Tanaka, S. Tamura and S. Arai, "Temperature dependence of threshold current density of GaInAsP/InP quantum-wire lasers," 「GaInAsP/InP量子細線レーザの発振しきい値電流の温度依存性」 *Nat. Conv. Res. of Japan Soc. Appl. Phys.*, 29p-ZH-3, Digest Ⅲ-p.1115, Hachioji, March 1998.

(7) T. Kojima, S. Tanaka, H. Yasumoto, S. Tamura and S. Arai, "Regrowth layer dependence of anisotropic polarization properties of PL from GaInAsP/InP quantum-wire structure," 「GaInAsP/InP量子細線構造のPL偏光特性の埋め込み層依存性」 *Nat. Conv. Res. of Japan Soc. Appl. Phys.*, 15p-YG-1, Digest Ⅲ-p.1236, Higashi-Hiroshima, September 1998.

(8) M. Tamura, T. Kojima, K. C. Shin, S. Tamura and S. Arai, "Fabrication of GaInAsP/InP quantum-wire structure by ECR dry-etching and hydrogen plasma cleaning," 「ECRドライエッチンングによるGaInAsP/InP量子細線構造の作製と水素プラズマクリーニング処理」 *Nat. Conv. Res. of Japan Soc. Appl. Phys.*, 28p-ZB-10, Digest Ⅲ-p.1092, Kanazawa, August 1995.

(9) M. Tamura, T. Kojima, T. Ando, S. Tamura, N. Nunoya and S. Arai, "Fabrication of GaInAsP/InP multiple-quantum-wire laser diodes by Cl_2-ECR dry-etching," 「ECRドライエッチンングによるGaInAsP/InP量子細線構造を有する電流注入型素子の試作」 *Nat. Conv. Res. of Japan Soc. Appl. Phys.*, 9p-C-7, Digest Ⅲ-p.1125, Fukuoka, September 1996.

(10) X. Y. Jia, T. Kojima, M. Tamura, S. Tamura and S. Arai, "Measurement size fluctuation of quantum-wire structure by electron-beam lithography," 「EB露光法により作製した量子細線構造のサイズ揺らぎ」 *Nat. Conv. Res. of Japan Soc. Appl. Phys.*, 9a-S-10, Digest Ⅱ-p.538, Fukuoka, September 1996.

(11) X. Y. Jia, T. Kojima, Y. Hayafune, S. Tamura, M. Watanabe and S. Arai, "Reduction of the size fluctuation of quantum-wire structures fabricated by proximity effect correction," 「近接効果補正露光による量子細線構造のサイズ揺らぎの低減」 *Nat. Conv. Res. of Japan Soc. Appl. Phys.*, 29a-X-4, Digest Ⅱ-p.586, Chiba, March 1997.

(12) S. Arai and T. Kojima, "GaInAsP/InP long-wavelength quantum-wire semiconductor lasers," 「GaInAsP/InP長波長帯量子細線半導体レーザ」 *Nat. Conv. Rec. of IEICE Japan*, (Invited) C-4-20, pp.266-267, Tokyo, September 1997.

(13) H. Nakaya, T. Kojima, S. Tanaka, S. Tamura and S. Arai, "Fabrication of 50nm-period of GaInAsP/InP compressively-strained quantum-wire lasers," 「周期50nm GaInAsP/InP圧縮歪量子細線レーザの作製」 *Nat. Conv. Res. of Japan Soc. Appl. Phys.*, 2a-ZC-5, Digest Ⅲ-p.1073, Akita, October 1997.

(14) S. Tanaka, T. Kojima, H. Nakaya, S. Tamura and S. Arai, "Regrowth temperature dependence of GaInAsP/InP single-layer quantum-well lasers," 「GaInAsP/InP単層量子井戸レーザの埋め込み成長温度依存性」 *Nat. Conv. Res. of Japan Soc. Appl. Phys.*, 29p-ZH-2, Digest Ⅲ-p.1115, Hachioji, March 1998.

(15) H. Nakaya, T. Kojima, S. Tanaka, H. Yasumoto, S. Tamura and S. Arai, "Gain spectrum measurement of GaInAsP/InP compressively-strained quantum-wire lasers," 「GaInAsP/InP圧縮歪量子細線レーザの光利得スペクトルの測定」 *Nat. Conv. Res. of Japan Soc. Appl. Phys.*, 29p-ZH-5, Digest Ⅲ-p.1116, Hachioji, March 1998.

(16) S. Arai and T. Kojima, "Nano-structure fabrication using lithography and GaInAsP/InP quantum-wire lasers," 「リソグラフィーによる極微構造形成とGaInAsP/InP量子細線レーザ」 電気化学会第65回大会, *Nat. Conv. Rec. of the Electrochemical Soc. of Japan*, (Invited) 特1H07, p.208, Meguro, April 1998.

(17) S. Tanaka, T. Kojima, H. Yasumoto, S. Tamura and S. Arai, "Fabrication of GaInAsP/InP compressively-strained single-quantum-well laser with AlInAs ESL," 「AlInAs ESL を有するGaInAsP/InP圧縮歪単層量子井戸レーザの作製」 *Nat. Conv. Res. of Japan Soc. Appl. Phys.*, 15a-A-9, Digest Ⅲ-p.993, Higashi-Hiroshima, September 1998.

(18) M. Madhan Raj, S. Toyoshima, Y. Saka, T. Kojima and S. Arai, "Analysis of threshold current of a high optical confinement semiconductor laser," 「高屈折率差光閉じ込め半導体レーザのしきい値電流解析」 *Nat. Conv. Res. of Japan Soc. Appl. Phys.*, 15a-A-19, Digest Ⅲ-p.997, Higashi-Hiroshima, September 1998.

(19) H. Yasumoto, T. Kojima, N. Nunoya, S. Tanaka and S. Arai, "Temperature dependences of 1.55μm GaInAsP/InP compressively-strained MQW lasers," 「1.55μm波長GaInAsP/InP圧縮歪多重量子井戸レーザの温度特性」 submitted to *Nat. Conv. Res. of Japan Soc. Appl. Phys.*, (28a-B-9), Noda, March 1999.

(20) S. Tanaka, T. Kojima, H. Yasumoto, M. Morshed, S. Tamura and S. Arai, "Fabrication of 1.55μm GaInAsP/AlGaInAs compressively-strained quantum-wire laser," 「1.55μm帯GaInAsP/AlGaInAs圧縮歪量子細線レーザの作製」 submitted to ***Nat. Conv. Res. of Japan Soc. Appl. Phys.***, (28p-B-8), Noda, March 1999.

(21) N. Nunoya, M. Nakamura, T. Kojima, S. Tanaka, I. Fukushi, S. Tamura and S. Arai, "GaInAsP/InP multiple-layered quantum-wire lasers fabricated by CH_4/H_2-RIE/OMVPE regrowth," 「CH_4/H_2-RIE/OMVPE再成長法によるGaInAsP/InP多層量子細線レーザ」 submitted to ***Nat. Conv. Res. of Japan Soc. Appl. Phys.***, (29p-ZL-19), Noda, March 1999.

IV. Technical Meetings and Symposia

(1) T. Kojima, M. Tamura, K. C. Shin, S. Tamura and S. Arai, "Fabrication of GaInAsP/InP compressively-strained single-layer quantum-wire lasers," ***13th Semiconductor Laser Symposium***, 24, p.24, Yokohama, March 1996.

(2) T. Kojima, M. Tamura, X. Y. Jia, S. Tamura, S. Arai, H. Nakaya and S. Tanaka, "Fabrication of nano-structures using EB-lithography and its application to GaInAsP/InP quantum-wire lasers," 「EB露光法による極微構造の作製とGaInAsP/InP量子細線レーザへの応用」 電子情報通信学会、レーザ・量子エレクトロニクス、信学技報, LQE96-86, pp.55-60, Tokyo, October 1996.

(3) T. Kojima, M. Tamura, X. Y. Jia, S. Tamura and S. Arai, "Fabrication of nano-structures using EB lithography and its application to long-wavelength quantum-wire lasers," ***The 3rd Int. Symposium on Quantum Effect Electron.***, 9, pp.38-43, Meguro, November 1996.

(4) T. Kojima, X. Y. Jia, H. Nakaya, S. Tanaka, S. Tamura, S. Arai and G. U. Bacher, "Lasing properties of GaInAsP/InP quantum-wire lasers," ***14th Semiconductor Laser Symposium***, 18, p.18, Yokohama, March 1997.

(5) T. Kojima, H. Nakaya, S. Tanaka, H. Yasumoto, S. Tamura and S. Arai, "Optical gain measurement of GaInAsP/InP quantum-wire lasers," ***15th Semiconductor Laser Symposium***, 19, p.19, Yokohama, March 1998.

(6) T. Kojima, H. Nakaya, S. Tanaka, H. Yasumoto, S. Tamura and S. Arai, "Fabrication of GaInAsP/InP quantum-wire lasers and evaluation of its optical gain characteristics," 「GaInAsP/InP量子細線レーザの作製とその光学利得特性評価」 電子情報通信学会技術研究報告、光エレクトロニクス、信学技報, OPE98-39, LQE98-33, pp.25-30, Tokyo, July 1998.

(7) T. Kojima, S. Tanaka, H. Yasumoto, S. Tamura, N. Nunoya and S. Arai, "Fabrication of GaInAsP/InP quantum wire lasers and evaluation of its optical gain characteristics," ***The 5th Int. Symposium on Quantum Effect Electron.***, 8, pp.32-37, Meguro, October 1998.

(8) S. Arai, M. Asada, K. C. Shin and T. Kojima, "GaInAsP/InP low dimensional quantum well lasers," ***The 29th Seminar on Science & Technology (Optoelectronics)***, (Invited) 3, pp.3-01-06, Meguro, February, 1996.

(9) B. Jenichen, G. Paris, H. T. Grahn, D. Luebbert, T. Baumbach, T. Kojima, S. Arai and A. Mazuelas, "Stress relaxation in $Ga_{0.22}In_{0.78}As_{0.80}P_{0.20}$ quantum wires on InP investigated by high-resolution x-ray diffractometry," ***The 5th Int. Symposium on Quantum Effect Electron.***, (Invited) 7, pp.26-31, Meguro, October 1998.

(10) N. Nunoya, M. Nakamura, T. Kojima, S. Tanaka, S. Tamura and S. Arai, "Low threshold current density (330A/cm^2) operation of 1.55μm GaInAsP/InP MQW-DFB lasers with separated periodic active regions," submitted to ***16th Semiconductor Laser Symposium***, 17, Yokohama, March 1999.